TESIS DE LA UNIVERSIDAD DE ZARAGOZA
2026
16

María Concepción Marcellán Vidosa

Estudio de la biomecánica corneal: modelo viscoelástico y aplicaciones

Director/es
Remón Martín, Laura
Ávila Gómez, Francisco Javier

ISSN 2254-7606

Prensas de la Universidad
Universidad Zaragoza

Universidad de Zaragoza
Servicio de Publicaciones

ISSN 2254-7606

Tesis Doctoral

ESTUDIO DE LA BIOMECÁNICA CORNEAL: MODELO VISCOELÁSTICO Y APLICACIONES

Autor

María Concepción Marcellán Vidosa

Director/es

Remón Martín, Laura
Ávila Gómez, Francisco Javier

UNIVERSIDAD DE ZARAGOZA
Escuela de Doctorado

Programa de Doctorado en Física

2025

Universidad Zaragoza
1542

Tesis Doctoral

ESTUDIO DE LA BIOMECÁNICA CORNEAL: MODELO VISCOELÁSTICO Y APLICACIONES

Autor

M.ª Concepción Marcellán Vidosa

Director/es

Francisco Javier Ávila Gómez

Laura Remón Martín

UNIVERSIDAD DE ZARAGOZA
Escuela de doctorado

Programa de Doctorado en Física

2025

AGRADECIMIENTOS

“ Solo no puedes, con amigos sí ”

Para muchos, su referente científico femenino es una figura lejana, admirable e inalcanzable. Yo tuve la inmensa suerte de tenerla cerca. Gracias, mamá, por enseñarme a mirar el mundo con curiosidad, por contagiarme tu amor por la ciencia y el conocimiento, y por demostrarme cada día que pensar también es una forma de amar. Solo aspiro a seguir tu ejemplo y sembrar en tus nietas la misma pasión que nos une.

A mis amigos y directores de tesis Laura Remón y Francisco Ávila, gracias por ser los faros en medio del camino. Sin vuestra ayuda, habría sido fácil perderse entre tantas rutas posibles. Vuestra guía y generosidad han sido esenciales para llegar a meta.

A Carlos, mi compañero de vida, gracias por sostenerme con tu calma, tu apoyo incondicional y tu generosidad con tu tiempo. Esta tesis es tan tuya como mía. Gracias por ayudarme a realizar mis sueños.

A mis pequeñas fieras, Laura e Isabel, gracias por vuestro amor desbordante, por acompañarme y por llenar de sentido cada página escrita. Ojalá este esfuerzo os inspire a desplegar las alas y volar tan alto como queráis.

A Pancho, mi padre, gracias por darme el último empujón cuando sentía que ya no podía más. Sin ti, esta aventura hubiera quedado incompleta. Y a mi hermano, por estar siempre ahí, apoyando cada una de mis locas aventuras, incluso cuando no te quede claro el sentido del viaje.

COMPENDIO DE PUBLICACIONES

Esta tesis se enmarca en la categoría 'Tesis por compendio de publicaciones' y consta de seis trabajos de investigación publicados en diversas revistas internacionales para optar al título de Doctor por la Universidad de Zaragoza. Todos los estudios se enmarcan en la misma temática: el estudio de la biomecánica corneal.

El capítulo 1 presenta con carácter introductorio, la revisión bibliográfica, los objetivos y justificación temática de los mismos. En el capítulo 2 se incluyen los trabajos científicos publicados. Los capítulos 3 y 4 presentan la discusión y principales conclusiones de la Tesis. Finalmente, el capítulo 5 presenta la bibliografía consultada. En el anexo I de acuerdo con el Real Decreto 99/2011, de 28 de enero, que regula las enseñanzas oficiales de Doctorado, se incluye el factor de impacto de las revistas y las áreas temáticas correspondientes a las publicaciones incluidas. Además, de la contribución del doctorando.

De acuerdo con la normativa, la primera página de este documento incluye el compendio de publicaciones junto con el Factor de Impacto (JIF/JCI: Factor-Categoría-Rango-Cuartil) de cada revista científica.

1. Ávila FJ, Marcellán MC, Remón L. On the Relationship between Corneal Biomechanics, Macrostructure, and Optical Properties. *J Imaging*. 2021;7(12):280.

   JCI (2021): 0,56-Imaging science & photographic technology-17/31-Q3

2. Marcellán MC, Remón L, Ávila FJ. Corneal hysteresis and intraocular pressure are altered in silicone-hydrogel soft contact lenses wearers. *Int Ophthalmol*. 2022;42(9):2801-2809.

   JIF (2022): 1,6- Ophthalmology- 50/62-Q4

   JCI (2022): 0,65- Ophthalmology-52/95-Q3

3. Del Barco Ó, Ávila FJ, Marcellán MC, Remón L. Corneal retardation time as an ocular hypertension disease indicator. *Biomed Phys Eng Express*. 2023;10(1):1088/2057-1976.

   JIF (2023): 1,3-Radiology, nuclear medicine & medical imaging-139/204-Q3

   JCI (2023):0,44-Radiology,nuclear medicine & medical imaging-132/204-Q3

4. Ávila FJ, Marcellán MC, Remón L. *In Vivo* Biomechanical Response of the Human Cornea to Acoustic Waves. *Optics*. 2023; 4(4):584-594.

   JIF (2023):1,1-Optics-94/119-Q4

   JCI (2023): 0,31-Optics-97/120-Q4

5. Ávila FJ, del Barco Ó, Marcellán MC, Remón L. A Comprehensive Study on Elasticity and Viscosity in Biomechanics and Optical Properties of the Living Human Cornea. *Photonics*. 2024; 11(6):524.

   JIF (2023): 2,1-Optics-59/119-Q2

   JCI (2023):0,61-Optics-56/120-Q2

6. Ávila FJ, del Barco O, Marcellán MC, Remón L. Aberrometric, Geometrical and Biomechanical Characterization of Sound-Induced Vibrational Modes of the Living Human Cornea. *Optics*. 2025; 6(1):5.

   JIF (2023):1,1-Optics-94/119-Q4

   JCI (2023): 0,31-Optics-97/120-Q4

ÍNDICE

RESUMEN

Esta tesis desarrolla nuevos métodos para evaluar las propiedades biomecánicas de la córnea, dada su relevancia en patologías ectásicas corneales, cirugía refractiva, así como en el diagnóstico y tratamiento del glaucoma. Con este objetivo, se ha propuesto un modelo teórico viscoelástico para caracterizar biomecánicamente la córnea. El desarrollo de dicho modelo ha permitido obtener expresiones analíticas que posibilitan, por primera vez, el cálculo *in vivo* de las componentes elástica y viscosa. Asimismo, se ha identificado el tiempo de retardo corneal como un biomarcador de la hipertensión ocular, lo que evidencia su importancia en la enfermedad ocular hipertensiva. Por otra parte, la influencia de la geometría corneal en la biomecánica ha sido analizada mediante tonometría de aire, demostrando la necesidad de incluir factores de corrección relacionados con el astigmatismo, de forma similar al enfoque aplicado al espesor central corneal. También se ha observado una relación entre la transparencia corneal, la macroestructura de la córnea y sus propiedades biomecánicas.

Finalmente, se ha desarrollado y calibrado un prototipo de resonador corneal basado en sonido de baja frecuencia, con el objetivo de caracterizar *in vivo* los modos de resonancia corneal, considerando aspectos geométricos, biomecánicos y aberrométricos.

ABSTRACT

This thesis presents new methods for evaluating the biomechanical properties of the cornea, given its relevance in ectatic corneal diseases, refractive surgery, and the diagnosis and treatment of glaucoma. To this end, a theoretical viscoelastic model has been proposed to characterize corneal biomechanics . The development of this model has enabled the derivation of analytical expressions that, for the first time, allow the *in vivo* calculation of both the elastic and viscous components. Furthermore, corneal retardation time has been identified as a potential biomarker for ocular hypertension, underscoring its significance in hypertensive eye disease. In addition, the influence of corneal geometry on biomechanics has been analyzed using air-puff tonometry, demonstrating the need to incorporate correction factors related to astigmatism—similar to those applied for central corneal thickness. A relationship has also been observed between corneal transparency, corneal macrostructure, and biomechanical properties.

Finally, a corneal resonator prototype based on low-frequency sound has been developed and calibrated, with the objective of characterizing the cornea's resonance modes *in vivo*, considering geometric, biomechanical, and aberrometric parameters.

ABREVIATURAS

Biomecánica corneal (BMC)

Elastografía de coherencia óptica (OCE)

Dioptría (D)

Asfericidad (Q)

Histéresis corneal (CH)

Modelo del Estado Sólido Lineal (MESL)

Cirugía refractiva (CR)

Queratocono (KC)

Factor de resistencia corneal (CRF)

Degeneración marginal pelúcida (DMP)

Presión intraocular (PIO)

La Laser assisted in Situ Keratomileusis (LASIK)

Ortoqueratología (Orto-K)

Lentes de contacto (LC)

Células ganglionares de la retina (CGR)

Disco óptico (DO)

Espesor central de la córnea (CCT)

Hipertensión ocular (HTO)

Ocular Response Analyzer (ORA)

Corneal Visualization Scheimpflug Technology (Corvis ST)

Presión intraocular compensada con la biomecánica corneal (PIO_b).

Primer valor de aplanación (P1)

Segundo valor de aplanación (P2)

Tomografía de coherencia óptica (OCT)

OCT vibracional (VOCT)

Densitometría corneal (DC)

Retardo corneal (τ)

Pneumatic viscoelastic damping"(PVD).

PIO umbral (PIO_u)

Tiempo de retardo umbral (τ_U)

LISTA DE FIGURAS

LISTA DE TABLAS

1. INTRODUCCIÓN

En este capítulo se abordarán aspectos fundamentales de la córnea desde una perspectiva tanto estructural como biomecánica. Se comenzará con una descripción detallada de la estructura, incluyendo sus capas y funciones esenciales en el sistema visual. A continuación, se explorará la biomecánica corneal (BMC), los diferentes modelos biomecánicos existentes y la importancia de su medición en diversas aplicaciones, tanto oftalmológicas como optométricas.

Se dedicará un apartado a los métodos y herramientas utilizados para evaluar la biomecánica corneal, con un enfoque particular en tecnologías *in vivo*. Además, se revisarán técnicas adicionales menos comunes, como la elastografía por coherencia óptica (OCE) y otras tecnologías que permiten obtener una visión más completa de la biomecánica corneal.

Por último, se estudiará la geometría corneal haciendo una revisión de las técnicas utilizadas para su medición y análisis. Estos parámetros son esenciales para comprender su comportamiento mecánico y su interacción con la presión intraocular.

1.1. Córnea

La córnea, junto con la película lagrimal, es la estructura refractiva más importante y es responsable de tres cuartas partes del poder refractivo del ojo. Una de sus principales características es la transparencia, debida a que es avascular [1]. Además, proporciona estabilidad mecánica al ojo, protegiéndolo de agentes externos [2], manteniendo una curvatura muy precisa y proporcionando una potencia aproximada de + 43,25 dioptrías (D)[1-3]. El radio de curvatura promedio de la primera superficie es de 7,7 mm y el radio posterior promedio de la segunda superficie es de 6,5 mm. Sin embargo, la cara anterior de la córnea no es una superficie esférica, sino que sufre un aplanamiento gradual según nos alejamos de su centro con un valor promedio de asfericidad (Q) de -0,26 que le proporciona aberración esférica positiva [4]. El espesor corneal central en la población sana

española es de 548,21 ± 30,7 µm, con un rango de 464 a 633 µm [5] que se va engrosando a medida que nos vamos hacia la periferia hasta alcanzar valores de 660-700 µm.

La córnea está compuesta por diversas capas. En el corte histológico de la figura 1, la capa más externa es el epitelio. A continuación, se encuentra la membrana de Bowman, seguida del estroma, la membrana de Descemet y, finalmente, el endotelio corneal. El epitelio tiene un grosor que varía entre 50 y 100 µm, y este grosor cambia según la localización geográfica, siendo más grueso en la parte inferior que en la superior y más grueso en la zona nasal que en la temporal. En el eje superior/inferior es significativamente más grueso que en el eje nasal/temporal [6]. La membrana de Bowman tiene un grosor de aproximadamente 12 µm. El estroma corneal es la capa más gruesa, con un grosor de aproximadamente 500 µm. La membrana de Descemet tiene un grosor de entre 4 y 10 µm, y, por último, el endotelio es la capa más fina, con un grosor de 5 µm [7].

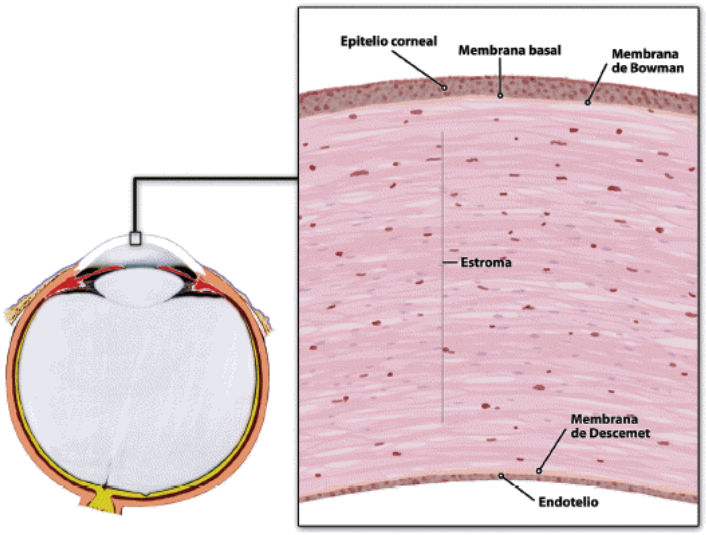

Figura 1: Corte histológico de la córnea. Imagen tomada de Fernández et al. [8].

Epitelio: Está formado por 4 a 6 capas de células. El epitelio se caracteriza por ser estratificado escamoso y no queratinizado, es la principal barrera contra patógenos y fluidos. Esta función se debe a las estrechas uniones entre las células y a la constante regeneración de células madre limbocorneales ubicadas en las capas basales del epitelio [9]. Morfológicamente está dividido en 3 tipos de células que residen cada una en su capa correspondiente (ver figura 2). En contacto directo con la lágrima, se encuentran dos capas de células superficiales planas o de descamación, que son hexagonales y presentan un

glicocálix fibrilar. Junto con las microvellosidades y micropliegues, esto favorece una mayor adherencia entre la lágrima y el epitelio [10].

En segundo lugar, hay tres filas de células alares que representan la transición entre las células superficiales y las basales. Estas células tienen numerosos desmosomas que las unen entre sí, facilitando la conexiónentre las células basales y superficiales [11].

Por último, una monocapa de células basales columnares descansa sobre la membrana basal, proporcionando adherencia entre las células epiteliales y el estroma. Estas células tienen una gran capacidad de mitosis, y su principal característica es que las células resultantes de esta división migran hacia la capa de células alares, donde se transforman en esas células. A medida que continúan su camino migratorio, se transforman en células superficiales. Este proceso dura aproximadamente una semana [9,10].

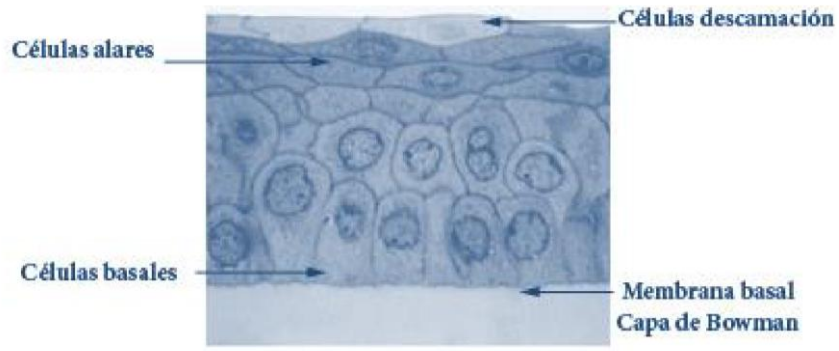

Figura 2: Esquema tipos de células epiteliales. Imagen tomada de la tesis de Lavilla [11].

Membrana de Bowman: Es acelular y está compuesta por colágeno, lo que la hace resistente a los traumatismos, aunque carece de capacidad regeneradora. Las fibras de colágeno más cercanas al estroma están entrelazadas y organizadas de manera aleatoria. Además, contiene mucoproteínas con una composición bioquímica similar a la del estroma[12].

Estroma: El estroma proporciona a la córnea el 90% de su espesor. Está formado por una matriz extracelular compuesta de colágeno y proteoglicanos, además de células estromales o queratocitos. Las células corneales son fibroblastos con morfología dendrítica, lo que les permite interconectarse y formar una red [13]. En el estroma anterior, su densidad es un 30% superior a la del estroma posterior [14]. Su función principal es la producción de colágeno y

proteoglicanos para la formación de la matriz extracelular [15]. La organización y estructura de esta matriz es fundamental para mantener la transparencia, las propiedades ópticas, la geometría y las propiedades biomecánicas de la córnea [10].

La matriz está formada por fibrillas de colágeno tipo I y V [10], empaquetadas en fibras más densas de pequeño diámetro (25-30 nm) [16] (figura 3). Estas fibrillas se disponen en paralelo, formando láminas (lamelas), y las capas de lamelas, a su vez, están organizadas de manera ortogonal [15]. El reducido tamaño de las microfibras (250-300 Å) [11] y su estrecha separación, del orden de 550 Å, evitan la dispersión luminosa [10]. Este empaquetamiento regular y homogéneo, junto con el pequeño diámetro de las fibras y su equidistancia, contribuyen a la transparencia corneal [17]. En la matriz también está presente el colágeno tipo IV, responsable de formar redes que aportan estabilidad mecánica [18]. Los proteoglicanos de la córnea se unen a las fibrillas de colágeno, favoreciendo su disposición y espaciamiento. Son determinantes para mantener la separación entre las fibras de colágeno, un factor clave en la transparencia corneal [19].

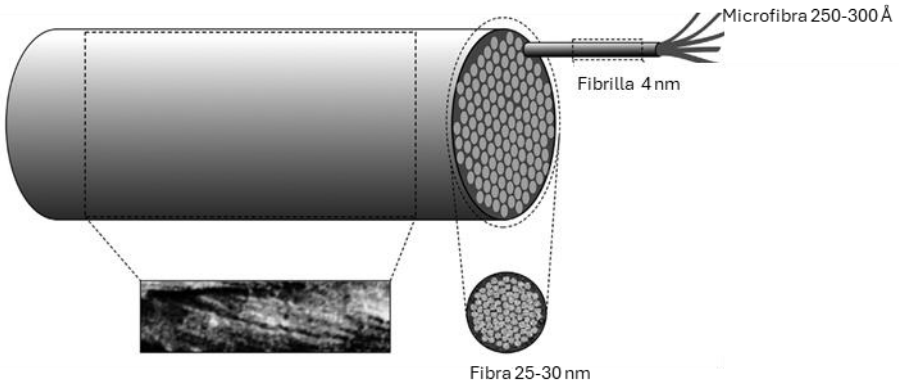

Figura 3: Estructura de las fibras de colágeno en el estroma corneal. Imagen tomada y modificada de Meek y Knupp [20].

El comportamiento mecánico de la córnea está determinado por su organización a nivel de microestructura y macroestructura. La distribución lamelar en el estroma no es completamente regular, ya que las láminas se entrecruzan con mayor densidad en el tercio anterior de la córnea que en el resto. Como se observa en la Figura 4, las laminillas están más entrelazadas en la parte anterior, mientras que en la posterior tienden a disponerse de manera más paralela, especialmente en la zona central. En la periferia media también se observa un mayor entrecruzamiento de fibras. En el limbo, las laminillas de anclaje parecen introducirse en el estroma desde las capas más profundas [20]. Las lamelas se

disponen de forma perpendicular entre sí en el centro y la media periferia corneal, orientadas en direcciones temporal-nasal e inferior-superior, como se observa en la Figura 5. En el limbo, su distribución es anular [15], aunque existe cierta discrepancia sobre la disposición exacta de este anillo de colágeno en el limbo esclerocorneal.

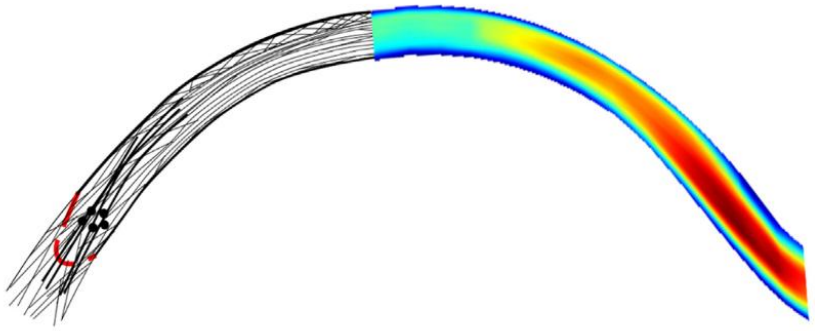

Figura 4: Distribución lamelar anteroposterior en el estroma. La escala de colores representa la densidad de fibras. Colores cálidos mayor densidad/ colores fríos menor densidad. Imagen tomada de Meek and Knupp [20].

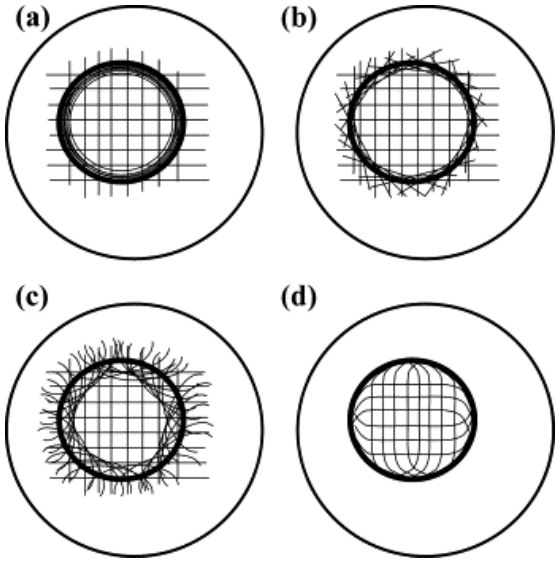

Figura 5: Esquemas de las 4 posibles organizaciones de las lamelas estromales en el limbo. En todas hay en el centro y periferia una distribución ortogonal. En **a)** fibrillas limbares formando un anillo discreto. En **(b)** y **(c)**, el colágeno en el limbo forma una red de anclaje al atravesar el limbo tangencialmente. En **(d)** el colágeno de la córnea se dobla cerca de la periferia para formar un anillo circular en el limbo. Imagen tomada de Meek and Boote [21].

Membrana de Descemet: Lámina basal gruesa segregada por el endotelio. Contiene componentes colágeno y no colágeno, los cuatro componentes son lamininas, colágeno tipo IV, nidógenos y perlecano. Su capacidad de regeneración tras un traumatismo, infección o lesión quirúrgica es limitada. Es de vital importancia para mantener la homeostasis corneal, siendo también una pieza clave para la transparencia corneal [22].

Endotelio corneal: Está formado por una única capa de células planas hexagonales, perfectamente unidas por sus lados. Esta disposición resulta altamente eficiente frente a la exposición intracelular al humor acuoso [23]. La estructura más importante del endotelio es la bomba sodio potasio (ATpasa), la cual contrarresta el flujo de agua hacia el estroma, preservando la transparencia corneal [24]. Con el envejecimiento, el número de células endoteliales disminuye, y las células vecinas deben expandirse para ocupar el espacio dejado [23].

1.2. Biomecánica

1.2.1. Definición

La biomecánica es la ciencia que aplica las leyes de la mecánica al estudio de las estructuras anatómicas y órganos de los seres vivos, considerando la influencia de las fuerzas externas e internas (cinética) y los movimientos (cinemática). Para ello, integra conocimientos de ingeniería, arquitectura, biofísica, anatomía, fisiología y otras disciplinas. La biomecánica se basa en modelos que permiten predecir el comportamiento, la resistencia, la fatiga y otros aspectos de distintas partes del cuerpo cuando están sometidas a condiciones específicas. Así, se desarrollan modelos matemáticos para comprender mejor los sistemas biológicos [25].

La biomecánica corneal analiza el equilibrio y la deformación de los tejidos ante fuerzas internas y externas [26], con el objetivo de mejorar el conocimiento sobre la fisiología y fisiopatología corneal, así como el diagnóstico y tratamiento de diversas patologías. Además, busca identificar patrones predictivos de su respuesta dinámica [10]. El estroma desempeña un papel importante en la forma, rigidez, transparencia y refracción de la córnea, representando aproximadamente el 90 % de su grosor [27]. En contraste, el epitelio y el endotelio tienen una influencia mínima en la biomecánica corneal. Por otro lado, la

membrana de Bowman, debido a su alta densidad de colágeno, parece tener un impacto significativo en la estructura corneal. Finalmente, aunque la contribución de la membrana de Descemet a la estabilidad corneal aún requiere mayor investigación, se considera que también desempeña un papel relevante [28].

La estabilidad de la córnea depende de factores intra y extra corneales. Estas fuerzas opuestas generan un equilibrio dinámico. En la tabla 1 se describen dichos factores [29].

Tabla 1: Factores intra y extra corneales que influyen en la biomecánica corneal.

Intra corneales	Extra corneales
- Microestructura ● Organización molecular del colágeno. - Macroestructura ● Geometría corneal. ● Espesor corneal.	- Presión intraocular. - Presión Atmosférica. - Tensión palpebral. - Tensión músculos extraoculares. - Tensión del músculo ciliar.

1.2.2. Propiedades y parámetros biomecánicos de la córnea

Biomecánicamente, la córnea se comporta como una membrana viscoelástica. Su matriz extracelular está compuesta por fibras de colágeno, que le otorgan resistencia a la carga (rigidez), y proteoglicanos, que le proporcionan una gran capacidad de absorción de energía (viscosidad), contribuyendo así a sus propiedades mecánicas [2]. Su característica más importante es precisamente este comportamiento viscoelástico, se comporta de forma parcialmente elástica como un sólido y parcialmente viscosa como un líquido [27].

Según la ley de Hooke, los sólidos elásticos se deforman de manera proporcional al esfuerzo aplicado y recuperan su forma original al cesar la fuerza. En cambio, en los líquidos viscosos, regidos por la ley de Newton, el esfuerzo aplicado es proporcional a la velocidad de deformación, pero no a la deformación en sí, lo que impide la recuperación de la forma original [30]. En este caso, no hay una recuperación de la deformación. Un comportamiento intermedio es el comportamiento viscoelástico, en el que el cuerpo sobre el que se aplica

el esfuerzo recupera parte de la deformación aplicada [31,32]. Además, su respuesta depende de la velocidad de deformación y de las fases de carga y descarga.

La córnea exhibe un comportamiento intermedio: tras la aplicación de una fuerza, recupera parte de la deformación, dependiendo de la velocidad de carga y descarga. Su respuesta es no lineal y depende del tiempo, lo que significa que se deforma lentamente y su recuperación no sigue exactamente el mismo patrón que la deformación inicial. De esta diferencia surge el concepto de histéresis corneal (CH), parámetro que mide la capacidad viscoelástica de la córnea para amortiguar, absorber y disipar energía [33]. Además, debido a su dependencia del tiempo, una carga más rápida genera una respuesta más rígida [34].

El módulo de Young describe la rigidez de un tejido elástico a través de la relación entre esfuerzo y deformación [32]. Cuanto mayor es su valor, mayor esfuerzo se requiere para deformar el tejido. En el caso del ojo, el coeficiente de rigidez ocular está determinado por el módulo de Young del globo ocular y refleja la resistencia de la córnea a la indentación, es decir, su capacidad estructural para resistir la deformación [10].

Otro parámetro relevante es el coeficiente de Poisson, que define la relación entre la deformación longitudinal y lateral [32]. Dado que la córnea no se deforma únicamente en la dirección de la fuerza aplicada, sino también en sentido perpendicular, su comportamiento se ve influenciado por la disposición de las fibras de colágeno en el estroma. Estas están organizadas en direcciones nasal-temporal y superior-inferior, lo que confiere a la córnea un comportamiento anisótropo, es decir, su deformación varía según la dirección de la fuerza ejercida [10,27]. Debido a su composición y estructura, la córnea se comporta como un tejido heterogéneo.

1.2.3. Modelos biomecánicos corneales

El objetivo de los modelos biomecánicos es describir la respuesta de un tejido ante una carga aplicada, correlacionando diferentes parámetros de entrada con los de salida para predecir posibles patologías o los efectos de distintos tratamientos. Debido a las propiedades viscoelásticas de la córnea [35] es necesario representar dos componentes: el elástico, que provoca una deformación instantánea, y el viscoso, que genera una deformación amortiguada [36]. Su modelización requiere la comprensión de los modelos

viscoelásticos, los cuales son difíciles de visualizar, por lo que suelen representarse mediante modelos mecánicos o reológicos.

En los materiales newtonianos, la viscosidad se representa mediante un pistón trabajando en un cilindro, lo que simboliza la disipación de energía. El comportamiento elástico, similar al de un sólido de Hooke, se representa habitualmente con un muelle, donde la energía está almacenada [30,31]. El comportamiento viscoelástico puede ser representado como una combinación de muelles y pistones. En la figura 6a, se observa un émbolo y un muelle acoplados en paralelo con un tablero, mostrando el modelo básico de viscoelasticidad de Kelvin-Voigt [32,37]. En la figura 6b, se muestra la curva de fluencia o creep/relajación del modelo de Kelvin-Voigt. Este modelo describe adecuadamente la deformación en los ensayos de esfuerzo, pero no es capaz de representar la relajación de manera precisa [37,38]. Otra característica importante de este modelo es que no se deforma de inmediato [39].

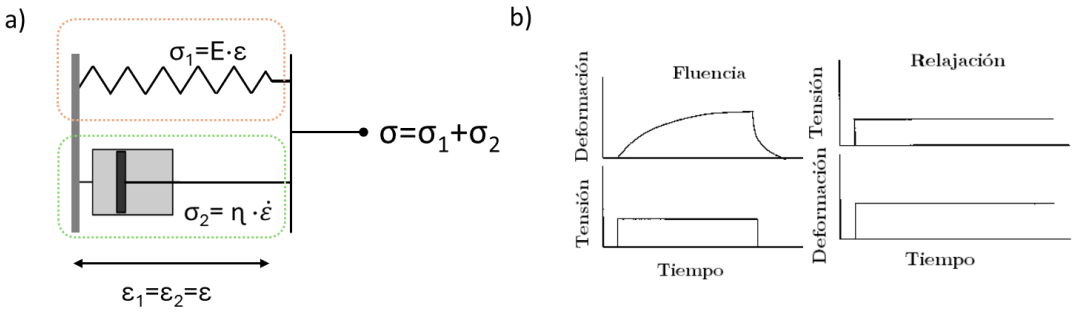

Figura 6: a) Representación esquemática del acoplamiento en paralelo de resorte y émbolo que definen el modelo viscoelástico de Kelvin-Voigt. Donde **σ** la tensión aplicada, **E** representa la constante elástica, **η** constante viscoelástica, **σ_1**tensión en el muelle, **σ_2** tensión en el émbolo, $\varepsilon_1=\varepsilon_2=\varepsilon$ elongación y $\dot{\varepsilon}$ corresponde a la velocidad de deformación del émbolo [32]. **b)** Representación de la curva de fluencia/relajación del modelo Kelvin-Voigt. Imagen tomada y modificada de Galindo [40].

Dentro de los modelos básicos viscoelásticos, el elemento de Maxwell (figura 7a) consiste en un muelle y un émbolo dispuestos en serie. Se caracteriza por una constante de elasticidad, **E,** y una de viscosidad, **η**. En la representación fluencia/relajación (figura7b), se observa que no representa fielmente el comportamiento viscoelástico, ya que la deformación crece linealmente con el tiempo, aunque la respuesta a la relajación si se ajusta a la realidad. Además, no recupera completamente la forma [37-39].

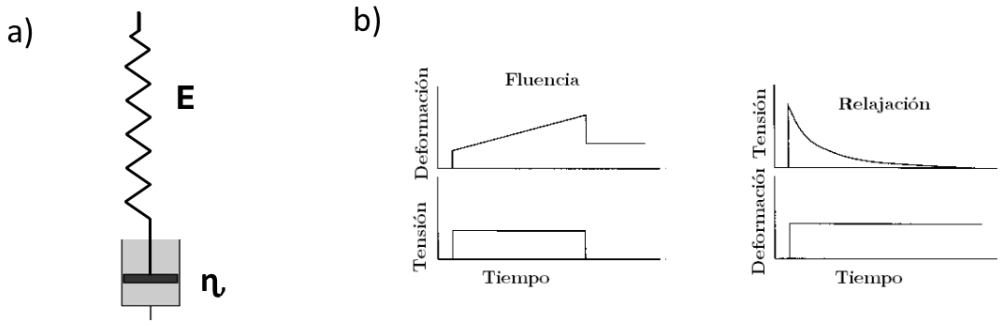

Figura 7: a) Representación esquemática del acoplamiento en serie de un muelle y émbolo del elemento de Maxwell [32]. **b)** Representación de la curva de fluencia/relajación del elemento Maxwell. Imagen tomada y modificada de Galindo[40].

Nótese que ni el modelo de Kelvin-Voigt ni el elemento de Maxwell logran reproducir la respuesta de un típico material viscoelástico por sí solo; es necesario combinar varios elementos [31,32]. El modelo de Maxwell consiste en un número arbitrario de elementos Maxwell conectados en paralelo y sometidos a un experimento de relajación del estrés (figura 8). En todos los elementos individuales, la deformación es la misma, la tensión total aplicada es la suma de las tensiones individuales experimentadas por cada elemento [32].

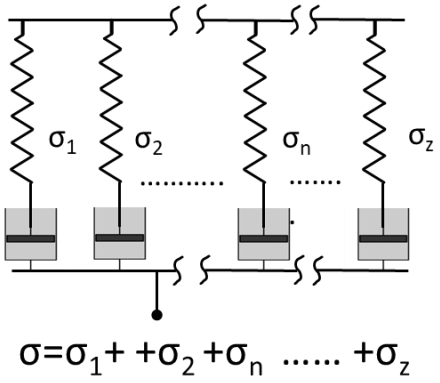

Figura 8: Representación esquemática del acoplamiento en paralelo de "z" elementos de Maxwell que definen el modelo viscoelástico de Maxwell [32].

Aunque estos modelos más complejos son precisos al representar las propiedades de los materiales viscoelásticos, generan modelos complicados que no tienen una única solución[41]. Para representar la córnea, se han propuesto modelos más sencillos basados en elementos finitos. Otra dificultad encontrada en la representación corneal es que esta tiene volumen, mientras que los modelos viscoelásticos reológicos son unidimensionales y no pueden considerar la deformación tridimensional de la córnea. Kling et al. [42] demostraron que existe una correlación entre la deformación de la córnea y la indentación en el ápex.

En consecuencia, al estar relacionada la deformación tridimensional de la córnea durante la tonometría por aire con la indentación puntual en el ápex, los modelos viscoelásticos corneales pueden simplificarse a una dimensión [43].

En 1973 Kobayashi et al. [35] propusieron un modelo viscoelástico de la córnea, utilizando un modelo reológico que combina dos unidades de Kelvin-Voigt y un muelle en serie (figura9).

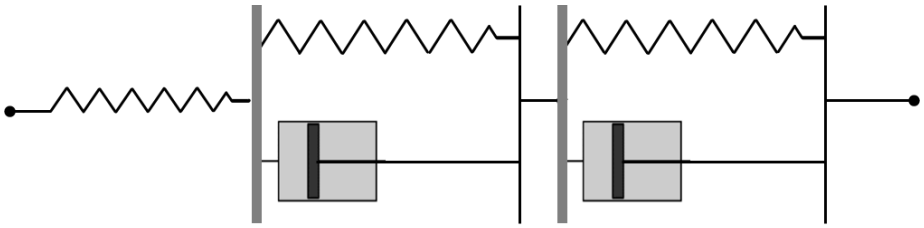

Figura 9: Representación esquemática del acoplamiento en serie del modelo de Kobayashi[35].

El modelo viscoelástico de Burgers modela el comportamiento de la córnea al considerar simultáneamente su elasticidad, elasticidad retardada y viscosidad. Este modelo combina en serie una unidad de Kelvin-Voigt y un elemento de Maxwell (figura 10a) [43]. Para definir este modelo, es necesario determinar el valor de cuatro parámetros. En general, este modelo representa bien la viscoelasticidad, como se puede observar en las gráficas de esfuerzo-relajación de la Figura 10b.

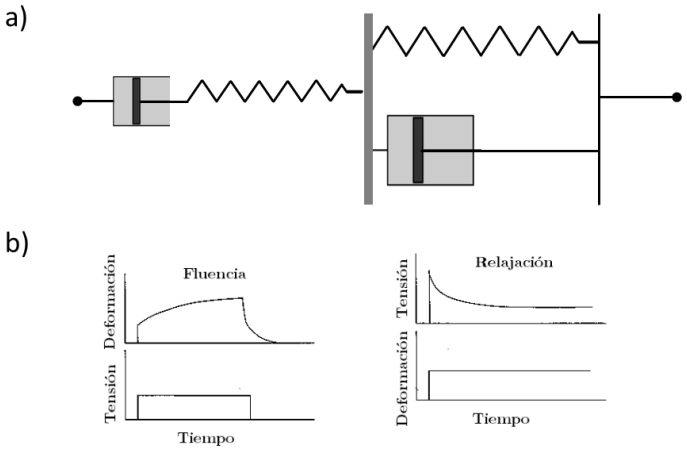

Figura 10: a) Representación esquemática del acoplamiento en serie del modelo de Burgers[43]. **b)** Representación de la curva de fluencia/relajación del modelo Burgers. Imagen tomada y modificada de Galindo [40].

Otro de los modelos utilizados para representar la córnea es el Modelo del Estado Sólido Lineal (MESL), que consiste en un muelle en serie con una unidad de Kelvin-Voigt [36,39] (figura 11a). Este modelo reacciona de inmediato y se recupera completamente como los materiales elásticos, pero su deformación y recuperación dependen del tiempo, similar a los materiales viscosos. Por esto, al aplicar una carga el muelle izquierdo se estira inmediatamente representado el comportamiento elástico de la córnea. Mientras que la unidad de Kelvin-Voigt representa la componente viscosa, el émbolo hace que la deformación sea lenta. Durante la descarga el muelle izquierdo se contrae inmediatamente pero es retenido por la unidad de Kevin-Voigt. De este modo se representa la dependencia con el tiempo de los materiales viscoelásticos [44]. En la figura 11b se muestra la curva de fluencia relajación del MESL, en la que se observa un comportamiento muy similar a los sólidos viscoelásticos. La primera parte de la curva corresponde al comportamiento elástico y la segunda al viscoso [45].

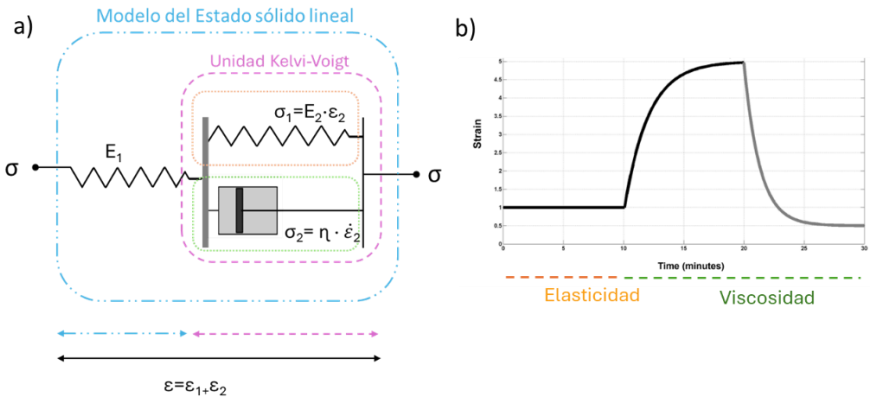

Figura 11: a) Representación esquemática del modelo lineal estándar representado por el acoplamiento en serie de un muelle y una Kelvin-Voigt. **E** es la elasticidad de los muelles, **η** es la viscosidad del émbolo, **σ** la tensión aplicada y **ε** la deformación inducida [36,39]. **b)** Curva de fluencia/relajación del MESL. Imagen tomada y modificada del trabajo de Lombardo et al. [45].

1.3. Biomecánica, aplicación en oftalmología y optometría

La biomecánica en la investigación y desarrollo en oftalmología actual tiene gran relevancia debido al potencial de sus aplicaciones tanto en el diagnóstico de patologías (ectasias corneales/glaucoma) como en la mejora de sus tratamientos [46]. Por otro lado, el auge de la cirugía refractiva hace que la investigación en biomecánica corneal sea fundamental para identificar a los pacientes con mayor riesgo de desarrollar ectasia iatrogénica tras la corrección del error refractivo con láser. Asimismo, existe la necesidad de mejora de la previsibilidad y eficacia de los protocolos de cirugía refractiva (CR) [11,28,47].

1.3.1. Ectasias corneales

Los desórdenes corneales ectásicos se definen como un conjunto de enfermedades de la córnea caracterizadas por un adelgazamiento progresivo y una alteración de su curvatura, acompañadas de protrusión, pero sin signos inflamatorios. Algunas de las enfermedades ectásicas no inflamatorias, ordenadas según su frecuencia de aparición, son: queratocono (KC) (ectasia corneal axial localizada), degeneración marginal pelúcida (ectasia corneal periférica), queratoglobo (ectasia corneal periférica) y queratocono posterior. Existe una relación entre los puntos de adelgazamiento máximo, la protrusión corneal máxima y el tipo de ectasia [10,48].

El debilitamiento de la arquitectura corneal, debido al adelgazamiento causado por la alteración de las fibras de colágeno, predispone a la ectasia. En estos casos, se pone de manifiesto la insuficiencia biomecánica de la córnea [10].

En la detección temprana de la ectasia y el seguimiento de su progresión, la topografía y tomografía corneal juegan un papel fundamental [49], ya que aumentan la capacidad para identificar la ectasia corneal en sus primeras etapas, particularmente antes de que el paciente desarrolle síntomas [50]. Sin embargo, incluso con todas estas herramientas, la medición directa de la biomecánica clínica sigue siendo primordial para mejorar la especificidad y sensibilidad en la identificación de casos leves, así como para caracterizar la susceptibilidad a la progresión de la ectasia [51].

Respecto a los valores de los parámetros biomecánicos hay variabilidad según los trabajos, Ortiz et al. [52] llegaron a la conclusión que los pacientes con queratocono la histéresis media corneal es de 7,5±1,2 mmHg y el factor de resistencia corneal (CRF) 6,2±1,9 mmHg. Mientras que Shahet et al. [53] obtuvieron un valor medio de CH 9,6±2,2 mmHg con un rango 4,7-16,7mmHg. Sedaghat et al. [54] midieron la histéresis en pacientes con queratocono y degeneración marginal pelúcida (DMP). obtuvieron para el KC una CH de 8,43±0,78mmHg y CRF de 7,19±1,11 mmHg, para la DMP una CH de 8,91±1,05 mmHg y CRF de 8,21±1,35 mmHg. En todos ellos existía un grupo control con sujetos sanos, llegando a la conclusión que la CH y CRF en ese grupo es significativamente mayor que en los pacientes con ectasia.

1.3.2. Cirugía refractiva

Aunque la cirugía refractiva presenta pocas complicaciones, una de las más graves es la ectasia corneal iatrogénica, cuya incidencia es del 0,033 % en un periodo de 8 años [55]. La ectasia asociada a Laser assisted in Situ Keratomileusis (LASIK) tiene una incidencia 4,5 veces mayor que la observada en queratectomía fotorefractiva [56]. Esta condición se caracteriza por un adelgazamiento estromal acompañado de una protrusión en la parte inferior de la córnea, lo que provoca un cierre de la curvatura corneal de 5D o más en comparación con las topografías postoperatorias [57]. La variación de los radios es distinta en cada meridiano, lo que genera un aumento del astigmatismo irregular y reduce significativamente la agudeza visual del paciente [11,27]. Entre los factores de riesgo se encuentran la miopía alta, el queratocono subclínico, un bajo espesor estromal, una zona óptica más grande y la realización de múltiples retoques [58].

Se ha planteado la hipótesis de que la progresión de la ectasia tras la cirugía refractiva está relacionada con propiedades biomecánicas alteradas y una descompensación estructural de la córnea, lo que resulta en un adelgazamiento del estroma y una protrusión [51]. Las propiedades biomecánicas de las córneas con ectasia postquirúrgica son muy similares a las observadas en córneas con queratocono, pero difieren significativamente en la mayoría de los parámetros de aquellas córneas que no han desarrollado ectasia tras la cirugía [27]. En cirugía refractiva corneal, la detección de formas leves de ectasia en el preoperatorio es esencial para prevenir su progresión en el postoperatorio. Por ello, es fundamental incluir

los parámetros biomecánicos en el protocolo preoperatorio, así como desarrollar herramientas que permitan relacionar la biomecánica con la geometría corneal.

1.3.3. Anillos intraestromales

Los segmentos intraestromales son pequeños dispositivos poliméricos que se introducen en el estroma corneal para regularizar la superficie corneal y corregir errores de refracción elevados. Se utilizan en el tratamiento del queratocono, las degeneraciones marginales pelúcidas, la ectasia post-LASIK y la miopía alta [59].

La forma y el tamaño de la sección transversal del implante, su diámetro y la longitud del arco, así como su posición de implantación, influyen en la forma postquirúrgica de la córnea y en la corrección refractiva resultante. Además, factores mecánicos, como la presión intraocular (PIO) y la biomecánica de los tejidos, juegan un papel importante y deben ser considerados al diseñar un nomograma [60]. En este contexto, resulta interesante la relación entre la modificación de la geometría corneal y la biomecánica.

1.3.4. Ortoqueratología

En optometría, los parámetros biomecánicos podrían ser interesantes para incluir en los protocolos ortoqueratológicos. Este tratamiento se basa en el moldeo corneal para corregir temporalmente defectos refractivos como la miopía. La ortoqueratología (Orto-K) utiliza lentes de contacto (LC) de geometría inversa. Con estas lentes de contacto de uso nocturno, se consigue aplanar la zona central de la córnea, lo que provoca que pase de forma prolata a oblata [61].

Una vez retiradas las lentes de contacto, la córnea no recupera su forma inmediatamente debido a las características viscoelásticas de la misma, lo que hace que durante algunas horas permanezca moldeada. El patrón de deformación viscoelástico producido por las lentes Orto-K es desconocido, se ve afectado tanto por las horas de uso de las lentes como por su diseño. Los modelos biomecánicos pueden desempeñar un papel importante en los

mecanismos de moldeo corneal, pero hasta el momento, son pocos los que logran predecir con precisión el resultado del tratamiento [62].

Por el contrario, el efecto del uso de las lentes Orto-K es muy evidente en la topografía, especialmente en el mapa refractivo. Se observa una disminución de la potencia en la región central y un aumento en la periferia ya desde la primera noche de uso. Tras una semana, se produce una estabilización del patrón topográfico. Estos cambios se deben principalmente a la redistribución del epitelio corneal, con un adelgazamiento en la zona central y un engrosamiento en la media periferia. El efecto de las lentes Orto-K no provoca cambios en todo el grosor corneal, ya que parece limitarse al epitelio corneal [63-66].

Por otro lado, la cuestión de si este tipo de lentes modifica la biomecánica corneal sigue siendo controvertida. Sin embargo, los últimos estudios indican que no se ha alterado significativamente la biomecánica corneal [67].

1.3.5. Glaucoma

El glaucoma es una neuropatía óptica crónica que se caracteriza por la pérdida de células ganglionares de la retina (CGR), degeneración progresiva del disco óptico, adelgazamiento de la capa de fibras nerviosas de la retina, aumento de la excavación del disco óptico (DO) y defectos del campo visual asociados [68].

En Europa, la prevalencia de glaucoma es del 2,93% entre las personas de 40 a 80 años [69]. Darbà y Marsà, en 2022, encontraron que en España la incidencia en entornos ambulatorios fue de 2,2 por 10.000 personas, mientras que en hospitales fue de 0,2 por 10.000 personas [70]. La fisiopatología del glaucoma está relacionada con el gradiente entre la presión intraocular y la presión arterial. Una PIO elevada junto con una presión arterial baja producen una disminución en el aporte sanguíneo, lo que conduce a un deterioro del transporte axonal en las fibras del nervio óptico, dañando los axones de las CGR en la lámina cribosa del nervio óptico [69,71].

Entre los factores de riesgo, la PIO alta se postula como uno de los que más influyen en la progresión del glaucoma, además de ser el único sobre el que se puede actuar actualmente. Los antecedentes familiares, el aumento de la edad, la raza, la miopía y el estado cardiovascular también influyen, aunque en menor medida [52,72,73]. Últimamente se está hablando de otro factor de riesgo: el grosor de la córnea central (CCT). Los resultados del

Ocular Hypertension Treatment Study y del Early Manifest Glaucoma Trial sugieren que los ojos con córneas delgadas tienen un mayor riesgo de desarrollar y progresar el glaucoma[54].

Por otro lado, se ha observado que las córneas con el mismo grosor pueden tener diferentes propiedades biomecánicas y viceversa. Existe evidencia de una fuerte relación entre la PIO y la CCT en sujetos sin glaucoma, pero esta relación es solo moderadamente fuerte en pacientes glaucomatosos [74]. De aquí la necesidad de introducir nuevos parámetros de diagnóstico, como la histéresis corneal.

Los pacientes con una PIO superior a 21 mmHg que no presentan alteraciones en el nervio óptico ni en el campo visual se denominan hipertensos oculares (HTO). Algunos de estos pacientes desarrollan glaucoma, mientras que otros no se ven afectados, a pesar de los valores elevados de presión intraocular [72]. También existen pacientes que presentan alteraciones en el campo visual y en la cabeza del nervio óptico, características del glaucoma, pero con valores de PIO normales. A esta condición se le denomina glaucoma normotenso [75]. Para explicar esta condición, es necesario considerar la histéresis corneal, dado que está relacionada tanto con su presencia y gravedad, como con la progresión estructural y funcional del glaucoma [76].

Una histéresis corneal más baja se asocia con un volumen menor del área del disco, una relación disco/copa disminuida y un grosor medio de fibras neurorretinianas más delgado en pacientes con glaucoma normotenso [77]. Las mediciones de histéresis corneal están asociadas con el riesgo de progresión del glaucoma. Los ojos con una CH más baja mostraron tasas más rápidas de pérdida del campo visual en comparación con aquellos con una CH más alta [75].

Los últimos estudios ponen de manifiesto la importancia de las propiedades biomecánicas de la córnea en los cambios de la cabeza del nervio óptico, lo que mejora la comprensión de los mecanismos fisiopatológicos implicados en el desarrollo del glaucoma [71-73,75,78-81].

1.4. Medida biomecánica corneal

Actualmente, existen diversas técnicas que permiten evaluar la biomecánica corneal, las cuales se clasifican en dos grupos: *in vivo* y *ex vivo*.

Dentro de las técnicas para medir la biomecánica corneal *in vivo*, se puede destacar los siguientes aparatos comerciales: Ocular Response Analyzer (ORA) (Reichert Technologies, Depew, NY, EE. UU.) y Corneal Visualization Scheimpflug Technology (Corvis ST) (Oculus Optikgeräte GmbH, Wetzlar, Alemania).

Ambos sistemas de medición emplean un pulso de aire para medir la respuesta biomecánica de la córnea. Otros sistemas menos utilizados incluyen la microscopía de Brillouin, el análisis ultrasonográfico de alta frecuencia, la elastografía por resonancia magnética y la elastografía de coherencia óptica [27,82,83]. La mayoría de los datos clínicos están relacionados con la respuesta biomecánica a un pulso de aire, por lo que estos métodos son los más utilizados [46].

La microscopía de Brillouin se basa en el fenómeno de dispersión de la luz, el cual resulta de la interacción entre los fotones que inciden en la superficie estudiada y la propagación de fluctuaciones termodinámicas en el medio. Dado que las velocidades de propagación de los fonones acústicos están asociadas con las propiedades mecánicas de la materia, la cuantificación del desplazamiento de frecuencia causado por la interacción acústico-óptica puede permitir la estimación de parámetros elásticos [84].

Entre los métodos *ex vivo* se encuentran la interferometría electrónica de patrón moteado y la interferometría de patrón moteado de corte radial [2].

1.4.1. Ocular Response Analyzer

Cuando el ORA salió al mercado en 2005, supuso un avance significativo al permitir la medición de la biomecánica corneal *in vivo*, ya que, anteriormente, el único método disponible para su medición era *ex vivo* [10]. Su función principal es proporcionar valores de presión intraocular, los cuales están correlacionados con los obtenidos mediante el tonómetro de Goldman, considerado el *gold* estándar en el diagnóstico de glaucoma.

Además, permite obtener valores de PIO compensada con la biomecánica corneal (PIOb), considerando el grosor de la córnea y la histéresis corneal. También proporciona valores de histéresis y el factor de resistencia corneal [46].

El sistema emite un pulso de aire que ejerce una presión con distribución gaussiana. Este pulso produce una primera fase de carga, donde la córnea se indenta, seguida por una segunda fase de descarga, en la cual la fuerza del pulso disminuye y la córnea vuelve a su posición normal. El punto máximo de la campana de Gauss coincide con el momento en el que la córnea pasa a ser ligeramente cóncava. De este modo, se obtiene un primer valor de presión (P1) que coincide con el punto en que la córnea pasa de convexa a plana, y un segundo valor de presión (P2) cuando la curvatura de la córnea vuelve de cóncava a plana mientras recupera su forma. Para detectar el aplanamiento, el sistema utiliza un sistema electroóptico de infrarrojos. Según la cantidad de luz infrarroja reflejada por la córnea, se obtienen los valores de P1 y P2. Cuando la córnea se aplana por primera vez, la luz infrarroja reflejada por ella alcanza un primer máximo (P1). Durante la fase de descarga, en el momento en que se produce la segunda aplanación, se genera otro máximo de reflexión, lo que da el valor de P2 [2,27,46,85].

La histéresis es la relación entre la deformación y la fuerza aplicadas sobre la córnea en función del tiempo, y se considera un valor de resistencia dinámica. Su valor está relacionado con los dos picos de aplanación. Debido a la naturaleza viscoelástica de la córnea, la presión del primer aplanamiento es distinta de la presión en el momento de la recuperación, tal como se muestra en la figura 12. Esto ocurre porque la córnea absorbe y disipa parte de la energía del pulso de aire. La diferencia entre estos dos valores determina el valor de histéresis (CH = P1 - P2), y su unidad de medida es mmHg [11,85,86].

El CRF mide la resistencia mecánica global de la córnea y representa sus propiedades elásticas. Este parámetro proporciona la resistencia estática a la deformación de la córnea. Es una medida empírica que se deriva de la expresión 1 [85,87,88].

$$CRF = (P1 - 0{,}70 - P2) - 3{,}08 \qquad \text{Expresión 1}$$

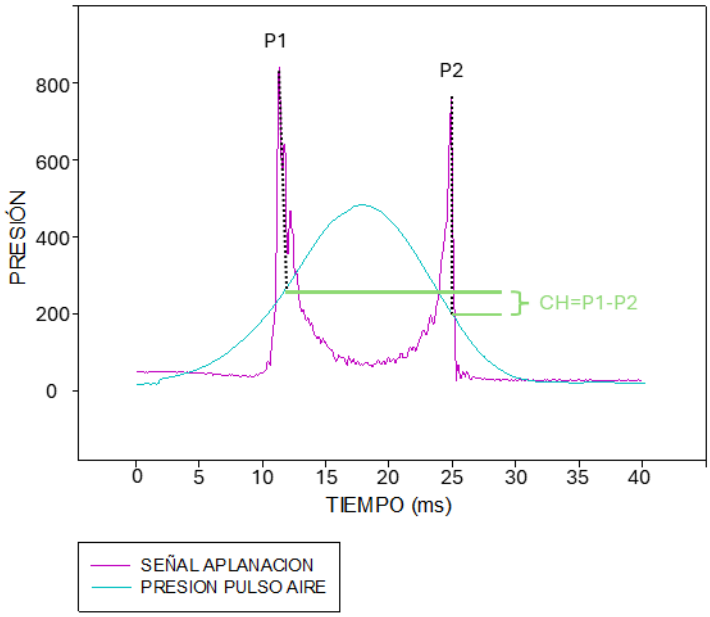

Figura 12: Representación gráfica de aplanación y presión de un paciente estudiado. Donde P1 corresponde al primer valor de aplanación y P2 al segundo dato de aplanación. Representación del cálculo de histéresis corneal (CH=P1-P2) en un paciente examinado.

1.4.2. Corneal Visualization Scheimpflug Technology

Es un tonómetro de no contacto que utiliza un pulso de aire para deformar la córnea hacia adentro y hacia afuera, pasando por dos momentos de aplanación. La principal diferencia con el ORA es que, en lugar de un sistema electroóptico de infrarrojos, utiliza una cámara ultra rápida de Scheimpflug. Realiza un barrido horizontal de 8 mm en el que captura 140 imágenes en 33 ms [89]. En la figura 13 se muestran las imágenes de la deformación producida por el pulso de aire. Otra diferencia es que la presión máxima es constante, mientras que en el ORA depende de P1. La principal medida que proporciona es la PIO correlacionada con Goldman y la PIO compensada biomecánicamente. También mide el espesor corneal. [2].

El Corvis ST mide los parámetros de deformación corneal basándose en la respuesta dinámica de la córnea. Algunos parámetros proporcionan datos precisos sobre el grado de deformación, considerando el desplazamiento máximo del ápex corneal en dirección antero-posterior durante la mayor concavidad. Otros parámetros detallan el tiempo y la velocidad de dicha deformación [46].

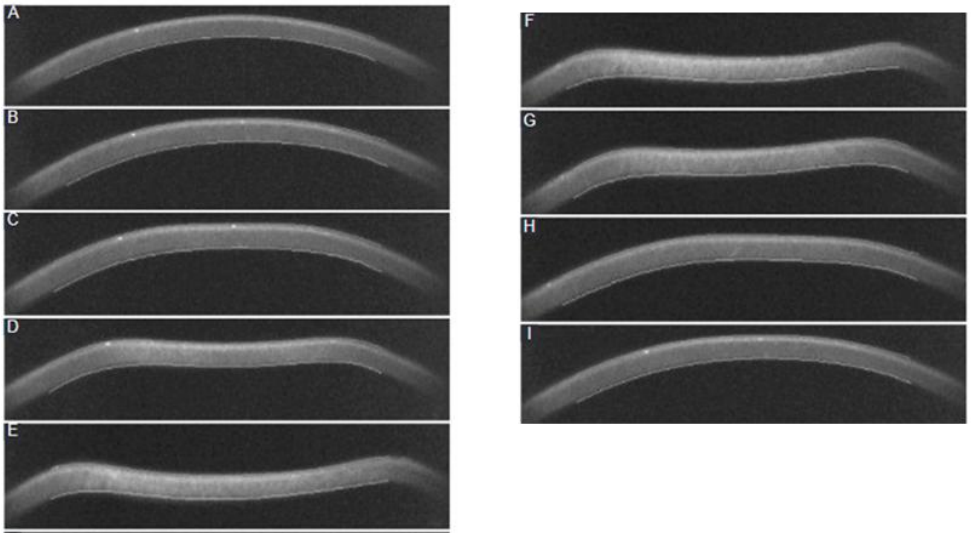

Figura 13: Imagen de Scheimpflug del Corvis ST durante el proceso de aplanación por el pulso de aire. Imagen tomada de Ramirez-Miranda et al. [2].

Los parámetros proporcionados por la ventana principal de diálogo del Corvist ST (figura 14) son los siguientes [46]:

- 1ª Aplanación: Se obtiene la velocidad y la cantidad de la primera aplanación.
- 2ªAplanación: Se obtiene la velocidad y la cantidad de la segunda aplanación.
- Concavidad más alta: El instante en que la córnea asume su máxima concavidad. Se da la distancia entre los picos, el radio de la máxima concavidad y la amplitud máxima de la deformación.
- Radio de Curvatura Normal: La córnea en su estado natural radio de curvatura.
- Radio cóncavo inverso: Inverso del radio de curvatura durante la fase cóncava.
- Espesor de la córnea: Medición del espesor de la córnea.
- PIO: Medición de la presión intraocular.
- PIOb: PIO corregida biomecánicamente.

Este instrumento no mide directamente la histéresis corneal, ni permite obtener todos los datos de presión y aplanamiento necesarios para modelizar biomecánicamente la córnea y alimentar los modelos. Por este motivo, se decidió utilizar el ORA para el desarrollo de esta tesis.

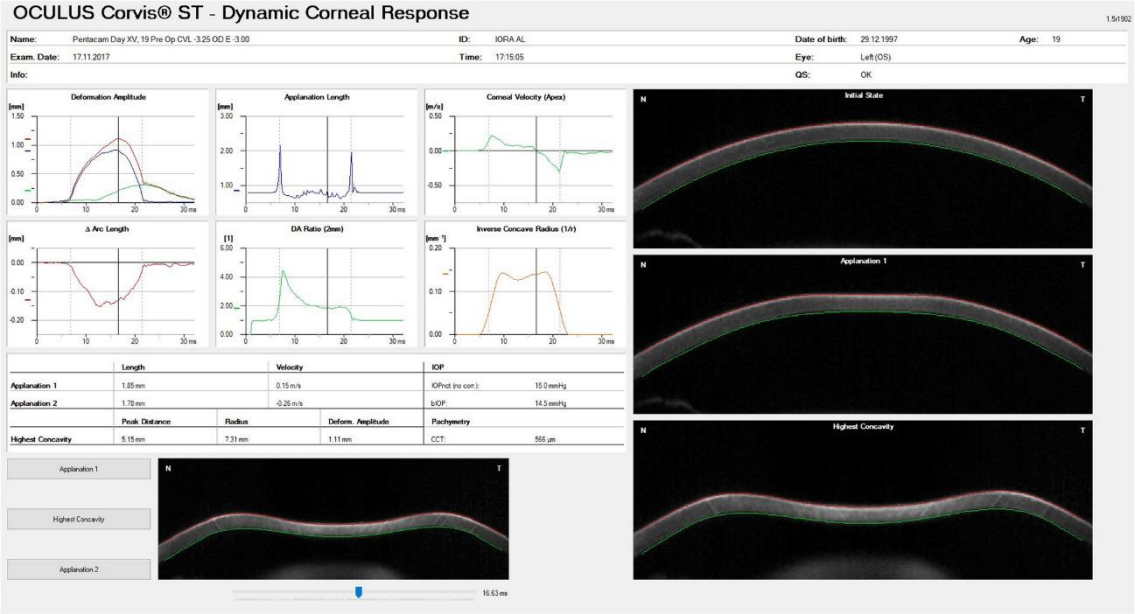

Figura 14: Parámetros estándar del Corvis ST. Imagen tomada de Esporcatte et al. [46].

1.4.3. Elastografía

La elastografía es una técnica para medir la elasticidad de los tejidos, mediante el análisis de la velocidad de las ondas transversales en estos. Dentro de las distintas modalidades de medición, se encuentra la que se combina con las técnicas de tomografía de coherencia óptica (OCT), lo que proporciona una resolución axial y lateral superior a la de la resonancia magnética. Esto hace que la elastografía de OCT sea la técnica más indicada para la estimación de la biomecánica corneal [90].

El módulo de Young está relacionado cuantitativamente con la velocidad de propagación de las ondas en el material estudiado (en los materiales más rígidos, la velocidad de propagación es mayor). La deformación de los tejidos produce ondas de cizallamiento, con propagación ortogonal a la fuerza aplicada [91]. Esta deformación se produce con un pulso breve de aire (menos de 1 ms) y de baja presión (0-60 Pa) [92]. Las ondas inducen una vibración en el tejido corneal, generando desplazamientos a escala submicroscópica. Este movimiento axial del ojo se registra mediante OCT. En resumen, el OCE utiliza un sistema para aplicar las fuerzas de estimulación y otro para observar el desplazamiento de los tejidos causado por las ondas mecánicas, lo que permite estimar las propiedades biomecánicas de la córnea.

1.4.4. Medida de la frecuencia natural de resonancia corneal.

La frecuencia natural de resonancia corneal se refiere a la frecuencia a la que debe oscilar la onda al propagarse por el tejido estudiado [90]. Se han utilizado diversas técnicas para estimular la córnea, como ondas de radio, ultrasonido, actuadores piezoeléctricos con control de vibraciones, transductores de nanopartículas magnéticas, pulsos de aire y sonido emitido por altavoces [90]. Se ha demostrado que la frecuencia natural está correlacionada linealmente con la raíz cuadrada del módulo de Young en un modelo elástico simple [90].

En 2015 Akca et al. [93] estudiaron los modos de resonancia in vitro con corneas de vaca, generando vibraciones con un altavoz y observándolas mediante OCT. Encontraron tres frecuencias de resonancia a 86 Hz, 200 Hz y 310 Hz. Los patrones vibracionales en la superficie corneal varían según la frecuencia: para 86 Hz se produce el modo fundamental de resonancia, mientras que para las otras dos frecuencias se generan oscilaciones a lo largo de la superficie (figura 15). La máxima amplitud de vibración observada fue de 8 µm a 86 Hz, para un nivel de presión sonora de 100 dB. Los autores concluyeron que la geometría y el grosor corneal, así como la edad y el módulo de rigidez, influyen en la resonancia corneal.

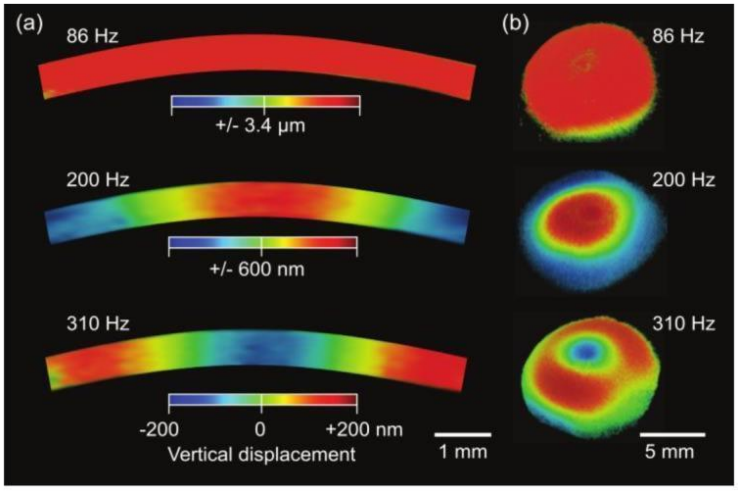

Figura 15: Modelos vibracionales experimentales de una córnea de vaca. Corte transversal**(a)** y 3D **(b)** de imágenes de vibrografía obtenidas con OCT para los distintos modos de resonancia. Imagen tomada del trabajo de Akca et al. [93].

En los últimos 5 años, se ha trabajado en la obtención de la frecuencia natural de resonancia de la córnea humana *in vivo*. Lan et al. [90,92], mediante elastografía de coherencia óptica, produjeron oscilaciones del orden de micras utilizando un pulso de aire de baja intensidad(13Pa). Encontraron un rango de frecuencias de resonancia entre 234 Hz y 277 Hz. En 2022, Crespo et al. [83] utilizaron OCT vibracional (VOCT), un método que consiste en generar la vibración de la córnea con un altavoz mediante ondas de presión sonora. Estas oscilaciones corneales fueron recogidas por un SD-OCT. Este sistema ha sido utilizado para medir in vitro la biomecánica de la piel, arterias, tendones, nervios y músculos. Testearon un rango de frecuencias entre 50 Hz y 250 Hz en pasos de 10 Hz y lograron identificar 5 picos de resonancia. El primer modo de resonancia se encontró a 73,5 ± 4,9 Hz. Si se hace una analogía con los trabajos relativos a la epidermis, se podría pensar que este modo corresponde a la componente celular de la córnea [94]. Los demás modos de vibración podrían estar relacionados con las redes de colágeno dentro del estroma [83]. Es de esperar que, debido a que la córnea tiene distintas capas e interfases, posea diferentes modos de resonancia [95].

1.5. Medidas geométricas y ópticas corneales

Los parámetros estructurales de la córnea, como el espesor, la curvatura y la geometría, influyen notablemente en la medición de su biomecánica corneal, dado que determinan cómo se distribuyen las fuerzas mecánicas a las que la córnea está sometida [29]. La córnea, como tejido viscoelástico, responde a la presión intraocular y a otras fuerzas externas de manera que su forma y rigidez pueden variar en función de su grosor y curvatura [96]. Estos factores estructurales influyen directamente en la evaluación de la respuesta biomecánica, dado que las tecnologías empleadas para su medición, como el ORA o el Corvis ST, se basan en la deformación corneal y la velocidad de recuperación ante un pulso de aire [46,85]. Por ello, la caracterización precisa de las medidas estructurales es esencial para interpretar los resultados biomecánicos y realizar evaluaciones exactas en diagnósticos y tratamientos relacionados con la salud ocular. Existen diversos dispositivos clínicos para la medición de estos parámetros, como los topógrafos, el Pentacam, OCT y el Galilei. En esta tesis se ha optado por el uso del Galilei, ya que permite medir los parámetros corneales tanto de la cara anterior como posterior de la córnea, CCT, aberraciones y, además, cuenta con un módulo de densitometría corneal (DC).

1.5.1. Galilei

El Galilei Dual Scheimpflug Analyser (Ziemer Ophthalmic Systems AG) es un sistema de no contacto diseñado para evaluar el segmento anterior del globo ocular, proporcionando información sobre las características geométricas y ópticas de la córnea. Esto se logra mediante la combinación de dos tecnologías comúnmente utilizadas en el diagnóstico oftalmológico: la topografía por discos de Plácido y las imágenes de Scheimpflug. Los discos de Placido ofrecen datos sobre la curvatura corneal, mejorando la precisión en el cálculo de la curvatura corneal anterior, mientras que la cámara de Scheimpflug proporciona información sobre la elevación [97]. Combinar ambas tecnologías nos proporciona información precisa de la curvatura, elevación, CCT y aberrometría corneales. Da información de la topografía de la cara anterior de la córnea y de la posterior. Proporciona un análisis en tres dimensiones del polo anterior, permitiendo obtener un mapa del espesor corneal. A nivel aberrométrico obtiene información acerca de la aberración óptica corneal, pero tambien es capaz de dar información de los coeficientes de Zernike por separado, lo que ayuda a entender como influyen las aberraciones de alto orden y las de bajo orden por separado. Tambien nos permite obtener la densitometría de la córnea y del cristalino [98].

En la toma de imágenes convencional, el plano del objeto, el plano de la lente y el plano de la imagen son paralelos entre sí. Las imágenes de Scheimpflug difieren de las técnicas convencionales en que el plano del objeto, el plano de la lente y el plano de la imagen se cruzan en línea recta, este hecho logra ampliar la profundidad de enfoque permitiendo obtener secciones ópticas de todo el segmento anterior del ojo [99]. El sistema Galilei usa una luz LED azul a 470 nm y mide 122.000 puntos por escaneo del segmento anterior del ojo, cubriendo 14 mm de diámetro [97]. Incluye dos cámaras de Scheimpflug rotatorias que capturan imagen de hendidura y hacen un barrido de los 0^0 a 180^0 corneales. La principal ventaja es que los datos de espesor de la córnea se promedian para compensar los errores de paralaje y movimiento, ya que en posiciones distintas del ápex corneal las cámaras subtienden distinto ángulo con el punto medido. De este modo se obtiene un valor de medición corregido en la ubicación correspondiente. El principio de imagen dual de Scheimpflug es independiente de las superficies curvas y, por lo tanto, permite una paquimetría precisa [99-101].

El módulo de densitometría de Galilei incluye una imagen tomográfica corneal de Scheimpflug, en la que se puede seleccionar manualmente el punto de estimación de la densitometría corneal y cristalina. El resultado se presenta en unidades estandarizadas de escala de grises, donde 0 representa la mínima retrodispersión de luz (máxima transparencia) y 100 representa la máxima retrodispersión de luz (mínima transparencia)[102,103]. En la figura 16 se ha seleccionado una sección horizontal de Scheimpflug, donde está marcada una ubicación posterior de la córnea para estimar la densitometría corneal en ese punto. Del mismo modo se puede obtener en cualquier estructura y meridiano su transparencia.

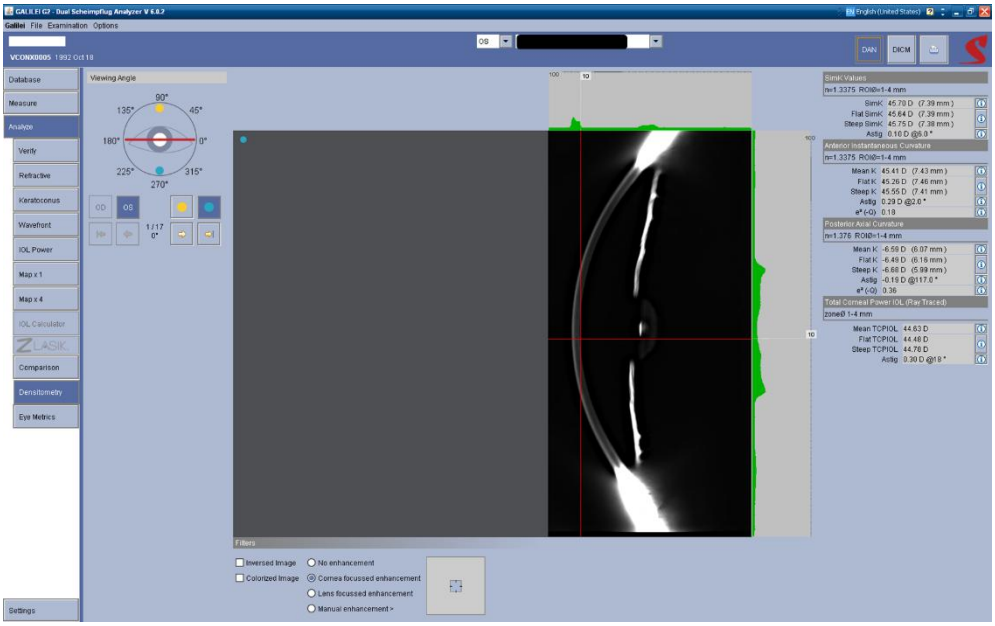

Figura 16: Módulo de estimación de DC con el instrumento Galilei G2. Imagen tomada de un paciente de esta tesis.

1.6. Motivación

La biomecánica es una rama de la biomedicina que estudia la estabilidad de los tejidos cuando se aplica una carga/presión externa. En particular, se habla de biomecánica corneal cuando se analizan los cambios dinámicos en el tejido corneal humano debido a deformaciones inducidas o a fluctuaciones de la presión intraocular [28,82]. Las propiedades biomecánicas corneales, como la elasticidad y la viscoelasticidad, pueden verse gravemente afectadas en patologías corneales degenerativas como el queratocono o en procedimientos de cirugía refractiva.

El desarrollo de la cirugía refractiva ha generado la necesidad de modificar la potencia corneal, lo cual se logra alterando su geometría y estructura mediante ablación láser [104]. Estos cambios, tanto microscópicos como macroscópicos en el estroma corneal, afectan su estabilidad y sus propiedades biomecánicas. Una de las complicaciones derivadas de la CR es la aparición de ectasias corneales, que podrían predecirse antes de la cirugía si se consideran los parámetros biomecánicos en la selección de candidatos. No obstante, en la fase pre-clínica del trastorno ectásico, los estudios topográficos y tomográficos no suelen revelar signos relevantes [51]. Por ello, es fundamental establecer nuevos criterios de selección de pacientes que permitan comprender, clasificar y tratar eficazmente las patologías ectásicas.

El queratocono es una patología ectásica en la que la red de colágeno del estroma se altera, debilitando la resistencia mecánica y provocando una protrusión corneal [105]. Esto reduce la calidad visual debido al aumento de las aberraciones óptica [106]. En particular, el KC puede generar una desestabilización biomecánica de la córnea que precede a su manifestación en la topografía [105].

Por otro lado, múltiples estudios respaldan que la principal causa fisiopatológica del glaucoma es una PIO elevada [78,107-109]. En su diagnóstico, la tonometría de Goldmann es la prueba de referencia [110] para la evaluación de la PIO. Esta técnica está estrechamente relacionada con el espesor central de la córnea [111] y con factores biomecánicos como la elasticidad, la viscosidad y la rigidez corneal [112]. Debido a esta relación, se ha planteado que alteraciones en la viscoelasticidad corneal podrían representar un factor de riesgo en el desarrollo del glaucoma [85].

A nivel optométrico, el estudio de la biomecánica corneal es relevante en el tratamiento ortoqueratológico y en la adaptación de lentes de contacto. Estas técnicas pueden modificar la geometría corneal y, en algunos casos, inducir edema corneal, lo que altera las propiedades biomecánicas de la córnea.

Por lo tanto, comprender la biomecánica corneal y su relación con los parámetros morfológicos es esencial para mejorar el diagnóstico, tratamiento y seguimiento de diversas patologías oculares, así como para optimizar procedimientos quirúrgicos, como la cirugía refractiva o tratamientos optométricos, como la ortoqueratología. A pesar de los avances en el estudio de la respuesta mecánica de la córnea, la falta de modelos viscoelásticos precisos y la ausencia de protocolos estandarizados en la práctica clínica siguen limitando la aplicación de estos conocimientos en oftalmología y optometría [2,10]. La modelización biomecánica de la córnea, junto con las nuevas herramientas de inteligencia artificial, abre la posibilidad de desarrollar simuladores innovadores que faciliten la toma de decisiones en la práctica clínica.

La presente tesis busca responder a las incertidumbres y problemáticas planteadas mediante el desarrollo de un nuevo modelo biomecánico para el análisis *in vivo* de la biomecánica corneal, así como el desarrollo de nuevos métodos de tonometría basados en resonancia por sonidos de baja frecuencia, con el objetivo de generar nuevo conocimiento en el campo de la biomecánica corneal.

Los estudios realizados durante el desarrollo de esta Tesis Doctoral se han llevado a cabo en el grupo de investigación TOL (*Tecnologías Ópticas Láser*) de la Universidad de Zaragoza. Este grupo pertenece al Instituto Universitario de Investigación en Ingeniería de Aragón (I3A) y forma parte de la división de Ingeniería Biomédica y Tecnologías de la Información y la Comunicación. Su actividad investigadora abarca diversas líneas dentro del campo de la óptica, con aplicaciones en metrología, medicina y comunicaciones. En la actualidad, el grupo TOL es un referente en investigación, reconocido por el Gobierno de Aragón durante los periodos 2020-2022 (E44_20R) y 2023-2025 (E44_23R).

1.7. Objetivos

Los objetivos generales de esta Tesis son dos:

1. Desarrollo de un modelo visco-elástico para el estudio de la biomecánica corneal.
2. Desarrollo de un nuevo método de tonometría ocular basado en resonancia corneal mediante sonido.

Para ello, se han definido cinco objetivos específicos:

1. Caracterización de propiedades estructurales macroscópicas, ópticas y biomecánicas en sujetos jóvenes y sanos.

2. Estudio de la influencia del uso de lentes de contacto de hidrogel de silicona durante dos periodos cortos de tiempo en la biomecánica corneal.
3. Desarrollo del modelo del estado sólido lineal para la obtención de las componentes elástica y viscosa *in vivo* mediante medidas experimentales de tonometría por aplanación con aire.
4. Propuesta de un nuevo biomarcador para la enfermedad hipertensiva ocular, basado en el tiempo de retardo corneal.
5. Desarrollo de un resonador de sonido de baja frecuencia como nuevo método de tonometría corneal. Para ello se llevaron a cabo los siguientes subobjetivos:

   5.2 Calibrado y testeo del resonador en estudio piloto para diferentes frecuencias de sonido.

   5.3 Caracterización de diferentes modos de resonancia corneal considerando aspectos geométricos, biomecánicos y aberrométricos.

1.8. Justificación de la temática

La falta de estandarización y protocolización de los parámetros biomecánicos puede conducir a un uso inadecuado de estos, lo que implica un desaprovechamiento de los recursos. Por ello, es fundamental adaptar la información para hacerla más comprensible y facilitar su interpretación clínica.

Con el enfoque expuesto a continuación, se ha logrado mejorar la comprensión de cómo se modifican los parámetros biomecánicos en función de las condiciones a las que está sometida la córnea. Esto ha permitido un mejor entendimiento de los factores y condiciones que influyen en dichos cambios, además de la propuesta de nuevos conceptos para profundizar en el conocimiento del estado biomecánico natural de la córnea y su comportamiento en patologías como la enfermedad hipertensiva ocular. Como resultado, se han desarrollado nuevas herramientas en el campo de la oftalmología para mejorar el diagnóstico, el tratamiento de patologías y la toma de decisiones tanto en cirugías refractivas como en su seguimiento postquirúrgico.

Durante el desarrollo de esta tesis, se han llevado a cabo diversas acciones de investigación y experimentación alineadas con los objetivos planteados. A continuación, se presentan las acciones realizadas para alcanzar los objetivos de la Tesis.

Objetivo 1: Para relacionar la estructura corneal con las propiedades biomecánicas y ópticas del ojo, se planteó un primer estudio en el que se determinó el índice de transparencia óptica, así como los parámetros biomecánicos y geométricos de la córnea. A partir de estos datos, se obtuvieron expresiones analíticas para modelizar la relación de los parámetros macroscópicos y biomecánicos de la córnea. Este trabajo se basa en el conocimiento de que la organización del estroma, con su patrón tridimensional de las fibras de colágeno, mantiene la córnea transparente y proporciona estabilidad estructural influyendo tanto en la geometría como en las propiedades biomecánicas [20]. Además, se investiga si el astigmatismo corneal influye de manera directa en los valores biomecánicos obtenidos con tonómetros de aire, encontrando la necesidad de implementar una compensación de los valores obtenidos para evitar la subestimación de los parámetros biomecánicos.

Objetivo 2: Para relacionar el uso de lentes de contacto (LCs) de hidrogel de silicona con la biomecánica corneal, se diseñó un protocolo con dos grupos de estudio, los cuales utilizaron LCs durante dos periodos de tiempo distintos (10 días y 20 días). Los sujetos fueron analizados mediante un tonómetro de aplanación por aire, específicamente con el Ocular Response Analyzer (ORA, Reichtert Instruments, Depew, NY, USA) y mediante imagen corneal de Scheimpflug para monitorizar los cambios producidos tanto en las propiedades biomecánicas como geométricas de la córnea.

Objetivo 3: Este objetivo tiene como finalidad la búsqueda de nuevos parámetros de diagnóstico para la enfermedad hipertensiva ocular, para ello se propone el desarrollo del modelo teórico viscoelástico corneal basado en el Modelo del Estado Sólido Lineal, y la definición del concepto de retardo corneal (τ). Una vez definido teóricamente el concepto, se ha buscado obtener su valor de forma empírica. Para ello, se recopilaron los datos de aplanación corneal de 200 pacientes utilizando el ORA.

Objetivo 4: Las medidas biomecánicas tradicionales proporcionan una medida de la viscoelasticidad, es decir, una evaluación conjunta de las componentes viscosa y elástica. Este objetivo parte de la necesidad de comprender en qué medida contribuyen por separado la componente viscosa y elástica a la biomecánica general. Para ello, se propone una metodología basada en la alimentación del modelo del estado sólido lineal mediante mediciones experimentales de tonometría corneal de aplanación por aire, con el fin de determinar las componentes elástica y viscosa. Este objetivo supone un hito, ya que es la primera vez que se obtienen de forma separada las componentes viscosa y elástica de la córnea *in vivo*. Otros trabajos han medido el módulo de elasticidad corneal por elastografía[90,92] u OCT vibracional [83], pero no el de viscosidad.

Objetivo 5: Hasta la fecha, los instrumentos utilizados en la práctica clínica generan una deformación de la córnea mediante un pulso de aire. Estas medidas se realizan en una zona central y dependen fuertemente de factores como el espesor corneal o su geometría, lo que puede sobreestimar (o infraestimar) de manera significativa la medida de la presión intraocular o las propiedades viscoelásticas de la córnea. Este objetivo surge de la necesidad de obtener un método de deformación corneal que afecte al tejido completo y

que, además, responda a sus propiedades ópticas, biomecánicas y geométricas. Para ello, se diseñó un generador de ondas de sonido de baja frecuencia para aplicación corneal, basado en las propiedades de resonancia natural de la córnea. Se llevó a cabo un estudio piloto en sujetos sanos y jóvenes, analizando la respuesta biomecánica y geométrica corneal para diferentes frecuencias vibracionales aplicadas. El objetivo es identificar las frecuencias que inducen los distintos modos de resonancia. Este estudio constituye el primer paso para la caracterización de los modos de resonancia corneal de la córnea humana *in vivo*, utilizando una nueva técnica totalmente no invasiva.

En la Tabla 2 se presenta una relación de los objetivos planteados para esta tesis y los artículos correspondientes, de los seis expuestos, en los que se ha dado justificación a cada uno de ellos.

Tabla 2: Resumen de los objetivos presentados en la Tesis y los artículos en los que se han llevado a cabo.

Objetivos	Artículo 2.1 https://doi.org/10.3390/jimaging7120280	Artículo 2.2 https://doi.org/10.1007/s10792-022-02270-0	Artículo 2.3 https://doi.org/10.1088/2057-1976/ad12fa	Artículo 2.4 https://doi.org/10.3390/opt4040043	Artículo 2.5 https://doi.org/10.3390/photonics11060524	Artículo 2.6 https://doi.org/10.3390/opt6010005
1	X	X	X	X	X	X
2		X				
3			X		X	
4			X	X	X	X
5				X		X
5.1				X		
5.2				X		X

2. PUBLICACIONES

La presente tesis se ha desarrollado en formato de compendio de publicaciones, concretamente, a partir de seis trabajos científicos publicados que se detallan a continuación:

2.1. On the relationship between corneal biomechanics, macrostructure, and optical properties

Ávila FJ, Marcellán MC, Remón L. On the Relationship between Corneal Biomechanics, Macrostructure, and Optical Properties. *J Imaging*. 2021;7(12):280. https://doi.org/10.3390/jimaging7120280

JCI (2021): 0,56-Imaging science & photographic technology-17/31-Q3

Journal of *Imaging*

MDPI

Article

On the Relationship between Corneal Biomechanics, Macrostructure, and Optical Properties

Francisco J. Ávila *, Maria Concepción Marcellán and Laura Remón

Departamento de Física Aplicada, Universidad de Zaragoza, 50009 Zaragoza, Spain; mcvidosa@unizar.es (M.C.M.); lauremar@unizar.es (L.R.)
* Correspondence: avila@unizar.es

Abstract: Optical properties of the cornea are responsible for correct vision; the ultrastructure allows optical transparency, and the biomechanical properties govern the shape, elasticity, or stiffness of the cornea, affecting ocular integrity and intraocular pressure. Therefore, the optical aberrations, corneal transparency, structure, and biomechanics play a fundamental role in the optical quality of human vision, ocular health, and refractive surgery outcomes. However, the inter-relationships of those properties are not yet reported at a macroscopic scale within the hierarchical structure of the cornea. This work explores the relationships between the biomechanics, structure, and optical properties (corneal aberrations and optical density) at a macro-structural level of the cornea through dual Placido–Scheimpflug imaging and air-puff tonometry systems in a healthy young adult population. Results showed correlation between optical transparency, corneal macrostructure, and biomechanics, whereas corneal aberrations and in particular spherical terms remained independent. A compensation mechanism for the spherical aberration is proposed through corneal shape and biomechanics.

Keywords: corneal biomechanics; corneal structure; corneal aberrations; optical density; Scheimpflug imaging; ocular response analyzer

Citation: Ávila, F.J.; Marcellán, M.C.; Remón, L. On the Relationship between Corneal Biomechanics, Macrostructure, and Optical Properties. *J. Imaging* **2021**, *7*, 280. https://doi.org/10.3390/jimaging7120280

Academic Editors: Constantino Carlos Reyes-Aldasoro and Alois Herkommer

Received: 27 October 2021
Accepted: 16 December 2021
Published: 18 December 2021

1. Introduction

Corneal biomechanics is a branch of biomedical sciences that deals with the analysis of the stability of the tissue when an external load or pressure is applied [1,2] or when the intraocular pressure fluctuates. The biomechanical properties of the cornea are responsible for its shape and integrity, acting as a unique convergence point between balanced ductility to preserve aspherical geometry (and correct ocular refraction), stiffness to compensate the intraocular pressure, and an ultrastructure that allows optical transparency. Biomechanical properties of the cornea can be affected by systemic diseases such as diabetes [3,4] or sclerosis [5,6]. In particular, corneal keratoconus may compromise the biomechanical stability, modifying the microstructure [7], weakening mechanical strength [8] and leading to corneal protrusion [9,10], inducing optical aberrations [11,12] that reduce the quality of vision or lead to transplants in advanced stages. The clinical relevance of the study of corneal biomechanics reached special interest with the development of refractive surgery techniques to modify the optical power of the cornea by laser ablation [13] or lenticular extraction [14]. These techniques consist of modifying the lamellar structure of cornea, causing a redistribution of mechanical stress. The biomechanical response is expected to provide the correct corneal curvature [15], and together with optical transparency, normal vision.

On the other hand, corneal transparency has been explained from the hierarchical structure of the cornea. At the molecular scale, X-ray scattering revealed how the collagen ultrastructure within the stroma is responsible for the tridimensional microstructure and consequently for the macroscopic geometry and biomechanics [16].

To date, the maximum spatial resolution of structural hierarchy achieved in living human eyes has been the microscopic scale using two-photon scanning microscopy [17].

However, only confocal microscopes are currently clinically available, and although they allow visualization of the cellular matrix, they are invisible for the stromal architecture [18]. In this sense, Scheimpflug imaging provides excellent tomographic measurements of the macrostructure of the cornea as well as optical density (transparency) [19], which is widely reported in anterior segment analysis for the assessment of normal and keratoconus or ectatic corneas [20] or refractive surgery [21]. Corneal biomechanics is usually assessed employing air-puff tonometry [22]; also, the combination of Scheimpflug imaging and air-puff tonometry has been successfully integrated, bringing excellent results in dynamic assessment of corneal biomechanics [23].

As stated, the molecular organization of the corneal stroma controls the optical transparency, macroscopic shape, and structural stability (biomechanics) [16]. In this work, we will investigate if the relationship between corneal transparency and optical properties, geometry, and biomechanics is preserved at the macroscopic level of the hierarchical structure.

The biomechanical properties, corneal geometry, and optical properties and densitometry measurements were collected from 102 eyes of 51 young-adult healthy subjects using Scheimpflug imaging and air-puff tonometry.

This work focuses on the inter-relationships of corneal biomechanics, optical, and structural properties to bring a comprehensive macroscale characterization of the cornea that can also provide future predictive models of corneal biomechanics.

2. Materials and Methods

2.1. Participants

This research was reviewed by an independent Ethical Committee of Research of the Health Sciences Institute of Aragon (Spain) approved with reference: C.P.-C.I.PI20/377 (approval date: 14 July 2020). Measurements procedure and data collection were carried out according to the tenets of the Declaration of Helsinki. All participants were informed about the nature, risks, and possible adverse consequences of the study and signed an informed consent document. The ethnicity of the participants involved in this study was European Caucasian, all of them students from the School of Optics and Optometry of the University of Zaragoza (Spain). A total of 102 eyes from 51 healthy young subjects (mean age 24 $\pm$ 5) were analyzed using dual Placido–Scheimpflug imaging and air-puff tonometry systems. None of them presented ocular pathologies, corneal disorders, or abnormal intraocular pressure. Exclusion criteria included contact lens wearers due to the influence of contact lens wear in corneal optical density, thickness, and spherical aberration [24].

2.2. Experimental Measurements

Clinical measurements were carried out at the laboratory of Optometry of the Department of Applied Physics of the University of Zaragoza and conducted by an experienced clinical optometrist. Both eyes of all participants were analyzed in a sequential procedure: First, optical and geometrical properties (see Table 1) were acquired by a dual Scheimpflug–Placido disk imaging system, and next, corneal biomechanics was assessed using an air-puff tonometer device.

2.2.1. Dual Placido–Scheimpflug Imaging: Structural and Optical Parameters

The Galilei Dual Scheimpflug Analyzer (Ziemer Ophthalmic Systems AG, Port, Switzerland) is a clinical optical system that combines Placido Disk imaging and a revolving Scheimpflug camera providing simultaneous acquisition of corneal topography based on the internal and external surfaces including eccentricity, astigmatism, pachymetry (measures of central middle and peripheral cornea), three-dimensional analysis of the cornea, power measures, wavefront aberration, and optical densitometry [25]. Figure 1 shows an example of wavefront aberration mapping and anterior segment Scheimpflug image from a participant of our study. Table 1 summarizes those Galilei outputs selected for data analysis.

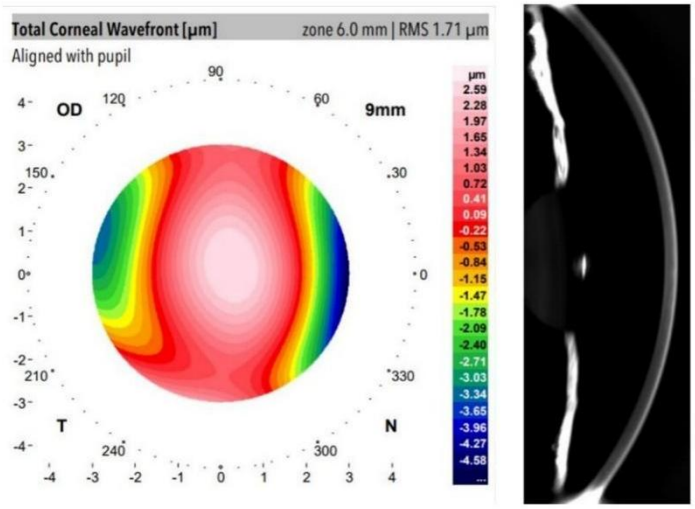

Figure 1. Total corneal wavefront aberration map (**left**) and anterior segment Scheimpflug image (**right**) from a volunteer of the study.

Table 1. Structural and optical parameters from the Galilei system considered of interest in our study. The total and spherical aberration wavefront were numerically evaluated by its root mean square (RMS) value.

Structural Parameters	Optical Parameters
Central Thickness Middle Thickness Peripheral Thickness	Total Aberration RMS Spherical Aberration RMS
Anterior Eccentricity Posterior Eccentricity Total Corneal Astigmatism	Optical Density

Optical Transparency Index Calculation

A Galilei device provides the degree of corneal and crystalline lens opacity by computing the relationship between the intensity of the illumination light and back-reflected rays expressed in standarized gray-scale units. It provides macroscopic visualization of the whole anterior segment of the eye by capturing full-angle imaging by rotating the Scheimpflug camera.

Scheimpflug imaging technology visualization is limited through strong scattering or opaque tissues such as the sclera, which is totally opaque due to irregular arrangement of collagen fibrils [16]. Nevertheless, toward the periphery of the iridocorneal angle in Scheimpflug images, a reference gray level from the sclera can be obtained from the Galilei outputs. In this work, the Optical Transparency Index (OTI) is defined and computed as:

$$\mathrm{OTI} = 100 \times \left[\frac{1}{OD_{Slcera}} (OD_{Sclera} - OD_{Cornea}) \right]. \quad (1)$$

The OD of the cornea and sclera (OD_{Cornea} and OD_{Sclera}) was the average of OD values acquired at the same lateral location corresponding to 4 rotational images acquired at 0°, 45°, 90°, and 135° meridians. Regarding OD_{Cornea}, the lateral location was the optical axis reference, and the final OD value of each individual frame (i.e., corresponding to a given oriented meridian) was the average of the anterior, central, and posterior axial depths of

the cornea. Figure 2 shows an example of an OD measurement at the posterior corneal location at a horizontal viewing angle.

OTI index ranges between 0 (total opacity) and 100 (absence of back-scattering light). The maximum value implies total corneal transmittance for the illumination wavelength underlying the understanding of corneal transparency.

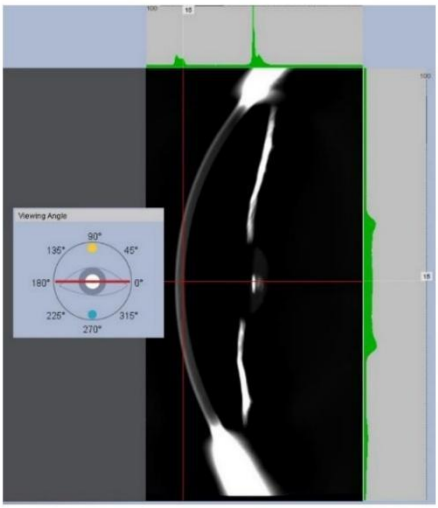

Figure 2. Optical density measurement at the posterior corneal location and horizontal viewing of the Scheimpflug camera.

2.2.2. Corneal Biomechanics Assessment

An Ocular Response Analyzer (ORA, Reichert Instruments, Depew, NY, USA) was employed to obtain measurements of corneal biomechanics. ORA is a non-invasive device based on air-puff applanation tonometry that measures intraocular pressure and corneal biomechanics, in particular corneal hysteresis (CH) and corneal resistance factor (CRF) parameters. Briefly, the corneal hysteresis can be defined as the energy dissipation when an external stress is applied, resulting in a time-dependent stain unlike purely elastic materials, which immediately recover their initial state once the stress stops. Whereas CH is a measurement of the viscoelasticity of the cornea, CRF is a measurement of the resistance (i.e., rigidity and/or elasticity) strongly associated to corneal thickness and then an indicator of the corneal pure elastic properties [26]. CRF and CH are related, but they do not describe the same biomechanical properties of the cornea.

CRF and CH are computed by quantifying the differential inward and outward corneal responses to an air pulse (see Figure 3) of approximately 24 milliseconds [27]. Once the first applanation is reached, the air pressure causes the cornea to move inward to a slight concavity and then back to a second applanation before recovering the natural shape.

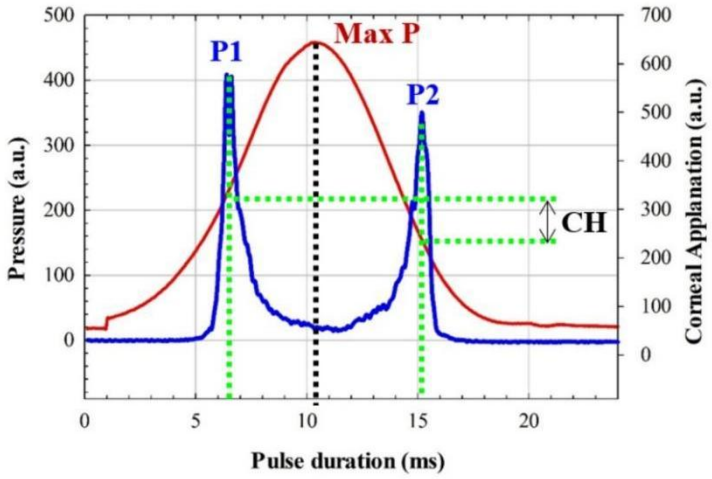

Figure 3. ORA measurement from a participant in our study. P1, P2, Max P, and CH correspond to the first and second applanation, maximum pressure, and corneal hysteresis, respectively.

Figure 3 shows an ORA measure from a participant of our study. From pressures P1 and P2 (corresponding to the first and second applanation pressures, respectively), CH and CRF are calculated as [28]:

$$CH = P1 - P2. \quad (2)$$

$$CRF = (P1 - 0.70 \times P2) - 3.08. \quad (3)$$

From an elastodynamic point of view, the first applanation is given when the air pulse compensates for the intraocular and atmospheric pressures. The stress–strain response of the cornea undergoes elastic deformation, whereas the second applanation pressure is affected by energy dissipation; that is, P1 can be related to the pure elastic properties of the cornea, whereas P2 is used for viscoelasticity estimation. For instance, a pure elastic cornea will provide a null CH value and symmetrical pressure curve (see Figure 3) during an ORA measurement, which implies an applanation pressures equalization condition, P1 = P2. In that sense, a stiffness parameter has been reported as the ratio between the resultant pressure at the first applanation and the deflection amplitude [29]. In this study, Equations (1) and (2) were employed to calculate P1 and P2 from ORA outputs (CRF and CH).

2.2.3. Data Analysis

Dataset Clustering

Data segmentation is usually applied for dimensionality reduction. In this work, OTI calculations computed from OD measurements made by the Galilei analyzer were found to be discrete values ranging from 78.5 to 81.5 (0.5 step size) for all subjects involved in this study. Table 2 shows the number of subjects (N) that presented a representative OTI value within the range found experimentally, those data are normally distributed (Shapiro–Wilk test), which motivated data clustering for graphical representation and data analysis. Each cluster contains the information of the mean values of each corneal parameter and its standard deviation. In that sense, graphical representation and statistical analysis have been performed on clustered data.

Table 2. Clustering of the OTI values as a function of the number of subjects (N).

OTI	N	Cluster
78.5	14	1
79.0	9	2
79.5	22	3
80.0	16	4
80.5	15	5
81.0	12	6
81.5	8	7

Figure 4 shows the standard deviation of the computed OTI value as a function of the number of subject per discrete OTI value, all of the values were below 1% of error. Therefore, any significant variability in the variance of the clusters will be due to that corneal parameter to be correlated. In that sense, data clustering provides separate visualization of the entire dataset as a function of the meaningful features.

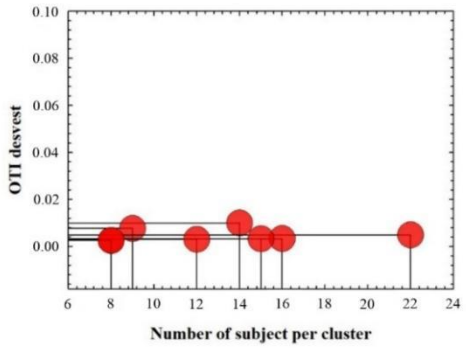

Figure 4. Standard deviation of OTI values as a function of the number of subjects per cluster.

Collected data were stored into an Excel spreadsheet and then migrated to Origin Lab software (Origin Lab Corp., Northampton, MA, USA) for graphical representations and statistical analysis.

Statistical analysis consisted of Spearman Rank Order Correlation and linear regression analysis in order to establish or discard significant relationships between geometrical and optical parameters. The Shapiro–Wilk test was used to test the normality and make valid the inferences of linear regression analysis (power of performed tests = 0.995 with alpha = 0.05). The significance of the linear regression models was also indicated by the F-test. Limits of agreement were used to quantify the agreement between those parameters in graphical representations. Statistics was performed using the advanced statistical tool of Origin Lab software.

3. Results

This section shows results of our study that are structured in the analysis of the relationship between optical density of the cornea and three main factors: optical aberrations, biomechanics, and macroscopic geometry of the cornea.

3.1. Optical Density and Corneal Aberrations

Figure 1 showed an example of the total aberration wavefont map and the corresponding Scheimpflug image from a participant measured with a dual Galilei imaging system. Total and spherical aberration RMS and OTI average values (mean of 102 eyes measurements) are shown in Table 3. Since spherical aberration is the dominant high-order term at the cornea [30], it was evaluated apart from the total aberration RMS values. The

statistical analysis (Spearman correlation) revealed no correlation between optical aberrations (neither total nor spherical term) and OTI values of the cornea. Whereas aberrations govern the correct focus of light and retinal image quality [31], it seems to be unrelated to the transparency of the cornea.

Table 3. Optical transparency index (OTI); Total aberration RMS (TA RMS); Spherical aberration RMS (SA RMS); and Spearman correlation analysis for the data collected from all participants of the study (* $p < 0.05$); ** $p < 0.005$).

OTI	TA RMS * (μm)	SA RMS ** (μm)	Spearman's *	Spearman's **
80.0 ± 0.9	1.45 ± 0.28	−0.15 ± 0.05	Failed, $p = 0.38$.	Failed, $p = 0.26$.

3.2. Optical Density and Corneal Macro-Structure

The cornea and sclera are composed mainly of type-I fibrillar collagen whose structural organization at the molecular scale is responsible for optical transparency. Due to the hierarchical structure of the cornea [32], the macroscopic structure is a consequence of the microscopic arrangement. This section investigates if the macroscopic structure of the cornea plays a role in the optical density or it disappears as a corneal transparency factor within the hierarachical organization. The total corneal astigmatism, anterior and posterior eccentricity, central, middle and peripheral thickness were measured and compared with the OTI index for all subjects.

Table 4 shows the mean values of thickness, corneal astigmatism, and eccentricity computed from the 102 measured eyes. The statistical analysis revealed that the corneal thickness and optical density are not related in young healthy subjects; however, both total corneal astigmatism and posterior eccentricity (i.e., the inner surface of the cornea) showed strong correlation with OTI parameters. These results imply that in the absence of pathological or physiological (aging) scattering contributions at the cornea, its optical transparency is related to the shape regardless of the thickness. Figure 5 shows the graphical representation of the cluster sampled OTI values as a function of total corneal astigmatism (Figure 5a) and posterior eccentricity (Figure 5b). The statistical analysis revealed positive correlation (Spearman, $R^2 = 0.87$) between OTI and total corneal astigmatism (TCA), the regression analysis (overall F-test $p = 0.003$) confirmed that OTI and TCA are related.

Regarding the posterior eccentricity (PE) of the cornea, Figure 5b shows negative correlation (Spearman, $R^2 = 0.94$) between OTI and PE; the results of the linear regression analysis provided the significant relationship (overall F-test $p = 0.003$). However, OTI and anterior eccentricity were found to be independent corneal parameters (see Table 3).

Table 4. Mean values of geometrical parameters and correlation results with OTI index.

Structural Parameter	Location	Mean Value	Spearman's
Corneal Thickness	Central	554 ± 30 μm	Failed, $p = 0.58$.
	Middle	601 ± 30 μm	Failed, $p = 0.42$.
	Peripheral	674 ± 69 μm	Failed, $p = 0.29$.
Corneal Astigmatism	Global	0.87 ± 0.34 Dpt.	$R^2 = 0.87$
Anterior Eccentricity	Global	0.24 ± 0.16	Failed, $p = 0.39$
Posterior Eccentricity	Global	0.42 ± 0.12	$R^2 = 0.94$

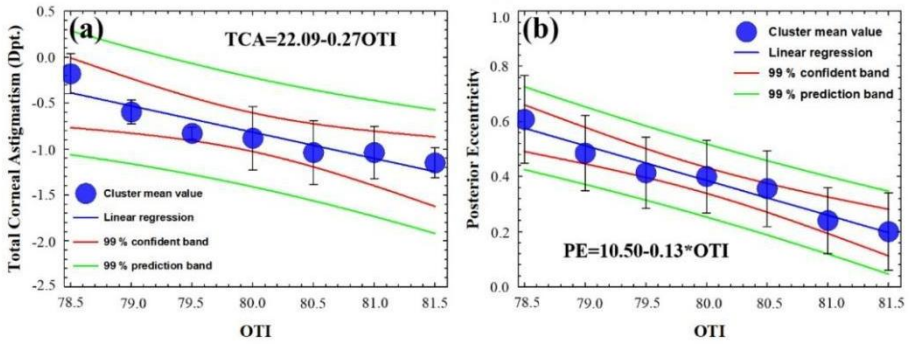

Figure 5. Mean clustered OTI values as function of total corneal astigmatism (TCA) (**a**) and posterior eccentricity (PE) (**b**) for all subjects. Standard deviation of the clustered data, equations, confident, and prediction bands of the regression analysis are included.

3.3. Optical Density and Corneal Biomechanics

This subsection investigates the impact of biomechanics on corneal transparency. Figure 6 shows a biomechanical image that represents the dynamic stress–strain response of the cornea during an air-puff applanation measurement at ORA device. The maximum deformation occurs at approximately 10 milliseconds. It can be observed how the distribution of the pressure curve is not symmetric but lopsided; this skewness is due to the viscoelastic nature of the cornea, while symmetric distributions correspond to corneas characterized by purely elastic biomechanical properties.

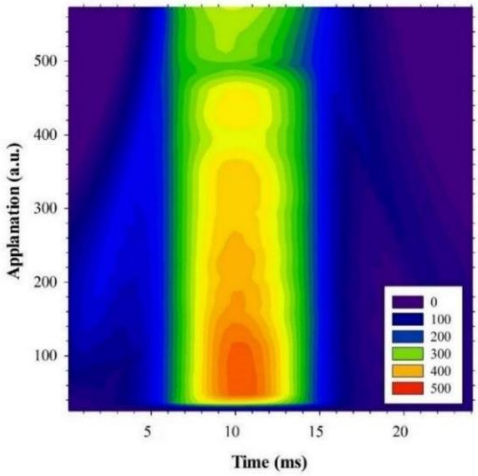

Figure 6. Dynamical representation of corneal applanation as a function of time from a volunteer of the study. Air pulse pressure is scaled in arbitrary units and shown in the bottom right corner legend.

As described in the Methods section, the ORA device provides CH and CRF biomechanical parameters. From them, we derived the applanation pressures P1 and P2, which are related to the pure elastic (P1) and viscoelastic (P2) properties of the cornea. Figure 7 shows the graphical representation of the clustered sampling OTI values as a function of P1 (Figure 7a) and P2 (Figure 7b). The statistical analysis revealed significant (negative) correlations of OTI with P1 and P2 ($R^2 = 0.96$ and $R^2 = 0.95$, respectively). The error bars that correspond to the standard deviation of the cluster mean value are within the prediction bands of the regression analysis (overall F-tests $p = 0.001$ and $p = 0.003$, respectively).

The statistical relationship between P1 and P2 with OTI proves that the optical density of the cornea is related to both elastic and viscosity properties from a macroscopic approach.

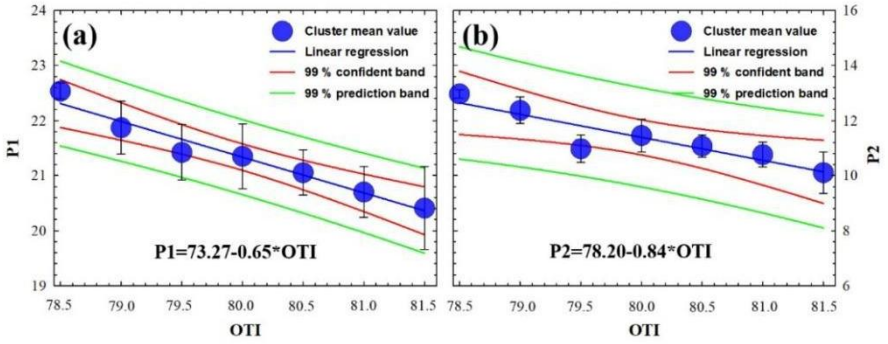

Figure 7. Mean clustered OTI values as function of first (**a**) and second applanation pressures (**b**) at the ORA device for all subjects. Standard deviation of the clustered data, equations, confidence, and prediction bands of the regression analysis are included.

3.4. Experimental Expression to Predict the Human Corneal Transparency through Macroscopic Parameters

The results above described deal with the separated investigation of the relationship between optical density and corneal parameters that describe the optical, biomechanical, and macro-structural properties of the cornea. In this last subsection, the presence (or lack of) relationships between those characterization parameters are investigated.

Regarding the macro-structural approach, Figure 8a shows a regression plot of PE versus TCA cluster mean values. The statistical results ($R^2 = 0.88$, $p = 0.0028$) revealed that as the total corneal astigmatism decreases, the posterior eccentricity significantly increases.

In this sense, it is obvious that the more direct the influence of the macro-structural shape on cornel aberrometry measurements, the less evident the relationship found between biomechanics and corneal aberrations. However, our findings did not show any statistical relationship in either total or spherical aberration (which is the dominant high-order term in the cornea) with respect to corneal biomechanics in young healthy subjects.

In that sense, corneal astigmatism is one of the low-order aberration terms that plays a fundamental role in ocular refraction; however, in terms of wave-front distortion, it does not increase the total RMS enough to show the dependence of total corneal aberrations with OTI or corneal biomechanics. However, understanding total corneal astigmatism as a measure of corneal asymmetry (structural parameter), Figure 8b shows the linear regression plot of applanation pressures (i.e., P1 and P2) versus total corneal astigmatism. The regression analysis revealed a strong dependence of the required pressures at ORA for first ($R^2 = 0.94$, $p = 0.001$) and second (($R^2 = 0.89$, $p = 0.002$) applanations as the corneal astigmatism increases; that is, the higher the corneal asymmetry (measured by astigmatism), the lower the required air pressure to flatten the cornea. It is worth highlighting that the higher correlation value corresponds to the first applanation pressure, which is related to pure elastic properties unlike P2, which is related to viscous properties.

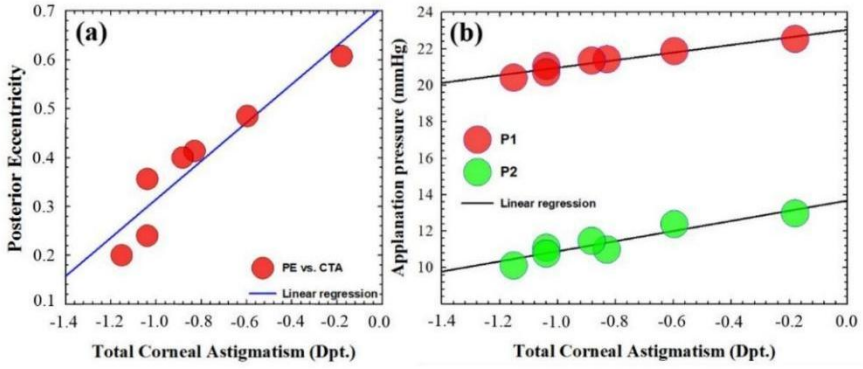

Figure 8. Mean clustered posterior eccentricity versus total corneal astigmatism values (**a**) and mean clustered applanation pressures at ORA versus total corneal astigmatism values (**b**). Linear regression fits are included.

Finally, multiple regression analysis revealed that corneal transparency can be modeled from those macroscopic parameters that showed significant correlation. OTI parameter can be predicted from a linear combination (significant dependence) of the following variables: P1($p = 0.13$), P2 ($p = 0.22$), TCA ($p = 0.15$), and PE ($p = 0.021$) (analysis of the variance of the multiple linear regression, $p = 0.018$) as:

$$\text{OTI} = 236{,}895 - [(7.817 \times \text{P1}) + (0.561 \times \text{P2}) + (4.458 \times \text{TCA}) + (18.497 \times \text{PE})]. \quad (4)$$

4. Discussion and Conclusions

Whereas the role of the corneal ultrastructure in the three-dimensional architecture at microscale, corneal transparency, and mechanical stability is well understood [16], the inter-relationships of those properties at the macroscale within the hierarchical corneal structure has not been investigated.

Considering that most of the medical devices for corneal analysis offer macro-structural resolution and information, in this study, we explore the relationship between the biomechanics, shape, and optical properties of the cornea in healthy young subjects. We analyzed wavefront aberration, optical density, geometrical parameters (thickness, eccentricity, and total corneal astigmatism) and corneal biomechanics using dual Placido–Scheimpflug analyzer and air-puff applanation tonometry systems, respectively.

Corneal aberrations and, in particular the spherical term, seem to have a compensation mechanism to keep stable the retinal image quality in the presence of intraocular scattering [31]; also, in traumatic injuries, corneal opacity appears together with high-order aberrations [33]. In particular, the decrease in optical density and corneal spherical aberration is correlated in contact lens wearers due to corneal swelling [24].

Although corneal astigmatism is one of the most representative low-order aberrations, in our work, we employed the total corneal astigmatism as a measure of the asymmetry in corneal shape (macro-structure parameter) instead of a wavefront distortion, since the contribution of astigmatism aberration term to the total aberration RMS was not enough to establish a relationship between corneal aberrations and OTI.

Regarding structural aspects, the corneal thickness and optical density change in dry eye syndrome, diabetes, and glaucoma [34] are correlated in edema processes such as corneal swelling associated with contact lens wear [24]. However, our findings showed that corneal thickness does not affect the optical transparency in healthy young subjects.

In addition, corneal surface irregularities are associated not only to optical aberrations but also to light scattering [35]. In that sense, our study also included as macro-structural parameters total corneal astigmatism and anterior and posterior eccentricities. As shown in the Results section, the higher the OTI value, the higher the corneal astigmatism and the lower the posterior eccentricity of the cornea. It is worth mentioning that only posterior

corneal eccentricity depends on corneal astigmatism [36], and as shown in the Results section, the total corneal astigmatism and posterior corneal eccentricity were negatively correlated ($R^2 = 0.88$, $p = 0.028$), which implies that the optical transparency and corneal macrostructure are related by means of the relative shape of the cornea independently of the thickness.

Focusing at the molecular scale, the structure of Type-I corneal collagen is responsible for the optical transparency and three-dimensional arrangement of the stroma [16]. The three-dimensional arrangement of the cornea determines its shape (geometry) and biomechanics [37]. Changes in corneal structure associated to aging or disease factors alter corneal biomechanics [38]. Thus, in our work, we also explored if biomechanics and corneal transparency are actually related at the macroscopic level of study. Results showed (see Figure 6) that both elastic- (P1) and viscoelastic-related parameters (P2) are strongly correlated with OTI; the viscoelastic parameter is more weakly correlated, which implies the dominance of the elastic property in corneal transparency.

Finally, a statistical relationship between biomechanics and corneal geometry (measured by total astigmatism) was found. That is, the corneal astigmatism, elastic, and viscoelastic properties of the cornea are related. It is worth mentioning that the dynamic corneal response depends not only on intrinsic biomechanical properties but also on intraocular pressure and corneal geometry [39]. In that sense, the ORA device provides corrected biomechanical measurements from intraocular pressure and central corneal thickness [23] but does not consider corneal astigmatism as a geometrical parameter affecting biomechanical assessment.

The relationship between corneal aberrations (in particular spherical term) and biomechanics has been previously stated in keratoconic eyes [40]. However, in young healthy subjects, the spherical aberration and corneal biomechanics are not related.

The independence of spherical aberration of corneal biomechanics in young healthy subjects could be explained by a feedback cycle compensation mechanism that occurs in the posterior cornea considering that biomechanical measurements are carried out at the anterior surface of the cornea: our results showed on the one hand that posterior eccentricity significantly increases as total astigmatism decreases, and on the other hand, the lower the total astigmatism of the cornea, the higher the applanation pressures at ORA (i.e., P1 and P2).

These results are consistent with the study reported by Li et al. [41], since their work concluded that the posterior corneal surface plays an important role in compensating for spherical aberration of the anterior corneal surface.

To conclude, within the hierarchical structure of the cornea, the nanoscopic scale leads to optical transparency, whereas the microscopic architecture models corneal biomechanics that impact the macroscale [16]. Previously to our work, Garzón et al. [42] reported a study on corneal densitometry and its correlation with aging, corneal thickness and curvature, and refractive error using Scheimpflug imaging; they found no correlation between optical transparency and refractive parameters. In our study, we expanded the analysis of those factors that could have an impact on corneal transparency.

In conclusion, if the macroscopic structure of the cornea is connected through optical and geometrical properties, its optical transparency can be modelled. Optical transparency measured through macroscale approaches is related to corneal biomechanics; in particular, the elastic property seems to be the dominant contribution. In addition, corneal astigmatism affects the biomechanical measurements in the sense that less applanation pressure is required as the total astigmatism increases, so future corrections must be calibrated into air-puff measurements to establish a compensation for asymmetric corneas and in short, avoid underestimation of the corneal biomechanics assessment.

Future research will expand this dataset to be incorporated into a predictive convolutional neural network including aging and pathological conditions to help us to develop predictive models in terms of the inter-relationships of the optical properties, structure, and biomechanics of the cornea.

Author Contributions: Conceptualization, F.J.Á.; methodology, F.J.Á.; validation, F.J.Á., L.R. and M.C.M.; formal analysis, F.J.Á.; investigation, F.J.Á.; data curation, F.J.Á.; writing—original draft preparation, F.J.Á.; writing—review and editing, F.J.Á., L.R. and M.C.M.; supervision, F.J.Á. All authors have read and agreed to the published version of the manuscript.

Funding: This research received no external funding.

Institutional Review Board Statement: The study was conducted according to the guidelines of the Declaration of Helsinki and approved by the Ethics Committee of Research of the Health Sciences Institute of Aragon (Spain) with reference: C.P.-C.I. PI20/377. Approval date: 14 July 2020.

Informed Consent Statement: Informed consent was obtained from all subjects involved in the study.

Conflicts of Interest: The authors declare no conflict of interest.

References

1. Piñero, D.P.; Alcón, N. Corneal biomechanics: A review. *Clin. Exp. Optom.* **2015**, *98*, 107–116. [CrossRef]
2. King, S.; Hafezi, F. Corneal biomechanics—A review. *Opthalmic. Physiol. Opt.* **2017**, *37*, 240–252. [CrossRef]
3. Del Buey, M.A.; Casas, P.; Caramello, C.; López, N.; de la Rica, M.; Subirón, A.B.; Lanchares, E.; Huerva, V.; Grzybowski, A.; Ascaso, F.J. An update on corneal biomechanical cornal differences between type-2 diabetic and nondiabetic patients. *J. Ophthalmol.* **2019**, *2019*, 7645352. [PubMed]
4. Beato, J.N.; Esteves-Leandro, J.; Reis, D.; Falcão, M.; Rosas, V.; Ângela, C.; Falcao-Reis, F. Structural and Biomechanical Corneal Differences between Type 2 Diabetic and Nondiabetic Patients. *J. Ophthalmol.* **2019**, *2019*, 3764878. [CrossRef]
5. Ayhan, Z.; Kaya, M.; Ozturk, T.; Arikan, G.; Birlik, M. Association between Skin Thickness Measurements with Corneal Biomechanical Properties and Dry Eye Tests in Systemic Sclerosis. *Ocul. Immunol. Inflamm.* **2019**, *27*, 1138–1143. [CrossRef] [PubMed]
6. Zimmermann, N.; Brandt, S.; Brünner, J.; Erb, C. Evaluation changes in corneal biomechanics in patients with systemic sclerosis. *Klin. Monbl. Augenheilkd.* **2019**, *236*, 806–815.
7. Parker, J.S.; van Dijk, K.; Melles, G.R. Treatment options for advanced keratoconus: A review. *Surv. Ophthalmol.* **2018**, *60*, 459–480. [CrossRef]
8. Roy, A.S.; Shetty, R.; Kummelil, M.K. Keratoconus: A biomechanical perspective on loss of corneal stiffness. *Indian J. Ophthalmol.* **2013**, *61*, 392–393. [CrossRef] [PubMed]
9. Binder, P.S.; May, C.H.; Grant, S.C. An Evaluation of Orthokeratology. *Ophthalmology* **1980**, *87*, 729–744. [CrossRef]
10. Ambrósio, R.; Correira, F.F.; Lopes, B.; Salomão, M.Q.; Luz, A.; Dawson, D.G.; Elsheikh, A.; Vinciguerra, R.; Vinciguerra, P.; Roberts, C.J. Corneal biomechanics in ectatic diseases: Refractive surgery implications. *Open Ophthalmol. J.* **2017**, *11*, 176–193. [CrossRef]
11. Aksoy, S.; Akkaya, S.; Özkurt, Y.; Kurna, S.; Açıkalın, B.; Şengör, T. Topography and higher order corneal aberrations of the fellow eye in unilateral kerato-conus. *Turk J. Ophthalmol.* **2017**, *47*, 249–254. [CrossRef]
12. Naderan, M.; Jahanrad, A.; Farjadnia, M. Ocular, corneal, and internal aberrations in eyes with keratoconus, forme fruste keratoconus, and healthy eyes. *Int. Ophthalmol.* **2018**, *38*, 1565–1573. [CrossRef]
13. Wilkinson, J.M.; Cozine, E.W.; Kahn, A.R. Refractive Eye Surgery: Helping Patients Make Informed Decisions About LASIK. *Am. Fam. Physician* **2017**, *95*, 637–644. [PubMed]
14. Zhang, Y.; Shen, Q.; Jia, Y.; Zhou, D.; Zhou, J. Clinical outcomes of SMILE and FS-LASIK used to treat myopia: A meta análisis. *J. Refract. Surg.* **2016**, *32*, 256–265. [CrossRef] [PubMed]
15. Sultan, M.B.; Mansberger, S.L.; Lee, P.P. Understanding the Importance of IOP Variables in Glaucoma: A Systematic Review. *Surv. Ophthalmol.* **2009**, *54*, 643–662. [CrossRef]
16. Meek, K.M.; Knupp, C. Corneal structure and transparency. *Prog. Retin. Eye Res.* **2015**, *49*, 1–16. [CrossRef] [PubMed]
17. Ávila, F.J.; Gambín, A.; Artal, P.; Bueno, J.M. In vivo two-photon microscopy of the human eye. *Sci. Rep.* **2019**, *9*, 10121. [CrossRef]
18. Petroll, W.M.; Robertson, D.M. In Vivo Confocal Microscopy of the Cornea: New Developments in Image Acquisition, Reconstruction, and Analysis Using the HRT-Rostock Corneal Module. *Ocul. Surf.* **2015**, *13*, 187–203. [CrossRef]
19. Otri, A.M.; Fares, U.; Al-Aqaba, M.A.; Dua, H.S. Corneal Densitometry as an Indicator of Corneal Health. *Ophthalmology* **2012**, *119*, 501–508. [CrossRef] [PubMed]
20. Belin, M.W.; Ambrósio, R. Scheimpflug imaging for keratoconus and ectatic disease. *Indian J. Ophthalmol.* **2013**, *61*, 401–406. [CrossRef] [PubMed]
21. Boulze-Pankert, M.; Dariel, R.; Hoffart, L. Corneal Scheimpflug Densitometry Following Photorefractive Keratectomy in Myopic Eyes. *J. Refract. Surg.* **2016**, *32*, 788–791. [CrossRef] [PubMed]
22. Qin, X.; Tian, L.; Zhang, H.; Chen, X.; Li, L. Evaluation of corneal elastic modulus based on Corneal Visualization Scheimpflug Technology. *Biomed. Eng. Online* **2019**, *18*, 42. [CrossRef] [PubMed]
23. Luce, D.A. Determining in vivo biomechanical properties of the cornea with an ocular response analyzer. *J. Cataract. Refract. Surg.* **2005**, *31*, 156–162. [CrossRef] [PubMed]

24. Motevasseli, T.; Baradaran-Rafii, A.; Yazdizadeh, F.; Karimian, F.; Fekri, S.; Baradaran-Rafii, A. Comparison between two scheimpflug anterior segment analyzers. *J. Ophthalmic Vis. Res.* **2017**, *12*, 23–29. [CrossRef]
25. Piñero, D.; Alcón, N. In vivo characterization of corneal biomechanics. *J. Cataract. Refract. Surg.* **2014**, *40*, 870–877. [CrossRef]
26. Kaushik, S.; Pandav, S.S. Ocular Response Analyzer. *J. Curr. Glaucoma Pract.* **2012**, *6*, 17–19. [CrossRef]
27. Lau, W.; Pye, D. A Clinical Description of Ocular Response Analyzer Measurements. *Investig. Opthalmology Vis. Sci.* **2011**, *52*, 2911–2916. [CrossRef]
28. Roberts, C.J.; Mahmoud, A.M.; Bons, J.P.; Hossain, A.; Elsheikh, A.; Vinciguerra, R.; Vinciguerra, P.; Ambrósio, R., Jr. Introduction of two novel stiffness parameters and interpretation of air puff bio-mechanical deformation parameters with a Dynamic Scheimpflug analyzer. *J. Refract. Surg.* **2017**, *33*, 266–273. [CrossRef] [PubMed]
29. Llorente, L.; Barbero, S.; Merayo, J.; Marcos, S. Total and corneal optical aberrations induced by laser in situ keratomileusis for hypero-pia. *J. Refract. Surg.* **2004**, *20*, 203–216. [CrossRef]
30. Pérez, G.M.; Manzanera, S.; Artal, P. Impact of scattering and spherical aberration in contrast sensitivity. *J. Vis.* **2009**, *9*, 19. [CrossRef]
31. Ávila, F.J.; Ares, J.; Collados, M.V.; Marcellán, M.C.; Remón, L. An Update on Corneal Imaging Techniques: From Macroscale to Nanostructure. *SN Compr. Clin. Med.* **2019**, *2*, 1–10. [CrossRef]
32. Shimizu, E.; Yamaguchi, T.; Tsubota, K.; Shimazaki, J. Corneal high-order aberrations in eyes with corneal scar after traumatic perfora-tion. *Eye Contact Lens* **2019**, *45*, 124–131. [CrossRef] [PubMed]
33. Lombardo, M.; Rosati, M.; Pileri, M.; Schiano-Lomoriello, D.; Serrao, S. evaluation of corneal optical properties in subjects wearing hydrogel etafilcon A contact lenses and the effect of administering mannitol-enriched sodium hyaluronate ophthalmic solution. *Clin. Ophthalmol.* **2014**, *8*, 2347–2354. [CrossRef] [PubMed]
34. Wegener, A.R.; Meyer, L.; Hauch, C.; Sacchetti, M.; Plateroti, R.; Lambiase, A. Changes of Corneal Transparency and Thickness in Dry–Eye Syndrome Single and in Combination With Other Ocular Diseases. *Investig. Opthalmol. Vis. Sci.* **2005**, *46*, 4473.
35. Spadea, L.; Maraone, G.; Verboschi, F.; Vingolo, E.M.; Tognetto, D. Effect of corneal light scatter on vision: A review of the literature. *Int. J. Ophthalmol.* **2016**, *9*, 459–464. [CrossRef]
36. Mohammadi, S.-F.; Khorrami-Nejad, M.; Hamidirad, M. Posterior corneal astigmatism: A review article. *Clin. Optom.* **2019**, *11*, 85–96. [CrossRef]
37. Whitford, C.; Studer, H.; Boote, C.; Meek, K.M.; Elsheikh, A. Biomechanical model of the human cornea: Considering shear stiffness and regional variation of collagen anisotropy and density. *J. Mech. Behav. Biomed. Mater.* **2015**, *42*, 76–87. [CrossRef]
38. Blackburn, B.J.; Jenkins, M.W.; Rollins, A.M.; Dupps, W.J. A Review of Structural and Biomechanical Changes in the Cornea in Aging, Disease, and Photochemical Crosslinking. *Front. Bioeng. Biotechnol.* **2019**, *7*, 66. [CrossRef] [PubMed]
39. Ariza-Gracia, M.A.; Zurita, J.F.; Piñero, D.P.; Rodriguez-Matas, J.F.; Calvo, B. Coupled biomechanical response of the cornea assessed by non-contact tonom-etry. A simulation study. *PLoS ONE* **2015**, *10*, e0121486. [CrossRef]
40. Piñero, D.P.; Alio, J.L.; Barraquer, R.I.; Michael, R.; Jiménez, R. Corneal biomechanics, refraction and corneal aberrometry in Keratoconus: An inte-grated study. *Investig. Opthalmol. Vis. Sci.* **2010**, *51*, 1948–1955. [CrossRef] [PubMed]
41. Li, X.; Wang, Y.; Dou, R. Aberration compensation between anterior and posterior corneal surfaces after Small incision lenticule extraction and Femtosecond laser-assisted laser in-situ keratomileusis. *Ophthalmic Physiol. Opt.* **2015**, *35*, 540–551. [CrossRef]
42. Garzón, N.; Poyales, F.; Illarramendi, I.; Mendicute, J.; Jáñez, Óscar; Caro, P.; López-Muñoz, A.; Argüeso, F. Corneal densitometry and its correlation with age, pachymetry, corneal curvature, and refraction. *Int. Ophthalmol.* **2017**, *37*, 1263–1268. [CrossRef]

2.2. Corneal hysteresis and intraocular pressure are altered in silicone-hydrogel soft contact lenses wearers.

Marcellán MC, Remón L, Ávila FJ. Corneal hysteresis and intraocular pressure are altered in silicone-hydrogel soft contact lenses wearers. *Int Ophthalmol*. 2022;42(9):2801-2809. https://doi.org/10.1007/s10792-022-02270-0

JIF (2022): 1,6- Ophthalmology- 50/62-Q4

JCI (2022): 0,65- Ophthalmology-52/95-Q3

Int Ophthalmol
https://doi.org/10.1007/s10792-022-02270-0

ORIGINAL PAPER

Corneal hysteresis and intraocular pressure are altered in silicone-hydrogel soft contact lenses wearers

María Concepción Marcellán · Laura Remón · Francisco J. Ávila

Received: 28 October 2021 / Accepted: 12 March 2022

Abstract

Purpose The aim of this work is to determinate the effects in the physical parameters in terms of intraocular pressure (IOP) and central corneal thickness (CCT) and corneal biomechanics in terms of corneal resistance factor (CRF) and corneal hysteresis (CH) of wearing silicone-hydrogel soft contact lenses (SiH-CLs) in young adult subjects during a short-term follow-up.

Methods 40 eyes of 20 healthy patients with a mean age of 22.87 ± 4.14 were involved in this study. Subjects with corneal diseases, dry eye, irregular astigmatism or who have been previous contact lens wearers were excluded. The ocular response analyzer (Reichert Ophthalmic Instruments) was used to measure CH, CRF and IOP and Scheimpflug imaging (the GALILEI™ Dual Scheimpflug camera analyzer, Ziemer) was used to measure CCT before and 10 days (Group 1) and 20 days (Group 2) after wearing the SiH-CLs.

Results IOP was significantly decreased 10 days after using the SiH-CLs ($p = 0.009$). Within the 20 days' period, Group 2 revealed an even more pronounced decrease in IOP ($p = 0.003$) while CH increased significantly ($p = 0.04$). CCT and CRF did not show a significant change during the period of SiH-CLs use. Our finding allowed obtaining an empirical expression that relates IOP, CCT, CRF and CH within a biomechanical compensation experimental model.

Conclusions Corneal biomechanical parameters and physical properties of the cornea may be altered due to SiH-CLs use. Our findings could have an impact on the management of glaucoma progression and ocular hypertension.

Keywords Corneal biomechanics · Soft contact lenses · Intraocular pressure · Glaucoma

Introduction

The biomechanical properties of the cornea are responsible of its stability and functionality with high impact in vision [1]. The cornea is characterized by elastic and viscoelastic properties [2] that play a fundamental role in refractive surgery [3], orthokeratology [4], keratoconus progression [5], glaucoma or corneal ectasia [6].

Refractive errors are very common human eye disorders and are leading causes of visual impairment worldwide. Soft contact lenses (CLs) are non-surgical vision correction alternatives to spectacles, with more than 140 million wearer's worldwide [7]. The developments in CLs design technologies have focused on comfortability, tear film stability, biocompatibility and the development of new materials [8]. On the one

M. C. Marcellán · L. Remón · F. J. Ávila (✉)
Departamento de Física Aplicada, Universidad de Zaragoza, C/ Pedro Cerbuna, 12, 50009 Zaragoza, Spain
e-mail: avila@unizar.es

Published online: 30 March 2022

hand, hydrogel CLs offer materials with good wettability, optical quality and comfortability. However, the oxygen permeability is moderate and this can lead to symptoms of dryness at the end of the day.

Oxygen-deficient metabolism (i.e., hypoxia) leads to metabolic changes and then to alterations in corneal biomechanics [9]. In this sense, silicone hydrogel CLs (SiH-CLs) have been chosen as the best option by new CLs users in the last decades [10]. This type of material provides more than five times oxygen permeability through the material compared to standard hydrogel materials [11], preventing the hypoxia-related [12] physiological changes within the corneal tissue and allowing patients wearing CLs for long daily use.

Despite the advantages of SiH-CLs, SiH materials present higher modulus of elasticity than conventional hydrogel lenses. Although the new generation of SiH-CLs have balanced the oxygen transmissibility obtaining a lower modulus of elasticity compared to the first generation, these two factors continue playing an important role in corneal biomechanics [13].

Some studies have reported topographic changes in both central and peripheral cornea [14, 15] after short-term CLs wearing including corneal swelling [16], optical aberrations [17] or loss of radial symmetry [18]. Those physical changes were observed in both soft hydrogel [19] and silicone hydrogel CLs [16].

In this sense, previous studies reported alterations in corneal biomechanics induced by long-term soft CLs wearing [20]. Lu et al. [21], reported alterations in the biomechanical properties of the cornea after wearing soft contact lenses during eye closure. Matalia et al. [22], demonstrated correlation between corneal stiffness and myopia. Few studies have investigated biomechanical changes after short-term period of wearing contact lenses [15, 23]. Tyagi et al. [15] reported changes in corneal thickness and morphology after analyzing different types of soft toric contact lenses materials (silicone hydrogel and hydrogel). Radaie-Moghadam et al. [23] studied the effect of toric soft contact lens wear on corneal biomechanical properties over a 3-month period.

The knowledge about any physical and/or biomechanical change in the short-term use of CLs could be crucial in occasional wearers, patients with corneal pathologies such as keratoconus, ectasia or glaucoma, in order to detect early contraindications or discard candidates for whom some transient biomechanical alterations may compromise the corneal stability.

In this sense, air-puff tonometers provide excellent measurement of corneal biomechanics [24] and have been successfully employed to analyze corneal alterations in glaucoma patients [25], keratoconus degeneration [26], or patients undergoing refractive surgery.

The aim of our work is to carry out a prospective observational study to determine the impact of wearing SiH-CLs on biomechanical and corneal physical parameters during 10 and 20 days of follow-up periods by combining non-contact air-puff tonometry and Scheimpflug imaging.

Methods

Participants

This research was reviewed by an independent ethical review board and conforms to the principles and applicable guidelines for the protection of human subjects in biomedical research (Ethical Committee of Research of the Health Sciences Institute of Aragon, Spain) approved with reference: C.P.-C.I.PI20/377. Measurements procedure and data collection were carried out according to the tenets of the Declaration of Helsinki. All participants were informed about the nature, risks and possible adverse consequences of the study and signed an informed consent document. The participants were European Caucasian population, non-wearers contact lenses students from the school of Optics and Optometry of the University of Zaragoza (Spain), a total of 40 eyes from 20 healthy young adult subjects (mean age of 22.87 ± 4.14 years old) were involved in the study.

Inclusion criteria consisted of age range between 18 and 28 years with myopia, hyperopia or astigmatism and best corrected visual acuity at distance at least of 20/20 for each eye. Exclusion criteria were history of using any type of contact lenses, corneal diseases or surgery, dry eye, or irregular astigmatism. In addition, patients who presented contact lens intolerance during the first day of use were excluded.

Contact lens use

The short-term wear time was divided into two different temporal intervals: 10 participants were asked to

wear SiH-CLs 8 h of uninterrupted daily use during 10 days, and the second group (10 participants) during 20 days with the same conditions.

Silicon hydrogel soft CLs of monthly replacement (Horizont Bio, Tiedra Farmacéutica S.L. Spain) were selected for this study. Table 1 shows the technical specifications:

Keratometric, pachymetric parameters and ocular refractive errors were measured using a dual Scheimpflug analyzer (see "Experimental Procedure" for details) and an open-view autorefractometer (Grand Seiko, WAM-5500), respectively. Subjective refraction and evaluation of the anterior segment of the eye were conducted by an experienced optometrist. Total diameter and the effective optic zone radius of the CLs were chosen following the manufacturer's guidelines.

Experimental procedure and data analysis

Ocular response analyzer (ORA, Reichert Instruments, Depew, NY, USA) is a non-contact air puff applanation tonometer that provides corneal hysteresis (CH) and corneal resistance factor (CRF) measurements. Briefly, CH can be defined as the energy dissipation when an external stress is applied resulting in a time-dependent stain unlike purely elastic materials, that immediately recover the initial state once the stress stops. Thus, CH is a function of the corneal viscoelastic behavior.

CRF is related to the pure elastic properties of the cornea [27]. Therefore, CH and CRF are representative parameters of the biomechanical properties of the cornea. ORA instrument also provides compensated IOP measurements independent of corneal biomechanics and pachymetry.

Table 1 Contact lenses technical specifications

Material	Fanfilcon A
Hydration	55%
Central Thickness	0.08 mm
Dk/t	110
Modulus	0.6 Mpa
Optical design	Aspheric
Border design	Round shape
UV filter	Class 1

In our study we first measured the central corneal thickness (CCT) using a dual Placido-Scheimpflug imaging analyzer (the GALILEI™ Dual Scheimpflug camera analyzer, Ziemer). Then, CCT measurement was incorporated to the operating interface of the ORA´s operating interface to start biomechanical measurements.

The measurement protocol was a simple sequential procedure: first Scheimpflug analyzer measures the CCT of the participant and next after incorporating this parameter to ORA instrument the compensated IOP (hereinafter IOP) CH and CRF are measured by air-puff applanation. Each final data were the average of three sequential experimental measurements.

The measurements were separated in two temporal groups: 10 and 20 days after SiH-CLs wearing. The control measurements were acquired after the first insertion of the CLs, the follow-up measurements were carried out two hours after asking the participants to remove the CLs once the wearing time ended. The reason for waiting two hours between contact lens removal and the measurements was motivated by the reported fluctuation [21] in corneal thickness after CL removal that recovers baseline values after 100 min.

Collected data were stored into an Excel spreadsheet. Every participant was identified by a reference number, no personal data were included. Once the experiment was finished, the spreadsheet was migrated to Origin Lab software (Origin Lab Corp.) for graphical representations and data analysis. The statistical analysis was performed using the advanced statistical tool including two-sample hypothesis tests and Spearman Rank Correlation Coefficient.

Results

Intrinsic biomechanical (CRF and CH) and biophysical (IOP and CCT) parameters were measured in a total of 40 eyes of 20 young healthy participants before and after wearing SiH-CLs. Two temporary periods of SiH-CLs use were considered in this study: 10 and 20 days, for which the described measurements were acquired immediately before and after starting and ending wearing periods.

Follow-up of biomechanical and physical parameters after SiH-CLs wearing

Figure 1 compares the IOP (Fig. 1a), CCT (Fig. 1b), CH (Fig. 1c) and CRF (Fig. 1d) values of the two groups of participants. The mean IOP showed a significant reduction after 10 ($p=0.009$) and 20 days ($p=0.003$) of SiH-CLs use. The pachymetry revealed a mean increase in CCT, although no significant differences were found, a slight edema was observed in the first group ($p=0.35$) which reverted to stabilization in the 20-days group ($p=0.48$), recovering the control values.

In addition, the analysis of the biomechanical parameters revealed how the use of SiH-CLs leaded to an increase in CH in both groups, showing a statistical shift in the 20-days group ($p=0.04$). On the other hand, the use of SiH-CLs did not significantly affect the CRF, however the behavior of this parameter (Fig. 1d) showed the opposite trend as observed in CCT (Fig. 1b), that is, a more accused decrease after 20 days of SiH-CLs wear ($p=0.13$) compared to the 10-days group ($p=0.32$).

For the sense of completeness, Fig. 2 compares the mean variation values of the parameters plotted in

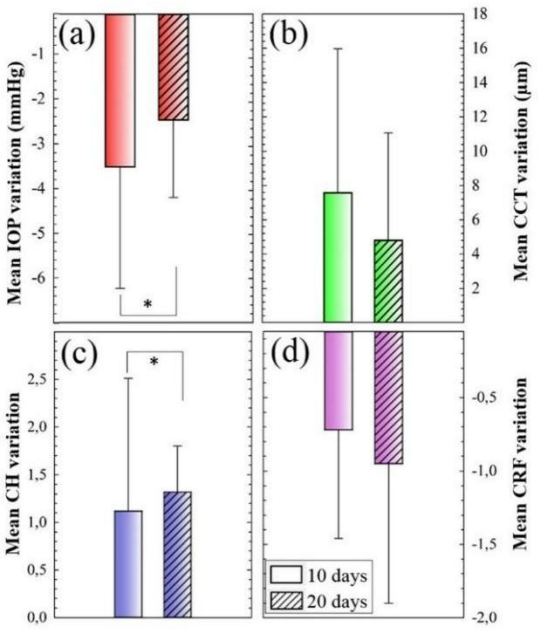

Fig. 2 Mean variation PIO (**a**), CCT (**b**), CH (**c**) and CRF (**d**) values of the two studied temporal groups (10 and 20 days). (*p < 0.05)

Fig. 1 Box diagrams of IOP (**a**), CCT (**b**), CH (**c**) and CRF (**d**) values comparing control measurements with each temporal group. For each box, the median (central line inside each box), the Q1 and Q4 quartiles (lower and higher borders of each box, respectively) and maximum and minimum values (whiskers) are shown. (*$p<0.05$; **$p<0.005$)

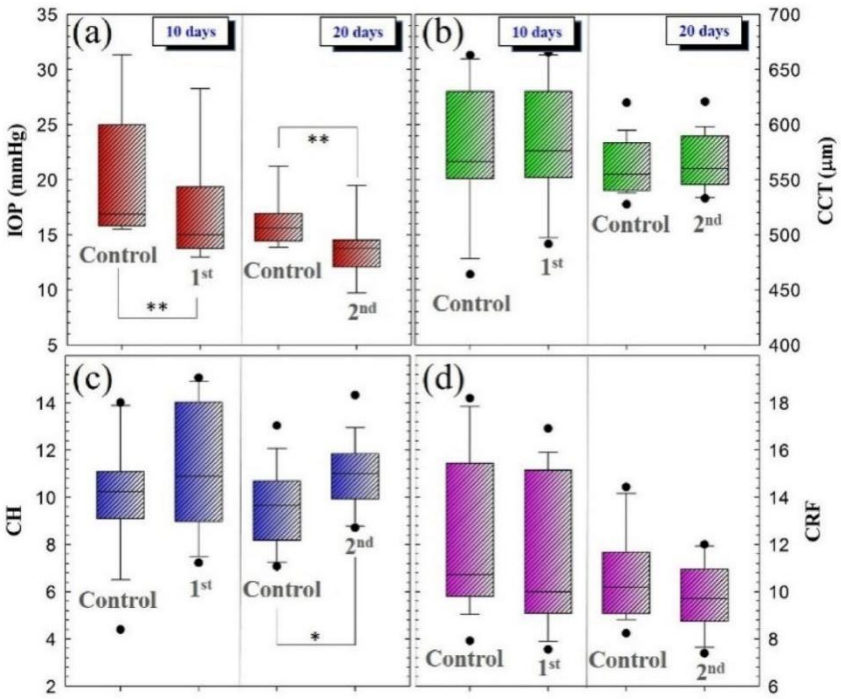

Fig. 1. This mean variation is calculated as the difference between the averaged values after SiH-CLs wearing and the control measurements. The bio-physical and biomechanical parameters that presented significant alterations as a consequence of SiH-CLs wearing were IOP ($p=0.008$) and CH ($p=0.04$), respectively.

In that sense, the increase in the time of SiH-CLs wearing implied a reduction in the variation in the IOP value and an increase in CH. Whereas CCT and CRF were not greatly affected by the use of SiH-CLs, those parameters showed opposite mean variations according to the behaviors observed in Fig. 1. That is, as the wearing time increases, the induced corneal edema is less pronounced while CRF shows higher variation in average rate.

Relationship between physical and biomechanical parameters

The results presented in Figs. 1 and 2 assessed the corneal alterations as a consequence of wearing SiH-CLs during two short follow-up periods measured by means of biomechanical (CH and CRF) and pure physical parameters (CCT and IOP). These alterations were quantified by measuring CH and CRF parameters. Nevertheless, for a better understanding on how the biophysics of the cornea is modified, it is necessary to investigate how the different properties are related.

A Spearman´s correlation analysis was performed by including the whole dataset (i.e., including both control and the two temporal groups) of the experiment. The statistical analysis revealed significant relationships between the biomechanical parameters and between physical and biomechanical data.

Panels (a) and (b) of Fig. 3 shows linear correlations between physical parameters (IOP and CCT) and the CRF parameter. In both cases, higher corneal resistance is related to higher IOP and corneal thickness with statistical significance (the results of the correlation are shown in the shaded boxes). CRF, IOP and CCT parameters are related by means of the following experimental fittings:

$$\mathrm{CRF} = 0.49 * \mathrm{IOP} + 2.84 \tag{1}$$

$$\mathrm{CRF} = 0.05 * \mathrm{CCT} - 22.86 \tag{2}$$

Figure 3d also relates the corneal thickness (CCT) and the viscoelastic property (CH) that according to the results, the greater the corneal pachymetry, the higher the viscoelasticity or the viscoelastic response of the corneal tissue under an external stress.

From data of Fig. 3c, the relationship between viscoelastic (CH) and elastic (CRF) properties can be analytically computed from Eq. (3):

$$\mathrm{CRF} = 0.34 \cdot e^{023 \cdot \mathrm{CH}} \tag{3}$$

The best mathematical fitting was an exponential function. This nonlinear behavior of the CRF as a function of the hysteresis can be explained by the transient viscous response of the cornea. This finding plays an important role in this study to explain one of the compensation mechanism acting as biomechanical response when the intraocular pressure fluctuates but the corneal thickness and resistance remain constants.

In this sense, biomechanical and physical corneal parameters that can be unified through an empirical biophysical expression by adding Eqs. (1), (2) and (3) as follow:

$$\mathrm{CRF} = \frac{1}{3} \cdot \left(0.49 \cdot \mathrm{IOP} + 0.05 \cdot \mathrm{CCT} + 0.34 \cdot e^{023 \cdot \mathrm{CH}} - 22.86\right) \tag{4}$$

From a dynamical point of view, Eq. (4) describes a biomechanical compensation model to explain how the viscoelastic response compensates for IOP and CCT imbalances, in order to preserve the corneal resistance.

Discussions and conclusions

Corneal swelling, shape alterations, refractive stability or induced optical aberrations are crucial factors for normal vision [1] that must also be specially controlled in severe corneal pathologies such as keratoconus [5], ectasia [28] or other ocular degenerative diseases with corneal manifestations such as glaucoma, for instance.

In this sense, there has been an increasing effort to understand how corneal biomechanics is affected by soft contact lenses wearing. It is well-known that both hydrogel and silicone hydrogel soft contact lenses induce structural corneal alterations: thickness [14], warpage [29] or morphology [16].

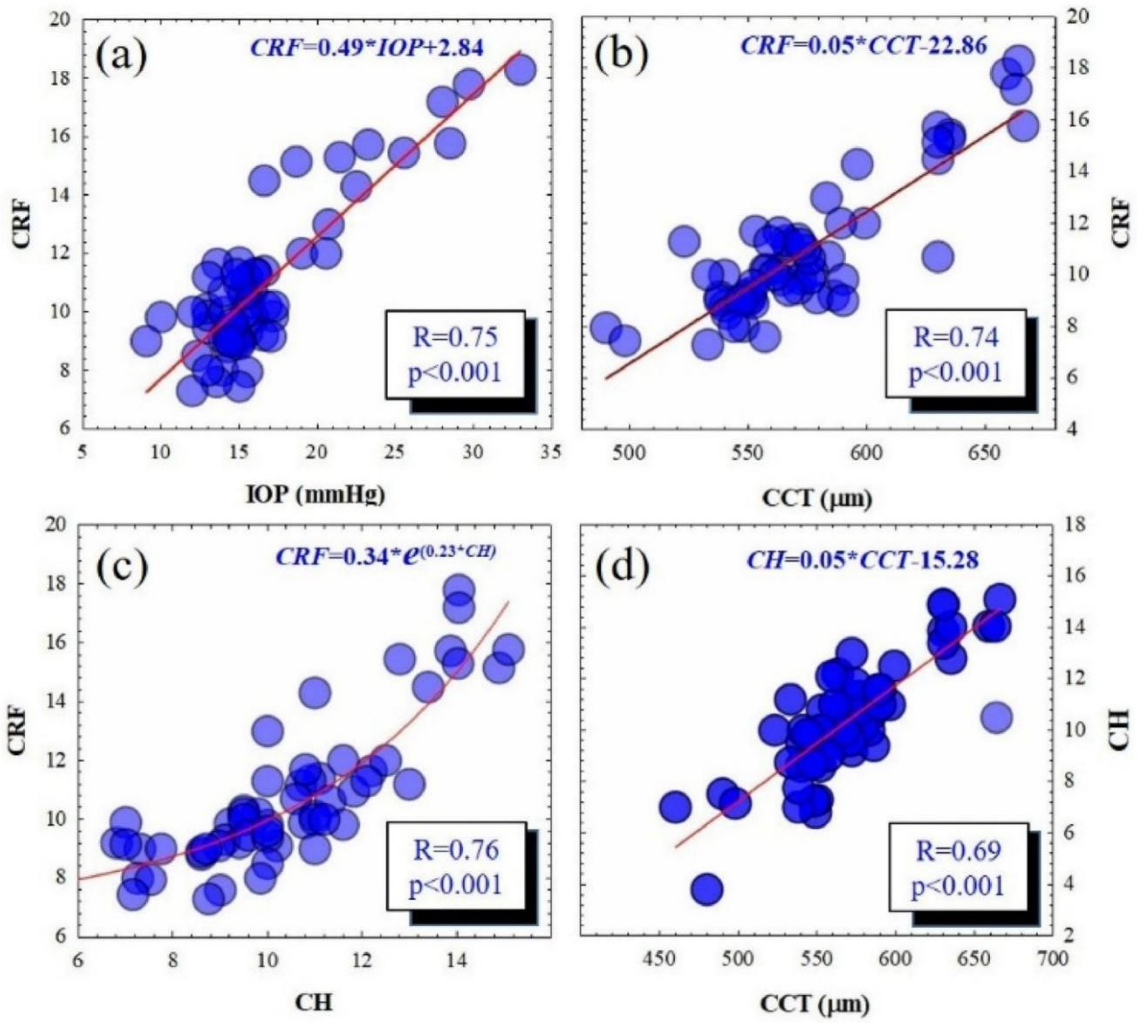

Fig. 3 Correlation and best mathematical fitting between physical and biomechanical parameters. The correlation results are shown within the shaded boxes

Lau and Pye [30] reported biomechanical overestimation measured with applanation tonometry due to the temporal hydration or induced corneal edema as a consequence of wearing hydrogel soft contact lenses. This overestimation is due to an increasing in corneal stiffness induced by corneal hyper-hydration.

In addition, Lu and coworkers studied biomechanical changes after inducing corneal edema by eye closure while wearing Hydroxyethyl-methacrylate soft CLs [21] during 3 h. Immediately after lens removal they found significant correlation between IOP and CRF with corneal thickness but no association of CH with corneal edema. Both CRF and CCT recovered the baseline values after 100 min. These two studies revealed short-term time-dependent changes in CRF and CCT because of the induced corneal edema.

In this work we have investigated the corneal biomechanics, IOP and CCT alterations after wearing SiH-CLs during two temporal groups: 10 and 20 days. Results herein showed that after 10 days the IOP is significantly reduced, whereas CH slightly increases and CRF and CCT remain without important variations.

The longer period of follow-up (20 days) revealed a stronger decrease in IOP and a statistical increase in CH. No induced edema or increased corneal stiffness (CRF) were observed. This inverse relationship can be explained by the La Place´s law: as the IOP increases the rigidity is greater and therefore the viscous damping reduces, that is, IOP and CH are negatively correlated [31, 32].

In this sense, Radaie-Moghadam and collaborators [23] extended the following time of corneal biomechanics after using soft toric contact lenses up to three months. They found a significant reduction in both CH and CRF after 1 month of CLs wearing, but not a significant variation in CCT or corneal swelling. This last finding is consistent with our results, however the main discrepancies in our study and the study by Radaie-Monghadam et al. [23] can be due to an absence of IOP analysis that could explain an increase in CH instead of the observed reduction in our study. A second discrepant factor may lie in the relationship between corneal biomechanics stiffness and the refractive error [22] and the fact that all the subjects were chosen to present regular astigmatism. Other factors such as contact lens properties or patient´s age difference could explain the discrepancies.

Although it is clear the direct influence of soft CLs wear in corneal biomechanics, a deep knowledge on how biomechanical and physical corneal parameters are related is necessary. In our work we have analyzed the whole data set of the study (including control and the two temporal groups) in order to find the possible relationships between pure physical (IOP and CCT) and biomechanical corneal parameters (CH and CRF).

Our results revealed that IOP is positively correlated to CRF, that is, the higher the elastic property the higher the measured IOP. CRF was also linearly associated with CCT, these finding are consistent with the results reported by Bhan et al. [33].

From a physiopathological point of view, an increase in CCT has been associated to ocular hypertension [34–36] what could explain the observed increase in CRF while measuring the IOP according to the results previously reported by Sha et al. [37]. They observed highest values of CRF (and therefore corneal rigidity) in ocular hypertension eyes. More recently, the positive correlation between corneal thickness and stiffness was demonstrated using optical coherence elastography [38].

In 2009, Mangouritsas et al. [39] reported a strong association between CH and CCT in healthy eyes that becomes weaker as IOP increases in glaucomatous eyes. Our results are in good agreement with this study as revealed a positive correlation between CH and CCT (Fig. 3d).

Finally, the exponential relationship found between CH and CRF allowed to obtain an analytical biophysical expression that unifies IOP, CH, CRF and CCF parameters. This equation allows explaining the follow-up biomechanics after SiH-CLs wearing represented in Fig. 1 as follow:

If the IOP decreases while CCT remains without significant fluctuations, in order to preserve the corneal resistance the viscoelastic response increase for mechanical compensation. These findings suggest that while the elastic property is weakening, the viscosity increases to compensate the corneal biomechanics and preserve ocular stability.

To conclude, unveiling the biomechanical properties of the human cornea is crucial for understanding the development of corneal diseases and new treatments. The main findings of our work lie in fact that the use of SiH-CL during a short-term period of wearing time reduces the IOP as the CH increases. Considering that CH has been proved a biomarker of visual field loss in glaucomatous eyes [40], future work of this study could help in the development of new biomechanical treatment against the progression of glaucoma.

Acknowledgements Authors would like to warmly thank "*TIEDRA* FARMACEUTICA S.L." (Spain) company for the donation of all contact lenses required in this study. Authors thanks the Department of Applied Physics of the University of Zaragoza (Spain) for the use of their equipment's.

Funding Open Access funding provided thanks to the CRUE-CSIC agreement with Springer Nature. No funding was received for this research.

Declarations

Conflict of interest Authors declare no conflicts of interest.

Ethical approval This study was approved by the Ethical Committee of Research of the Health Sciences Institute of Aragon, Spain (C.P.-C.I.PI20/377). Measurements procedure and data collection were carried-out according to the tenets of the Declaration of Helsinki.

Informed consent All participants were informed about the nature, risks and possible adverse consequences of the study and signed an informed consent document.

References

1. Kling S, Hafezi F (2017) Corneal biomechanics—a review. Opthal Physiol Opt 37(3):240–252
2. Woo S, Kobayashi A, Schlegel W (1972) Non linear material properties of intact cornea and sclera. Exp Eye Res 14(1):29–39
3. Damgaard IB, Reffat M, Hjortdal J (2018) Review of corneal biomechanical properties following LASIK and SMILE for myopia and myopic astigmatism. Open Ophthalmol J 12:164–174
4. Lam AK, Hon Y, Leung Y (2019) Association between long-term orthokeratology responses and corneal biomechanics. Sci Rep 29(1):12566
5. Catalán-Lopez S, Cadarso-Suarez L, López-Ratón M (2018) Corneal biomechanics in unilateral keratoconus and fellow eyes with a scheimpflug-based tonometer. Optom Vis Sci 95(7):608–615
6. Esporcate LPG, Salomao MQ, Lopes BT (2020) biomechanics diagnosis of the cornea. Eye Vis (Lond) 7:9
7. Nichols JJ, Willcox MDP, Bron AJ (2013) Members of the TFOS international workshop on contact lens discomfort. The TFOS international workshop on contact lens discomfort: executive summary. Invest Ophthalmol Vis Sci 54:TFOS7–TFOS13
8. Stapleton F, Stretton S, Papas E (2006) Silicone hydrogel contact lenses and the ocular surface. Ocul Surf 4:24–43
9. Papas EB (2014) The significance of oxygen during contact lens wear. Contact Lens Anterior Eye 37(6):394–404
10. Sankaridurg P, Lazon de la Jara P, Holden B (2013) The future of silicone hydrogels. Eye Contact Lens 39:125–129
11. Seitz ME, Wiseman ME, Hilker I (2017) Influence of silicone distribution and mobility on the oxygen permeability of model silicone hydrogels. Polymer 118:150–162
12. Sweeney DF (2013) Have silicone hydrogel lenses eliminated hypoxia? Eye Contact Lens 39:53–60
13. Ballesteros JF (2017) Cambios corneales físicos y fisiológicos inducidos por el módulo de elasticidad del lente de contacto. J Chem Inf Model 53(9):1689–1699
14. Bailey IL, Carney LG (1973) Corneal changes from hydrophilic contact lenses. Am J Optom Arch Am Acad Optom 50:299–304
15. Tyagi CM, Read S (2010) Regional changes in corneal thickness and shape with soft contact lenses. Optom Vis Sci 87(8):567–575
16. Alba-Bueno F, Beltran-Masgoret A, Sanjuan C (2009) Corneal shape changes induced by first and second generation silicone hydrogel contact lenses in daily wear. Cont Lens Anterior Eye 32:88–92
17. Lu F, Mao X, Qu J, Xu D, Che J (2003) Monochromatic wavefront aberrations in the human eye with contact lenses. Optom Vis Sci 80:135–141
18. Arranz I, Gonzalez-Garcia MJ, Galarreta DJ (2003) Low water content hydrogel contact lenses (HCL) induce corneal Irregularity. Invest Ophthalmol Vis Sci 44:3701
19. Schornack M (2003) Hydrogel contact lens-induced corneal warpage. Cont Lens Anterior Eye 26:153–159
20. Çavdarli C, TopÇu-Yilmaz (2018) Does long-term soft contact lens wear affect corneal and anterior chamber parameters? Turk J Ophthalmol 48:166–170
21. Lu F, Xu S, Qu J (2006) Central corneal thickness and corneal hysteresis during corneal swelling induced by contact lens wear with eye closure. Invest Ophthalmol Vis Sci 52(6):3207–3214
22. Matalia J, Francis M, Gogri P (2017) Correlation of corneal biomechanical stiffness with refractive error and ocular biometry in a pediatric population. Cornea 36(10):1221–1226
23. Radaie-Moghadam S, Hashemi H, Jafarzadehpur E (2016) Corneal biomechanical changes following toric soft contact lens wear. J Ophthalmic Vis Res 11(2):131–135
24. Luce DA (2005) Determining in vivo biomechanical properties of the cornea with an ocular response analyzer. J Cataract Refract Surg 31:156–162
25. Sullivan-Mee M, Billingsley SC, Patel AD (2008) Ocular Response Analyzer in subjects with and without glaucoma. Optom Vis Sci 85:463–470
26. Pinero DP, Alio JL, Barraquer RI (2010) Corneal biomechanics, refraction, and corneal aberrometry in keratoconus: an integrated study. Invest Ophthalmol Vis Sci 51:1948–1955
27. Piñero D, Alcón N (2014) In vivo characterization of corneal biomechanics. J Cataract Refract Surg 40:870–877
28. Salomao MQ, Hofling-Lima AL, Esporcatte LPG (2020) The role of corneal biomechanics for the evaluation of ectasia patients. Int J Environ Res Public Health 17:2113
29. Alipour F, Letafatnejad M, Hooshang-Beheshtnejad A et al. (2016) Corneal biomechanical findings in contact lens induced corneal warpage. J Opthalmol ID: 5603763
30. Lau W, Pye D (2011) Changes in corneal biomechanics and applanation tonometry with induced corneal swelling. Invest Ophthalmol Vis Sci 52:3207–3214
31. Orssenjo GJ, Pye DC (1999) Determination of the true intraocular pressure and modulus of elasticity of the human cornea in vivo. Bull Math Biol 61:551–572
32. Roberts C (2014) Concepts and misconceptions in corneal Biomechanics. J Cataract Refract Surg 40:862–869

33. Bhan A, Browning A, Shah S (2002) Thickness on intraocular pressure measurements with the pneumotonometer, Goldmann applanation tonometer, and Tono-Pen. Invest Ophthalmol Vis Sci 43:1389–1392
34. Argus WA (1995) Ocular hypertension and central corneal thickness. Ophthalmology 102:1810–1812
35. Wolfs RCW, Klaver CCW, Vingerling JR (1997) Distribution of central corneal thickness and its association with intraocular pressure: the Rotterdam Eye Study. Am J Ophthalmol 123:767–772
36. Copt RP, Thomas R, Mermoud A (1999) Corneal thickness in ocular hypertension, primary open-angle glaucoma and normal tension glaucoma. Arch Ophthalmol 117:14–16
37. Shah S, Laiquzzaman M, Mantry S (2008) Ocular response analyser to assess hysteresis and corneal resistance factor in low tension, open angle glaucoma and ocular hypertension. Clin Exp Ophthalmol 36(6):508–513
38. Vantipally S, Jiasong L, Manmohan S (2018) Effects of thickness on corneal biomechanical properties using optical coherence elastography. Optom Vis Sci 95(4):299–308
39. Mangouritsas G, Morphis G, Mourtzoukos S (2009) Association between corneal hysteresis and central corneal thickness in glaucomatous and nonglaucomatous eyes. Acta Ophthalmol 87:901–905
40. Medeiros FA, Meira-Freitas D, Lisboa R (2013) Corneal hysteresis as a risk factor for glaucoma progression: a prospective longitudinal study. Ophthalmology 120:1533–1540

2.3. Corneal retardation time as an ocular hypertension disease indicator.

Del Barco Ó, Ávila FJ, Marcellán MC, Remón L. Corneal retardation time as an ocular hypertension disease indicator. *Biomed Phys Eng Express*. 2023;10(1). https://doi.org/10.1088/2057-1976/ad12fa

JIF (2023): 1,3-Radiology, nuclear medicine & medical imaging-139/204-Q3

JCI (2023):0,44-Radiology,nuclear medicine & medical imaging-132/204-Q3

IOP Publishing Biomed. Phys. Eng. Express 10 (2024) 015014 https://doi.org/10.1088/2057-1976/ad12fa

Biomedical Physics & Engineering Express

PAPER

Corneal retardation time as an ocular hypertension disease indicator

RECEIVED
19 September 2023

REVISED
17 November 2023

ACCEPTED FOR PUBLICATION
6 December 2023

PUBLISHED
14 December 2023

Oscar del Barco[1,*], Francisco J Ávila[2], Concepción Marcellán[2] and Laura Remón[2]

[1] Laboratorio de Óptica, Instituto Universitario de Investigación en Óptica y Nanofísica, Universidad de Murcia, Campus de Espinardo, E-30100, Murcia, Spain
[2] Departamento de Física Aplicada, Universidad de Zaragoza, E-50009, Zaragoza, Spain
* Author to whom any correspondence should be addressed.

E-mail: obn@um.es

Keywords: corneal viscoelastic models, non-contact tonometry, ocular hypertension diseases, glaucoma

Abstract

Objective. A detailed analysis of the corneal retardation time τ as a highly related parameter to the intraocular pressure (IOP), and its plausible role as an indicator of ocular hypertension disease. *Approach.* A simple theoretical expression for τ is derived within the corneal viscoelastic model of Kelvin-Voigt with 3 elements. This retardation time can be easily calculated from the well-known signal and pressure amplitudes of non-contact tonometers like the Ocular Response Analyzer (ORA). Then, a population-based study was performed where 100 subjects aged from 18 to 30 were analyzed (within this group, about 10% had an elevated IOP with more than 21 mmHg). *Main results.* A clear relationship between the corneal retardation time and the corneal-compensated intraocular pressure (IOP_{cc}) was found, underlying the risk for ocular hypertensive (OHT) subjects with lower τ values to develop hypertension illnesses (due to the inability of poorly viscoelastic corneas to absorb IOP fluctuations, resulting in probable optic nerve damage). *Significance.* Our results might provide an useful tool to systematically discern which OHT patients (and even those with normal IOP values) are more likely to suffer glaucoma progression and, consequently, ensure an early diagnosis.

1. Introduction

Corneal biomechanics (CB) is a branch of biophysical sciences that deals with deformation and equilibrium of corneal tissue when any external force is applied. In this sense, the mechanical properties of the corneal tissue depend on the specific organization of fibres, cells and ground substance within the structure. Collagen in Bowman's layer and stroma make a significant contribution to corneal elasticity, whereas the ground substance would give the viscous behaviour (Garcia-Porta *et al* 2014). The increasing interest in CB is due to, among others, its role in the detection and management of ectatic disease (Ortiz *et al* 2007, González-Méijome *et al* 2008, Roy and Dupps 2011, Ambrósio *et al* 2017, Padmanabhan and Elsheikh 2023) and an accurate estimation of IOP to manage pathological diseases such as glaucoma (Liu and Roberts 2005, Asejczk-Widlicka *et al* 2019, Consejo *et al* 2019, Susanna *et al* 2019, Chan *et al* 2021, Catania *et al* 2023).

There are different material models which describe with more or less accuracy the corneal biomechanics. In this respect, we can mention the visco-hyperelastic model, where a highly nonlinear elastic response is achieved when very large strains are applied (Ariza-Gracia *et al* 2015, Whitford *et al* 2018, Liu *et al* 2020), the viscoelastic model (i.e. the material's elastic stress-strain relationship depends on the strain rate) (Fraldi *et al* 2016, Maczynska *et al* 2019) or the finite element methods, where a complete 3D model of the cornea is designed to study its mechanical behaviour (Sánchez *et al* 2014, Simonini *et al* 2016). On the other hand, one-dimensional (1D) rheological models have been useful to describe the viscoelastic properties of the cornea (Glass *et al* 2008, Han *et al* 2014, Jannesari *et al* 2018), though they are not meant to study the 3D corneal deformation.

In this regard, 1D models consist of parallel and/or series combinations of springs and dashpots which mimic the elastic and/or viscous character of the cornea. Thus, a Kelvin-Voigt model with an additional spring can reproduce the instantaneous deformation of the cornea (Glass *et al* 2008), while a four-element viscoelastic model (i.e. the Burgers model) has also been selected for modeling the corneal biomechanics

(Jannesari *et al* 2018). More recently, a more sophisticated rheological model that takes into account the elastic and viscous effects of cornea, crystalline lens and the whole eyeball has been reported (Jimenez-Villar *et al* 2022). Although more complex models with a greater number of elements (i.e. springs and/or dashpots) should be more accurate in corneal modeling (Kok *et al* 2014, Jannesari *et al* 2018), these approaches might not present a unique mathematical solution, due to the higher-order differential equations inherent in these models. So, as clearly stated by Jannesari *et al* (2018), rheological models combining simplicity with accuracy are desired.

Furthermore, it has been amply demonstrated that CB influences IOP measurements (Medeiros and Weinreb 2006, Grise-Dulac *et al* 2012, Brown *et al* 2018). For that matter, the corneal-compensated intraocular pressure provided by the non-contact tonometer ORA is less influenced by corneal biomechanics (Medeiros and Weinreb 2006, Hager *et al* 2008, Lee *et al* 2019), so it might be a reliable parameter to characterize OHT subjects. As it is well-known, an elevated IOP is the major risk factor for developing glaucoma (De Moraes *et al* 2012, Matlach *et al* 2019), however, this is not the unique factor. It has been reported glaucomatous damage at low IOP values (Anderson 2003), whereas no significant glaucoma progression has been found at IOPs greater than 22 mmHg (Kass *et al* 2002).

In this connection, the gold standard method widely used by ophthalmologists to evaluate structural changes in the optic nerve head (ONH) or the retinal nerve fiber layer (RNFL) and assist in the diagnosis of glaucoma has been the fundus photography (Chakrabarti *et al* 2016). The main advantage of this technique is its simplicity and cost-effectiveness, despite the clinical examination of ONH and RNFL is subjective and qualitative, leading to considerable intra- and inter-observer variability in assessing the ONH among qualified specialists. Alternative methods such as optical coherence tomography (OCT) (Geevarghese *et al* 2021), scanning laser polarimetry (SLP) (Lemij and Reus 2008), and confocal scanning laser ophthalmoscopy (CSLO) (Yaghoubi *et al* 2015) have been developed to evaluate nerve fiber loss and optic disc changes in glaucoma. Nonetheless, these retinal imaging instruments are costly and present some drawbacks, among them, the susceptibility of CSLO to inter-observer variabilities or the inability of SLP method to provide both RNFL and ONH data. Additionally, selective perimetry techniques such as short-wavelength automated perimetry (SWAP) and frequency-doubling technology (FDT) perimetry have been extensively studied as adjuncts to standard automated perimetry evaluation (Sharma *et al* 2008).

Accordingly, the aim of this work is to yield a reasonable indicator related to the viscoelastic corneal quality, which might be useful to discern which OHT subjects are more probable to develop ocular hypertensive disorders such as glaucoma. This parameter is the corneal retardation time τ, that is, the time in which about 63% of the final corneal strain is determined (Brinson and Brinson 2008, Jannesari *et al* 2018), and might serve as an indicator of how elastic or viscous a cornea should be. In other words, this metric would measure the cornea's ability to absorb IOP fluctuations. As we will show in this article, the τ parameter might explain why some OHT subjects (and even those with normal IOP values) should undergo glaucoma progression, while others not.

The paper is organized as follows. In section 2 we describe our 1D corneal viscoelastic model to derive a practical expression for the corneal retardation time τ, as a function of the corneal applanation pressures and their first derivatives. A detailed explanation of our methods to calculate the τ parameter is performed in section 3, and our corneal retardation results concerning a population of 100 healthy young subjects is presented in section 4. Finally, we discuss and summarize our results in section 5.

2. Theoretical calculation of the corneal retardation time

Let us first introduce the theoretical model for the corneal biomechanics, in order to derive a simple and useful expression for the corneal retardation time τ (i.e. our crucial parameter which might be used as a plausible OHT disease indicator).

When loaded, the cornea demonstrates some instantaneous deformation (purely elastic behavior) followed by a progressive viscoelastic deflection. This trend can be fairly described by the Kelvin-Voigt viscoelastic model of three elements (KVM) (please, see figure 1) where the dashpot η symbolizes the time-dependent viscous resistance to the applied force, and springs E_1 and E_2 mimic the purely elastic behavior (Glass *et al* 2008). When a stress σ is applied, a corneal strain ϵ is induced. This configuration allows an instantaneous deformation of the cornea through spring E_2. More precisely, the right-hand spring E_2 stretches immediately upon loading. Then, the dashpot η then takes up the stress, transferring the load to the second spring E_1 as it slowly varies over time. Upon unloading, E_2 contracts immediately and the left-hand spring slowly shortens, being held back by the dashpot.

Though more sophisticated 1D rheological models have been recently studied (Jannesari *et al* 2018, Jimenez-Villar *et al* 2022), we have chosen the KVM over other viscoelastic approaches (such as the Zener or Burgers models) for two reasons: its ability to mimic the corneal response to an applied force (as above-mentioned, an instantaneous deformation followed by a progressive viscoelastic deflection) and the limited number of independent variables (thus, reducing its mathematical complexity). As currently

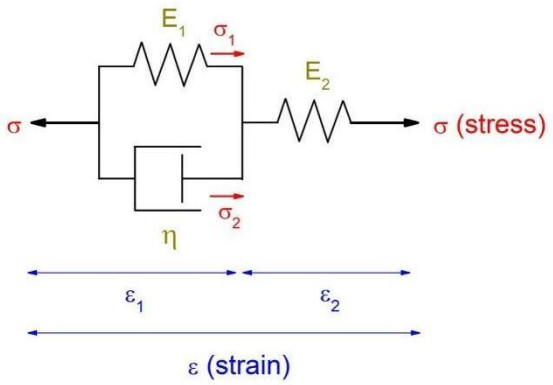

Figure 1. Kelvin-Voigt viscoelastic model of three elements for the corneal biomechanics. This configuration allows an instantaneous deformation of the cornea through spring E_2 and a progressive deflection though the parallel component of dashpot η and spring E_1. Upon unloading, E_2 contracts immediately and the left-hand spring slowly shortens, being held back by the dashpot.

explained by Torres *et al* (2022), the Kelvin-Voigt model is quite appropriate and straightforward to characterize the viscoelasticity of the cornea, as well as it has been experimentally validated with artificial phantom corneas (Glass *et al* 2008).

Our KVM relates the applied stress (σ) to the corneal strain (ϵ) through the following set of equations (Kelly 2013)

$$\begin{aligned} &\sigma = \sigma_1 + \sigma_2 \qquad \epsilon = \epsilon_1 + \epsilon_2 \qquad \sigma_1 = E_1\epsilon_1 \\ &\sigma = E_2\epsilon_2 \qquad \sigma_2 = \eta\dot{\epsilon}_1, \end{aligned} \tag{2.1}$$

and $\dot{\epsilon}_1$ corresponds to the strain rate of the parallel elements. Assuming the cornea to be axisymmetric, a single elastic constant should govern corneal behavior (Glass *et al* 2008), so we can identify $E_1 = E_2 = E$. After Laplace transforming, the constitutive relation can be written as (Kelly 2013)

$$E\epsilon + \eta\dot{\epsilon} = 2\sigma + \tau\dot{\sigma}, \tag{2.2}$$

where $\dot{\sigma}$ is the stress rate and $\tau = \eta/E$ stands for the corneal retardation time. The latter parameter describes the time dependent response of the cornea with respect to the applied load.

On the other hand, non-contact tonometers such as ORA applanate the cornea in two instants, when the strain is minimum. Consequently, the strain rate cancels at these applanation moments and $\dot{\epsilon} = 0$. So, from equation (2.2) we can write for the first applanation time $t_{ap,1}$

$$\begin{aligned} E\epsilon(t_{ap,1}) &= 2\sigma(t_{ap,1}) + \tau\dot{\sigma}(t_{ap,1}) \\ &= -2|\sigma(t_{ap,1})| + \tau|\dot{\sigma}(t_{ap,1})|, \end{aligned} \tag{2.3}$$

where it is assumed a compressive stress ($\sigma(t_{ap,1}) < 0$) during the load stage ($\dot{\sigma}(t_{ap,1}) > 0$). Moreover, for the second applanation time (also a compressive regime with $\sigma(t_{ap,2}) < 0$), we have

$$\begin{aligned} E\epsilon(t_{ap,2}) &= 2\sigma(t_{ap,2}) + \tau\dot{\sigma}(t_{ap,2}) \\ &= -2|\sigma(t_{ap,2})| - \tau|\dot{\sigma}(t_{ap,2})|, \end{aligned} \tag{2.4}$$

and now, during the unload process, $\dot{\sigma}(t_{ap,2}) < 0$. Provided that the strain at applanation is the same for both load-unload processes (i.e. $\epsilon(t_{ap,1}) = \epsilon(t_{ap,2})$), we obtain the following expression for the corneal retardation time τ from equations (2.3) and (2.4)

$$\tau = \frac{2(|\sigma(t_{ap,1})| - |\sigma(t_{ap,2})|)}{|\dot{\sigma}(t_{ap,1})| + \dot{\sigma}(t_{ap,2})}. \tag{2.5}$$

Let us now analyze how the different pressures act on the anterior and posterior corneal surfaces at applanation (please, see figure 2). The intraocular pressure IOP on the posterior surface of the cornea is subtracted to the sum of the tonometer applied pressure $P_t(t_{ap,i})$ and the tear film pressure s, so as to obtain the resultant intraocular pressure at applanation $P_r(t_{ap,i})$ (Liu and Roberts 2005, Glass *et al* 2008, Kotecha *et al* 2015)

$$P_r(t_{ap,i}) = P_t(t_{ap,i}) + s - \text{IOP}, \quad \text{for } i = 1, 2. \tag{2.6}$$

This radial stress $P_r(t_{ap,i})$ can be related to the membrane stress $\sigma(t_{ap,i})$ in the KVM via the Laplace law (Glass *et al* 2008)

$$\sigma(t_{ap,i}) = \frac{R_c}{2e}P_r(t_{ap,i}), \quad \text{for } i = 1, 2, \tag{2.7}$$

where R_c and e state for the corneal radius of curvature and corneal thickness, respectively. Therefore, introducing equation (2.7) into (2.5) and performing some elementary calculations, we derive the final expression for the corneal retardation time

$$\tau = \frac{2(|P_1| - |P_2|)}{|\dot{P}_1| + |\dot{P}_2|} = \frac{2\ \text{CH}}{|\dot{P}_1| + |\dot{P}_2|}, \tag{2.8}$$

where $P_i = P_t(t_{ap,i})$ are the tonometer applanation pressures, $\text{CH} = |P_1| - |P_2|$ the corneal hysteresis and $\dot{P}_i$ the tonometer applanation pressures rates. One observes that the corneal retardation time τ is directly related to CH, but with a clear different behaviour and physical meaning, as will be examined in the next sections.

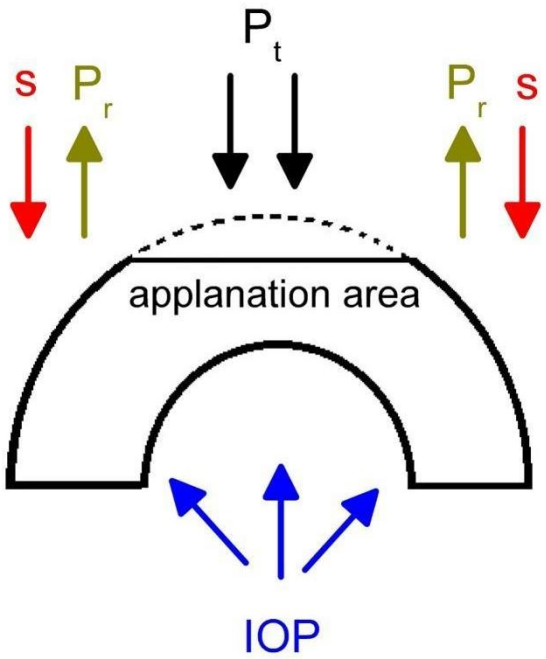

Figure 2. Pressures acting during applanation tonometry. The intraocular pressure IOP on the posterior surface of the cornea is subtracted to the sum of the tonometer applied pressure P_t and the tear film pressure s so as to obtain the resultant intraocular pressure at applanation P_r.

3. Methods

To our purpose, a total number of 200 eyes from 100 healthy European Caucasian subjects (mean age 24 ± 5 years old) were involved in the study. Within this group, about 10% had an elevated IOP with more than 21 mmHg, and only patient number #278 had been undergoing medical treatment for elevated IOP and diagnosed glaucoma disease during the measurements. The inclusion criterion was to be aged between 18 to 30 years old, whereas subjects with history of ocular pathologies, corneal injuries or surgery, contact lens wearers or irregular astigmatism were excluded. This study was reviewed by an ethical review board and conforms to the tenets of the Declaration of Helsinki (Ethical Committee of Research of the Health Sciences Institute of Aragón, Spain) approved with reference C.P.-C.I.PI20/377. All participants were informed about the nature of the project and signed an informed consent document.

Hence, participants involved in this study were divided into two groups: control (with intraocular pressure values less than 21 mmHg) and ocular hypertensive (where IOP_{cc} is greater or equal than 21 mmHg), all of them (as previously mentioned) healthy subjects without ophthalmological clinical manifestations, except for patient number #278 with diagnosed glaucoma disease (please, see table 1). This differentiation will be more necessary and evident when we study the corneal retardation time as a function of the intraocular pressure, as described in figure 7 of the next section.

The applanation pressure data were collected with the non-contact tonometer Ocular Response Analyzer (ORA®; Reichert Ophthalmic Instruments, Depew, NY) which measures, apart from the Goldmann-correlated IOP (IOP_g) and the corneal-compensated IOP (IOP_{cc}), some biomechanical properties such as the corneal hysteresis (CH) (related to the capacity of the cornea to absorb and dissipate energy) or the corneal resistance factor (CRF). This last metric is thought to be a better indicator of the corneal viscoelasticity than CH (Gatinel 2007).

The ORA device generates a 25 ms collimated air jet to deform the cornea and uses an infrared (IR) detection system in which the IR emitter is aligned on one side of the cornea with an IR detector (Roberts 2014). As the cornea deforms under the applied air pressure, it rapidly traverses a state of applanation, causing the reflected IR light to align with the detector. As a result, the captured light increases significatively and a spike in the IR signal is recorded. Hereafter, the cornea takes on a slight concave shape, to then move outward in another applanation state. Finally, the cornea recovers its normal configuration state. In our study, four measures were carried out for each subject's eye in order to get averaged values.

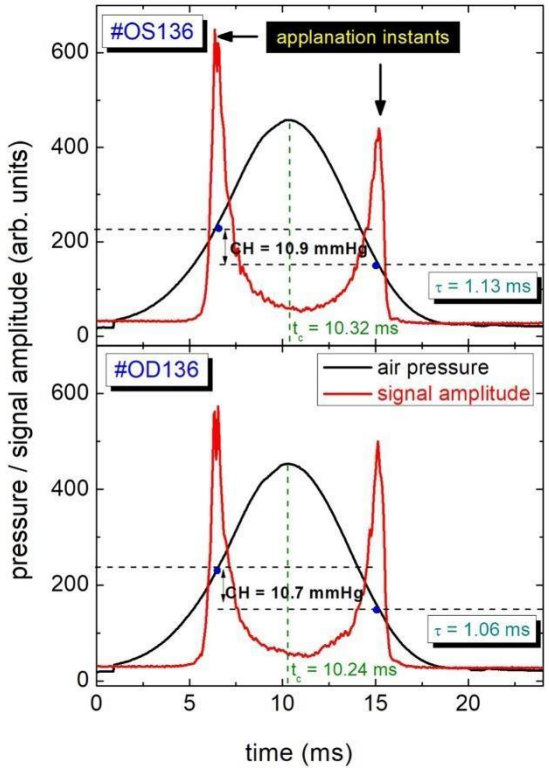

Figure 3. ORA's pressure and signal amplitudes for subject #136 in our population, where the upper (bottom) panel shows the results for the left (right) eye. The gaussian center t_c (located near the corneal concave state), corneal hysteresis CH and corneal retardation time τ (as calculated via equation (2.8)) are also shown.

Table 1. Control population and OHT subjects that participated in our study.

Control population ($IOP_{cc} < 21$ mmHg)	ocular hypertensive ($IOP_{cc} \geqslant 21$ mmHg)
90 subjects	10 subjects
mean $IOP_{cc} = (16.38 \pm 2.52)$ mmHg	mean $IOP_{cc} = (22.43 \pm 1.10)$ mmHg

In this sense, the accurate method to determine the corneal retardation time τ was performed via the two ORA's characteristic curves: the signal amplitude (corresponding to the IR light which is reflected off the surface of the cornea during perturbation) and the pressure amplitude (i.e. the external applied pressure $P_t(t)$ as depicted in figure 2). The last curve can be fairly fitted by the following gaussian profile ($0.985 < R^2 < 0.997$ in all cases)

$$P_t(t) = P_{t,0} + \exp\left[-0.5\left(\frac{t - t_c}{\Delta t}\right)^2\right], \qquad (3.1)$$

where Δt stands for the pressure amplitude width, and the gaussian center t_c is located near the corneal concave state. Hence, we have represented in figure 3 both the pressure and signal amplitudes versus time for subject #136 in our population, where the upper (bottom) panel shows the results for the left (right) eye. As easily noticed, the pressure curve conforms a clear gaussian shape in accordance with equation (3.1), where the gaussian center t_c is also depicted.

Once this gaussian fit is performed, the signal amplitude provides the two applanation pressures P_1 and P_2 (via the sharp peaks in both panels) and the corresponding corneal hysteresis CH (which resulted to be 10.9 mmHg for the left eye and 10.7 mmHg for the right eye, respectively). The pressure rates $\dot{P}_i$ can be analytically evaluated from the first derivatives of the tonometer pressures. Ergo, the corneal retardation time τ is calculated via equation (2.8) (for subject #136, this parameter was 1.13 (1.06) ms for the left (right) eye, respectively). These corneal retardation time results are fairly close to the average mean of the

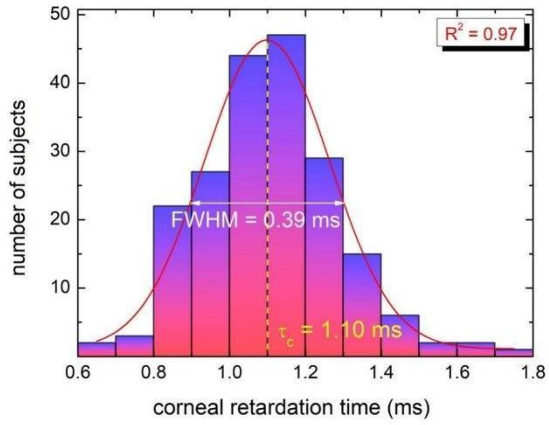

Figure 4. Histogram representation of the corneal retardation time τ of our study population (200 eyes from 100 young subjects) calculated via equation (2.8). A clear gaussian shape ($R^2 = 0.97$) centered at 1.10 ms and FWHM of 0.39 ms is found. Elastic corneas are associated with low τ values (about 13.5% in our case) while elevated corneal retardation times are related to more viscoelastic corneas (roughly a 13% of our population).

total population, as explained in detail in the next section.

4. Results

In this section we deal with the fundamental results concerning the corneal retardation time of our young population, and its important relationship with the intraocular pressure IOP.

To this aim, the histogram illustrated in figure 4 shows the corneal retardation time τ (calculated via equation (2.8)) of the 100 subjects that participated in the study. It can be observed an explicit gaussian profile centered at 1.10 ms with a full width half maximum (FWHM) of 0.39 ms. The R-squared parameter for this gaussian fit was 0.97. In view of these results it can be assumed that for a young and healthy population, the corneal retardation time should be ranged between 0.90 and 1.30 ms, where more elastic corneas are associated with low τ values (about 13.5% in our case). In addition, elevated corneal retardation times are related to viscoelastic corneas (roughly a 13% of our population), not necessarily being pathological cases those subjects with upper or lower τ values (though, in the later scenario, a clear connection with higher intraocular pressures is found, as briefly discussed).

On the other hand, it is expected that our biomechanical parameter should be directly correlated to the time interval between the two applanation times Δt_{ap}. That is, more elastic (viscoelastic) corneas, which entail lower (higher) τ values, might take less (more) time during the applanation interval. In such a case (not shown in this work), the linear coefficient of determination resulted to be $R^2 = 0.46$ for $\Delta t_{ap} = t_{ap,2} - t_{ap,1}$. Subsequent data analysis (please, see figure 5) demonstrated that the optimized time interval corresponded to $\Delta t_{ap,opt} = 1.5t_{ap,2} - 0.5t_{ap,1}$, where now $R^2 = 0.72$. This time lapse is depicted in the inset of figure 5, however different applanation time intervals might also be considered for our study (with $R^2 > 0.45$, in all cases). As a matter of fact, the optimized time interval for subject #OS231 was 18.46 ms, fairly shorter than patient #OS174 with a time lapse of 20.49 ms. This may be interpreted assuming that the cornea of the former subject is more elastic (that is, it takes less time between both applanation times) than subject #OS174, with a more viscoelastic cornea. Moreover, these findings should be affected by the intraocular pressure, because elastic corneas with low IOP values might take longer to recover its original shape than viscoelastic corneas of OHT subjects. This relationship between the τ parameter and the IOP will be treated in detail shortly.

But before embarking on this study, let us first analyze an important biomechanical parameter like the corneal hysteresis CH and its dependence on the corneal-compensated IOP_{cc} in our population (please, see figure 6). Assuming that normal IOP ranges from 10 to 21 mmHg (Badakere *et al* 2021), one notices that both parameters are not correlated, in consistency with previous published work (Luce 2005), where no statistical significance was found. For this reason, we have not differentiated between control and OHT populations. Nevertheless, it can be observed that low CH values (such as subjects #OD278 or #OS231) also possess high intraocular pressures and an possible risk of glaucoma progression. This result agrees with prior reported research, where low corneal hysteresis is thought to be related to the risk and development of glaucoma (Prata *et al* 2012, Deol *et al* 2015), though there is no consensus on this topic. As stated by Roberts (2014), low CH should not be interpreted as a

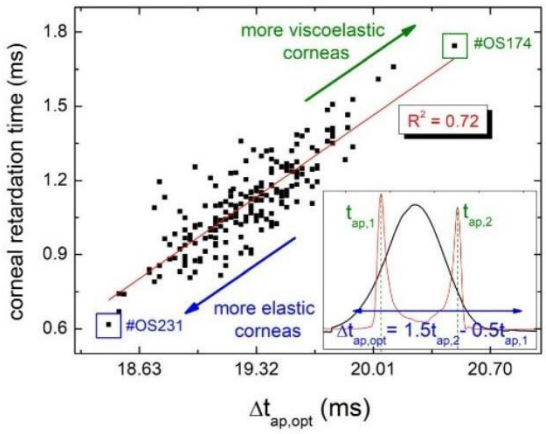

Figure 5. Corneal retardation time τ of our study population versus the optimized time interval $\Delta t_{ap,opt}$ (over which the biomedical data are highly correlated, with $R^2 = 0.72$). The inset shows more clearly this optimized applanation lapse. It can also be appreciated that lower (higher) τ values correspond to more elastic (viscoelastic) corneas.

damaged cornea, and further work is required to determine what component contributing to this viscoelastic parameter correlates to damage at the optic nerve. In our study, when the corneal hysteresis CH is divided by the sum of the first derivatives of the applanation pressures $\dot{P}_i$ (please, see again equation (2.8)), the uncorrelated scheme illustrated in figure 6 turns to a well-defined linear dependence, as immediately discussed.

Accordingly, our fundamental result is exhibited in figure 7(a) where the corneal retardation time τ is represented as a function of IOP_{cc}. Now, a clear linear dependence is found (with a coefficient of determination $R^2 = 0.70$), where lower τ values are mostly associated with higher intraocular pressures. This can be easily understood since more pressurized corneas will behave more elastically than those with lower IOPs. So, for instance, subjects #OD170 or #OS174 have the highest τ values in our study (which should be connected with small IOPs) but it cannot be assured that such corneas are the most viscoelastic of our population. This fact should be corroborated with a relevant number of ocular hypotony patients, though it does not constitute a subject of study in our current research.

Nonetheless, this is not a fundamental rule. Indeed, after inspection of figure 7(a), one notices that for similar IOP_{cc} values (such as for subjects #231, #193 or #278), the corneal viscoelastic behavior is different. Whereas subject #193 possess good viscoelastic corneas for both eyes (greater than the average of 1.10 ms, as illustrated in figure 4), other OHT patients like #231 or #278 have more elastic corneas (that is, with lower τ values). This means that the corneas of subject #193 would be more prepared to absorb IOP fluctuations (and avoid possible glaucoma progression) than the other OHT patients. As a consequence, hypertensive subjects with low corneal retardation times should be periodically monitored, in order to prevent possible optical nerve damage. Moreover, even normal IOP subjects present significant differences between their τ values, although these patients are not considered as a "risky population". In this sense, at a normal IOP of 18.4 mmHg (please note the vertical dashed line in figure 7), subject #OD209 exhibits a more elastic cornea (0.79 ms) than patient #OS224, where the corneal retardation time resulted to be 1.24 ms (a 57% higher than the latter). Additionally, the corneal elasticity of subject #OD209 (quantified by our τ parameter) is similar to some OHT patients in our study, so such normal IOP subjects should also be controlled, despite they do not belong to a risk group.

For the sake of clarity, we have also illustrated the corneal retardation time τ for the control population (Figure 7(b)) and OHT subjects (Figure 7(c)). Clearly, the linear correlation between the τ parameter and the intraocular pressure IOP_{cc} for the control group is even increased (as compared to the whole population), while no significant correlation for OHT subjects is found. This fact reflects the difficulty in predicting the corneal retardation time for our ocular hypertensive population, probably due to the small number of OHT participants in our study (please, see again table 1).

5. Discussion

Summarizing, a detailed analysis of the corneal retardation time τ of a young population (200 eyes from 100 healthy subjects) has been carried out. Our results show that this parameter is highly correlated with the corneal-compensated intraocular pressure IOP_{cc} supplied by ORA tonometer, underlying the risk for OHT subjects with lower τ values to develop

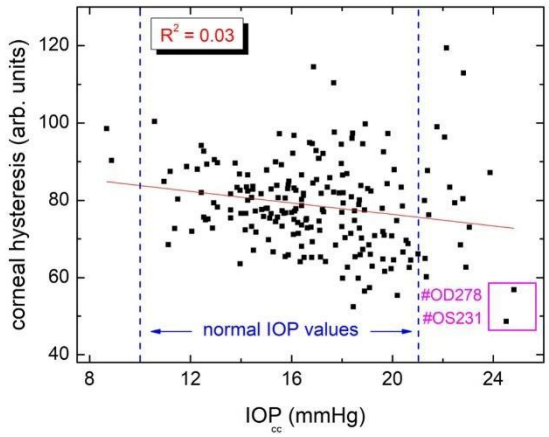

Figure 6. Corneal hysteresis CH as a function of the corneal-compensated intraocular pressure IOP_{cc} for our study population. It can be noticed that both parameters are highly uncorrelated, in consistency with previous reported research (Luce 2005). On the other hand, low CH subjects like #OD278 or #OS231 possess high intraocular pressures and an possible risk of glaucoma progression.

hypertension diseases (due to the inability of the poorly viscoelastic cornea to absorb IOP fluctuations). Indeed, viscous damping of the cornea should be crucial since increased damping capacity of the eye may actually buffer hazardous IOP fluctuations, diminishing the stress/strain on the optic nerve and peripapillary scleral tissues (Kaushik and Pandav 2012).

Furthermore, some authors argue that IOP_{cc} is overestimated (Martinez *et al* 2006) in comparison with the gold standard technique in measuring IOP, that is, the Goldmann applanation tonometry (Lee *et al* 2018). Thus, a possible discrepancy between our results for the τ parameter and the corneal-compensated intraocular pressure should be expected. However, given that all IOP_{cc} values in our population might be affected by the same (or similar) scale factor, the linear dependence depicted in figure 7 should remain the same, with comparable R-squared parameters.

As previously stated, the fundamental aim of our work is to yield an useful tool (i.e. the corneal retardation time τ) to systematically discern which ocular hypertensive patients are more likely to develop OHT diseases and ensure an early diagnosis. Among them, glaucoma plays a leading role since this eye illness is the most common cause of irreversible blindness and affects about 80 million people worldwide, with many more undiagnosed (Tribble *et al* 2023).

In this sense, our work might help in glaucoma diagnosis (as compared to previous existing methods already mentioned in the Introduction) due to the easiness and robustness of our method. More specifically, it is straightforward to measure the corneal retardation time τ with non-contact tonometers (i.e. via our equation (2.8) and the applanation pressures provided by such instruments). Besides, these values are not affected by subjective or qualitative factors, so the τ parameter can be considered a strong biomechanical indicator not subject to intra- or interobserver variabilities. Also, it has been suggested in the literature that increased viscoelasticity of ocular tissues may have a protective role in glaucoma (Murphy *et al* 2017, Del Buey-Sayas *et al* 2021), so the τ parameter could be an important metric to diagnose this disease, playing a leading role in explaining normotensive glaucoma. Instead, our method does not provide information about structural changes in the optic nerve head or the retinal nerve fiber layer, so a proper glaucoma diagnosis might not be guaranteed (and other techniques such as the fundus photography or optical coherence tomography are needed).

It has been widely reported in the literature that the major risk factors for glaucoma are genetics, age and an elevated IOP, so, intraocular pressure should be adequately controlled to avoid visual field deterioration. Beyond the diagnosis, the prediction of the future glaucoma progression of an individual patient is often extremely difficult for clinicians, due to the mix of the abovementioned risk factors. In this regard, corneal thickness, corneal hysteresis or horizontal and vertical cup-disc ratio constitute additional OHT risk factors (apart from an elevated IOP). As reported by Murphy *et al* (2017), about 3050% of glaucoma patients have normal IOP values, becoming evident that other elements should be taken into account. Provided the large number of independent risk factors, it might not seem plausible that a unique parameter as the corneal retardation time would effectively serve as a OHT indicator.

Nevertheless, the validity of our theoretical approach (as given by the fundamental equation (2.8) for the τ parameter) is based on the strength of the Kelvin-Voigt model to imitate the corneal viscoelastic

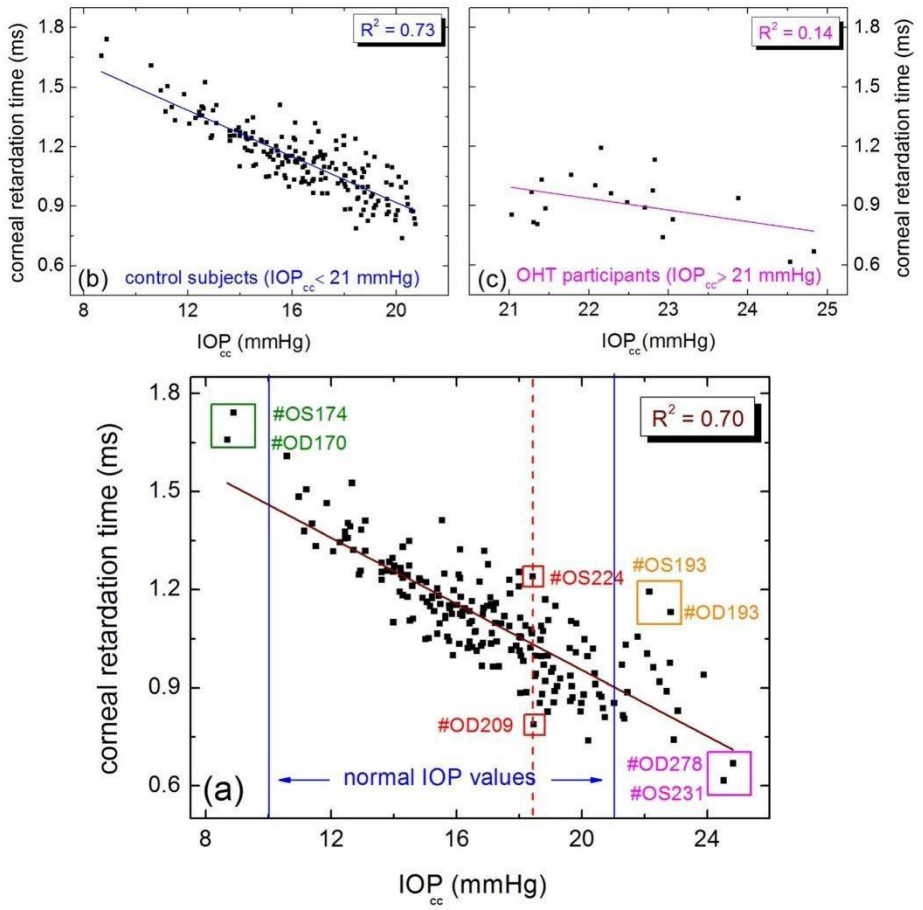

Figure 7. (a) Corneal retardation time τ of our study population (calculated via equation (2.8)) as a function of the corneal-compensated IOP_{cc} given by ORA. It can be observed that both parameters are highly correlated with a linear coefficient of determination $R^2 = 0.70$. On the other hand, it can be argued that OHT subjects like #OD278 (who was receiving medication for elevated IOP and possess a particularly elastic cornea with $\tau = 0.67$ ms) should be more likely to develop glaucoma than other OHT subjects with more viscoelastic corneas (like patient #OS193 in our population). Furthermore, the upper panels represent the τ parameter for (b) our control population and (c) OHT participants. A clear linear correlation is found for the control group, while no significant correlation is obtained for our OHT population.

behaviour. In other words, the τ metric constitutes a valuable indicator of the corneal viscoelastic quality. However, its validity is subject to obtaining well-defined signals via non-contact tonometers (please, see again figure 3): irregular signals with no evident applanation peaks will not give reliable corneal retardation time values.

In fact, our proposal is consistent with previous reported glaucoma research (Matsuura *et al* 2017) where it is suggested that careful consideration should be given to patients whose eyes are applanated fast in the first and second applanations (please, see again our fundamental results concerning the applanation time interval in figure 5, which are directly related to the τ parameter shown in figure 7(a)). Additionally, the loss of corneal viscoelasticity (which is correlated with lower τ values in our model) is a risk factor that can lead an ocular hypertensive subject to develop glaucoma disease (Roberts *et al* 2023). For that matter, the corneal retardation time might represent an early detector of those complications associated with ocular hypertension before clinical signs manifest. Nonetheless, such suspected glaucoma patients should be periodically monitored to confirm this fact.

Among the potential limitations encountered during our study, we can mention the reduced number of OHT subjects (in comparison with the normal IOP patients) and the difficulty in finding some OHT clinical cases. It is worth mentioning that our young study population consisted of 100 healthy subjects and, within this group, about 10% had an elevated IOP with more than 21 mmHg (only patient #278 was medically monitored due to its high IOP). Certainly, an increased number of OHT subjects is needed for a

conclusive statement about the utility of the corneal retardation time as an ocular hypertension disease indicator. Moreover, it could be interesting to include participants with pathological conditions such as diabetic retinopathy or glaucoma for a more comprehensive analysis, as well as considering another age group. In addition, it should be studied the effects of physical parameters such as central corneal thickness (CCT) or corneal morphology on corneal biomechanics (in line with the proposals by Marcellán *et al* 2022) which is a subject of ongoing research by our group.

Acknowledgments

Oscar del Barco gratefully thanks Alfonso Jimenez Villar for helpful discussions on 1D corneal rheological models. The authors acknowledge the funding grant from Departamento de Ciencia, Universidad y Sociedad del Conocimiento del Gobierno de Aragón (research group E44−23R).

Data availability statement

The data cannot be made publicly available upon publication because they contain sensitive personal information. The data that support the findings of this study are available upon reasonable request from the authors.

Conflicts of interest

The authors declare no conflict of interest.

ORCID iDs

Oscar del Barco https://orcid.org/0000-0001-7502-9164
Francisco J Ávila https://orcid.org/0000-0002-9068-7728
Concepción Marcellán https://orcid.org/0000-0002-7516-3029
Laura Remón https://orcid.org/0000-0002-3979-4528

References

Ambrósio R *et al* 2017 Integration of scheimpflug-based corneal tomography and biomechanical assessments for enhancing ectasia detection *J. Refract. Surg.* **33** 434–43
Anderson D R 2003 Collaborative normal tension glaucoma study *Curr. Opin. Ophthalmol.* **14** 86–90
Ariza-Gracia M A *et al* 2015 Coupled biomechanical response of the cornea assessed by non-contact tonometry a simulation study *PLoS One* **10** e0121486
Asejczk-Widlicka M *et al* 2019 Data analysis of the ocular response analyzer for improved distinction and detection of glaucoma *J. Opt. Soc. Am.* A **36** B71–6
Badakere S V *et al* 2021 Agreement of intraocular pressure measurement of icare ic200 with goldmann applanation tonometer in adult eyes with normal cornea ophthalmol *Glaucoma* **4** 238–43
Brinson H F and Brinson L C 2008 *Polymer Engineering Science and Viscoelasticity* (Springer) (https://doi.org/10.1007/978-0-387-73861-1)
Brown L *et al* 2018 The influence of corneal biomechanical properties on intraocular pressure measurements using a rebound self-tonometer *J. Glaucoma* **27** 511–8
Catania F *et al* 2023 Corneal biomechanics assessment with ultra high speed scheimpflug camera in primary open angle glaucoma compared with healthy subjects: a meta-analysis of the literature *Curr. Eye Res.* **48** 161–71
Chakrabarti L *et al* 2016 Automated detection of glaucoma from topographic features of the optic nerve head in color fundus photographs *J. Glaucoma* **25** 590–7
Chan E *et al* 2021 Changes in corneal biomechanics and glaucomatous visual field loss *J. Glaucoma* **30** 246–51
Consejo A *et al* 2019 *Corneal Properties of Keratoconus Based on Scheimpflug Light Intensity Distribution Investig. Ophthalmol. Vis. Sci.* **60** 3197–203
De Moraes C G *et al* 2012 Effect of treatment on the rate of visual field change in the ocular hypertension treatment study observation group *Invest. Ophthalmol. Vis. Sci.* **53** 1704–9
Del Buey-Sayas M A *et al* 2021 Corneal biomechanical parameters and central corneal thickness in glaucoma patients, glaucoma suspects, and a healthy population *J. Clin. Med.* **10** 2637
Deol M *et al* 2015 Corneal hysteresis and its relevance to glaucoma *Curr. Opin. Ophthalmol.* **26** 96–102
Fraldi M *et al* 2016 Visco-elastic and thermal-induced damaging in time-dependent reshaping of human cornea after conductive keratoplasty *Mech. Time-Depend. Mater.* **21** 45–59
Garcia-Porta N *et al* 2014 *Corneal biomechanical properties in different ocular conditions and new measurement techniques ISRN Ophthalmol* **2014** 724546
Gatinel D 2007 Evaluating biomechanic properties of the cornea Cataract. Refract *Surg. Today Eur.* **25** 36–9
Geevarghese A *et al* 2021 *Optical Coherence Tomography and Glaucoma Annu. Rev. Vis. Sci. 15;7* 693–726
Glass D H *et al* 2008 A viscoelastic biomechanical model of the cornea describing the effect of viscosity and elasticity on hysteresis *Invest. Ophthalmol. Vis. Sci.* **49** 3919–26
González-Méijome J M *et al* 2008 Pilot study on the influence of corneal biomechanical properties over the short term in response to corneal refractive therapy for myopia *Cornea* **27** 421–6
Grise-Dulac A *et al* 2012 Assessment of corneal biomechanical properties in normal tension glaucoma and comparison with open-angle glaucoma, ocular hypertension, and normal eyes *J. Glaucoma* **21** 486–9
Hager A *et al* 2008 Effect of central corneal thickness and corneal hysteresis on tonometry as measured by dynamic contour tonometry, ocular response analyzer, and Goldmann tonometry in glaucomatous eyes *J. Glaucoma* **17** 361–5
Han Z *et al* 2014 Air puff induced corneal vibrations: theoretical simulations and clinical observations *J. Refract. Surg.* **30** 208–13
Jannesari M *et al* 2018 Numerical and clinical investigation on the material model of the cornea in Corvis tonometry tests: differentiation between hyperelasticity and viscoelasticity *Mech. Time Depend. Mater.* **23** 373–84
Jimenez-Villar A *et al* 2022 Rheological eye model to determine elastic and viscoelastic properties of the cornea and crystalline lens *Invest. Ophthalmol. Vis. Sci.* **63** 2395–A0198
Kass M A *et al* 2002 The ocular hypertension treatment study: a randomized trial determines that topical ocular hypotensive medication delays or prevents the onset of primary open-angle glaucoma *Arch. Ophthalmol.* **120** 701–13
Kaushik S and Pandav S S 2012 Ocular response analyzer *J. Curr. Glaucoma Pract.* **6** 17–9
Kelly P 2013 Solid mechanics part I: an introduction to solid mechanics *Solid Mechanics Lecture Notes* University of Auckland (https://pkel015.connect.amazon.auckland.ac.nz/SolidMechanicsBooks/Part_I/index.html)

Kok S *et al* 2014 Calibrating corneal material model parameters using only inflation data: an ill-posed problem *Int. J. Numer. Methods Biomed. Eng.* **30** 1460–75
Kotecha A *et al* 2015 Tonometry and intraocular pressure fluctuation *Glaucoma* **1** 98–108
Lee S Y *et al* 2018 Utility of Goldmann applanation tonometry for monitoring intraocular pressure in glaucoma patients with a history of laser refractory surgery *PLoS One* **13** e0206564
Lee K M *et al* 2019 Association of corneal hysteresis with lamina cribrosa curvature in primary open angle glaucoma *Invest. Ophthalmol. Vis. Sci.* **60** 4171–7
Lemij H G and Reus N J 2008 New developments in scanning laser polarimetry for glaucoma *Curr. Opin. Opthalmol.* **19** 136–40
Liu J and Roberts C J 2005 Influence of corneal biomechanical properties on intraocular pressure measurement: quantitative analysis *J. Cataract Refract. Surg.* **31** 146–55
Liu T *et al* 2020 Characterization of hyperelastic mechanical properties for youth corneal anterior central stroma based on collagen fibril crimping constitutive model *J. Mech. Behav. J. Mech. Behav.* **103** 103575
Luce D A 2005 Determining in vivo biomechanical properties of the cornea with an ocular response analyzer *J. Cararact. Refract. Surg.* **31** 156–62
Maczynska E *et al* 2019 Assessment of the influence of viscoelasticity of cornea in animal ex vivo model using air-puff optical coherence tomography and corneal hysteresis *J. Biophotonics* **12** e201800154
Marcellán M C *et al* 2022 Corneal hysteresis and intraocular pressure are altered in silicone-hydrogel soft contact lenses wearers *Int. Ophthalmol.* **42** 2801–9
Martinez J M *et al* 2006 Ocular response analyzer versus goldmann applanation tonometry for intraocular pressure measurements *Invest. Ophthalmol. Vis. Sci.* **47** 4410–4
Matlach J *et al* 2019 Investigation of intraocular pressure fluctuation as a risk factor of glaucoma progression *Clin. Ophthalmol.* **13** 9–16
Matsuura M *et al* 2017 Using CorvisST tonometry to assess glaucoma progression *PLoS One* **12** e0176380
Medeiros F A and Weinreb R N 2006 Evaluation of the influence of corneal biomechanical properties on intraocular pressure measurements using the ocular response analyzer *J. Glaucoma* **15** 364–70
Murphy M L *et al* 2017 Corneal hysteresis in patients with glaucoma-like optic discs, ocular hypertension and glaucoma *BMC Ophthalmol.* **17** 1–8
Ortiz D *et al* 2007 Corneal biomechanical properties in normal, postlaser in situ keratomileusis, and keratoconic eyes *J. Cataract Refract. Surg.* **33** 1371–5
Padmanabhan P and Elsheikh A 2023 Keratoconus: A Biomechanical Perspective *Curr. Eye Res.* **48** 121–9
Prata T S *et al* 2012 Association between corneal biomechanical properties and optic nerve head morphology in newly diagnosed glaucoma patients *Clin. Experiment. Ophthalmol.* **40** 682–8
Roberts C J 2014 Concepts and misconceptions in corneal biomechanics *J. Cararact. Refract. Surg.* **40** 862–9
Roberts C J *et al* 2023 Comparison of elastic and viscoelastic biomechanical metrics in ocular hypertension and normal controls *Invest. Ophthalmol. Vis. Sci.* **64** 4720
Roy A S and Dupps W J Jr. 2011 Patient-specific computational modeling of keratoconus progression and differential responses to collagen cross-linking *Investig. Ophthalmol. Vis. Sci.* **52** 9174–87
Sánchez P *et al* 2014 Biomechanical and optical behavior of human corneas before and after photorefractive keratectomy *J. Cataract Refract. Surg.* **40** 905–17
Sharma P *et al* 2008 Diagnostic tools for glaucoma detection and management *Surv. Ophthalmol.* **53** S17–32
Simonini I *et al* 2016 Theoretical and numerical analysis of the corneal air puff test *J. Mech. Phys. Solids* **93** 118–34
Susanna B N *et al* 2019 Corneal biomechanics and visual field progression in eyes with seemingly well-controlled intraocular pressure *Ophthalmology* **126** 1640–6
Torres J *et al* 2022 Torsional wave elastography to assess the mechanical properties of the cornea *Sci. Rep.* **12** 8354
Tribble J R *et al* 2023 Neuroprotection in glaucoma: Mechanisms beyond intraocular pressure lowering *Mol. Aspects Med.* **92** 101193
Whitford C *et al* 2018 A viscoelastic anisotropic hyperelastic constitutive model of the human cornea *Biomech. Model. Mechanobiol.* **17** 19–29
Yaghoubi M *et al* 2015 Confocal scan laser ophthalmoscope for diagnosing glaucoma: a systematic review and meta-analysis *Asia Pac. J. Ophthalmol.* **4** 32–9

2.4. *In Vivo* Biomechanical Response of the Human Cornea to Acoustic Waves.

Ávila FJ, Marcellán MC, Remón L. *In Vivo* Biomechanical Response of the Human Cornea to Acoustic Waves. *Optics*. 2023; 4(4):584-594. https://doi.org/10.3390/opt4040043

JIF (2023):1,1-Optics-94/119-Q4

JCI (2023): 0,31-Optics-97/120-Q4

optics

MDPI

Article

In Vivo Biomechanical Response of the Human Cornea to Acoustic Waves

Francisco J. Ávila *, Maria Concepción Marcellán and Laura Remón

Departamento de Física Aplicada, Facultad de Ciencias, Universidad de Zaragoza, 50009 Zaragoza, Spain; mcvidosa@unizar.es (M.C.M.); lauremar@unizar.es (L.R.)
* Correspondence: avila@unizar.es

Abstract: The cornea is the optical window to the brain. Its optical and structural properties are responsible for optical transparency and vision. The shape, elasticity, rigidity, or stiffness are due to its biomechanical properties, whose stability results in ocular integrity and intraocular pressure dynamics. Here, we report in vivo observations of shape changes and biomechanical alterations in the human cornea induced by acoustic wave pressure within the frequency range of 50–350 Hz and the sound pressure level of 90 dB. The central corneal thickness (CCT) and eccentricity (e^2) were measured using Scheimpflug imaging and biomechanical properties [corneal hysteresis (CH) and intraocular pressure (IOP)] were assessed with air-puff tonometry in six young, healthy volunteers. At the specific 150 Hz acoustic frequency, the variations in e^2 and CCT were 0.058 and 7.33 µm, respectively. Biomechanical alterations were also observed in both the IOP (a decrease of 3.60 mmHg) and CH (an increase of 0.40 mmHg).

Keywords: corneal biomechanics; corneal resonance; acoustic vibrometry

check for updates

Citation: Ávila, F.J.; Marcellán, M.C.; Remón, L. In Vivo Biomechanical Response of the Human Cornea to Acoustic Waves. *Optics* **2023**, *4*, 584–594. https://doi.org/10.3390/opt4040043

Academic Editors: Yongji Liu and Thomas Seeger

Received: 21 September 2023
Revised: 25 October 2023
Accepted: 14 November 2023
Published: 17 November 2023

1. Introduction

Corneal biomechanics [1,2] depends on the distribution of the collagen fibers within the stroma. The corneal type-I fibrillary collagen arrangement allows the maintenance of the three-dimensional structure and transparency of the corneal stroma [3]. Knowledge of the biomechanical properties (BMPs) of the cornea allows us to ensure the success of refractive surgery [4] or the diagnosis and follow up of corneal pathologies such as keratoconus, a progressive degeneration that can lead to corneal transplantation.

The clinical relevance of BMPs has attracted special interest with the development of surgery techniques to modify the refractive power of the cornea via laser ablation [5] or lenticular extraction [6]. These techniques consist of modify the lamellar structure of the cornea, causing redistribution of mechanical stress. The biomechanical response is expected to provide the correct corneal curvature [7,8] and normal vision.

Various methods based on different inherent principles have been developed to characterize corneal biomechanics in vivo. The most commonly used approaches involve the use of air-puff tonometry, such as the Ocular Response Analyzer (ORA), which is a non-invasive device that measures the intraocular pressure (IOP) and corneal biomechanics, including corneal hysteresis (CH) and corneal resistance factor (CRF) parameters [9]. The ORA device has been extensively used to explore the impact of corneal biomechanics on myopia development [10], asymmetry of visual field defects in glaucoma [11], the effect of soft contact lens use in healthy subjects [12], or corneal changes due to degenerative keratoconus disease [13].

The development of optical techniques, such as the Scheimpflug camera or optical coherence tomography (OCT), allows the direct monitoring of corneal deformation following air perturbations (e.g., CORVIS ST) [14,15]. In recent years, new technologies, including Brillouin microscopy [16] and corneal elastography techniques [17,18], have emerged as potential tools for in vivo corneal biomechanical evaluation. Moreover, the

finite element methods (a type of in silico method) are playing a fundamental role in corneal modelling simulations in several studies to evaluate and establish predictive models of corneal biomechanics [19–21].

Due to its inherent elastic properties, the cornea can behave as a biomechanical resonance system under the action of certain mechanical vibrations [22], and then the cornea can be considered a biomechanical resonant oscillator when external perturbations are applied [23,24].

In this respect, sound-induced corneal vibrometry has previously been reported to explore the corneal vibrational modes. Akca et al. [25] reported the visualization of the resonance modes of ex vivo corneas using low-power sound waves and OCT imaging. In addition, these vibrational resonance modes of the cornea are sensitive to the IOP [26].

Therefore, the corneal resonance induced by acoustic waves seems to be sensitive to both the shape and the biomechanics of the cornea. This work presents an acoustic wave generator to induce subtle modifications in corneal shape that can alters corneal biomechanics within the physiological range. We show the first in vivo observations of corneal biomechanics and shape changes due to acoustic pressure within the range 50–350 Hz at a maximum pressure level of 90 dB. The technique utilizes an arbitrary waveform generator, a sound amplifier, a subwoofer, a Scheimpflug camera (Galilei G2; Ziemer Ophthalmic Systems AG, Port, Switzerland), and an ORA (Reichert Instruments, Depew, NY, USA) tonometer. Shape parameters, including the CCT and e^2, and biomechanical measure (CH and IOP) changes were analyzed in six healthy volunteers as a function of the oscillating frequency of the sound wave generator.

2. Materials and Methods

2.1. Experimental Corneal Acoustic Wave Generator

Figure 1a shows a schematic diagram of the custom-built instrument. The acoustic waves are generated via a function/arbitrary waveform (FWG) generator (RSGD 805, RS PRO, RS Components Ltd, Northants, UK) with maximum output frequency of 5 MHz, 125 MSa/s sample rate, and resolution frequency of 1 µHz (14-bit vertical resolution). The output wave can be generated as a sine, square, ramp, pulse, Gaussian noise, or arbitrary forms. The output is connected to a sound amplifier (SA), which drives a full-range subwoofer (SW) (FR8, VISATON GmbH & Co, Haan, Germany) to produce acoustic pressure at the corneal plane. Figure 1 shows a real picture of the set up, vertically orientated for clinical measurements.

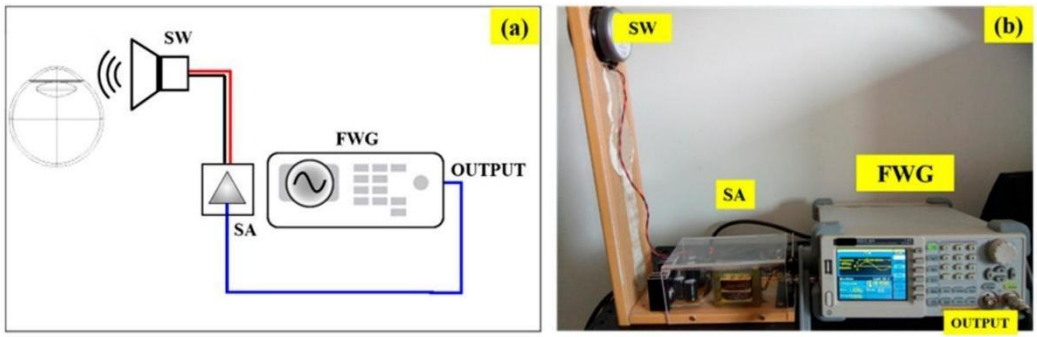

Figure 1. (**a**) Schematic of the corneal acoustic wave generator. (**b**) Real picture of the apparatus in real-time operation. FWG represents the waveform generator for acoustic waves, SA is the sound amplifier, and SW is a subwoofer that emits the sound wave directed towards the eyeball.

2.2. Instrument Calibration

A sinusoidal waveform signal was generated at the FWG for two different amplitudes (peak-to-peak voltage): 1 and 2 Vpp. The sound pressure level was measured in dB

using a digital sound meter placed at 100 mm from the SW, as a function of the signal frequency. Figure 2 shows the measured acoustic pressure (dB) for a frequency range between 50 and 350 Hz (with a step size of 50 Hz) for two different amplitude values. For in vivo corneal testing, we chose the lower amplitude that provided a maximum pressure of 90 dB at the maximum frequency (350 Hz), with a modulation of 11 dB within the range of tested frequencies.

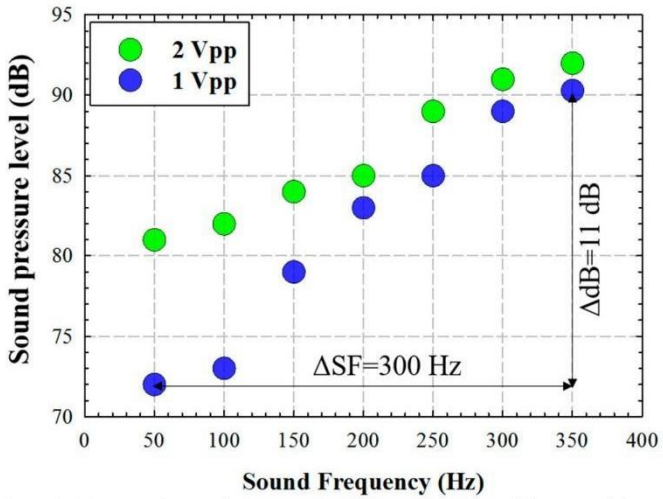

Figure 2. Measured sound pressure (in dB) as a function of the sound frequency for two different Vpp amplitudes generated at the FWG.

2.3. Experimental Measurements

Six volunteers (33 ± 9 years old) were included in the study. The measurements were carried out at the Visual Science and Instrumentation Lab of the University of Zaragoza (Zaragoza, Spain). The participants did not have any ocular diseases, glaucoma, or corneal complications that could affect the measurements. Dual Placido–Scheimpflug imaging (Galilei G2) and air-puff tonometry (ORA) commercial devices (ORA, Reichert Instruments, Depew, NY, USA) were employed to obtain morphometric data for shape characterization and biomechanical assessment, respectively, as shown in Table 1.

Table 1. Summary of the parameters measured in the experimental procedure. CCT: central corneal thickness; IOP: intraocular pressure; CH: corneal hysteresis.

Shape Parameters	Biomechanical Parameters
CCT (μm)	IOP (mmg)
Eccentricity (e^2)	CH (mmHg)

2.3.1. Galilei Dual Scheimpflug Analyzer: Shape Parameters

The Galilei Dual Scheimpflug Analyzer (Galilei G2; Ziemer Ophthalmic Systems AG, Port, Switzerland) is an advanced clinical optical system that combines Placido Disk imaging with a revolving Scheimpflug camera [14]. This integration allows for the simultaneous capture of corneal topography information from both the internal and external surfaces of the cornea. The device captures two corneal images for each analyzed meridian, and the Galilei G2 software (version G4) overlays these images to enhance the accuracy of corneal parameter estimation. The central corneal thickness (CCT) and eccentricity (e^2) were extracted for each participant and sound frequency. Three measurements of good quality, as indicated via the Galilei G2 software, were captured at each session to assess repeatability, using the 16-picture (i.e., 16 corneal meridians) scan mode. Corneal shape involved the CCT

and e^2 measures. While variations in CCT correspond to tissue compression, eccentricity values reveal the rate of corneal flattening due to sound pressure waves.

2.3.2. Ocular Response Analyzer: Biomechanical Assessment

Ocular Response Analyzer (ORA, Reichert Instruments, Depew, NY, USA) is a non-contact air-puff applanation tonometer that provides corneal hysteresis (CH) and corneal resistance factor (CRF) measurements [9]. CH refers to the dissipation of energy when an external stress is applied to the cornea. Unlike purely elastic materials that immediately return to their initial state once the stress is removed, the cornea exhibits time-dependent stress. On the other hand, the CRF measures the resistance of the cornea, encompassing aspects of rigidity and/or elasticity. CH and the IOP were measured for each volunteer for different sound wave frequencies. Each experimental measurement was the average of four measurements of good quality.

2.3.3. Pneumatic Viscoelastic Damping

CH deals with the inherent viscous damping nature of the human cornea [27]. CH can be defined as the biomechanical property that describes the biophysics of the corneal viscoelastic nature when the tissue is deformed by an external load (air pulses). In that sense, CH is the corneal capability to absorb and dissipate energy such as mechanical stress or intraocular pressure [28].

The proposed method delivers sound waves to the corneal tissue with a sine-wave form at a given amplitude and angular frequency (see Section 2); those waves create back-and-forth oscillations of the air molecules, creating a wave pressure. This study deals with the transition of the "pneumatic tonometry" concept [29], the principle of which is based on corneal depression against the IOP due to the injection of an air column flow.

In this work, we introduce the concept of pneumatic viscoelastic damping (*PVD*) as the variation in CH as a consequence of a sound wave pressure (swp) as a function of the sound frequency (v), defined as:

$$PVD\ (v) = 100 \times \left(\frac{\mathrm{CH_{swp}} - \mathrm{CH_0}}{\mathrm{CH_0}} \right) \quad (1)$$

Let us consider a viscoelastic cornea under external pressures. When loaded, the cornea exhibits immediate deformation (pure elastic component) that is damped by the viscous component followed by creep deformation (viscoelastic damping) [30]. More elastic corneas are prone to greater deformation due to a decreased viscoelasticity response [27] (i.e., lower CH values); in this sense, *PVD* reflects the ability of the cornea to modify its elastic and viscous properties under dynamic load conditions. Positive *PVD* values correspond to an increased viscosity component. On the contrary, *PVD* negative values indicate a reduced capability to absorb and dissipate energy as the elasticity the predominant component.

3. Results

3.1. Corneal Shape Changes as a Function of the Sound Frequency

Understanding the acoustic sinusoidal wave reaching the corneal surface as an external sound pressure perturbation applied to a viscoelastic material, an observed deformation or structural change is expected in relation to the relaxed state (i.e., FWG off). As described in Section 2.3, the structural changes in the corneal tissue were quantified via computing the CCT and e^2 parameters from Scheimpflug imaging. Figure 3 shows the mean values for six volunteers as a function of the sound frequency compared to the control baseline mean values (FGW off). The results showed that, at a given sound frequency, the corneal tissue reaches the lowest values of e^2 and CCT. In particular, the most sensitive sound frequency was 150 Hz, which resulted in an average reduction of 0.058 in e^2 (Figure 3a) and 7.33 µm in CCT (Figure 3b) compared to the relaxed state.

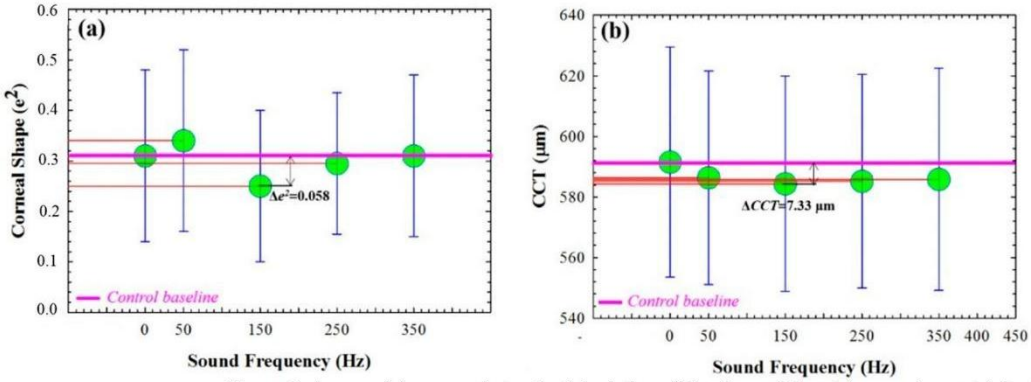

Figure 3. Averaged (mean and standard deviation of the six participants) corneal eccentricity (**a**) and central corneal thickness (**b**) measured as a function of the sound frequency. Red lines intersect the mean values for e^2 and CCT.

Figure 4 displays an example from one volunteer of the Scheimpflug output elevation maps for a regular measurement (upper row, instrument off) and a measurement taken while the acoustic wave generator was operating at 150 Hz for anterior and posterior corneal surfaces. The images demonstrate quantitative modifications in both the anterior and posterior surfaces during the presence of the sound pressure.

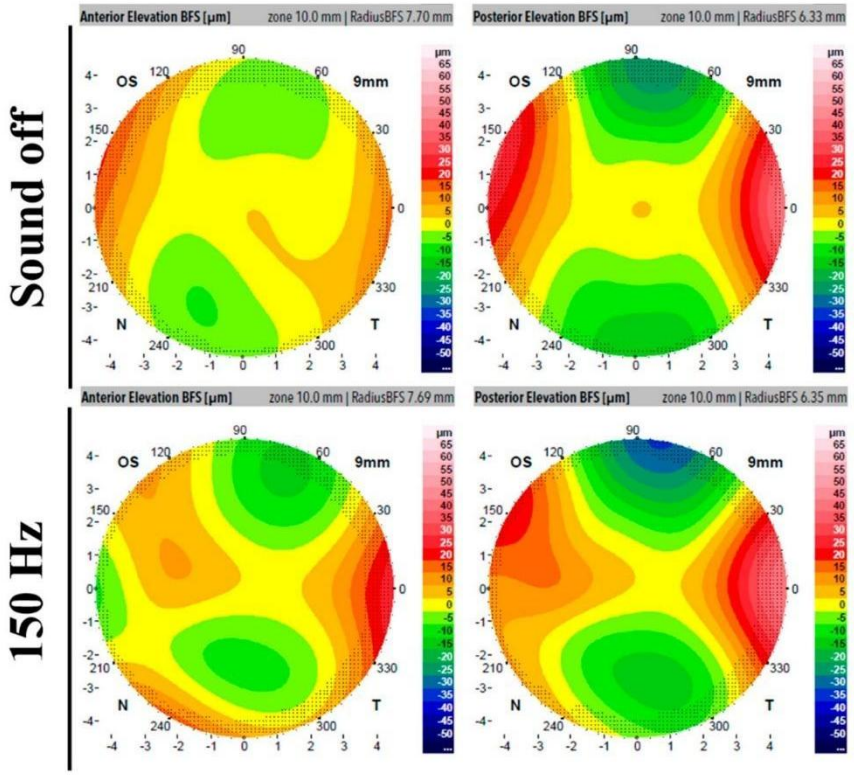

Figure 4. Scheimpflug output elevation maps corresponding to a regular measurement (upper row, instrument off) and a measurement during the acoustic wave generator operating at 150 Hz. The right and left column correspond to anterior and posterior corneal surface elevation, respectively.

3.2. Biomechanical Variations and Sound Frequency

The previous section showed how the frequency modulation of the sound pressure at a constant signal amplitude can induce slight changes in corneal shape, specifically in the central thickness, to the order of a few microns. These changes, unlike those produced via air-puff tonometry at a macroscopic scale, are microscopic in nature. However, even at the microscopic scale, this section presents evidence of how acoustic pressure can induce measurable biomechanical changes in the cornea. Figure 5 shows the mean IOP values for six healthy young adult subjects as a function of the sound frequency. The average control value falls within the normal range established between 11 and 21 mmHg [27]. According to our findings, the IOP is reduced for all the tested frequencies (Figure 5a), reaching a minimum value at 150 Hz that corresponds to an absolute difference of 3.60 mmHg with respect to the control baseline (pink line).

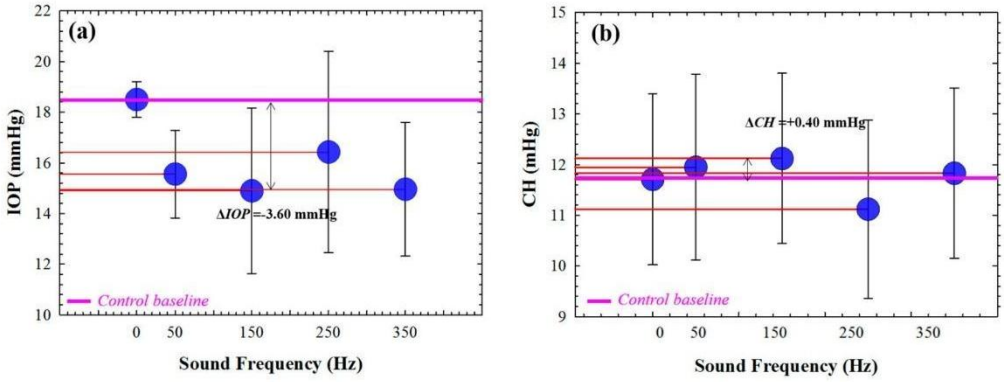

Figure 5. The averaged (mean and standard deviation of the six participants) IOP (**a**) and CH (**b**) measured as a function of the sound frequency. Red lines intersect the mean values for IOP and CH.

Regarding the viscoelastic property measured using the CH parameter, it shows a maximum value (an increase of 0.40 mmHg with respect to the average control value) for 150 Hz. Those preliminary results suggest that the application of acoustic waves can alter the corneal biomechanics, specifically reducing both the IOP and CH at a specific sound frequency of 150 Hz.

The air-puff system enables the acquisition of stress–strain dynamic measurements during the duration of the air pulse. Figure 6 illustrates a comparison of the air pulse pressure curves and corneal applanation responses (averaged value of the six volunteers) under normal operation (with the acoustic wave generator off) and with the application of acoustic wave pressure at 150 Hz. It can be observed that the application of external sound pressure causes less air pressure to reach the first applanation of the cornea (Figure 6a). This fact can be associated with reduced corneal stiffness, which aligns with the results presented in Figure 6b, where the first applanation occurs earlier when acoustic waves are applied. It is noteworthy that in Figure 6b, an intersection is observed on the left side of the graph between the applanation curves corresponding to normal measurements (blue line) and measurements taken during acoustic pressure (green line). A statistical comparison was performed via applying Student's *t*-test, revealing significant differences in both air-puff pressure ($p = 0.036$) and applanation waveforms ($p = 0.039$), respectively.

While the cornea still undergoes deformation due to the air pressure (sound off), the effect of acoustic interaction alters the viscoelastic properties over time, causing the cornea to begin relaxation at a point where it is still deforming.

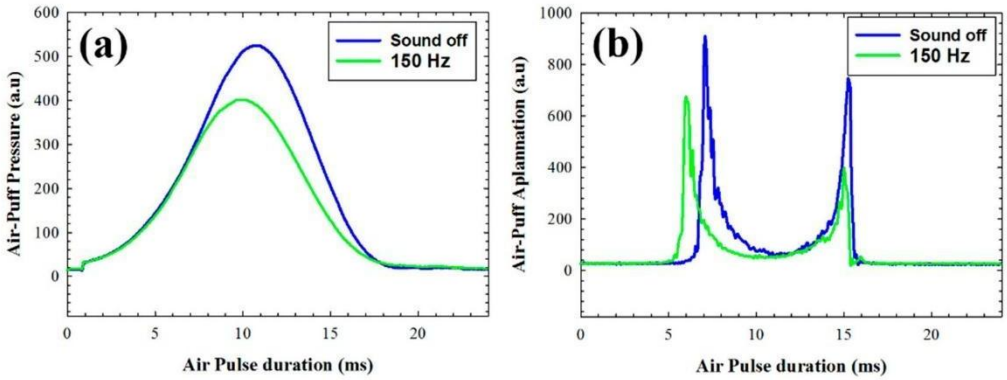

Figure 6. The air-puff pressure and applanation averaged response curves during an air-pulse time lapse for a normal measurement (**a**) and during acoustic pressure application (**b**).

Pneumatic Viscoelastic Damping for Different Sound Wave Frequencies

Figure 7 shows the *PVD* values for different sound frequencies. At the specific frequency of 150 Hz, the *PVD* showed a maximum value of +3.75% (green box) which corresponds to an increased viscosity with respect to the baseline viscoelasticity (pink line). In agreement with the data shown in Figure 5b, the maximum *PVD* value occurs for the same sound frequency at which an increasing CH is observed. On the contrary, negative values for *PVD* (red box in Figure 7) correspond to decreased CH values with respect to the control baseline.

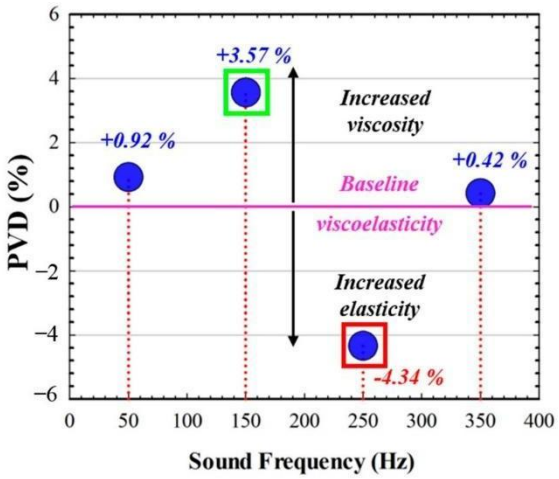

Figure 7. *PVD* (%) mean values as a function of the sound frequency. Vertical red dotted lines show the relative position of the mean *PVD* values with respect to the baseline viscoelasticity. Green and red boxes indicate the maximums positive and negative minimums *PVD* values, respectively.

3.3. Shape and Biomechanical Stability during Cornea and Acoustic Wave Interactions

The previous sections showed how the application of acoustic pressure by means of our proposed acoustic wave generator can alter the corneal shape at a microscopic scale and modify its biomechanical properties. This raises the question of whether these changes remain stable over time or whether they fluctuate randomly. To address this question, we conducted four consecutive measurements on a volunteer while applying the specific frequency of 150 Hz using both Scheimpflug imaging and the ORA analyzer. The results of these measurements are presented in Figure 8.

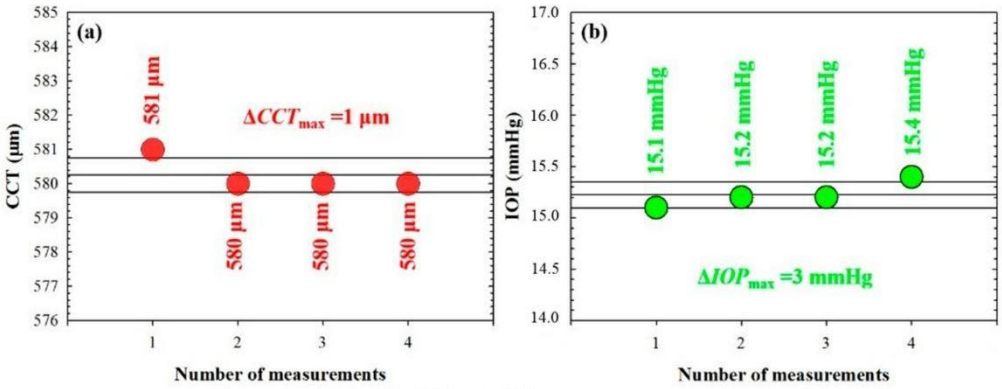

Figure 8. Sequential CCT and IOP measurements in one volunteer at the same experimental conditions (acoustic generator operating at 150 Hz and 1 Vpp). (**a**,**b**) Horizontal black lines represent the reference bands for the experimental values (central, upper and lower correspond to mean and control lines for a standard deviation error of ±1%, respectively). ΔCCT_{max} and ΔIOP_{max} are the maximum variation found for CCT and IOP values, respectively.

4. Discussion and Conclusions

The corneal shape and transparency are related to biomechanical properties, and the elastic component plays a dominant role [31]. Based on the corneal pneumatic tonometry concept [29], we developed a clinically orientated instrument to deliver acoustic waves to the corneal plane by combining a function/arbitrary waveform generator and a wide-range subwoofer mounted in a vertical orientation. The system was first calibrated via placing a digital sound meter at the position at which the corneal apex should be aligned. Sinusoidal signals at two different peak-to-peak amplitude voltages (1 and 2 Vpp.) were generated within the range frequency of 50–350 Hz (50 Hz step), obtaining a maximum sound pressure around 90 dB (see Figure 1) at the maximum frequency (350 Hz).

As a proof of concept, we tested the instrument on six healthy volunteers in a lab-conducted experiment. In the experimental set up, two commercially available ophthalmic devices were employed to establish a set of measurements of biomechanics and corneal biometry using the Ocular Response Analyzer (ORA, Reichter) and dual Scheimpflug tomography and Placido topography (Ziemer Ophthalmic Systems, AG) systems.

Previously to our work, Akca et al. [25] reported the observation of three corneal vibrational modes using sound waves within the frequency range of 50–400 Hz in ex vivo bovine ocular globes. They found a vibration amplitude of ~8 µm for a fundamental mode in the range of 80–120 Hz and at the sound pressure level of 100 dB.

In our work, we delivered acoustic sinusoidal acoustic waves in the frequency range of 50–350 Hz (1 Vpp. amplitude) and a 90 dB pressure level at the living human cornea, using a custom corneal acoustic waveform generator (see the description in Section 2.1). Corneal changes were visualized using a dual Scheimpflug camera and Placido rings analyzer and an Ocular Response Analyzer to monitor the corneal structure and biomechanics, respectively.

We found a reduction in the central corneal thickness of 7.33 µm at the sound frequency of 150 Hz together with a flattening of the corneal eccentricity of 0.058 (e^2) (see Figure 3). These results are visualized in the elevation maps shown in Figure 4. The application of acoustic waves can then induce measurable axial deformation in the cornea that is consistent with the results of Akca et al. [25] in ex vivo corneas.

On the one hand, the application of acoustic waves induces an IOP decrease (on average) from 18.5 ± 0.71 to 14.9 ± 3.27 mmHg at a sound frequency of 150 Hz; this induced change is within the reported physiological transient variations in the IOP [32,33].

In this sense, corneal hysteresis (CH) reacts to elevated IOP levels, rendering the tissue more elastic and reducing the viscous component; this alteration in CH due to an elevated IOP is considered a biomarker of glaucoma disease [27]. Agarwal et al. [34] evaluate the relationship between the IOP and CH before and after applying prostaglandin analogue therapy in 57 patients with glaucoma; they found a correlated reduction in the IOP of 18.8%, with increased CH in 5.2%. Our results showed an IOP reduction of 19.46% and an increase in CH of 3.5% during acoustic pressure application with respect to the baseline reference values (see Figure 5), which are in agreement with those reported by Agarwal et al.

On the other hand, Herndon et al. [35] compared the CCT values in normal and hypertensive eyes; they found significantly greater CCT values in normal eyes compared with those of ocular hypertension patients. In addition, the positive linear correlation between the CCT and IOP was demonstrated by Wei et al. [36] in a healthy young population, so a decrease in IOP implies a reduction in CCT. In good agreement, our results showed a reduction in CCT of 1.16% as a consequence of the decrease of 18.8% in IOP as a consequence of acoustic pressure application at 150 Hz.

Finally, the pneumatic viscoelastic damping (*PVD*) concept was introduced as the adaptive capability of the human cornea to modify its viscoelasticity by modulating the elastic and viscous components when low-magnitude external forces are loaded, such as sound wave pressures. We found two specific sound frequencies at which both scenarios occur: at 150 Hz, *PVD* showed positive values that correspond to a mean increase of +0.40 in CH and maximum corneal deformation (see Figure 3), consistent with an increased viscous component. On the contrary, at 250 Hz the *PVD* turned into negative values that are (as described in Section 2.3.3) related to an increased elastic component.

These preliminary results suggest that the corneal shape and biomechanical alterations due to sound wave pressure depend not only on the minimum pneumatic load to interact with the tissue but also on the specific oscillating frequency.

To conclude, we present a new and versatile system to generate acoustic waves for corneal applications. As a proof of concept, the system was tested on six volunteers, delivering a maximum sound pressure of 90 dB of sinusoidal acoustic waves at the range of 50–350 Hz (50 Hz step size). At the given frequency of 150 Hz, we found corneal deformation and changes in both IOP and CH that are consistent with those in the reported literature. Therefore, the application of acoustic waves allows us to modify the corneal biomechanics and the structure of the cornea in physiological transient physiological variations.

The main limitations were the small size of the sample, which did not allow the whole statistical analysis of the results, although the main goal was to demonstrate a proof of concept of biomechanical response in the human cornea's interaction with acoustic waves. The exposure time to sound waves was 10 s per measure to ensure continuous acoustic pressure before, while, and just after Scheimpflug and air-puff tonometry measures. The upcoming clinical study will include larger sound pressure exposure times to track whether changes in corneal biomechanics occur due to the time-dependent properties associated to the viscous damping nature of the human stroma. Future work will include a clinical study in a large population as a function of age and pathological conditions such as hypertensive and glaucomatous eyes, including contact lens wearers, and patients undergoing refractive surgery and minimally invasive glaucoma surgery. Those future steps will allow us to investigate changes in *PVD* over time.

Author Contributions: Conceptualization, F.J.Á.; methodology, F.J.Á., M.C.M. and L.R.; formal analysis, F.J.Á.; investigation, M.C.M. and L.R.; writing—original draft preparation, F.J.Á.; writing—review and editing, F.J.Á., M.C.M. and L.R.; project administration, F.J.Á.; funding acquisition, F.J.Á. All authors have read and agreed to the published version of the manuscript.

Funding: This research was funded by FUNDACIÓN BANCARIA IBERCAJA, grant number, 223221: JIUZ-2021-CIE-01.

Institutional Review Board Statement: The study was conducted in accordance with the Declaration of Helsinki, and approved by the Ethics Committee of the Health Sciences Institute of Aragon, Spain. (protocol code: C.P.-C.I. PI20/377, date of approval: 14 July 2020).

Informed Consent Statement: Informed consent was obtained from all subjects involved in the study.

Data Availability Statement: Data are contained within the article.

Acknowledgments: The authors thank Julio Amaré and Juanjo Lanuza from the "Departamento de Fisica Aplicada" of the University of Zaragoza for their technical support in the electronic design and mechanical assembly of the corneal waveform generator.

Conflicts of Interest: The authors declare no conflict of interest.

References

1. Piñero, D.P.; Alcón, N. Corneal biomechanics: A review. *Clin. Exp. Optom.* **2015**, *98*, 107–116. [CrossRef]
2. Kling, S.; Hafezi, F. Corneal biomechanics—A review. *Ophtalmic. Physiol. Opt.* **2017**, *37*, 240–252. [CrossRef]
3. Wilson, A.; Marshall, J. A review of corneal biomechanics: Mechanisms for measurement and the implications for refractive surgery. *Indian J. Ophthalmol.* **2020**, *68*, 2679–2690. [PubMed]
4. Meek, K.M. Corneal collagen-its role in maintaining corneal shape and transparency. *Biophys. Rev.* **2009**, *1*, 83–93. [CrossRef] [PubMed]
5. Fernández, J.; Rodríguez-Vallejo, M.; Martínez, J.; Tauste, A.; Piñero, D.P. Corneal biomechanics after laser refractive surgery: Unmasking differences between techniques. *J. Cataract. Refract. Surg.* **2018**, *44*, 390–398. [CrossRef] [PubMed]
6. Cao, K.; Liu, L.; Yu, T.; Chen, F.; Bai, J.; Liu, T. Changes in corneal biomechanics during small-incision lenticule extraction (SMILE) and femtosecond-assisted laser in situ keratomileusis (FS-LASIK). *Lasers Med. Sci.* **2020**, *35*, 599–609. [CrossRef]
7. Wallace, H.B.; McKelvie, J.; Green, C.R.; Misra, S.L. Corneal Curvature: The Influence of Corneal Accommodation and Biomechanics on Corneal Shape. *Transl. Vis. Sci. Technol.* **2019**, *8*, 5. [CrossRef]
8. Wu, D.; Liu, C.; Li, B.; Wang, D.; Fang, X. Influence of Cap Thickness on Corneal Curvature and Corneal Biomechanics After SMILE: A Prospective, Contralateral Eye Study. *J. Refract. Surg.* **2020**, *36*, 82–88. [CrossRef]
9. Kaushik, S.; Pandav, S.S. Ocular Response Analyzer. *J. Curr. Glaucoma Pract.* **2012**, *6*, 17–19. [CrossRef]
10. Du, Y.; Zhang, Y.; Zhang, Y.; Li, T.; Wang, J.; Du, Z. Analysis of potential impact factors of corneal biomechanics in myopia. *BMC Ophthalmol.* **2023**, *23*, 143. [CrossRef]
11. Choi, E.J.; Kim, K.N.; Song, M.Y.; Hwang, Y.H. Correlation between Interocular Asymmetry of Corneal Hysteresis and Visual Field Defect in Glaucoma. *Korean J. Ophthalmol.* **2023**, *37*, 112–119. [CrossRef] [PubMed]
12. Marcellán, M.C.; Remón, L.; Ávila, F.J. Corneal hysteresis and intraocular pressure are altered in silicone-hydrogel soft contact lenses wearers. *Int. Ophthalmol.* **2022**, *42*, 2801–2809. [CrossRef] [PubMed]
13. Sedaghat, M.R.; Momeni-Moghaddam, H.; Kangari, H.; Moradi, A.; Akbarzadeh, R.; Naroo, S.A. Changes in corneal biomechanical parameters in keratoconus eyes with various severities after corneal cross-linking (CXL): A comparative study. *Eur. J. Ophthalmol.* **2023**, *3*, 2114–2122. [CrossRef] [PubMed]
14. Baptista, P.M.; Ambrosio, R.; Oliveira, L.; Meneres, P.; Beirao, J.M. Corneal Biomechanical Assessment with Ultra-High-Speed Scheimpflug Imaging During Non-Contact Tonometry: A Prospective Review. *Clin. Ophthalmol.* **2021**, *15*, 1409–1423. [CrossRef]
15. Karmiris, E.; Tsiripidis, K.; Gartaganis, P.S.; Totou, S.; Vasilopoulou, M.G.; Patelis, A.; Giannakis, I.; Chalkiadaki, E. Comparison of intraocular pressure obtained by Goldmann applanation tonometer, Corvis ST and an airpuff tonometer in healthy adults. *Eur. J. Ophthalmol.* **2021**, *32*, 951–959. [CrossRef]
16. Eltony, A.M.; Shaom, P.; Yun, S.H. Measuring mechanical anisotropy of the cornea with Brillouin microscopy. *Nat. Commun.* **2022**, *13*, 1354. [CrossRef]
17. Sun, M.G.; Son, T.; Crutison, J.; Guaiquil, V.; Lin, S.; Nammari, L.; Klatt, D.; Yao, X.; Rosenblatt, M.I.; Royston, T.J. Optical coherence elastography for assessing the influence of intraocular pressure on elastic wave dispersion in the cornea. *J. Mech. Behav. Biomed. Mater.* **2022**, *128*, 105100. [CrossRef]
18. Lan, G.; Twa, M.D.; Song, C.; Feng, J.; Huang, Y.; Xu, J.; Qin, J.; An, L.; Wei, X. In vivo corneal elastography: A topical review of challenges and opportunities. *Comput. Struct. Biotechnol. J.* **2023**, *21*, 2664–2687. [CrossRef]
19. Qin, X.; Tian, L.; Zhang, H.; Zhang, D.; Jie, Y.; Zhang, H.X.; Li, L. Determine Corneal Biomechanical Parameters by Finite Element Simulation and Parametric Analysis Based on ORA Measurements. *Front. Bioeng. Biotechnol.* **2022**, *10*, 862947. [CrossRef]
20. Hsu, F.L.; Shih, P.J.; Wang, I.J. Development and validation of an intuitive biomechanics-based method for intraocular pressure measurement: A modal analysis approach. *BMC Ophthalmol.* **2023**, *23*, 124. [CrossRef]
21. Zhao, G.P.; Zhai, H.T.; Xiang, H.Z.; Wu, L.M.; Chen, Q.O.; Chen, C.; Zhou, M. Biomechanical study of cornea response under orthokeratology lens therapy: A finite element analysis. *Int. J. Numer. Methods Biomed. Eng.* **2023**, *39*, e3691. [CrossRef]
22. Wardosanidze, Z.V. About the possible acoustic functions of the eye. *Am. J. Biom. Sci. Res.* **2021**, *15*, 79–81. [CrossRef]
23. Coquart, L.; Depeursinge, C.; Gurnier, A.; Ohayon, R. A fluid-structure interaction problem in biomechanics: Prestressed vibrations of the eye by the finite element method. *J. Biomech.* **1992**, *25*, 1105–1118. [CrossRef] [PubMed]

24. Shih, P.J.; Guo, Y.R. Resonance frequency of fluid-filled and prestressed spherical shell—A model of the human eyeball. *J. Acoust. Soc. Am.* **2016**, *139*, 1784. [CrossRef] [PubMed]
25. Akca, B.I.; Chang, E.W.; Kling, S.; Ramier, A.; Scarcelli, G.; Marcos, S.; Yun, S.H. Observation of sound-induced corneal vibrational modes by optical coherence tomography. *Biomed. Opt. Express* **2015**, *6*, 3313–3319. [CrossRef]
26. Ramier, A.; Tavakol, B.; Yun, S.H. Effect of intraocular pressure on the vibrational resonance of the cornea measured by optical coherence tomography. *Investig. Ophthalmol. Vis. Sci.* **2017**, *58*, 4326.
27. Zimprich, L.; Diedrich, J.; Bleeker, A.; Schweitzer, J.A. Corneal Hysteresis as a Biomarker of Glaucoma: Current Insights. *Clin. Ophthalmol.* **2020**, *14*, 2255–2264. [CrossRef]
28. Jammal, A.A.; Medeiros, F.A. Corneal hysteresis: Ready for prime time? *Curr. Opin. Ophthalmol.* **2022**, *33*, 243–249. [CrossRef]
29. Walter, R.E.; Kitovitz, T.L. An experimental and theoretical study of the pneumatic tonometer. *Exp. Eye Res.* **1972**, *13*, 14–23.
30. Kobayashi, A.S.; Staberg, L.G.; Schlegel, W.A. Viscoelastic properties of the human cornea. *Exp. Mech.* **1973**, *13*, 497–503. [CrossRef]
31. Ávila, F.J.; Marcellán, M.C.; Remón, L. On the relationship between corneal biomechanics, macrostructure, and optical properties. *J. Imaging* **2021**, *7*, 280. [CrossRef] [PubMed]
32. Martin, X.D. Normal intraocular pressure in man. *Ophthalmologica* **1992**, *205*, 57–63. [CrossRef] [PubMed]
33. Bakke, E.F.; Hisdal, J.; Semb, S.O. Intraocular Pressure Increases in Parallel with Systemic Blood Pressure during Isometric Exercise. *Investig. Opthalmol. Vis. Sci.* **2009**, *50*, 760–764. [CrossRef]
34. Agarwal, D.; Ehrlich, J.; Shimmyo, M.; Radcliffe, N. The relationship between corneal hysteresis and the magnitude of intraocular pressure reduction with topical prostaglandin therapy. *Br. J. Ophthalmol.* **2011**, *96*, 254–257. [CrossRef]
35. Herndon, L.W.; Choudhri, S.A.; Cox, T.; Damji, K.F.; Shields, M.B.; Allingham, R.R. Central corneal thickness in normal, glaucomatous, and ocular hypertensive eyes. *Arch. Ophthalmol.* **1997**, *115*, 1137–1141. [CrossRef] [PubMed]
36. Wei, W.; Fan, Z.; Wang, L.; Li, Z.; Jiao, W.; Li, Y. Correlation Analysis between Central Corneal Thickness and Intraocular Pressure in Juveniles in Northern China: The Jinan City Eye Study. *PLoS ONE* **2011**, *9*, e104842. [CrossRef] [PubMed]

2.5. A Comprehensive Study on Elasticity and Viscosity in Biomechanics and Optical Properties of the Living Human Cornea.

Ávila FJ, del Barco Ó, Marcellán MC, Remón L. A Comprehensive Study on Elasticity and Viscosity in Biomechanics and Optical Properties of the Living Human Cornea. *Photonics*. 2024; 11(6):524. https://doi.org/10.3390/photonics11060524

JIF (2023): 2,1-Optics-59/119-Q2

JCI (2023):0,61-Optics-56/120-Q2

photonics

MDPI

Article

A Comprehensive Study on Elasticity and Viscosity in Biomechanics and Optical Properties of the Living Human Cornea

Francisco J. Ávila [1,*], Óscar del Barco [2], María Concepción Marcellán [1] and Laura Remón [1]

[1] Departamento de Física Aplicada, Universidad de Zaragoza, 50009 Zaragoza, Spain
[2] Laboratorio de Óptica, Instituto Universitario en Óptica y Nanofísica, Universidad de Murcia, Campus de Espinardo, 30100 Murcia, Spain; obn@um.es
* Correspondence: avila@unizar.es

Abstract: Corneal biomechanics is a hot topic in ophthalmology. The biomechanical properties (BMPs) of the cornea have important implications in the management and diagnosis of corneal diseases such as ectasia and keratoconus. In addition, the characterization of BMPs is crucial to model the predictability of a corneal surgery intervention, the outcomes of refractive surgery or the follow-up of corneal diseases. The biomechanical behavior of the cornea is governed by viscoelastic properties that allow, among other structural implications, the damping of excess intraocular pressure and the reduction of damage to the optic nerve. Currently, the most versatile and complete methods to measure corneal viscoelasticity are based on air-puff corneal applanation. However, these methods lack the ability to directly measure corneal viscosity. The aim of this work is to propose a new methodology based on the analysis of corneal air-puff measurements through the standard linear solid model (SLSM) to provide analytical expressions to separately calculate the elastic and time-dependent (corneal retardation time and viscosity) properties. The results show the mean values of elasticity (E), viscosity (η) and corneal retardation time (τ) in a sample of 200 young and healthy subjects. The influence of elasticity and viscosity on viscoelasticity, high-order corneal aberrations and optical transparency is investigated. Finally, the SLSM fed back from experimental E and η values is employed to compare the creep relaxation response between a normal, an ocular hypertension patient and an Ortho-K user. Corneal biomechanics is strongly affected by intraocular pressure (IOP); however, corneal hysteresis (CH) analysis is not enough to be employed as a risk factor of glaucoma progression. Low values of CH can be accompanied by high or low corneal elasticity and viscosity depending on the IOP threshold from which the time-dependent biomechanical properties trends are reversed.

Keywords: corneal biomechanics; standard linear solid model; corneal viscoelasticity; corneal elasticity; corneal viscosity; corneal retardation time; ocular hypertension; Ortho-K; ocular response analyzer; corneal Scheimpflug imaging

Citation: Ávila, F.J.; del Barco, Ó.; Marcellán, M.C.; Remón, L. A Comprehensive Study on Elasticity and Viscosity in Biomechanics and Optical Properties of the Living Human Cornea. *Photonics* **2024**, *11*, 524. https://doi.org/10.3390/photonics11060524

Received: 29 April 2024
Revised: 25 May 2024
Accepted: 29 May 2024
Published: 31 May 2024

1. Introduction

The hierarchical architecture of the cornea is responsible for the structure and transparency due to its collagen-based lamellar organization [1,2]. X-ray scattering has revealed how the molecular collagen fibrils provide the mechanical properties of corneal tissue [3]. In particular, the spring-like and viscous crimp mechanisms are governed by the micro- and nanoscale collagen structure. The elasticity of the cornea is enabled by the springs that straighten the supramolecular torsion of tropocollagen, while the viscosity responds to a curling mechanism of the fibrils [4]. In this sense, the cornea exhibits a viscoelastic nature with differentiated elastic and time-dependent (viscous) properties.

Biomechanical properties (BMPs) of the cornea can be understood as the dynamic response of the cornea to applied external forces [5]. BMPs have revolutionized the anterior

chamber subspeciality in ophthalmology, allowing powerful competition in the prognosis and diagnosis of surgery treatments [6] and corneal diseases [7], respectively. The main methodologies for in vivo assessment of corneal BMPs are based on air-puff tonometry [8], elastography [9] and Brillouin microscopy approaches [10]. The most widespread approaches include the ocular response analyzer (ORA) [11] and corneal Scheimpflug visualization (Corvis-ST) [12], which consist of corneal applanation tonometry and provide the estimation of viscoelastic parameters and measurements of intraocular pressure (IOP).

Brillouin scattering allows the longitudinal modulus to be quantified from the analysis of the Doppler Brillouin frequency shift [13]. This technique has successfully characterized biomechanical differences between normal, keratoconic and post-refractive surgery corneas [14] due to its ability to observe mechanical anisotropy of the cornea [10].

Elastography methods include magnetic resonance imaging, ultrasound elastography and the emerging optical coherence elastography [9], which provides micrometric scale measurements of corneal stiffness and structural properties. In this sense, our group recently reported a promising tool based on a sound pressure generator for in vivo observation of the biomechanical response of the cornea to low-frequency acoustic waves [15].

The methodologies mentioned above are in progress on how to perform a rapid non-invasive biomechanical assessment of the cornea with sufficient spatial resolution to also provide reliable structural information. Obtaining accurate measures of biomechanical parameters is essential for the reliable predictability of mathematical models that reproduce the behavior of the cornea under normal and pathological conditions.

Under conditions of transient stress, the human cornea behaves as a viscoelastic material [16]. Various methods have been used to mathematically model the viscoelastic nature of the human cornea, particularly the Kelvin–Voigt, Maxwell and standard solid models [17].

Glass et al. proposed a modified Kelvin–Voigt model to evaluate the effect of elastic and viscosity properties on hysteresis (measure of the viscoelastic damping of the cornea [18]) in a corneal phantom [19]. Su et al. proposed a hyper-viscoelastic approach combining the Mooney–Rivlin hyperelastic and modified Maxwell models for the specific simulation of trephine and suture in corneal surgery [20]. Whitford et al. developed the first constitutive model for corneal viscoelastic representation by combining complex anisotropy, shear stiffness and fibrillar collagen density [21].

Recently, the standard solid model was proposed for the simulation of thermoviscoelasticity of the human cornea [22] due to its reasonable predictability for loads applied to the cornea on a constant or transient basis.

The study of corneal biomechanics through mathematical models achieves greater robustness if feedback with experimental data (or at least derivable from experimental measurements) is possible.

The aim of this work is to introduce a new methodology based on the analysis of air-puff corneal applanation measurements and corneal Scheimpflug imaging with the three-element standard linear solid model (SLSM) to provide experimental analytical expressions to calculate separated elastic and time-dependent (i.e., viscous property and corneal retardation time) of the human cornea in vivo.

2. Materials and Methods

2.1. Participants

Two hundred young healthy volunteers participated in the study (mean age 21.07 $\pm$ 3.13 years old). None of them had a diagnosis of glaucoma or hypertensive ocular disease or had undergone refractive surgery. In addition, a patient diagnosed with ocular hypertension (intraocular pressure 24.8 mmHg) and an Ortho-K contact lens user were recruited to compare normal response from their variations in biomechanical properties in tensile creep relaxation tests. The motivation to include a comparison with these two types of patients was the growing concern regarding glaucoma disease and to explore the biomechanical complications of orthokeratology.

This study was reviewed by an ethical review board (Ethical Committee of Research of the Health Sciences Institute of Aragón, Spain. Reference C.P.-C.I.PI20/377) according to the tenets of the Declaration of Helsinki. All participants were informed about the nature and risks of the study and signed an informed consent document.

2.2. In Vivo Corneal Assessment: Geometrical, Optical and Biomechanical Corneal Parameters

The Galilei dual Scheimpflug analyzer (Galilei G2; Ziemer Ophthalmic Systems AG, Port, Switzerland) and the ocular response analyzer device (ORA, Reichert Instruments, Depew, NY, USA) were used to measure geometrical and optical (optical density and corneal aberrometry) corneal parameters and provide a biomechanical assessment of the living human cornea. Table 1 summarizes the description of the parameters as a function of the employed technology.

Table 1. Geometrical (R_{cor}, CCT), optical (OD, SA, trefoil and coma) and biomechanical parameters (IOP_{cc} and CH) measured for morphometric, optical and biomechanical corneal assessment.

Parameter [Units]	Technology	Description
Rcor (mm)	Dual Scheimpflug analyzer	Mean corneal radii
2·Xcor (mm)	Dual Scheimpflug analyzer	Corneal applanation diameter
CCT (μm)	Dual Scheimpflug analyzer	Central corneal thickness
OD (n.u)	Dual Scheimpflug analyzer	Optical density
SA (μm)	Dual Scheimpflug analyzer	Spherical aberration
Trefoil (μm)	Dual Scheimpflug analyzer	Trefoil term
Coma (μm)	Dual Scheimpflug analyzer	Coma term
IOP_{cc} (mmHg)	ORA	Corneal-compensated intraocular pressure
CH (mmHg)	ORA	Corneal hysteresis

The measurements were carried out at the visual optics laboratory of the University of Zaragoza (Spain) by an experienced clinical optometrist. All data were incorporated into an Excel database without including more personal data than the date of birth and an identification code. Graphical representations and numerical simulations were carried out using Origin Lab software 2024b (Origin Lab Corp., Northampton, MA, USA) and Matlab2019b (the MathWorks Inc., Natick, MA, USA) programming language.

2.3. The Three-Element Standard Linear Solid Model

Figure 1 shows the three-element standard linear solid model (SLSM) [23], which is obtained by adding a spring series with a Kelvin–Vogt (KV) unit (blue box in Figure 1). The KV model consists of a spring coupled in parallel with a dash pot that represents the viscoelastic component of the model. E is the elasticity of the springs, η is the viscosity of the dash pot, σ is the applied stress (or external load) and ε is the strain, respectively. The third element consists of an extra spring (E_1) that forms the purely elastic behavior of the system. In the three-element SLSM, the Kelvin–Voigt representation is used to distinguish it from the Maxwell representation. The model is oriented in the plane of the corneal lamellae, where the air pressure from the tonometer is perpendicular to our viscoelastic model with 3 elements. In this orientation, the model aligns with the forces generated in the lamellae and represents the elongation and shortening of the lamellae as the wall stress in the cornea changes during measurement.

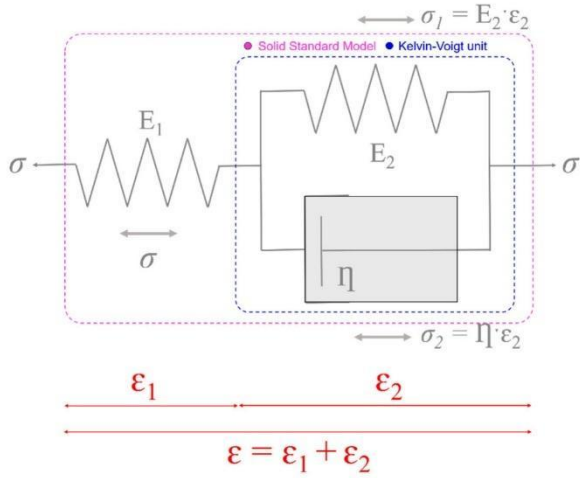

Figure 1. Representation of three elements of the standard linear solid model. E, η, σ and ε correspond to elasticity, viscosity, applied stress and induced strain, respectively.

From the Figure 1, the equations for the SLSM are [23]:

$$\begin{aligned} \sigma &= \sigma_1 + \sigma_2 \\ \sigma &= E_1 \varepsilon_1 \\ \sigma_1 &= E_2 \varepsilon_2 \\ \sigma_2 &= \eta \dot{\varepsilon_2} \\ \varepsilon &= \varepsilon_1 + \varepsilon_2 \end{aligned} \tag{1}$$

where $\dot{\varepsilon}$ is the stress rate. The constitutive law for the SLSM is given by [23]:

$$\sigma + \left(\frac{\eta}{E_1 + E_2}\right) \dot{\sigma} = \left(\frac{E_1 \cdot E_2}{E_1 + E_2}\right) \varepsilon + \left(\frac{E_1 \eta}{E_1 + E_2}\right) \dot{\varepsilon} \tag{2}$$

Assuming the cornea to be axisymmetric, a single elastic constant should govern the corneal behavior, so we can identify $E_1 = E_2$ [19]. Consequently, the constitutive law for the standard solid model can be written as:

$$\sigma + \left(\frac{\eta}{2E}\right) \dot{\sigma} = \left(\frac{E}{2}\right) \varepsilon + \left(\frac{\eta}{2}\right) \dot{\varepsilon} \tag{3}$$

In addition, the cornea is considered an isotropic spherical membrane with constant thickness and the load on the cornea is assumed to be uniform. If the SLSM is loaded (considering a step function for the stress σ), the response is given by solving the differential equation (Equation (3)):

$$\varepsilon(t) = \sigma_0 \left[\frac{1}{E} + \frac{1}{E}\left(1 - e^{-(\frac{E}{\eta})t}\right)\right] \tag{4}$$

Notice that, immediately after applying the load stress, the strain will be entirely from the lone spring (E1). Thus, in fact, $\varepsilon(0) = \sigma_0/E$.

When the stress is removed, the absence of load ($\sigma = 0$) reduces the constitutive law to:

$$\left(\frac{E}{2}\right) \varepsilon + \left(\frac{\eta}{2}\right) \dot{\varepsilon} = 0 \tag{5}$$

and the relaxation response is:

$$\varepsilon(t) = \frac{\sigma_0}{E} e^{-(\frac{E}{\eta})t} \left(e^{(\frac{E}{\eta})t_u} - 1 \right) \quad (6)$$

where the time t begins at the zero load event at which the stress is applied. The point at which the stress is removed is given by t_u. Then, Equations (4) and (6) can predict the response of the model (strain) under stress given the values for elasticity and viscosity. The next section attemps to develop analitical expressions for the calculation of E and η from air-puff corneal applanation measurements.

2.4. Experimental Calculation of Elastic and Time-Dependent Biomechanical Properties

The ORA device provides invaluable mechanical information beyond the CRF, CH and IOP parameters provided by commercial software. Figure 2a shows a representative measurement showing both signals corresponding to the force of the air jet applied to the cornea and the deformation monitored by electro-optical detection. The red waveform shows two peaks (P1 and P2) representing the first and second applanation events as the cornea moves inward and outward, respectively. The green Gaussian-shaped curve corresponds to the delivered pressure and is responsible for the forward and backward corneal displacement phases. At the moment of maximum corneal deformation, the Gaussian reaches maximum peak.

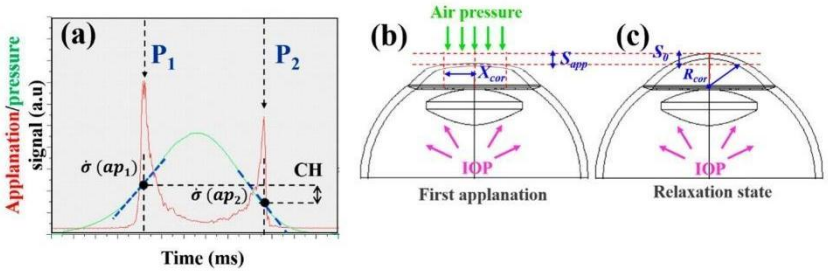

Figure 2. (**a**) Representation of the ocular anterior chamber during air-puff tonometry. S_0 and R_{cor} correspond to the sagitta of the area of air jet application and corneal curvature radius before applanation. (**b**) At the first applanation event, $S_{app} = -S_0$. The diameter of the area of applanation if given by $2 \cdot X_{cor}$. (**c**) Representation of the applanation/pressure signals during air-puff tonometry ORA measurement. P1, P2, CH, $\dot{\sigma}(ap_1)$ and $\dot{\sigma}(ap_2)$ are the first and second applanation pressures, corneal hysteresis and first and second pressure rates at the moment of the two applanation events, respectively.

In this sense, Figure 2b represents the first applanation event, where the applied stress (σ_{P1}) on the anterior corneal surface is given by [19]:

$$\sigma_{P1} = \frac{P_{r,1} \cdot R_{cor}}{2 \cdot CCT} \quad (7)$$

where R_{cor} and CCT are the original corneal radius and central corneal thickness, respectively. $P_{R,1}$ is the resulting pressure in the first applanation event [24]:

$$P_{r,1} = P_1 + P_{tf} - IOP \quad (8)$$

where P_1, P_{tf} and IOP are the first applanation pressure, the tear film surface pressure and the intraocular pressure, respectively. Once the measurement is completed, the cornea returns to its original state and shape (Figure 2c).

The air jet applies stress on a total corneal diameter of $2{\cdot}X_{cor}$, which subtends an arc length in the relaxed state, L_{cor} [19]:

$$L_{cor} = 2{\cdot}CCT\left[\sin^{-1}\left(\frac{X_{cor}}{R_{cor}}\right)\right] \quad (9)$$

When the cornea is completely applanated (i.e., corneal sagitta is S_{app}), $L_{cor} = L_{flatt} = 2 \cdot X_{cor}$, then the induced strain (ε_{flatt}) by the applanation pressure P_1 can be calculated from Equation (4) [19]:

$$\varepsilon_{flatt} = \frac{L_{cor} - L_{flatt}}{L_{cor}} = \frac{X_{cor}}{CCT{\cdot}\sin^{-1}\left(\frac{X_{cor}}{CCT}\right)} - 1 \quad (10)$$

Once the values for stress σ_{P1} and strain ε_{flatt} for the first applanation are known, corneal elasticity can be calculated:

$$E = \frac{\sigma_{P1}}{\varepsilon_{flatt}} \quad (11)$$

On the other hand, the corneal retardation time τ is the time in which about 63% of the final corneal strain is determined [25,26]. This metric would measure the cornea's ability to absorb IOP fluctuations. Recently, our group developed a theoretical method to derive a practical expression for this parameter [27] once the applanation pressures (P_1 and P_2) and their first derivatives are known (please, see again Figure 2a):

$$\tau = \frac{2CH}{\left|\dot{\sigma}(ap_1)\right| + \left|\dot{\sigma}(ap_2)\right|} \quad (12)$$

The accurate method to determine the applanation pressures is performed via the two ORA characteristic curves: the applanation signal (corresponding to the IR light that is reflected off the surface of the cornea during perturbation) and the pressure amplitude (please, see again Figure 2a). The last curve can be fairly fitted by a Gaussian profile with a high confidence level ($0.985 < R^2 < 0.997$ in all cases) [27]. Then, the applanation signal provides the two applanation pressures P_1 and P_2 (via the sharp peaks in both panels), whereas the derivatives of the applanation pressures $\dot{\sigma}(ap_1)$ and $\dot{\sigma}(ap_2)$ can be analytically evaluated from the first derivatives of the fitted Gaussian profile.

Once the time-dependent parameter τ is computed, the corneal viscosity can be easily obtained by the following expression:

$$\eta = E{\cdot}\tau = 2{\cdot}\frac{\sigma_{P1}{\cdot}CH}{\varepsilon_{flatt}{\cdot}\left(\left|\dot{\sigma}(ap_1)\right| + \left|\dot{\sigma}(ap_2)\right|\right)} \quad (13)$$

2.5. Statistical Analysis

Experimental data are stored in an Excel spreadsheet and then migrated to Origin Lab software 2024b (Origin Lab Corp., Northampton, MA, USA) for statistical analysis and graphical representations. Statistical analysis consists of Spearman rank order correlation and regression analysis. Data shown in Figure 4 are modeled by a piecewise 2 segment linear regression for which the threshold values correspond to the point of discontinuity obtained as a result of the regression analysis. Limits of agreement and confident bands are used to quantify the agreement between the given parameters in graphical representations. Statistics is performed using the advanced statistical tool from Origin Lab software.

3. Results

3.1. Efect of IOP on Elastic, Viscoelastic and Viscous Properties of the Cornea

The aim of this section is to investigate how fluid pressure within the eyeball impacts corneal biomechanics due to its relevance to glaucoma disease [28]. Table 1 shows the representative mean values of IOP, geometric and biomechanical parameters for all participants

in this study. Elasticity, tau and viscosity are calculated using Equations (11), (12) and (13), respectively.

Figure 3 represents CH as a function of the IOP. As the intraocular pressure increases, the ability of the cornea to absorb and dissipate excess mechanical energy reflects a decrease in CH measurements, with a significant negative correlation ($R^2 = -0.49$, $p < 0.001$).

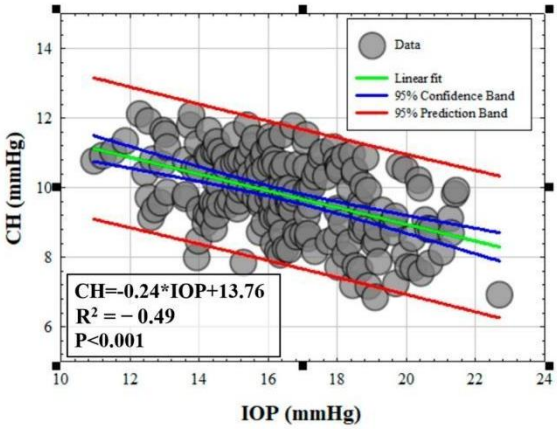

Figure 3. CH as a function of the IOP_{cc} for all participants involved in the study. The blue line corresponds to the best linear fitting of the negative correlation found between both variables.

Figure 4 shows the experimental values for elasticity (Figure 4a) and viscosity (Figure 4b) of the human cornea as a function of the IOP_{cc}. The results show piecewise linear behavior with statistical correlations of $R^2 = 0.81$ ($p < 0.0001$) and $R^2 = 0.80$ ($p < 0.0001$), respectively.

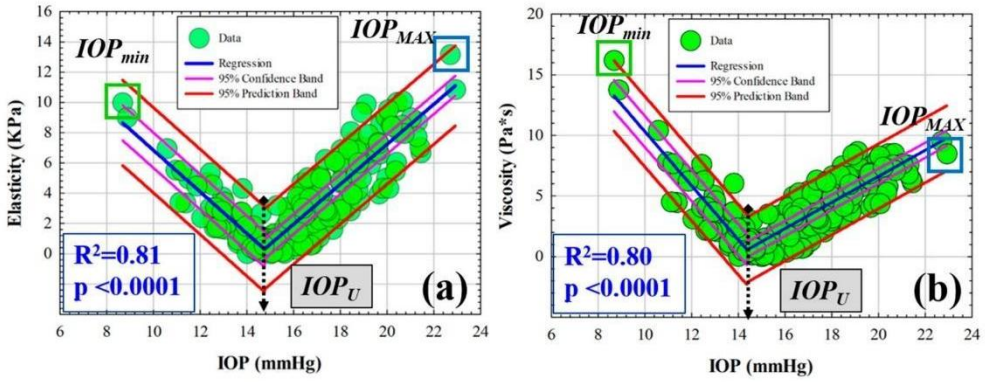

Figure 4. Elasticity (**a**) and viscosity (**b**) as a function of the intraocular pressure. The blue lines correspond to the piecewise linear fitted intervals. The green and blue boxes indicate the minimum (IOP_{min}) and maximum (IOP_{max}) IOP of the intervals separated by the IOP threshold (IOP_u).

The two-segment linear regressions for E and η are given by experimental fitting expressions 14 and 15. We find a threshold IOP value (IOP_u) of 14.45 mmHg, for which the intervals are defined. For IOP values less than 14.45 mmHg, the elastic and viscous components of the cornea are negatively correlated, i.e., elasticity and viscosity decrease as the IOP increases up to IOP_u. However, for IOP values higher than IOP_u, the trend is reversed and both elastic and viscous properties increase as a function of IOP.

$$E(IOP) = \begin{cases} \frac{9.33\cdot(IOP_u - IOP) + 0.21\cdot(IOP - IOP_{min})}{IOP_u - IOP_{min}}, & IOP_{min} \leq IOP \leq IOP_u \\ \frac{0.21\cdot(IOP_{MAX} - IOP) + 11.30\cdot(IOP - IOP_u)}{IOP_{MAX} - IOP_u}, & IOP_u \leq IOP \leq IOP_{MAX} \end{cases} \quad (14)$$

$$\eta(IOP) = \begin{cases} \frac{14.33\cdot(IOP_u - IOP) + 0.47\cdot(IOP - IOP_{min})}{IOP_u - IOP_{min}}, & IOP_{min} \leq IOP \leq IOP_u \\ \frac{0.47\cdot(IOP_{MAX} - IOP) + 9.98\cdot(IOP - IOP_u)}{IOP_{MAX} - IOP_u}, & IOP_u \leq IOP \leq IOP_{MAX} \end{cases} \quad (15)$$

3.2. Retardation Time as a Biomechanical Behavior Threshold: Role of Elasticity and Viscosity on Corneal Viscoelasticity

Corneal retardation time (τ) has been reported as a good biomarker of corneal viscoelasticity [26], which, in collusion with the CH parameter, provides combined information regarding elastic and viscous properties. At this point, it is crucial to ask a fundamental question: what is the elastic response of the cornea when its viscoelastic behavior changes?

Figure 5 shows the elasticity calculated from all subjects as a function of the retardation time (τ). The elastic property of the cornea shows an almost symmetric behavior around a given value of the retardation time τ_U = 1.22 ms. For those corneas characterized by a retardation time less than 1.22 ms, elasticity decreases as viscoelasticity increases. However, an inverse behavior is observed for values of $\tau_U \geq 1.22$ ms.

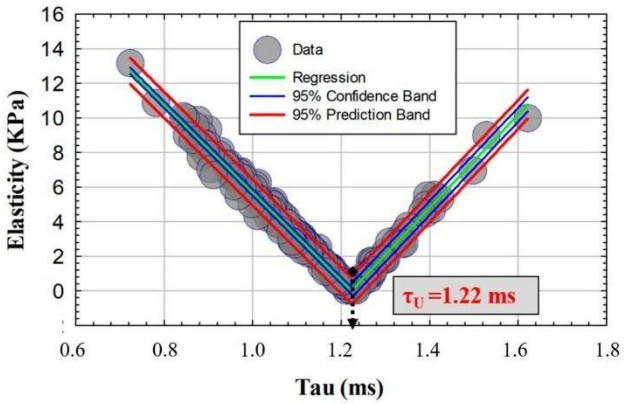

Figure 5. Elasticity as a function of the retardation time. The red dotted line indicates the threshold retardation time (τ_U) separating the trend intervals.

From the data observed in Figure 5, there appears to be a threshold in the retardation (τ_U) time, beyond which the elastic behavior of the cornea is reversed. To understand the influence of this threshold on the evaluation of viscoelasticity, Figure 6 shows the influence of the elasticity and viscosity on corneal hysteresis for values of $\tau_U \leq 1.22$ ms (Figures 6a and 6b, respectively) and for values of retardation time greater than τ_U (Figures 6c and 6d). For retardation times less than 1.22 ms, both the viscosity (Figure 6a) and elasticity (Figure 6b) components contribute to an increase in corneal hysteresis with parabolic correlation (R^2 = 0.60 and R^2 = 0.59, respectively). However, an interesting phenomenon is observed for corneas exhibiting retardation times larger than 1.22 ms. If corneal viscosity (Figure 6c) or elasticity (Figure 6d) increases, the viscoelasticity measured by the CH parameter decreases, with a statistically significant negative linear trend ($R^2 = -0.66$ and $R^2 = -0.14$, respectively). It is worth highlighting that, while for $\tau_U \leq 1.22$ ms, the corneal hysteresis shows a similar dependence on viscosity and elasticity, for retardation times greater than τ_U, the main contribution to viscoelasticity comes from the viscous component.

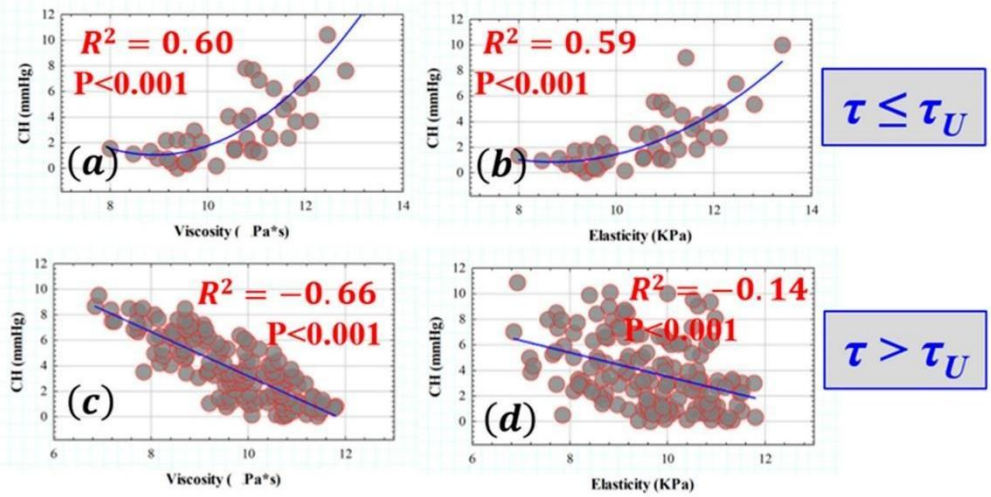

Figure 6. CH as a function of viscosity (**a**) and elasticity (**b**) for retardation time values below the thresold (τ_u) and CH versus Η (**c**) and E (**d**) for suprathreshold τ values.

3.3. Influence of Elasticity and Time-Dependent Parameters on Corneal Optical Properties

The ultrastructure of the stromal lamellae (formed by type-I collagen fibrils) is responsible for corneal optical transparency [3]. In addition, the three-dimensional architecture at the microscopic level has an important implication for the corneal biomechanics [5]. In this sense, this section studies the influence of elasticity and time-dependent corneal properties on both corneal transparency (quantified by optical density measures) and high-order corneal aberrations.

Table 2 shows the representative mean values of optical density (OD), spherical aberration (SA), trefoil and coma terms of the study sample.

Table 2. (**a**) Mean values (±standard deviation) for the corneal-compensated intraocular pressure (IOP_{cc}), central corneal thickness (CCT), corneal radius (R_{cor}), corneal hysteresis (CH), elasticity (E), viscosity (Η) and tau (τ) parameters. (**b**) Mean values (± standard deviation) for the OD, SA, trefoil and coma of all participating subjects.

(a)						
IOP_{cc} (mmHg)	**CCT (μm)**	**R_{cor} (mm)**	**CH (mmHg)**	**E (KPa)**	**Η (Pa· s)**	**T (ms)**
16.51 ± 2.32	555.75 ± 29.49	7.89 ± 0.30	9.78 ± 1.16	3.44 ± 2.67	3.57 ± 2.39	1.12 ± 0.13
(b)						
OD (pd/μm)	**SA (μm)**		**Trefoil (μm)**		**Coma (μm)**	
0.034 ± 0.004	−0.15 ± 0.08		0.19 ± 0.13		0.27 ± 0.14	

Figure 7 shows the relationships found between viscosity and corneal optical density (OD). Optical density increases moderately with viscosity (R^2 = 0.28) (i.e., optical transparency decreases as viscosity increases). No relationships are found between elasticity and optical density.

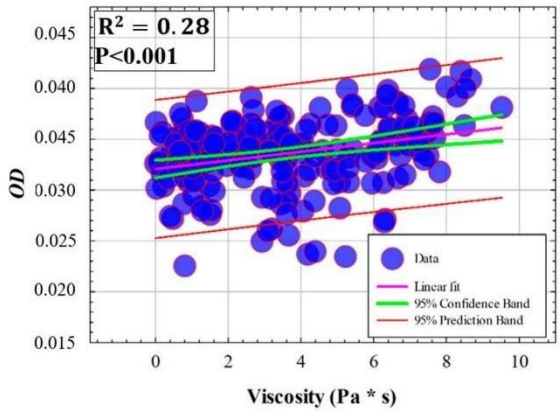

Figure 7. Optical density values as a function of the viscous component. Green lines correspond to the statistical linear fitting ($R^2 = 0.28$, $p < 0.001$).

With respect to corneal optical imperfections measured by high-order aberrometry, Figure 8 shows the correlations found between elasticity and retardation time with the coma term. The data shown in Figure 8a indicate how increasing corneal elasticity correlates ($R^2 = -0.23$) with a descent in the amount of coma term. On the contrary, longer retardation times are related to an increase in corneal coma (Figure 8b).

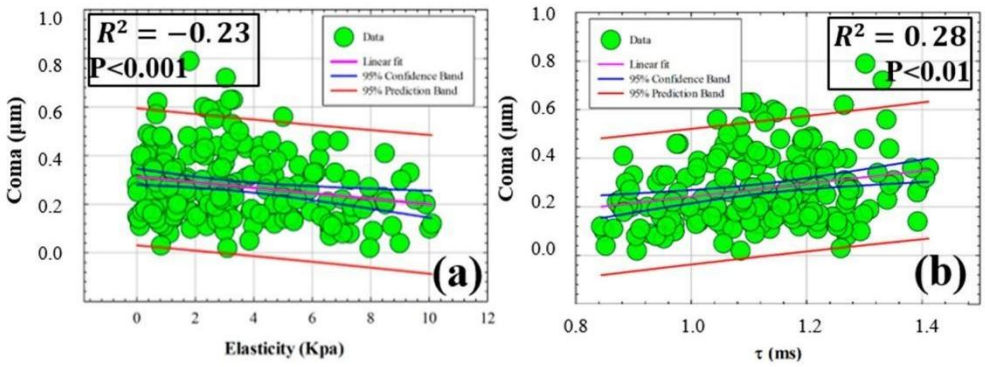

Figure 8. Coma high-order term as a function of elasticity (**a**) and corneal retardation time (**b**). Red lines correspond to the best linear fittings of the data.

3.4. Creep Relaxation Response of the Human Cornea as a Function of Elasticity and Viscosity

Once the elastic and time-dependent biomechanical properties of the human cornea are experimentally derived from ORA measures and Scheimpflug imaging, the SLSM (see Section 2.3) can be fed back from the experimental data for the simulation of creep and stress relaxation behavior under real conditions. Table 3 shows the experimental values of elasticity and viscosity for the representative mean value of our study sample, for an ocular hypertensive patient and for a healthy user of Ortho-K contact lenses.

Table 3. Elasticity (E) and viscosity (η) for a normal cornea (mean value of 200 healthy subjects), for an ocular hypertensive patient and a healthy Ortho-K contact lens wearer.

	Normal Cornea	Ocular Hypertensive	Ortho-K User
E (Kpa)	3.44	13.23	3.13
η (Pa · s)	3.57	8.62	3.47

The data shown in Table 3 are entered as inputs into the solid model to perform a creep and stress relaxation response over a time of 10 s. The ocular hypertensive patient showed a drastic increase in both elastic (+42.2%) and viscous (+82.85%) components. However, the Ortho-K user experienced a slight reduction in E (−9.44%) and almost negligible variation in η (−2.84%).

Figure 9 compares the creep relaxation test between a pathological eye and Ortho-K contact lens wearer with the normal response of a population of 200 healthy young subjects. In agreement with the mean values shown in Table 3, the Ortho-K wearer showed an almost negligible relaxation response compared with normal corneas, while a slightly weaker reduction is seen in the creep response. The ocular hypertensive patient showed a rapid stabilization of the creep (Figure 9a) and relaxation curves (Figure 9b), with a significantly reduced response compared with the normal representative curves (Figure 9, blue lines).

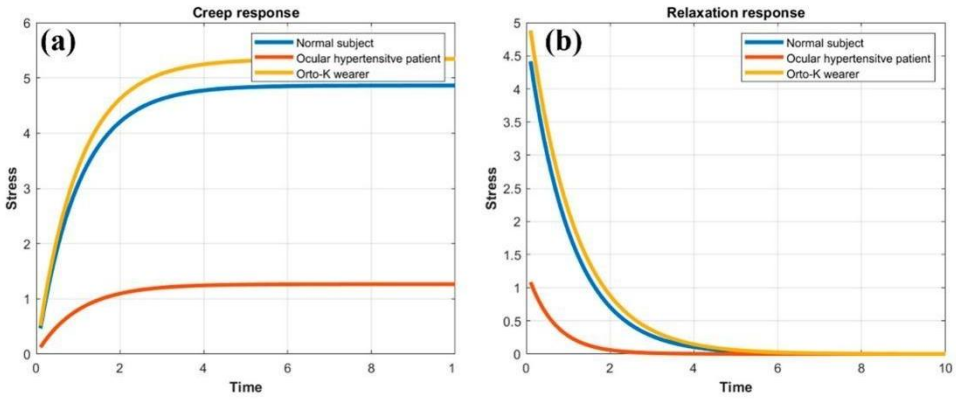

Figure 9. Comparative creep (**a**) and relaxation (**b**) tensile tests for normal corneas (blue curve), an ocular hypertensive patient (red curve) and an Ortho-K contact lens user (orange curve).

4. Discussion and Conclusions

We proposed a simple experimental methodology to obtain information on separated elastic and viscous components from the viscoelastic properties of the living human cornea. The results from the ocular response analyzer combined with geometric information from corneal Scheimpflug imaging allowed us to calculate the corneal retardation time [24] (τ), the corneal elasticity (E) and finally the corneal viscosity (η) from a large sample of young subjects.

To the best of our knowledge, this is the first work presenting the experimental derivation of viscous and elastic components from measurements of living human corneas combining non-contact tonometry and Scheimpflug imaging. In addition, we presented analytical expressions to calculate both elastic moduli and time-dependent biomechanical properties of the human cornea.

The SLSM was employed here to model the human cornea and obtain the creep and stress relaxation response from experimental data by solving the constitutive stress–strain equation of the constitutive law for the loading and unloading conditions of the system.

Biomechanical and geometric experimental data from ORA measurements and Scheimplug imaging were acquired from 200 eyes of healthy young subjects (See Table 1). From these data, E (Kpa), τ (ms) and η (Pa*s) were calculated.

Mikula et al. found a mean elastic moduli value of 3.05 Kpa through the axial cornea measured using acoustic radiation force elasticity microscopy [29]. In agreement, we found an average elastic modulus of 3.44 ± 2.67 Kpa.

Rahmati et al. [30] conducted in-depth research into the biomechanics of keratoconic corneas (KCs), focusing on the viscoelastic properties of both healthy and pathological patients via a finite element optimization algorithm. Though this paper reported interesting conclusions on corneal viscosity in KC patients, the main population of our work consisted of healthy subjects (with one exceptional case of possible glaucoma). Moreover, the authors described the corneal viscoelasticity via the shear deformation parameter, whereas the goal of our research was to separate both viscoelastic contributions, that is, the elastic modulus and viscous component at a time. Nevertheless, the study of biomechanical properties in keratoconic corneas is a matter for future research by our group.

Francis et al. reported a methodology for obtaining corneal viscous properties by analyzing the temporal corneal deflection signal from air-puff applanation in a large sample of normal subjects and patients with keratoconus [31]. In particular, they analyzed the deformation data using the standard linear solid and Kelvin–Voigt models. Unfortunately, they did not detect a significant corneal viscous response of the cornea and concluded that viscous properties cannot be computed from air-puff applanation. Our proposed methodology allowed us to experimentally measure (and calculate analytically) the viscous property of the human cornea in vivo; we found an average value for normal corneas of 3.57 ± 2.39 [Pa $\cdot$ s].

The discrepancies between our study and that published by Francis et al. reside in the adequate definition of a time-dependent biomechanical parameter that relates the viscosity and elasticity, such as the previously reported corneal retardation time [27].

Considering that intraocular pressure (IOP) is the main clinically interesting force affecting the cornea (and its implications on the optical nerve and glaucoma disease), Figure 1 explores the influence of IOP on corneal hysteresis (CH). A negative correlation was found between IOP and CH in accordance with previous studies [32–34].

Therefore, the higher the IOP, the lower the CH and, therefore, the lower the ability of the cornea to dissipate and/or absorb energy from an excess of intraocular pressure.

In this sense, the influence of IOP on the separated elastic and viscous components is analyzed in Figure 4.

A piecewise asymmetric linear behavior was found between IOP, E and η for an IOP threshold value of IOP_U = 14.45 mmHg. A negative linear correlation between E and η with IOP was found for values of IOP lower than IOP_u. However, for intraocular pressure measurements greater than 14.45 mmHg, both the elastic and viscous components of the cornea increased with IOP.

This seemingly anomalous behavior can be better understood by analyzing the results shown in Section 3.2. The corneal retardation had a limit of 1.22 ms, from which the corneal elasticity reversed its behavior (Figure 5).

Considering the threshold value of τ = 1.22 ms, we investigated the influence of separated elasticity and viscosity on corneal hysteresis.

In 2008, Glass et al. [19] reported a methodology based on a viscoelastic model to evaluate how the individual contribution of viscous and elastic components affected corneal hysteresis (i.e., corneal viscoelasticity) in a corneal phantom. They concluded that low hysteresis can be related to either low and high elasticity, depending on the viscous component.

In agreement, our finding revealed that, for low values of retardation time, an increase in both elasticity and viscosity implied a growth in CH. But, consequently, for retardation times higher than 1.22 ms, the dependence of the elastic component on CH decreased and

governed a clear correlation of viscosity with corneal hysteresis. As the viscosity increased the CH decreased, with negative significant correlation.

Therefore, for corneal retardation times greater than 1.22 ms, the cornea showed a predominant viscous behavior. That is, the cornea was capable of absorbing energy but lost the ability to dissipate energy.

Optimal visual acuity is contingent upon corneal transparency. Corneal infections, contact lens complications, chemical injuries or neovascularization are causes of corneal opacification. However, corneal surgery for refractive error correction such as photorefractive keratectomy and accelerated cross-linking for the treatment of degenerative keratoconus can lead to permanent corneal opacification in healthy patients [35]. These last two corneal surgery techniques involve a redistribution of corneal stiffness and biomechanical remodeling.

In this sense, Section 3.3 analyzed the influence of elastic and viscous components on corneal transparency quantified by optical densitometry measurements (corneal Scheimpflug imaging). The results showed a linear dependence on the optical density (OD) but no statistical relationship with elasticity (See Figure 7). Our findings revealed a decrease in optical transparency (i.e., higher optical density) as the viscosity increased.

The results shown in Figure 8 are especially relevant for refractive surgery to better understand how photorefractive laser ablation redistributes the corneal stiffness and how this affects the appearance of higher order aberrations such as coma.

On the other hand, one-dimension tensile creep and stress relaxation tests are usually performed to analyze the viscoelastic nature of the cornea [36,37]. SLSM allowed us to simulate feedback creep relaxation tests from calculated experimental data. The creep and relaxation responses of normal (mean value of 200 healthy subjects), ocular hypertensive and Ortho-K contact lens user were compared. The patient with ocular hypertension showed a drastically reduced response in both creep and relaxation responses compared with normal eyes; however, the Ortho-K user showed a weak and reduced response in the creep response only.

The results obtained in the creep relaxation tests can help to better understand the management of glaucoma and the biomechanical impact of the use of Ortho-K contact lenses for the temporal correction of ametropia.

Finally, it is necessary to emphasize why it is clinically revelant to obtain the separated elastic and viscous components with respect to the viscoelastic measure. Elasticity and viscosity properties arise from different mechanisms governed by the structural arrangement of type-I fibrillary collagen at micro- and nanoscales. Low values of viscosity or elasticity cannot be detected in hysteresis measures and results, as both properties play potentially offsetting ways [19].

Then, let us supose that, under normal physiological conditions, the cornea exhibits a compensatory biomechanical mechanism in which the product E*η remains constant, that is, viscoelasticity is balanced by the individual contributions of the viscous and elastic components. In this sense, Figure 10a shows the product E*η for a range of IOP between 10 and 22 mmHg. It can be seen that, for an IOP range located aproximately between 14 and 16 mmHg, E*η is practically constant; however, outside that range, the trends are again reversed according to the results previously shown. Green and orange boxes delimit pairs of experimental values exhibiting a similar E*η product, which would be equivalent to presenting equal measures of viscoelasticity.

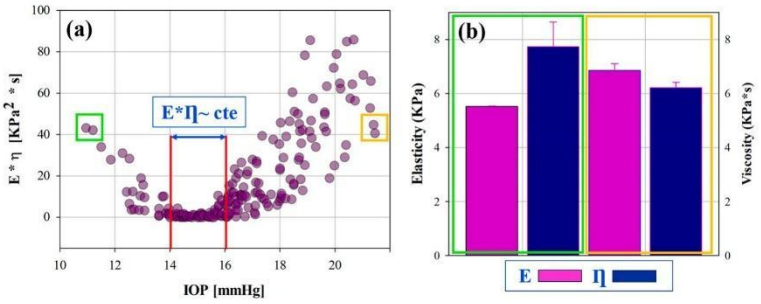

Figure 10. E*Ƞ as a function of the IOP (**a**) and averaged values of E and Ƞ corresponding to the green and orange boxes marked (**b**), respectively.

This would be a clinical disagreement, since the corresponding IOP values are at the extremes of the range. However, if the viscoelasticity is separated into its main components, the elastic and viscous parameters reveal significant differences that could be hidden in viscoelastic measures. While the values of the green and orange boxes appear similar in viscoelasticity (Figure 10a), the individual components of E and Ƞ reveal that the cornea becomes more elastic and less viscous as a result of the intraocular pressure.

It is well known that the measure of viscoelasticity (corneal hysteresis) is not strongly correlated to IOP [38]; a moderate correlation ($R^2 = -0.49$) was found in this study. Low values of viscosity or elasticity cannot be detected in hysteresis measures, as both properties play potentially offsetting ways [19]. The improved outcomes of obtaining separated measures of elasticity and viscosity are directly related to glaucoma patients; lower measured values of CH can be clinically interpreted as a risk factor of glaucoma damage [ref]; however, the elasticity or viscosity can be a stronger contribution with the progression of glaucoma.

To conclude, we present a new methodology to experimentally calculate the separate corneal elasticity and viscosity components of the viscoelasticity measurement by feeding the standard linear solid model with experimental air-puff applanation tonometry and corneal Scheimplug imaging.

Ocular biomechanics is strongly affected by intraocular pressure. Low values of hysteresis should not be considered on their own as risk factors in glaucomatous optic neuropathy; however, the behaviors of the viscous and elastic components should be considered. For subthreshold IOP values of 14.45 mmHg, corneal hysteresis increases with elasticity and viscosity. However, for values above the IOP threshold, low values of viscoelasticity are related to an increase in the viscous and elastic components, with a clear predominance of the viscous property. Results also show that changes in corneal optical density and high-order aberrations can be reflected in both elastic and time-dependent biomechanical properties.

Author Contributions: Conceptualization, F.J.Á.; methodology, F.J.Á. and Ó.d.B.; software, F.J.Á.; validation, F.J.Á. and Ó.d.B.; formal analysis, F.J.Á. and Ó.d.B.; investigation, F.J.Á., Ó.d.B., M.C.M. and L.R.; resources, F.J.Á.; data curation, F.J.Á. and Ó.d.B.; writing—original draft preparation, F.J.Á. and Ó.d.B.; writing—review and editing, F.J.Á. and Ó.d.B.; visualization, L.R. and M.C.M.; supervision, F.J.Á.; project administration, F.J.Á.; funding acquisition, F.J.Á. All authors have read and agreed to the published version of the manuscript.

Funding: This research was funded by "Departamento de Ciencia, Universidad y Sociedad del Conocimiento del Gobierno de Aragón (research group E44−23R)".

Institutional Review Board Statement: This study was conducted in accordance with the Declaration of Helsinki, and approved by the Ethics Committee of the Health Sciences Institute of Aragon, Spain. (protocol code: C.P.-C.I. PI20/377, date of approval: 14 July 2020).

Informed Consent Statement: Informed consent was obtained from all subjects involved in the study.

Data Availability Statement: Dataset is available upon reasonable request.

Conflicts of Interest: The authors declare no conflicts of interest.

References

1. Meek, K.M. Corneal collagen–its role in maintaining corneal shape and transparency. *Biophys. Rev.* **2009**, *1*, 83–93. [CrossRef] [PubMed]
2. Espana, E.M.; Birk, D.E. Composition, structure and function of the corneal stroma. *Exp. Eye Res.* **2020**, *198*, 108137. [CrossRef] [PubMed]
3. Meek, K.M.; Knupp, C. Corneal structure and transparency. *Prog. Retin. Eye Res.* **2015**, *49*, 1–16. [CrossRef] [PubMed]
4. Bell, J.S.; Hayes, S.; Whitford, C.; Sanchez-Weatherby, J.; Shebanova, O.; Terrill, N.J.; Sørensen, T.L.M.; Elsheikh, A.; Meek, K.M. Tropocollagen springs allow collagen fibrils to stretch elastically. *Acta Biomater.* **2022**, *142*, 185–193. [CrossRef] [PubMed]
5. Chong, J.; Dupps, W.J., Jr. Corneal biomechanics: Measurement and structural correlations. *Exp. Eye Res.* **2021**, *205*, 108508. [CrossRef] [PubMed]
6. Wilson, A.; Marshall, J. A review of corneal biomechanics: Mechanisms for measurement and the implications for refractive surgery. *Indian J. Ophthalmol.* **2020**, *68*, 2679–2690. [PubMed]
7. Marinescu, M.; Dascalescu, D.; Constantin, M.; Coviltir, V.; Burcel, M.; Darabus, D.; Ciuluvica, R.; Stanila, D.; Potop, V.; Alexandrescu, C. Corneal Biomechanics—An Emerging Ocular Property with a Significant Impact. *Maedica* **2022**, *17*, 925–930. [PubMed]
8. Kaushik, S.; Pandav, S.S. Ocular Response Analyzer. *J. Curr. Glaucoma Pract.* **2012**, *6*, 17–19. [CrossRef] [PubMed]
9. Lan, G.; Twa, M.D.; Song, C.; Feng, J.; Huang, Y.; Xu, J.; Qin, J.; An, L.; Wei, X. In vivo corneal elastography: A topical review of challenges and opportunities. *Comput. Struct. Biotechnol. J.* **2023**, *21*, 2664–2687. [CrossRef]
10. Eltony, A.M.; Shao, P.; Yun, S.H. Measuring mechanical anisotropy of the cornea with Brillouin microscopy. *Nat. Commun.* **2022**, *13*, 1354. [CrossRef]
11. Terai, N.; Raiskup, F.; Haustein, M.; Pillunat, L.E.; Spoerl, E. Identification of biomechanical properties of the cornea: The ocular response analyzer. *Curr. Eye Res.* **2012**, *37*, 553–562. [CrossRef] [PubMed]
12. Salouti, R.; Bagheri, M.; Shamsi, A.; Zamani, M. Corneal Parameters in Healthy Subjects Assessed by Corvis ST. *J. Ophthalmic Vis. Res.* **2020**, *15*, 24–31. [CrossRef] [PubMed]
13. Yun, S.H.; Chernyak, D. Brillouin microscopy: Assessing ocular tissue biomechanics. *Curr. Opin. Ophthalmol.* **2018**, *29*, 299–305. [CrossRef] [PubMed]
14. Zhang, H.; Asroui, L.; Tarib, I.; Dupps, W.J., Jr.; Scarcelli, G.; Randleman, J.B. Motion-Tracking Brillouin Microscopy Evaluation of Normal, Keratoconic, and Post-Laser Vision Correction Corneas. *Am. J. Ophthalmol.* **2023**, *254*, 128–140. [CrossRef] [PubMed]
15. Ávila, F.J.; Marcellán, M.C.; Remón, L. In Vivo Biomechanical Response of the Human Cornea to Acoustic Waves. *Optics* **2023**, *4*, 584–594. [CrossRef]
16. Kobayashi, A.S.; Staberg, L.G.; Schlegel, W.A. Viscoelastic properties of human cornea. *Exp. Mech.* **1973**, *13*, 497–503. [CrossRef]
17. Lakes, R.S. *Viscoelastic Solids*; CRC Press: Boca Raton, FL, USA, 1999; pp. 15–61.
18. Zimprich, L.; Diedrich, J.; Bleeker, A.; Schweitzer, J.A. Corneal Hysteresis as a Biomarker of Glaucoma: Current Insights. *Clin. Ophthalmol.* **2020**, *14*, 2255–2264. [CrossRef] [PubMed]
19. Glass, D.H.; Roberts, C.J.; Litsky, A.S.; Weber, P.A. A Viscoelastic Biomechanical Model of the Cornea Describing the Effect of Viscosity and Elasticity on Hysteresis. *Investig. Ophthalmol. Vis. Sci.* **2008**, *49*, 3919–3926. [CrossRef] [PubMed]
20. Su, P.; Yang, Y.; Xiao, J.; Song, Y. Corneal hyper-viscoelastic model: Derivations, experiments, and simulations. *Acta Bioeng. Biomech.* **2015**, *17*, 73–84.
21. Whitford, C.; Movchan, N.V.; Studer, H.; Elsheikh, A. A viscoelastic anisotropic hyperelastic constitutive model of the human cornea. *Biomech. Model. Mechanobiol.* **2018**, *17*, 19–29. [CrossRef]
22. Ahmed, H.M.; Salem, N.M.; Al-Atabany, W. Human cornea thermo-viscoelastic behavior modelling using standard linear solid model. *BMC Ophthalmol.* **2023**, *23*, 250. [CrossRef] [PubMed]
23. Kelly, P. Solid Mechanics Part I: An Introduction to Solid Mechanics Solid Mechanics Lecture Notes University of Auckland. 2013. Available online: https://pkel015.connect.amazon.auckland.ac.nz/SolidMechanicsBooks/Part_I/index.html (accessed on 29 April 2024).
24. Liu, J.; Roberts, C.J. Influence of corneal biomechanical properties on intraocular pressure measurement: Quantitative analysis. *J. Cataract. Refract. Surg.* **2005**, *31*, 146–155. [CrossRef] [PubMed]
25. Brinson, H.F.; Brinson, L.C. *Polymer Engineering Science and Viscoelasticity*; Springer: Berlin/Heidelberg, Germany, 2008.
26. Jannesari, M.; Mosaddegh, P.; Kadkhodaei.; Kasprzak, H.; Jabbarvand Behrouz, M. Numerical and clinical investigation on the material model of the cornea in Corvis tonometry tests: Differentiation between hyperelasticity and viscoelasticity. *Mech. Time Depend. Mater.* **2018**, *23*, 373–384. [CrossRef]
27. Barco, O.; Ávila, F.J.; Marcellán, C.; Remón, L. Corneal retardation time as an ocular hypertension disease indicator. *Biomed. Phys. Eng. Express* **2024**, *10*, 015014. [CrossRef] [PubMed]
28. Deol, M.; Taylor, D.A.; Radcliffe, N.M. Corneal hysteresis and its relevance to glaucoma. *Curr. Opin. Ophthalmol.* **2015**, *26*, 96–102. [CrossRef] [PubMed]

29. Mikula, E.R.; Jester, J.V.; Juhasz, T. Measurement of an Elasticity Map in the Human Cornea. *Investig. Ophthalmol. Vis. Sci.* **2016**, *57*, 3282–3286. [CrossRef] [PubMed]
30. Rahmati, S.M.; Razaghi, R.; Karimi, A. Biomechanics of the keratoconic cornea: Theory, segmentation, pressure distribution, and coupled FE-optimization algorithm. *J. Mech. Behav. Biomed. Mater.* **2021**, *113*, 104155. [CrossRef] [PubMed]
31. Francis, M.; Matalia, H.; Nuijts, R.M.M.A.; Haex, B.; Shetty., R.; Sinha Roy, A. Corneal Viscous Properties Cannot Be Determined From Air-Puff Applanation. *J. Refract. Surg.* **2019**, *35*, 730–736. [CrossRef] [PubMed]
32. Dana, D.; Mihaela, C.; Raluca, I.; Miruna, C.; Catalina, I.; Miruna, C.; Schmitzer, S.; Catalina, C. Corneal hysteresis and primary open angle glaucoma. *Rom. J. Ophthalmol.* **2015**, *59*, 252–254.
33. Nossair, A.A.; Kassem, M.K.; Eltanamly, R.M.; Alahmadawy, Y.A. Corneal Hysteresis, Central Corneal Thickness, and Intraocular Pressure in Rheumatoid Arthritis, and Their Relation to Disease Activity. *Middle East Afr. J. Ophthalmol.* **2021**, *28*, 174–179.
34. Murtagh, P.; O'Brien, C. Corneal Hysteresis, Intraocular Pressure, and Progression of Glaucoma: Time for a "Hyst-Oric" Change in Clinical Practice? *J. Clin. Med.* **2022**, *11*, 2895. [CrossRef] [PubMed]
35. Blanco-Dominguez, I.; Duch, F.; Reyes, J.; Polo, V.; Abad, J.M.; Gomez-Barrera, M.; Olate-Perez, Á. Permanent corneal opacification after refractive surgery with a combined technique: Photorefractive keratectomy (PRK) and accelerated cross-linking (PRK Xtra) in healthy patients. *J. Français D'ophtalmologie* **2021**, *44*, e141–e143. [CrossRef] [PubMed]
36. Abyaneh, M.H.; Wildman, R.D.; Ashcroft, I.A.; Ruiz, P.D. A hybrid approach to determining cornea mechanical properties in vivo using a combination of nano-indentation and inverse finite element analysis. *J. Mech. Behav. Biomed. Mater.* **2013**, *27*, 239–248. [CrossRef] [PubMed]
37. Lombardo, G.; Serrao, S.; Rosati, M.; Lombardo, M. Analysis of the viscoelastic properties of the human cornea using Scheimpflug imaging in inflation experiment of eye globes. *PLoS ONE* **2014**, *9*, e112169. [CrossRef]
38. Touboul, D.; Roberts, C.; Kérautret, J.; Garra, C.; Maurice-Tison, S.; Saubusse, E.; Colin, J. Correlations between corneal hysteresis, intraocular pressure, and corneal central pachymetry. *J. Cataract. Refract. Surg.* **2008**, *34*, 616–622. [CrossRef]

2.6. Aberrometric, Geometrical and Biomechanical Characterization of Sound-Induced Vibrational Modes of the Living Human Cornea.

Ávila FJ, del Barco O, Marcellán MC, Remón L. Aberrometric, Geometrical and Biomechanical Characterization of Sound-Induced Vibrational Modes of the Living Human Cornea. *Optics*. 2025; 6(1):5. https://doi.org/10.3390/opt6010005

JIF (2023):1,1-Optics-94/119-Q4

JCI (2023): 0,31-Optics-97/120-Q4

optics

MDPI

Article

Aberrometric, Geometrical, and Biomechanical Characterization of Sound-Induced Vibrational Modes of the Living Human Cornea

Francisco J. Ávila [1,*], Óscar del Barco [2], Maria Concepción Marcellán [1] and Laura Remón [1]

[1] Departamento de Física Aplicada, Facultad de Ciencias, Universidad de Zaragoza, 50009 Zaragoza, Spain
[2] Laboratorio de Óptica, Instituto Universitario de Investigación en Óptica y Nanofísica, Universidad de Murcia, 30100 Murcia, Spain
* Correspondence: avila@unizar.es

Abstract: Repeatable and reliable assessment of corneal biomechanics with spatial resolution remains a challenge. Vibrational Optical Computerized Tomography (V-OCT), based on sound-wave elastography, has made it possible to investigate the natural resonant modes of the cornea and obtain the elastic moduli non-invasively. This pilot study presents a characterization of four corneal vibrational modes from aberrometric, geometrical, and biomechanical approaches in the living human cornea of five healthy volunteers by combining a corneal sound-wave generator, dual Placido–Scheimpflug corneal imaging, and the Ocular Response Analyzer (ORA) devices. Sound-induced corneal wavefront aberration maps were reconstructed as a function of sound frequency and isolated from the natural state. While maps of low-order aberrations (LOA) revealed symmetric geometrical patterns, those corresponding to high-order aberrations (HOA) showed complex non-symmetric patterns. Corneal geometry was evaluated by reconstructing corneal elevation maps through biconical fitting, and the elastic and viscous components were calculated by applying the standard linear solid model to the ORA measurements. The results showed that sound-wave modulation can increase high-order corneal aberrations significantly. Two frequencies rendered the corneal shape more prolate (50 Hz) and oblate (150 Hz) with respect to the baseline, respectively. Finally, both the elastic and viscous properties are sensitive to sound-induced vibrational modes, which can also modulate the corneal stress-strain response. The cornea exhibits natural resonant modes influenced by its optical, structural, and biomechanical properties.

Keywords: corneal vibrational modes; sound-wave vibrometry; corneal aberrations; corneal biomechanics; corneal viscosity; corneal elasticity

Academic Editor: Marco Gandolfi

Received: 10 December 2024
Revised: 24 January 2025
Accepted: 3 February 2025
Published: 5 February 2025

Citation: Ávila, F.J.; Barco, Ó.d.; Marcellán, M.C.; Remón, L. Aberrometric, Geometrical, and Biomechanical Characterization of Sound-Induced Vibrational Modes of the Living Human Cornea. *Optics* **2025**, *6*, 5. https://doi.org/10.3390/opt6010005

1. Introduction

Ocular biomechanics focuses on the dynamic response the cornea when an external stress is applied [1]. This response, typically measured through air-puff corneal deformation, reflects the cornea's elastic and viscoelastic properties [1,2]. The cornea's intrinsic biomechanical characteristics are determined by its extracellular matrix (corneal stroma), which ensures optical transparency, mechanical stability, and tissue shape [3]. Factors such as hydration levels [4], environmental conditions, metabolic influences [5], and age [6] can alter these properties. Pathological and external factors, including increased intraocular pressure (IOP) [7], contact lens wear [8], laser refractive surgery [9], or diseases like keratoconus [10], glaucoma [11], and corneal ectasia [12,13], can further disrupt the biomechanical stability of the cornea.

Given the critical role of corneal biomechanics in ocular health, various tools have been developed to assess these properties. Among the most widely used are the Ocular Response Analyzer (ORA; Reichert Technologies) and the Oculus Corvis ST (OCULUS Optikgeräte GmbH), both of which employ non-contact air-puff tonometry. The ORA measures corneal viscoelasticity [14,15] through corneal hysteresis (CH), a parameter that has been extensively studied as a biomarker for glaucoma [16,17], Fuchs' dystrophy [18], and biomechanical changes in keratoconus and post-LASIK patients [19]. Meanwhile, the Corvis ST combines tonometry with high-speed Scheimpflug imaging, offering dynamic parameters that have been applied to studying keratoconus [20,21], orthokeratology [22], dry eye [23], and myopia-related biomechanical alterations [24].

Although these devices provide rapid assessments, they do not directly measure intrinsic biomechanical properties. Computational modeling, such as the viscoelastic models proposed by Glass et al. [25], has been employed to infer these properties from the devices' measurements. Recently, our group proposed a methodology based on ORA measurements and the standard linear solid model to derive distinct analytical expressions for elastic and time-dependent biomechanical parameters, including retardation time and viscosity [26].

Emerging technologies, like elastography imaging, have also gained prominence in biomechanics. Optical Coherence Elastography (OCE) provides spatially resolved measurements of the elastic modulus by analyzing the propagation of mechanical shear waves [27–29]. However, these measurements can be influenced by factors like corneal curvature, thickness [30], intraocular pressure [31], and even systemic variables such as heartbeat and respiration [32], potentially leading to inaccuracies.

This study aims to build on this foundation by investigating the biomechanical response of the living human cornea under acoustic stimulation. Specifically, we seek to characterize changes in wavefront aberrometry, corneal geometry, and stress-strain responses across four vibrational frequency modes (50, 150, 250, and 350 Hz). By integrating these findings, this work provides new insights into the dynamic behavior of corneal biomechanics, offering potential advancements in the diagnosis and treatment of biomechanical disorders.

2. Materials and Methods

2.1. Subjects

Five healthy Caucasian participants (35 ± 10 years old) were recruited to participate in the study. Measurements were performed at the Vision Sciences Laboratory of the University of Zaragoza (Zaragoza, Spain). Exclusion criteria included elevated intraocular pressure (IOP), glaucoma, contact lens wearers, and patients undergoing refractive surgery or corneal complications that could alter measurements results. Demographic information is shown in Table 1.

Table 1. Demographic information of the cohort studied. N: number of participants; std: standard deviation; IOP: intraocular pressure.

Demographic Information (N = 5)	
Male/female	2/5
Age (mean ± std)	35 ± 10
Ethnicity	Caucasian
Ophthalmic History	Not found
Medical History	Not found
IOP (mean ± std)	15.32 ± 2.94 mmHg

The present study was conducted in accordance with the Declaration of Helsinki and approved by the Ethics Committee of the Health Sciences Institute of Aragon, Spain (protocol code: C.P.-C.I. PI20/377; date of approval: 14 July 2020).

2.2. Experimental Measurements

A corneal acoustic wave generator [33] was used to obtain geometric, biomechanical, and total corneal wavefronts for four different sound frequencies from a sine wave signal applied at a maximum pressure of 90 dB. These sound frequencies were 50, 150, 250, and 350 Hz. Commercial dual Placido–Scheimpflug imaging (Galilei G2; Ziemer Ophthalmic Systems AG, Port, Switzerland) and the Ocular Response Analyzer (ORA, Reichert Instruments, Depew, NY, USA) devices were used to obtain the data summarized in Table 2.

Table 2. Summary of experimental parameters required for wavefront aberration, geometrical, and biomechanical analysis, the information provided, and the instrument from which they were acquired.

Parameter	Information	Instrument
Zernike coefficients (mode number) [μm]	Corneal wavefront aberrometry	Galilei G2
Pupil aperture [mm]	Area of the wavefront measurement	Galilei G2
Q-factor	Corneal asphericity	Galilei G2
Flat R_1 [mm]	Flat corneal radius	Galilei G2
Steep R_2 [mm]	Steep corneal radius	Galilei G2
CH [mmHg]	Corneal hysteresis	ORA
CRF [mmHg]	Corneal resistant factor	ORA
IOP [mmHg]	Intraocular pressure	ORA

2.3. Wavefront Analysis

Corneal Zernike coefficients were obtained from the Galilei G2 measurements for 6 mm of corneal zone (aperture), and those mode number were used to reconstruct wavefront aberration (WA) maps as a function of sound frequency using Equation (1).

$$WA(\rho,\theta) = \sum_{n=0}^{\infty} \sum_{m=-n}^{n} c_n^m \times Z_n^m(\rho,\theta) \quad (1)$$

Equation (1) represents the corneal wavefront aberration in the Zernike polynomial expansion according to the Optical Society of America (OSA) standards [34]. Here, Z_n^m and c_n^m and are the Zernike modes and coefficients, respectively. The subscript n and superscript m correspond to the radial order and angular frequency. Figure 1 shows a representation of the Zernikes modes provided by the Galilei G2 device.

The root mean square (RMS) metric was used to numerically compare the influence of sound waves on corneal WA, calculated as follows:

$$RMS = \sqrt{\sum_{j=3}^{14} c_j^2} \quad (2)$$

where $j = \frac{n(n+2)+m}{2}$. Then, the RMS was calculated for low-order and high-order aberrations (LOA and HOA, respectively).

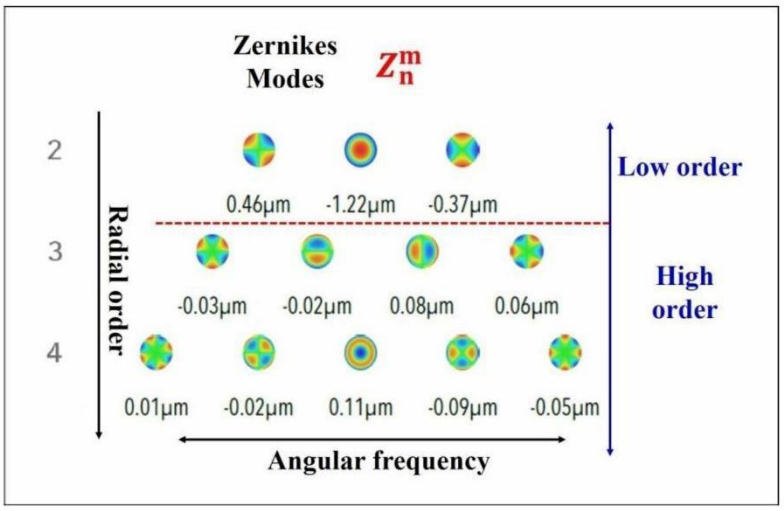

Figure 1. Scheme of Zernike coefficients provided by Galilei G2 device.

2.4. Corneal Surface Reconstruction

The geometrical information provided by the Galilei device (i.e., the Q-factor and radii of curvature) was employed to reconstruct the corneal surfaces for each sound frequency using the equation of the sagittal curve for a biconic surface, that can be expressed in Cartesian coordinates, as in [35]:

$$z(x,y) = \frac{\frac{x^2}{R_x} + \frac{y^2}{R_y}}{1 + \sqrt{1 - (1+Q_x)\frac{x^2}{R_x} - (1+Q_y)\frac{y^2}{R_y}}} \quad (3)$$

Here, R_x, R_y, Q_x, and Q_y are the radii of curvature (i.e., flat and steep principal corneal meridians) and conic constants of the cornea. Equation (3) allows for fitting the cornea to a biconic surface, from which the mean corneal elevation is calculated and analyzed in Section 3.2.

2.5. Biomechanical Model

The ORA device was employed to extract the parameters required to calculate the elastic and time-dependent parameters (i.e., corneal retardation time and viscous component) of the cornea, as reported in [26]. The elasticity, retardation time, and viscosity were employed to simulate creep-relaxation tests as a function of sound frequency in Section 3.3.

2.6. Statistical Analysis and Image Reconstruction Processing

A statistical analysis was applied to aberrometric data to explore differences in the mean values among the different sound frequencies. Basically, the analysis consisted of performing the Shapiro–Wilk test to check the normality of the data and then the One-Way Repeated Measures Analysis of Variance (One-Way RM ANOVA). Graphical representations and statistics were carried out in Origin Lab v.13 software (OriginPro 2024, Origin Lab Corp., Northampton, MA, USA). Wavefront aberration maps and corneal surface reconstructions were carried out using custom-written scripts in Matlab2019b (the MathWorks Inc., Natick, MA, USA).

3. Results

3.1. Wavefront Aberrometry

Figure 2 shows the averaged amplitude values (i.e., the mean of the five participants) of the Zernike coefficients of the corneal WA for the relaxed state (Figure 2a) and for different sound-wave frequencies (Figure 2b–e). The data show how different sound frequencies modulate each individual Zernike coefficient in terms of low and high aberration. Figure 3 shows the low- and high-order aberration root mean square (LOA and HOA RMS, respectively) values as a function of sound frequency. The maximum WA deviations differ for LOA and HOA: while for 250 Hz LOA increases by up to 11.98% (Figure 3a) with respect to the relaxed state (i.e., when the sound-wave generator is off), the maximum RMS variation occurs at 150 Hz for HOA (Figure 3b). Furthermore, this observed increase in the RMS value of 21.92% was found to be significantly higher (one-way Anova test, $p = 0.039$) than the reference (control) RMS value. Although RMS modulation as a function of sound frequency was observed in both LOA and HOA, no significant differences were found between the rest of the values represented.

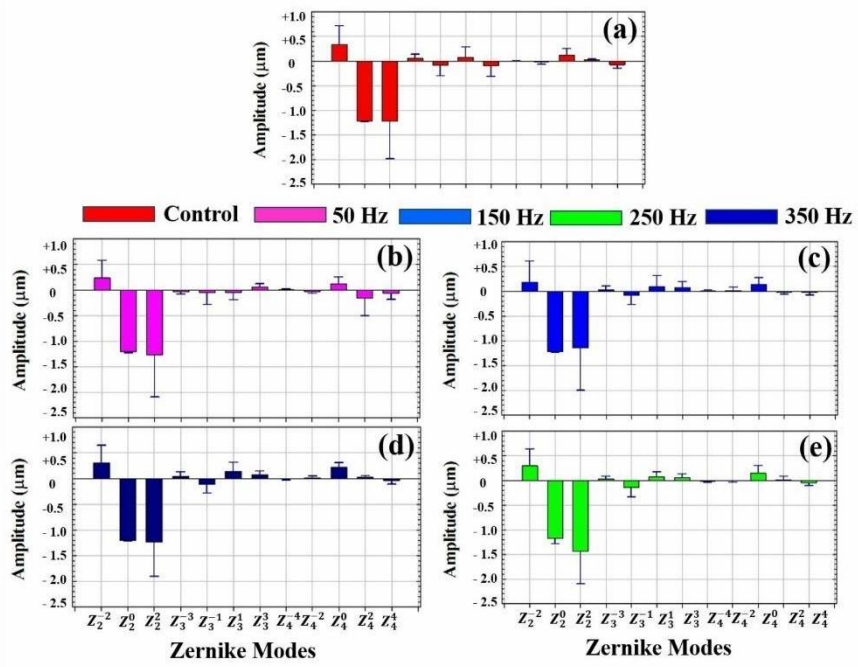

Figure 2. Average amplitude values of each Zernike mode number for control (relaxed state) (**a**) and for each sound frequency (**b**–**e**).

To complete the WA description, Figure 4 shows the reconstructed wavefront aberration maps for LOA and HOA as a function of sound frequency. The first and third rows show the original WA map for LOA and HOA, respectively. To highlight the induced effects by sound waves, the second and fourth rows show the WA maps with subtracted control aberrometric data ('control–LOA WA' and 'control–HOA WA', respectively). It can be observed how WA LOA maps show symmetric geometric patterns, while the HOA maps show complex irregular patterns.

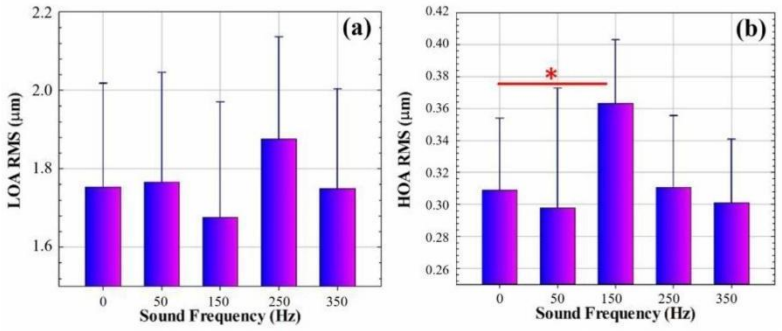

Figure 3. Average RMS values for low-order (**a**) and high-order aberrations (**b**) RMS values (LOA and HOA RMS, respectively) as a function of sound frequency. Asterisk indicates statistically significant difference ($p < 0.005$).

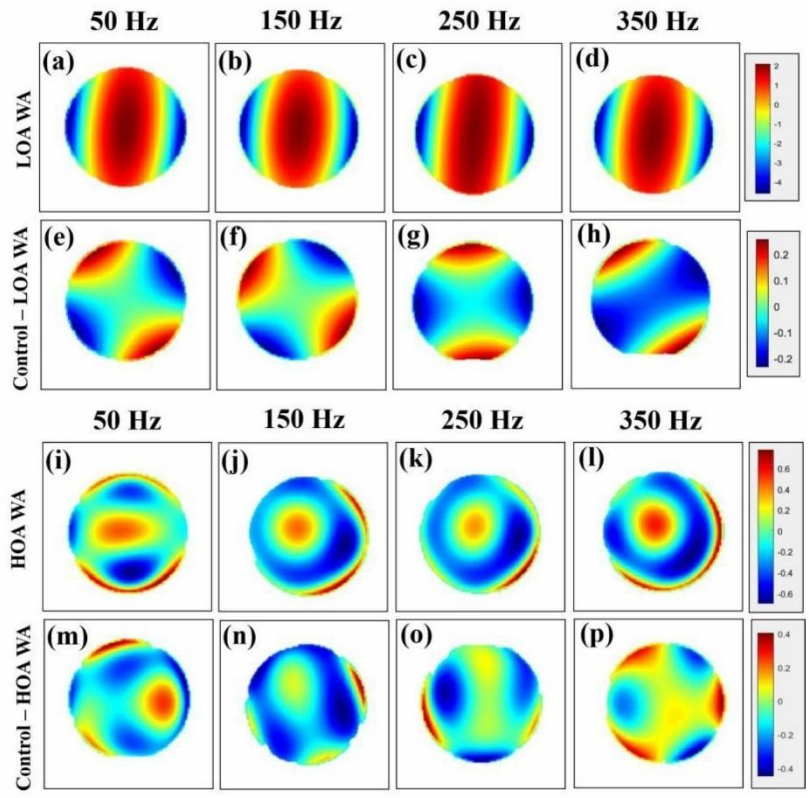

Figure 4. Top row and third row: low- (**a**–**d**) and high-order (**i**–**l**) wavefront aberration (LOA WA and HOA WA, respectively) maps as a function of sound frequency. Second and fourth rows: wavefront aberration maps isolated from control measurements [Control–LOA (**e**–**h**) and HOA WA (**m**–**p**), respectively].

The wavefront results showed that, although sound-induced mechanical vibrations can modulate the low-order aberration (LOA) terms, none of the sound frequencies induced a significant variation in these terms. On the contrary, the frequency of 150 Hz induced a significant increase in corneal high-order aberrations (HOA) with respect to the baseline corneal values. Reconstruction of the wavefront aberration maps allowed visualization of

the formation of regular patterns in LOA (Figure 4), while for HOA, complex and asymmetric WA maps were observed. These patterns suggest localized biomechanical responses influenced by collagen fiber distribution and corneal viscoelasticity, as corroborated by Crespo et al. [36] and Silver et al. [37].

3.2. Corneal Geometry

Corneal surfaces were reconstructed from the mean radii of curvature and conic constants using the biconical equation described in Section 2.3. Figure 5a shows the fit of the corneal surface corresponding to the mean corneal geometric parameters in the relaxed state. This elevation map was set as a reference to be subtracted from those reconstructed for the different sound frequencies. As an example, Figure 5b,c shows the relative elevation maps induced by the application of sound waves for 150 and 350 Hz frequencies. While for 150 Hz an asymmetric meridional elevation is observed, for the 350 Hz frequency the induced elevation appears to be negligible.

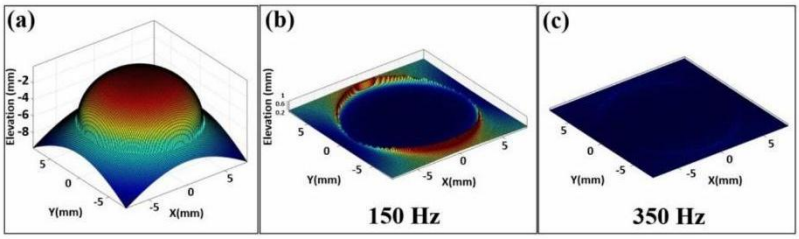

Figure 5. Corneal surfaces reconstructed using biconic fit. (**a**): control surface; (**b**,**c**): reconstructed surfaces for 150 Hz and 350 Hz, respectively.

Figure 6a shows the mean corneal elevation as a function of sound frequency. It is important to highlight how, depending on the applied frequency, depressions or elevations can be observed. The geometric analysis was complemented by the analysis of corneal asphericity; Figure 6b shows the mean Q-factor measured by Scheimpflug images for the control (baseline) and for the different sound frequencies. As shown, the most oblate induced deformation occurs for 150 Hz, which corresponds to the maximum corneal elevation (Figure 6a). In contrast, the maximum depression observed for 50 Hz (Figure 6a) corresponds to the most prolate deformation at the same frequency (Figure 6b).

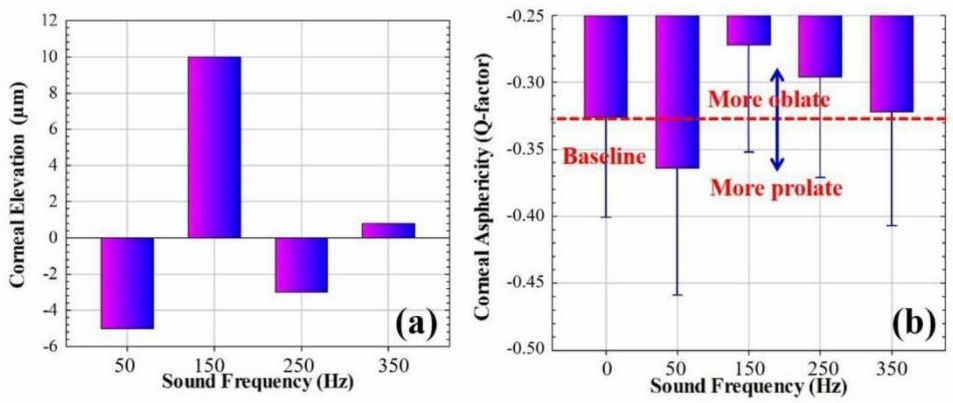

Figure 6. Mean corneal elevation (**a**) and corneal asphericity (**b**) as a function of sound frequency.

The geometrical analysis consisted of corneal elevation analysis computed from the biconical surface corneal fit and asphericity measurements. The maximum corneal elevation was found for the 150 Hz frequency, which corresponded to the most oblate Q-factor. On the other hand, the 50 Hz frequency induced the maximum corneal depression and showed the most prolate deformation of the four sound frequencies. In contrast, the 350 Hz frequency induced negligible changes with respect the baseline values.

3.3. Biomechanical Analysis

Finally, this subsection analyzes the influence of the mechanical vibration of sound waves on corneal biomechanics. A previously reported standard linear solid model [34] applied to ORA measurements was used to extract the elastic and viscous properties of the cornea as a function of sound frequency. Figure 7 shows the average elasticity and viscosity values for the relaxed state (i.e., sound frequency = 0 Hz) and for four different sound frequencies. The maximum modulation of corneal elasticity occurs for the sound frequency of 250 Hz, while 250 Hz induces the maximum increase in the viscous component. However, for the frequency of 350 Hz, both elasticity and viscosity decrease by relatively similar percentages (decreases of 3.53% and 2.74%, respectively). This fact stands out from the wavefront and geometrical analyses, for which this sound frequency seemed to be innocuous.

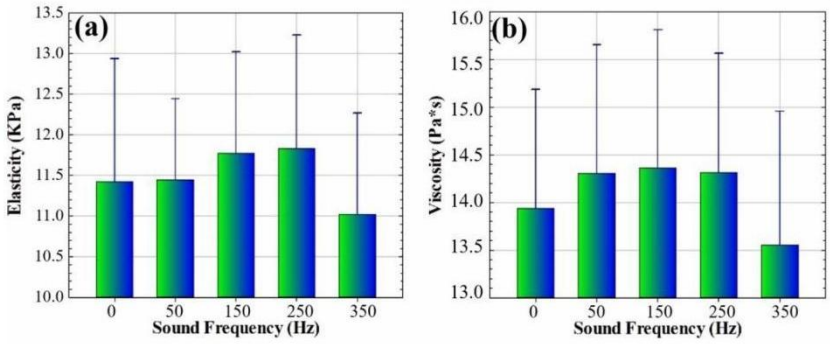

Figure 7. The average (mean of the 5 subjects) elasticity (**a**) and viscosity (**b**) parameters for the relaxed state and four sound frequencies.

The calculated biomechanical parameters were used to feed a previously reported standard linear solid model [34] and then to perform a creep-relaxation (C-R) test as a function of sound frequency. Panels (a) and (b) of Figure 8 show a C-R test with an integration time of 6 s for different sound frequencies. It can be observed that the sound frequency modulates both the creep and relaxation responses. Figure 8c,d show the responses marked in the red rectangles in the above figures for the first second of the C-R test, and those ranges show the largest distances with respect to the control responses, which are given for the frequency of 250 Hz.

The biomechanical analysis consisted of calculating the elastic and viscous components of the cornea using a standard linear solid model (SLSM), previously reported in [26]. The maximum variation in corneal elasticity occurred for 250 Hz, while the maximum increase in the viscous component occurred for 150 Hz. However, the maximum reduction in both elasticity and viscosity was given for 350 Hz.

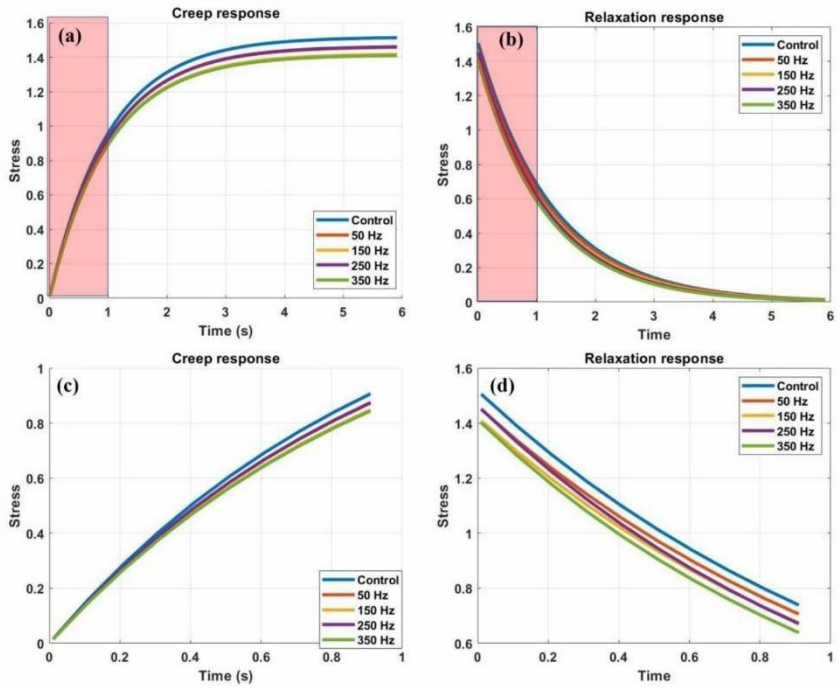

Figure 8. (**a**,**b**) Creep-relaxation test for different sound frequencies and integration time of 6 s. (**c**,**d**) Enlarged view of red rectangles for better visualization of sound-wave modulation in stress-strain curves.

4. Discussion

Since the first observation of sound-induced vibrational modes of the cornea almost a decade ago by Akca et al. [38], the stimulation of the cornea through its natural resonance frequency has attracted the interest of researchers working on the development of new advanced techniques for the assessment of corneal biomechanics.

We have recently reported on the effect of sound-induced mechanical vibration on the corneal biomechanics of the living human cornea [33] for a discrete range of sound frequencies between 50 and 350 Hz at a maximum sound pressure of 90 dB. The study reported by Akca et al. [38] revealed an amplitude of vibration of 8 μm in the fundamental resonant mode between 80 and 120 Hz for a sound pressure of 100 dB in enucleated corneas of bovine eyes. In good agreement, our findings showed a variation of 7.33 μm in central corneal thickness at the frequency of 150 Hz (90 dB sound pressure) in living human corneas [33].

Lan et al. [39] reported an elastography-based OCT method to quantify the corneal natural resonant frequency in living human eyes by air-pulse stimulation. Although they found a dependence of the dominant natural frequency on corneal thickness, this frequency appeared to be constant for different stimulation pressures and measurement distances. Specifically, they found a natural corneal resonant frequency of the living human cornea of 259 Hz. The same group quantified the natural resonant frequency range of the cornea by inducing submicron corneal vibrations using low-power microliter air pulses [40]. They found a corneal natural frequency range of 234–277 Hz in a measured region of 2.5×2.5 mm^2 centered at the corneal apex, with an application time of 28.6 s. This range was found to be repeatable over a smaller area (1 mm^2) and shorter application time (0.9 s).

Subsequently, Crespo et al. [36], used vibrational OCT imaging for the assessment of the elastic modulus of the living human cornea by resonant frequency excitation. They found five peak resonant frequencies at 73.5, 120.4, 148.7, 207.0, and 239.0 Hz and suggested that peaks two to five might correspond to different collagen networks in the stroma, while peak 1 was related to corneal cellular components.

The latter hypothesis was later confirmed by Silver et al. [37], demonstrating that vibrational OCT can isolate the cellular component of the cornea. Lan et al. [39] demonstrated that different components of the natural frequency spectrum can correspond to different tissue structures and thus characterize different heterogeneities of biological structures.

The natural resonant frequency of the cornea can be altered by variations in intraocular pressure, elasticity, or corneal thickness [41] and has been proposed as a biomarker for corneal biomechanics. The objective of this pilot study was to characterize the induced effects of four sound-induced vibrational modes in the living human cornea from a multimodal analysis based on wavefront aberrometry, geometry, and biomechanics.

In our previous study [26], we introduced the concept of Pneumatic Viscoelastic Damping (PVD) as the ability of the cornea to modify its viscoelastic properties under dynamic loading conditions. Those results showed PVD values of +3.57% and −4.34% for the frequencies of 150 and 250 Hz, respectively. While positive PVD values were associated with an increase in viscosity, an increase in corneal elasticity corresponded to negative PVD values. The possibility of obtaining the separated elastic and viscous components of the human cornea in vivo allowed us to corroborate that the maximum increase in viscosity and elasticity indeed occur at 150 and 250 Hz, respectively.

The SLSM model [33] also allowed the simulation of stress-relaxation tests with the calculated biomechanical properties; such tests showed how vibrational modes can affect both creep and relaxation behaviors. In particular, the application of specific sound frequencies in vibrometry allows for obtaining faster deformation and stress relaxation under the same external load conditions (see Figure 8).

Table 3 summarizes the variations induced by each sound frequency on wavefront aberration, corneal geometry, and biomechanics. The frequency of 50 Hz has the ability to reduce HOA, flatten the corneal surface, and increase corneal viscosity; however, this sound frequency does not induce any effect on LOA or elastic properties.

Table 3. Percentage of variation with respect to reference parameters studied as a function of vibrational mode. Low-order and high-order aberrations (LOA and HOA); corneal asphericity (Q-value); elasticity and viscous corneal biomechanical components.

	50 Hz	**150 Hz**	**250 Hz**	**350 Hz**
		Wavefront		
LOA	↑ 0.70%	↓ 5.10%	↑ 11.98%	↓ 6.70%
HOA	↓ 3.62%	↑ 21.92%	↓ 14.43%	↓ 3.15%
		Corneal geometry		
Q value	↑ 11.66%	↓ 16.56%	↓ 9.20%	↓ 1.23%
		Biomechanics		
Elasticity	↑ 0.18%	↑ 3.05%	↑ 3.56%	↓3.53%
Viscosity	↑ 2.65%	↑ 3.05%	↑ 2.71%	↓ 2.74%

At 150 Hz, LOAs are reduced by 5.10%, while HOAs showed a significant increase in RMS values (21.92%, $p = 0.039$) compared to the baseline wavefront aberration.

The observed significant increase in HOAs at 150 Hz aligns with studies reporting resonant frequency effects on corneal biomechanics [42]. Frequencies near natural resonant

modes can amplify certain biomechanical responses, potentially explaining the pronounced HOA variations.

Lower frequencies (e.g., 50 Hz) primarily impacted corneal shape and did not significantly alter HOAs, possibly due to insufficient energy to excite low-order modes. Higher frequencies (350 Hz) may not effectively couple with the cornea's structural properties, leading to minimal aberration changes.

The cornea becomes more oblate (a Q factor increase of 16.56%) and the elastic and viscous components are affected in exactly the same proportion: both increase by 3.05%. This frequency provides the maximum increase in viscosity of the studied vibrational modes. A frequency of 250 Hz shows an inverse behavior compared to 150 Hz in the wavefront analysis; while LOAs increase, HOAs decrease, as shown in Table 3. The corneal geometry becomes more oblate and both elasticity and viscosity increase. This frequency provides the maximum elastic modulation with respect to the other vibrational modes.

Finally, at 350 Hz all the parameters studied are reduced: wavefront aberration, corneal geometry, and biomechanics. It is important to note that the corneal geometry seemed to be insensitive to the specific frequency of 350 Hz; however, it is the only frequency capable of reducing the elastic and viscous components of the corneal biomechanics.

5. Conclusions

In conclusion, the cornea exhibits vibrational modes whose behavior is influenced by its mechanical, structural, and optical properties. These modes are being considered as biomarkers of corneal biomechanics and can reveal critical information in pathological processes such as corneal keratoconus [43].

Low-frequency sound vibrometry provides a non-invasive way to analyze different natural corneal vibrational modes that are sensitive to wavefront aberration, macrostructure, and biomechanical properties such as elasticity and viscosity. The integration of aberrometry and the interaction of sound-wave vibrometry can achieve a more comprehensive understanding of how mechanical and optical corneal aberrations correlate and investigate how vibrational wavefront aberration patterns are altered, identifying areas of potential weakness before surgery or corneal pathologies.

Finally, knowledge of how the elastic and viscous properties of the cornea respond to different vibrational modes reflects the cornea's ability to compensate for mechanical stress, helping the physician improve clinical outcomes and minimize post-corneal surgery complications.

Future research will focus on the integration of sound-wave corneal vibrometry into new approaches based on structural contrast mechanisms to investigate how different vibrational modes can characterize the corneal tissue and reveal physiological or pathological alterations not detected in current diagnostic modalities.

Author Contributions: Conceptualization, F.J.Á.; methodology, F.J.Á., Ó.d.B., M.C.M. and L.R.; formal analysis, F.J.Á.; investigation, Ó.d.B., M.C.M. and L.R.; writing—original draft preparation, F.J.Á.; writing—review and editing, F.J.Á. and Ó.d.B.; project administration, F.J.Á.; funding acquisition, F.J.Á. All authors have read and agreed to the published version of the manuscript.

Funding: This research was funded by Fundación Bancaria Ibercaja, grant number 223221: JIUZ-2021-CIE-01.

Institutional Review Board Statement: The study was conducted in accordance with the Declaration of Helsinki and approved by the Ethics Committee of the Health Sciences Institute of Aragon, Spain (protocol code: C.P.-C.I. PI20/377; date of approval: 14 July 2020).

Informed Consent Statement: Informed consent was obtained from all subjects involved in the study.

Data Availability Statement: All data generated in this study are shown in the manuscript.

Acknowledgments: The authors thank Julio Amaré and Juanjo Lanuza from the "Departamento de Fisica Aplicada" of the University of Zaragoza for their technical support in the electronic design and mechanical assembly of the corneal waveform generator.

Conflicts of Interest: The authors declare no conflicts of interest.

References

1. Marinescu, M.; Dascalescu, D.; Constantin, M.; Coviltir, V.; Burcel, M.; Darabus, D.; Ciuluvica, R.; Stanila, D.; Potop, V.; Alexandrescu, C. Corneal Biomechanics—An Emerging Ocular Property with a Significant Impact. *Maedica* **2022**, *17*, 925–930. [CrossRef] [PubMed]
2. Kobayashi, A.S.; Staberg, L.G.; Schlegel, W.A. Viscoelastic properties of human cornea. *Exp. Mech.* **1973**, *13*, 497–503. [CrossRef]
3. Espana, E.M.; Birk, D.E. Composition, structure and function of the corneal stroma. *Exp. Eye Res.* **2020**, *198*, 108137. [CrossRef]
4. Hatami-Marbini, H.; Etebu, E. Hydration dependent biomechanical properties of the corneal stroma. *Exp. Eye Res.* **2013**, *116*, 47–54. [CrossRef]
5. Schweitzer, C.; Korobelnik, J.F.; Boniol, M.; Cougnard-Gregoire, A.; Le Goff, M.; Malet, F.; Rougier, M.B.; Delyfer, M.N.; Dartigues, J.F.; Delcourt, C. Associations of biomechanical properties of the cornea with environmental and metabolic factors in an elderly population: The ALIENOR study. *Investig. Ophthalmol. Vis. Sci.* **2016**, *57*, 2003–2011. [CrossRef]
6. Kamiya, K.; Shimizu, K.; Ohmoto, F. Effect of aging on corneal biomechanical parameters using the ocular response analyzer. *J. Refract. Surg.* **2009**, *25*, 888–893. [CrossRef] [PubMed]
7. David, R.; Zangwill, L.; Briscoe, D.; Dagan, M.; Yagev, R.; Yassur, Y. Diurnal intraocular pressure variations: An analysis of 690 diurnal curves. *Br. J. Ophthalmol.* **1992**, *76*, 280–283. [CrossRef] [PubMed]
8. Marcellán, M.C.; Remón, L.; Ávila, F.J. Corneal hysteresis and intraocular pressure are altered in silicone-hydrogel soft contact lenses wearers. *Int. Ophthalmol.* **2022**, *42*, 2801–2809. [CrossRef] [PubMed]
9. Bao, F.; Lopes, B.T.; Zheng, X.; Ji, Y.; Wang, J.; Elsheikh, A. Corneal Biomechanics Losses Caused by Refractive Surgery. *Curr. Eye Res.* **2023**, *48*, 137–143. [CrossRef]
10. Esporcatte, L.P.G.; Salomão, M.Q.; Lopes, B.T.; Sena, N.; Ferreira, É.; Filho, J.B.R.; Machado, A.P.; Ambrósio, P., Jr. Biomechanics in keratoconus diagnosis. *Curr. Eye Res.* **2023**, *48*, 130–136. [CrossRef] [PubMed]
11. Elhusseiny, A.M.; Scarcelli, G.; Saeedi, O.J. Corneal Biomechanical Measures for Glaucoma: A Clinical Approach. *Bioengineering* **2023**, *10*, 1108. [CrossRef] [PubMed]
12. Salomão, M.Q.; Hofling-Lima, A.L.; Gomes Esporcatte, L.P.; Lopes, B.; Vinciguerra, R.; Vinciguerra, P.; Bühren, J.; Sena, N., Jr.; Luz Hilgert, G.S.; Ambrósio, R., Jr. The Role of Corneal Biomechanics for the Evaluation of Ectasia Patients. *Int. J. Environ. Res. Public Health* **2020**, *17*, 2113. [CrossRef] [PubMed]
13. Esporcatte, L.P.G.; Salomão, M.Q.; Junior, N.S.; Machado, A.P.; Ferreira, É.; Loureiro, T.; Junior, R.A. Corneal biomechanics for corneal ectasia: Update. *Saudi J. Ophthalmol.* **2022**, *36*, 17–24. [CrossRef] [PubMed]
14. Lau, W.; Pye, D. A clinical description of Ocular Response Analyzer measurements. *Investig. Ophthalmol. Vis. Sci.* **2011**, *52*, 2911–2916. [CrossRef] [PubMed]
15. Luce, D.A. Determining in vivo biomechanical properties of the cornea with an ocular response analyzer. *J. Cataract Refract. Surg.* **2005**, *31*, 156–162. [CrossRef] [PubMed]
16. Zimprich, L.; Diedrich, J.; Bleeker, A.; Schweitzer, J.A. Corneal Hysteresis as a Biomarker of Glaucoma: Current Insights. *Clin. Ophthalmol.* **2020**, *14*, 2255–2264. [CrossRef]
17. Sit, A.J.; Chen, T.C.; Takusagawa, H.L.; Rosdahl, J.A.; Hoguet, A.; Chopra, V.; Richter, G.M.; Ou, Y.; Kim, S.J.; WuDunn, D. Corneal Hysteresis for the Diagnosis of Glaucoma and Assessment of Progression Risk: A Report by the American Academy of Ophthalmology. *Ophthalmology* **2023**, *130*, 433–442. [CrossRef] [PubMed]
18. del Buey, M.A.; Cristóbal, J.A.; Ascaso, F.J.; Lavilla, L.; Lanchares, E. Biomechanical properties of the cornea in Fuchs' corneal dystrophy. *Investig. Ophthalmol. Vis. Sci.* **2009**, *50*, 3199–3202. [CrossRef]
19. Ortiz, D.; Piñero, D.; Shabayek, M.H.; Arnalich-Montiel, F.; Alió, J.L. Corneal biomechanical properties in normal, post-laser in situ keratomileusis, and keratoconic eyes. *J. Cataract Refract. Surg.* **2007**, *33*, 1371–1375. [CrossRef]
20. Lopes, B.T.; Roberts, C.J.; Elsheikh, A.; Vinciguerra, R.; Vinciguerra, P.; Reisdorf, S.; Berger, S.; Koprowski, R.; Ambrósio, R., Jr. Repeatability and Reproducibility of Intraocular Pressure and Dynamic Corneal Response Parameters Assessed by the Corvis ST. *J. Ophthalmol.* **2017**, *2017*, 8515742. [CrossRef] [PubMed]
21. Borderie, V.; Beauruel, J.; Cuyaubère, R.; Georgeon, C.; Memmi, B.; Sandali, O. Comprehensive Assessment of Corvis ST Biomechanical Indices in Normal and Keratoconus Corneas with Reference to Corneal Enantiomorphism. *J. Clin. Med.* **2023**, *12*, 690. [CrossRef]

22. Zhang, P.; Wu, J.; Jiang, J.; Zhang, X.; Ran, Z.; Jiang, F.; Zheng, X.; Wang, J.; Elsheikh, A.; Bao, F. Evaluation of changes in corneal biomechanics after orthokeratology using Corvis ST. *Contact Lens Anterior Eye* **2024**, *47*, 102100. [CrossRef]
23. Long, Q.; Wang, J.; Yang, X.; Jin, Y.; Ai, F.; Li, Y. Assessment of Corneal Biomechanical Properties by CorVis ST in Patients with Dry Eye and in Healthy Subjects. *J. Ophthalmol.* **2015**, *2015*, 380624. [CrossRef]
24. Wang, X.; McAlinden, C.; Zhang, H.; Yan, J.; Wang, D.; Wei, W.; Mi, S. Assessment of corneal biomechanics, tonometry and pachymetry with the Corvis ST in myopia. *Sci. Rep.* **2021**, *11*, 3041. [CrossRef]
25. Glass, D.H.; Roberts, C.J.; Litsky, A.S.; Weber, P.A. A Viscoelastic Biomechanical Model of the Cornea Describing the Effect of Viscosity and Elasticity on Hysteresis. *Investig. Ophthalmol. Vis. Sci.* **2008**, *49*, 3919–3926. [CrossRef] [PubMed]
26. Ávila, F.J.; del Barco, Ó.; Marcellán, M.C.; Remón, L. A Comprehensive Study on Elasticity and Viscosity in Biomechanics and Optical Properties of the Living Human Cornea. *Photonics* **2024**, *11*, 524. [CrossRef]
27. Kwon, S.J.; Jeong, M.K. Advances in ultrasound elasticity imaging. *Biomed. Eng. Lett.* **2017**, *7*, 71–79. [CrossRef] [PubMed]
28. Lan, G.; Aglyamov, S.R.; Larin, K.V.; Twa, M.D. In Vivo Human Corneal Shear-wave Optical Coherence Elastography. *Optom. Vis. Sci.* **2021**, *98*, 58–63. [CrossRef] [PubMed]
29. Ramier, A.; Tavakol, B.; Yun, S.H. Measuring mechanical wave speed, dispersion, and viscoelastic modulus of the cornea using optical coherence elastography. *Opt. Express* **2019**, *27*, 16635–16649. [CrossRef]
30. Han, Z.; Li, J.; Singh, M.; Aglyamov, S.R.; Wu, C.; Liu, C.H.; Larin, K.V. Analysis of the effects of curvature and thickness on elastic wave velocity in cornea-like structures by finite element modeling and optical coherence elastography. *Appl. Phys. Lett.* **2015**, *106*, 233702. [CrossRef] [PubMed]
31. Larin, K.V. Investigating Elastic Anisotropy of the Porcine Cornea as a Function of Intraocular Pressure With Optical Coherence Elastography. *J. Refract. Surg.* **2016**, *32*, 562–567.
32. Lan, G.; Gu, B.; Larin, K.V.; Twa, M.D. Clinical Corneal Optical Coherence Elastography Measurement Precision: Effect of Heartbeat and Respiration. *Transl. Vis. Sci. Technol.* **2020**, *9*, 3. [CrossRef]
33. Ávila, F.J.; Marcellán, M.C.; Remón, L. In Vivo Biomechanical Response of the Human Cornea to Acoustic Waves. *Optics* **2023**, *4*, 584–594. [CrossRef]
34. Thibos, L.N.; Applegate, R.A.; Schwiegerling, J.T.; Webb, R. Standards for reporting the optical aberrations of eyes. *J. Refract. Surg.* **2002**, *18*, S652–S660. [CrossRef] [PubMed]
35. Blanco-Martínez, I.; González-Méijome, J.M.; Faria-Ribeiro, M. Linear fitting of biconic surfaces for corneal modeling. *J. Opt. Soc. Am. A Opt. Image Sci. Vis.* **2024**, *41*, 288–295. [CrossRef] [PubMed]
36. Crespo, M.A.; Jimenez, H.J.; Deshmukh, T.; Pulido, J.S.; Saad, A.S.; Silver, F.H.; Benedetto, D.A.; Rapuano, C.J.; Syed, Z.A. In Vivo Determination of the Human Corneal Elastic Modulus Using Vibrational Optical Coherence Tomography. *Transl. Vis. Sci. Technol.* **2022**, *11*, 11. [CrossRef]
37. Silver, F.H.; Benedetto, D.A.; Rapuano, C.J.; Syed, Z.A. Identification of the Vibrational Optical Coherence Tomography Corneal Cellular Peak. *Transl. Vis. Sci. Technol.* **2023**, *12*, 11.
38. Akca, B.I.; Chang, E.W.; Kling, S.; Ramier, A.; Scarcelli, G.; Marcos, S.; Yun, S.H. Observation of sound-induced corneal vibrational modes by optical coherence tomography. *Biomed. Opt. Express* **2015**, *6*, 3313–3319. [CrossRef] [PubMed]
39. Lan, G.; Aglyamov, S.; Larin, K.V.; Twa, M.D. In vivo human corneal natural frequency quantification using dynamic optical coherence elastography: Repeatability and reproducibility. *J. Biomech.* **2021**, *121*, 110427. [CrossRef]
40. Lan, G.; Larin, K.V.; Aglyamov, S.; Twa, M.D. Characterization of natural frequencies from nanoscale tissue oscillations using dynamic optical coherence elastography. *Biomed. Opt. Express* **2020**, *11*, 3301–3318. [CrossRef] [PubMed]
41. McAuley, R.; Nolan, A.; Curatolo, A.; Alexandrov, S.; Zvietcovich, F.; Varea Bejar, A.; Marcos, S.; Leahy, M.; Birkenfeld, J.S. Co-axial acoustic-based optical coherence vibrometry probe for the quantification of resonance frequency modes in ocular tissue. *Sci. Rep.* **2022**, *12*, 18834. [CrossRef] [PubMed]
42. Lan, G.; Shi, Q.; Wang, Y.; Ma, G.; Cai, J.; Feng, J.; Huang, Y.; Gu, B.; An, L.; Xu, J.; et al. Spatial Assessment of Heterogeneous Tissue Natural Frequency Using Micro-Force Optical Coherence Elastography. *Front. Bioeng. Biotechnol.* **2022**, *10*, 851094. [CrossRef] [PubMed]
43. Koprowski, R.; Ambrósio, R., Jr. Quantitative assessment of corneal vibrations during intraocular pressure measurement with the air-puff method in patients with keratoconus. *Comput. Biol. Med.* **2015**, *66*, 170–178. [CrossRef] [PubMed]

3. DISCUSIÓN

La presente tesis se centra en el análisis de la biomecánica corneal y en la propuesta de modelos biomecánicos orientados a mejorar la comprensión del comportamiento viscoelástico de la córnea. Con el desarrollo del MESL, se introducen nuevos conceptos relacionados las propiedades temporales (retardo corneal y viscosidad) y elásticas de la biomecánica corneal, los cuales resultan de gran interés para el diagnóstico y tratamiento de patologías en las que la biomecánica corneal desempeña un papel crucial. Asimismo, se propone una alternativa al tradicional pulso de aire para la evaluación de la biomecánica corneal, basada en el desarrollo de un nuevo resonador corneal mediante ondas de sonido de baja frecuencia.

Dado que esta tesis se presenta en formato de compendio de artículos, cada publicación incluye su propia discusión y comparación con la literatura existente. Por este motivo, a continuación, se exponen de forma conjunta las principales aportaciones derivadas del conjunto de publicaciones presentadas.

La principal propiedad de la córnea es su transparencia óptica, la cual ha sido asociada con parámetros geométricos y biomecánicos [20]. Uno de los logros de este trabajo es la obtención del primer modelo empírico que relaciona la transparencia corneal con la geometría y la biomecánica de la córnea. En la literatura, es frecuente el estudio de las causas de la edematización y la pérdida de transparencia, así como los esfuerzos por establecer de forma clara las interrelaciones entre estos factores y su aplicación clínica [113].

En este trabajo se plantea que, desde un punto de vista biomecánico, la transparencia corneal está más influenciada por la componente elástica de la córnea que por la viscosa. Otra de las relaciones encontradas indica que, a mayor astigmatismo corneal, menor es la presión necesaria para lograr el aplanamiento corneal, siendo este un factor influyente que puede infraestimar las medidas si no es tenido en cuenta.

Se destaca, por tanto, la necesidad de introducir un nuevo parámetro de compensación al medir la presión intraocular mediante aplanación, como es el astigmatismo, además del espesor central corneal [54].

Otro factor que modifica la geometría y transparencia corneal es el uso de lentes de contacto, ya que disminuyen el aporte de oxígeno a la córnea [114], lo que produce un déficit metabólico corneal que introduce cambios en su biomecánica [46]. Nuestro trabajo pone de manifiesto que el uso de lentes de contacto de hidrogel de silicona durante periodos cortos altera la biomecánica corneal, provocando una disminución de la presión intraocular y un incremento en la histéresis corneal. Estos cambios en la PIO y la CH se deben a los mecanismos compensatorios que modulan las propiedades elásticas y viscosas para mantener el equilibrio corneal, estando relacionados con la le ley de Laplace´s, la cual indica que un aumento de la PIO incrementa la rigidez y reduce la capacidad de absorción de energía [34,115].

Desde una perspectiva biomecánica, se observan mecanismos compensatorios entre la viscoelasticidad y la PIO. En el globo ocular existen otros mecanismos de autorregulación, como los que mantienen el flujo sanguíneo del nervio óptico y la retina. La regulación del flujo sanguíneo en la red de capilares de la lámina cribosa del nervio óptico está mediada tanto por la PIO como por la presión arterial [116]. El propósito de estos equilibrios es preservar la integridad y función ocular.

Como resultado de la investigación de esta Tesis, se ha logrado un modelado experimental corneal que relaciona la presión intraocular, factores físicos y biomecánicos de la córnea. Esta relación sugiere que un mayor espesor corneal se asocia con una mayor respuesta elástica del tejido corneal.

Los mecanismos de compensación biomecánica se activan ante variaciones en la PIO. Roberts et al. [34,88] sostienen en sus investigaciones que es fundamental considerar la combinación de PIO y viscoelasticidad corneal (histéresis corneal) como un factor de riesgo en pacientes con hipertensión ocular. Dada la relación inversa entre estos parámetros, se incrementa la probabilidad de que estos pacientes desarrollen glaucoma. Por este motivo, el desarrollo de nuevas técnicas para la medición de la biomecánica corneal resulta de gran interés, ya que los instrumentos actuales no miden directamente las propiedades viscoelásticas, sino que se basan en expresiones analíticas [39]. En este sentido, nuestro trabajo aporta valor al obtener dichas expresiones de manera empírica.

Como se ha comentado anteriormente, uno de los objetivos de esta tesis es separar las componentes viscosa y elástica para lograr un mejor entendimiento de las propiedades biomecánicas de la córnea. Para ello, ha sido necesario analizar distintos modelos de representación viscoelástica. Dada la existencia de múltiples modelos aplicables a la córnea, en las siguientes líneas se justifica el uso del Modelo del Estado Sólido Lineal. Se han propuesto diversos modelos viscoelásticos, entre ellos los modelos de Kelvin-Voigt, Estado Sólido Lineal, Maxwell, Kobayashi y Burgers [35,39]. El modelo de Maxwell fue descartado debido a su comportamiento de fluencia indefinida y la falta de recuperación completa, ya que se basa únicamente en un componente viscoso puro [36]. El modelo de Kelvin-Voigt tampoco resulta adecuado, debido a que carece de un componente puramente viscoso; por ello, su respuesta a la deformación no es inmediata [39]. Por su parte, los modelos de Kobayashi y Burgers presentan una mayor complejidad matemática, lo que dificulta su aplicación práctica. El Modelo del Estado Sólido Lineal, en cambio, representa eficazmente el comportamiento viscoelástico de la córnea, ya que permite distinguir de forma clara la respuesta puramente elástica de la viscoelástica y simular adecuadamente el comportamiento viscoelástico de la córnea, ya que ofrece una respuesta inmediata similar a la de un material elástico, y una recuperación completa tras la descarga [39].

Una vez comprendida la utilidad del MESL, se abordan los conceptos derivados de su desarrollo matemático [30,44]. En primer lugar, se introduce el tiempo de retardo corneal (τ), un parámetro que mide la capacidad de la córnea para absorber las fluctuaciones de la PIO. Para analizar este comportamiento, se utilizaron datos de pacientes divididos en dos grupos: un grupo control y otro con hipertensión ocular sin glaucoma. El objetivo fue observar cómo reacciona la córnea ante procesos de deformación y recuperación. El parámetro biomecánico τ representa el tiempo que tarda la córnea en recuperar su forma tras una deformación. Córneas con un comportamiento predominantemente elástico presentan valores bajos de τ, lo que indica una recuperación rápida. En cambio, córneas con una mayor componente viscoelástica muestran una recuperación más lenta y, por tanto, valores elevados de τ. Cabe destacar que los pacientes con tiempos de retardo reducidos requieren un seguimiento más riguroso, ya que podrían estar en mayor riesgo de sufrir daño en el nervio óptico, independientemente de que presenten o no una presión intraocular elevada. Para comprender la relevancia del parámetro τ, es fundamental considerar los mecanismos viscoelásticos compensatorios. Glass et al. [39] demostraron que, aunque no se observen cambios en la histéresis corneal, sí pueden producirse alteraciones

en la viscosidad y elasticidad, lo que afecta de manera compensatoria a la histéresis. Por ejemplo, en pacientes con queratocono se ha observado una histéresis baja [117] y un módulo elástico reducido [118], lo cual sugiere la existencia de un mecanismo compensatorio. Otro caso representativo es la disminución de la histéresis con la edad [39], a pesar de que se sabe que la córnea tiende a endurecerse con el envejecimiento debido al aumento en el diámetro de las fibrillas de colágeno [119]. Estos fenómenos reflejan cómo los mecanismos viscoelásticos compensatorios contribuyen a mantener la integridad corneal, y refuerzan la importancia de calcular por separado las componentes viscosa y elástica de la córnea. Aunque en el pasado se desarrollaron modelos teóricos para describir estas propiedades, nunca se había logrado medirlas *in vivo*. Glass et al. [39] destacaron la necesidad de evaluar la elasticidad y viscosidad en córneas vivas, mientras que Ahmed et al. [36] señalaron las dificultades asociadas a dichas mediciones, incluyendo la falta de equivalencia entre condiciones *ex vivo* e *in vivo*. El desarrollo del MESL ha permitido obtener estos parámetros de forma independiente. Así, se ha logrado calcular la elasticidad corneal con un valor estimado de 3,44 ± 2,67 kPa. Además, por primera vez se ha medido *in vivo* la viscosidad de la córnea (η = 3,57 ± 2,39 Pa·s), ya que hasta ahora solo se había obtenido mediante mediciones *in vitro* [39,90].

Una vez desarrollados los parámetros derivados del MESL, es fundamental justificar su aplicación clínica. Para ello, debe considerarse la correlación inversa entre la PIO y la viscoelasticidad, ampliamente documentada en la literatura [120-122]. En nuestro estudio, se observó que, para tiempos de retardo inferiores a 1,22 ms, la histéresis corneal muestra una dependencia similar tanto de la viscosidad como de la elasticidad. No obstante, cuando los tiempos de retardo superan un umbral crítico, el principal componente que contribuye a la histéresis es el componente viscoso. Nuestra principal aportación clínica radica en la identificación de valores umbral a partir de los cuales el comportamiento viscoelástico de la córnea cambia de forma significativa. En particular, se halló que, para una PIO inferior a 14,45 mmHg, la propiedad viscosa de la córnea tiende a aumentar. Este hallazgo es relevante, ya que según Roberts et al. [123], una córnea con mayor viscosidad presenta un menor riesgo de desarrollar glaucoma. Para tiempos de retardo corneal superiores a 1,22 ms, la córnea mostró un comportamiento predominantemente viscoso. En otras palabras, fue capaz de absorber energía, pero perdió eficiencia en su capacidad de disiparla. Estos hallazgos podrían tener implicaciones relevantes en el diagnóstico y tratamiento del glaucoma. Se plantea la hipótesis de que los pacientes que reciben tratamiento para el

control de la PIO y logran mantener sus valores por debajo del umbral de 14,45 mmHg, presentan una menor pérdida de campo visual y menor afectación del nervio óptico en comparación con aquella cuya PIO se mantiene por encima de dicho valor. En conclusión, para un abordaje diagnóstico y terapéutico adecuado del glaucoma, no es suficiente con medir la presión intraocular. Es esencial considerar también parámetros biomecánicos, como la histéresis corneal, el valor PIO umbral (PIOu) y el tiempo de retardo corneal. Cuando se observa una histéresis corneal disminuida junto con un valor de τ por debajo del umbral (indicando predominio del componente elástico), se puede esperar una mayor probabilidad de progresión glaucomatosa. Es importante destacar que una disminución de la viscosidad corneal se ha asociado con un mayor riesgo de desarrollar glaucoma [123].

Para comprender el comportamiento biomecánico de la córnea, se realizaron pruebas de *stress-strain* alimentando el modelo viscoelástico con parámetros experimentalmente medidos. Estas pruebas compararon un grupo control con pacientes que presentaban hipertensión ocular y otro usuario de lentes de geometría inversa "Orto-K".

El objetivo del tratamiento ortoqueratológico es modificar la refracción del paciente mediante el moldeo epitelial, permitiendo así una visión emétrope durante el día [124]. El usuario de lentes Orto-K mostró una mayor respuesta al estrés biomecánico en comparación con el grupo control, mientras que los valores de relajación fueron similares en ambos grupos. Estos pacientes presentan una elasticidad ligeramente reducida, lo cual favorece el mantenimiento de la deformación corneal inducida durante la noche. En la tesis de Pérez Corral [125], se concluye que los pacientes sometidos a orto-K presentan una mayor rigidez corneal por la mañana, la cual tiende a disminuir a lo largo del día. Este hallazgo sugiere la necesidad de profundizar en el estudio de las variaciones biomecánicas diarias inducidas por este tratamiento.

En comparación con el grupo control, el paciente con hipertensión ocular mostró una respuesta reducida tanto al estrés como a la relajación. Es decir, con menores niveles de estrés ya se producen cambios estructurales, y los tejidos se deforman más rápidamente que en sujetos sanos. Además, debido a una respuesta más lenta durante la fase de relajación, la recuperación biomecánica de la córnea es también más prolongada. Cabe destacar que el disco óptico no posee una estructura estática. La lámina cribosa puede experimentar un desplazamiento anteroposterior inducido por aumentos tanto en la PIO como en la presión intracraneal [126]. En este contexto, Azuara-Blanco et al. [127] observaron

desplazamientos del disco óptico tras aumentos bruscos de la PIO, mientras que Hocaoğlu et al. [126] detectaron desplazamientos en pacientes normotensos con valores elevados de histéresis corneal. Considerando estos estudios y su relación con las curvas de estrés/relajación observadas en pacientes con hipertensión ocular, podría sugerirse que estos factores podrían contribuir a la pérdida de fibras nerviosas en la cabeza del nervio óptico.

El segundo objetivo principal de esta Tesis ha sido el desarrollo de un nuevo método de tonometría basado en resonancia natural de la córnea. Los métodos actuales, basados principalmente en tonometría de aplanación, se ven afectados por factores como el espesor y la forma de la córnea, lo que puede conducir a estimaciones incorrectas tanto de las propiedades biomecánicas como de la PIO [128-130]. Además, técnicas que implican la deformación de la córnea, transformando su forma natural convexa en una configuración cóncava mediante pulsos de aire, pueden no ser adecuadas para pacientes con córneas gravemente comprometidas, como aquellos que han sido sometidos a un trasplante corneal. En estos casos, la medición precisa de la PIO resulta técnicamente compleja [131]. Por lo tanto, se vuelve imprescindible contar con un instrumento capaz de proporcionar mediciones fiables en este tipo de pacientes, considerando que la incidencia de glaucoma post-queratoplastia se estima en un 21,5 % [132].

Los resultados obtenidos han demostrado la respuesta biomecánica de la córnea a diferentes frecuencias de vibración de sonido. Se ha introducido un nuevo concepto conocido como “pneumatic viscoelastic damping” (PVD). Este parámetro mide la capacidad de la córnea para modificar sus propiedades elásticas y viscosas bajo una carga dinámica. Valores positivos indican un comportamiento predominantemente viscoso, mientras que valores negativos reflejan un comportamiento más elástico, con menor capacidad para absorber y disipar energía.

Se identificaron dos frecuencias específicas, 150 Hz y 250 Hz, que afectan la viscoelasticidad corneal al modular sus componentes elásticos y viscosos. A 150 Hz, el parámetro PVD mostró valores positivos, lo que indica un aumento en el componente viscoso, resultando en una reducción tanto de la histéresis como de la PIO. En contraste, a 250 Hz, el PVD presentó valores negativos, lo que sugiere un comportamiento más elástico de la córnea, con una menor capacidad de absorber y disipar energía a esa frecuencia. Se determinó la frecuencia de sonido a la cual la córnea alcanza la deformación máxima de 7 µm, que

corresponde a una vibración sonora de 150 Hz. Akca et al. [93] encontraron, en modelos corneales córneas *ex vivo*, una deformación de 8 µm para frecuencias entre 80-120 Hz.

Existen diferentes modos de resonancia de la córnea. Para distintas frecuencias, la córnea vibra con diversas intensidades, dependiendo de las capas de la córnea que se estimulen. Estos modos de vibración han sido previamente estudiados en la epidermis: entre 50-70 Hz se estimula el componente celular, mientras que entre 100-120 Hz se activa el colágeno[83,133]. Al comparar los modos de vibración de la epidermis con nuestros resultados, hemos identificado un modo de resonancia a 50 Hz. Considerando que la mayoría de las células de la córnea se encuentran en el epitelio y el estroma anterior [134], es posible que el epitelio anterior de la córnea esté siendo sometido a vibraciones. Esto tiene relevancia particular en patologías que afectan al epitelio, como el queratocono. Estudios previos han demostrado que las alteraciones en la capa epitelial ocurren en las etapas tempranas de esta enfermedad [135]. Daher et al. identificaron un pico de resonancia entre 50-70 Hz y, mediante análisis histológico, determinaron que la densidad celular corneal es mayor en el primer tercio de la córnea [136]. Por otro lado, a 150 Hz se observa la frecuencia de resonancia más alta, lo cual podría estimular las fibras de colágeno, como sugieren Crespo et al. [83], al correlacionar este modo de vibración con los estudiados en la epidermis. En cuanto a los modos de vibración a 250 Hz y 350 Hz, se requiere un estudio adicional, ya que la literatura actual no aborda estas frecuencias. Sin embargo, hemos observado que, a 250 Hz, el comportamiento de la córnea es inverso al observado a 150 Hz. En relación con la frecuencia de 350 Hz, se destaca que esta frecuencia no altera la geometría de la córnea y tiene la capacidad de reducir tanto la elasticidad como la viscosidad corneal.

3.1. Limitaciones.

Esta sección enumera las limitaciones encontradas a lo largo de esta tesis, explicando las razones detrás de dichas limitaciones.

Una de las principales limitaciones es la edad de las muestras estudiadas. En este sentido, los estudios se han centrado principalmente en sujetos sanos y jóvenes.

Otra limitación se refiere al uso de los nuevos parámetros biomecánicos para el diagnóstico y tratamiento del glaucoma. Es necesario contar con un mayor número de pacientes que presenten una PIO superior a 21 mmHg, específicamente aquellos con hipertensión ocular. Aunque trabajar con pacientes que tienen tensiones oculares dentro de los rangos normales ayuda a establecer las bases teóricas, es fundamental expandir la muestra para incluir a pacientes con patologías específicas como el glaucoma.

En cuanto a los estudios piloto realizados con el resonador corneal, la principal limitación radica en la cantidad de pacientes examinados. No obstante, es importante señalar que las pruebas de concepto sirven como base para la planificación de investigaciones más amplias y detalladas.

Otro aspecto que considerar es la falta de evaluación del nervio óptico y sus cambios estructurales en el contexto del diagnóstico y tratamiento del glaucoma. Esto plantea la necesidad de nuevas líneas de investigación.

3.2. Líneas futuras de investigación.

Esta tesis abre varias líneas de investigación futuras, ya que ha establecido las bases conceptuales que deben ser estandarizadas para su incorporación en la práctica clínica. Además, abre el campo para el diseño de nuevas técnicas de medición.

Concretamente, las líneas propuestas son las siguientes:

- Investigación sobre la relación entre la viscoelasticidad y la pérdida de campo visual: Dado que la bibliografía muestra una clara relación entre la histéresis corneal y la pérdida de campo visual, los trabajos futuros deberían explorar el potencial uso de lentes de contacto como tratamiento en pacientes glaucomatosos[71,73,75,79].
- Estudio del tiempo de retardo corneal: Este parámetro debe investigarse en pacientes con glaucoma normotenso y HTO como posible indicador diagnóstico. También se debe estudiar si los pacientes con τ inferior a τ umbral (τu) presentan una mayor prevalencia de progresión del glaucoma.
- Investigación en pacientes con PIO inferior al valor umbral: Es necesario determinar si los pacientes diagnosticados con glaucoma y una PIO inferior al valor umbral experimentan una menor pérdida de campo visual y una menor pérdida de fibras del nervio óptico.
- Estudio de usuarios de ortoqueratología: Es crucial realizar un estudio en usuarios de ortoqueratología para comprender cómo los componentes viscosos y elásticos afectan la deformación corneal mantenida durante la noche. Esto permitirá utilizar parámetros biomecánicos para predecir el efecto de este tratamiento.
- Investigar cómo los diferentes modos vibratorios pueden caracterizar el tejido corneal y revelar alteraciones fisiológicas o patológicas que no se detectan con las modalidades diagnósticas actuales.

4. CONCLUSIONES

Tras la discusión de los principales resultados obtenidos, se han obtenido las siguientes conclusiones con relación a los objetivos de la Tesis:

1. **Relación entre la estructura macroscópica de la córnea y sus propiedades:** La estructura macroscópica de la córnea está estrechamente relacionada con sus propiedades ópticas, biomecánicas y geométricas. El astigmatismo corneal afecta las mediciones biomecánicas; para evitar la subestimación de las medidas de la BMC, es crucial considerar tanto el espesor central corneal como el astigmatismo corneal del paciente.

2. **Disminución de la presión intraocular tras el uso de lentes de contacto**: Se observa una disminución significativa de la PIO tras el uso de lentes de contacto blandas a partir de 20 días de uso.

3. **Se ha conseguido separar la componente elástica y viscosa de la córnea mediante la implementación del modelo viscoelástico propuesto**. Esta nueva información puede resultar de gran utilidad en el tratamiento y seguimiento de enfermedades como el glaucoma, el queratocono y en cirugía refractiva.

4. **Nuevo biomarcador: retardo corneal.** La introducción del nuevo biomarcador "tau" permite conocer la capacidad real de la córnea para amortiguar las oscilaciones de la PIO.

5. **Modos de resonancia corneal:** Las propiedades viscosas, elásticas, estructurales y ópticas de la córnea determinan sus modos de resonancia natural. Se ha identificado que la frecuencia de resonancia de la córnea humana ocurre a 150 Hz, con una deformación máxima de 7,33 µm. El conocimiento de estos modos vibracionales refleja la capacidad de la córnea para compensar el estrés mecánico, lo cual puede ser crucial para el manejo de resultados clínicos y reducir las complicaciones posteriores a la cirugía corneal.

5. BIBLIOGRAFÍA

1. Eghrari AO, Riazuddin SA, Gottsch JD. Overview of the Cornea: Structure, Function, and Development. *Prog Mol Biol Transl Sci*. 2015;134:7-23. doi:10.1016/bs.pmbts.2015.04.001

2. Ramirez-Miranda A, Mangwani-Mordani S, Arteaga-Rivera JY, et al. Importance and use of corneal biomechanics and its diagnostic utility. Importancia y uso de la biomecánica corneal y su utilidad diagnóstica. *Cir Cir*. 2023;91(6):848-857. doi:10.24875/CIRU.23000260

3. Olsen T. On the calculation of power from curvature of the cornea. *Br J Ophthalmol*. 1986;70(2):152-154. doi:10.1136/bjo.70.2.152

4. Piñero Llorens DP. Topografía y tomografía corneal. En: García Gonzalez M, Teus Guezala MA, eds. *Cirugía refractiva corneal láser*. SECOIR España;2022:57-64

5. Gros-Otero J, Arruabarrena-Sánchez C, Teus M. Espesor corneal central en una población sana española *Arch Soc Esp Oftalmol*. 2011;86(3):73-76. doi:10.1016/j.oftal.2010.12.008

6. Reinstein DZ, Archer TJ, Gobbe M, Silverman RH, Coleman DJ. Epithelial thickness in the normal cornea: three-dimensional display with Artemis very high-frequency digital ultrasound. *J Refract Surg*. 2008;24(6):571-581. doi:10.3928/1081597X-20080601-05

7. Clout NJ, Hohenester E. A model of FAS1 domain 4 of the corneal protein beta(ig)-h3 gives a clearer view on corneal dystrophies. *Mol Vis*. 2003;9:440-448.

8. Fernández A, Moreno J, Prósper F, García M, Echeveste J. Regeneración de la superficie ocular: stem cells/células madre y técnicas reconstructivas. *An Sist Sanit Navar*. 2008;31(1):53-69. doi:10.4321/s1137-66272008000100005

9. Vidal Candela MT. *Estudio sobre los parámetros que afectan a la calidad de la cirugía en pacientes intervenidos de queratomileusis in situ asistida mediante láser excímer (Lasik)*. Tesis Doctoral. Universidad Miguel Hernández de Elche; 2003.

10. Buey Sayas MÁ del, Peris Martínez C. Biomecánica corneal: concepto, desarrollo y aplicaciones clínicas. En: *Biomecánica y arquitectura corneal*. Elsevier España; 2014:3-10.

11. Lavilla García L, Cristóba. *Biomecánica corneal en cirugía LASIK*. Tesis Doctoral. Universidad de Zaragoza; 2013.

12. Tamura Y, Konomi H, Sawada H, Takashima S, Nakajima A. Tissue distribution of type VIII collagen in human adult and fetal eyes. *Invest Ophthalmol Vis Sci*. 1991;32(9):2636-2644.

13. Hahnel C, Somodi S, Weiss DG, Guthoff RF. The keratocyte network of human cornea: a three-dimensional study using confocal laser scanning fluorescence microscopy. *Cornea*. 2000;19(2):185-193. doi:10.1097/00003226-200003000-00012

14. Møller-Pedersen T, Ehlers N. A three-dimensional study of the human corneal keratocyte density. *Curr Eye Res*. 1995;14(6):459-464. doi:10.3109/02713689509003756

15. Espana EM, Birk DE. Composition, structure and function of the corneal stroma. *Exp Eye Res*. 2020;198:108137. doi:10.1016/j.exer.2020.108137

16. Hassell JR, Birk DE. The molecular basis of corneal transparency. *Exp Eye Res*. 2010;91(3):326-335. doi:10.1016/j.exer.2010.06.021

17. Massoudi D, Malecaze F, Galiacy SD. Collagens and proteoglycans of the cornea: importance in transparency and visual disorders. *Cell Tissue Res*. 2016;363(2):337-349. doi:10.1007/s00441-015-2233-5

18. Lizarbe MA. El colágeno, ¿un cemento biológico que mantiene la arquitectura y plasticidad tisular? En: *Horizontes culturales: las fronteras de la ciencia: 2000*. Espasa Calpe España; 2001:119-137.

19. Rada JA, Cornuet PK, Hassell JR. Regulation of corneal collagen fibrillogenesis in vitro by corneal proteoglycan (lumican and decorin) core proteins. *Exp Eye Res*. 1993;56(6):635-648. doi:10.1006/exer.1993.1081

20. Meek KM, Knupp C. Corneal structure and transparency. *Prog Retin Eye Res*. 2015;49:1-16. doi:10.1016/j.preteyeres.2015.07.001

21. Meek KM, Boote C. The organization of collagen in the corneal stroma. *Exp Eye Res*. 2004;78(3):503-512. doi:10.1016/j.exer.2003.07.003

22. de Oliveira RC, Wilson SE. Descemet's membrane development, structure, function and regeneration. *Exp Eye Res*. 2020;197:1080-90. doi:10.1016/j.exer.2020.108090

23. Rocío Guadalupe Contreras-Corona RG, Anaya-Pava EJ, Gallegos-Valencia AJ, Villarreal-Maíz JA. Densidad y morfología de células del endotelio corneal en adultos jóvenes del norte de México. *Rev Mex Oftalmol.* 2014;88(3):99-103.

24. Bonanno JA. Molecular mechanisms underlying the corneal endothelial pump. *Exp Eye Res*. 2012;95(1):2-7. doi:10.1016/j.exer.2011.06.004

25. Izquierdo M, Arteaga R. Cinesiología y biomecánica de la actividad física y el deporte: concepto y revisión histórica. En: Izquierdo M, ed. *Biomecánica y Bases Neuromusculares de la Actividad Física y el Deporte*. Medica Panamericana;2008:1-15

26. Fung YC. Biomechanics: Mechanical Properties of Living Tissues. 2 ed. Berlin Heidelberg: Springer; 2013.

27. Buey Sayas MÁ del, Peris Martínez C. Factores que influyen sobre la biomecánica corneal. En: *Biomecánica y arquitectura corneal*. Elsevier España; 2014:11-22.

28. Kling S, Hafezi F. Corneal biomechanics - a review. *Ophthalmic Physiol Opt*. 2017;37(3):240-252. doi:10.1111/opo.12345

29. Torres RM, Merayo-Lloves J, Jaramillo MA, Galvis V. Biomecánica de la córnea. *Arch Soc Esp Oftalmol*. 2005;80(4):215–23.

30. Oliver Olivella X. Mecánica de medios continuos para ingenieros. Ediciones UPC; 2002.

31. Valiente Cancho A. Curso de comportamiento mecánico de materiales: elasticidad y viscoelasticidad. Madrid: García-Maroto; 2018

32. Shaw MT, MacKnight WJ. Introduction to polymer viscoelasticity. 3 ed. Hoboken;2005.

33. Jones Romero O, Bacardí Zapata PA, Páez Candelaria Y, Romero García LI, Alba Carcasé Y, Gondres Legró KM. Biomecánica corneal y glaucoma. Revi Cubana Oftalmol. 2017;30(3):1–11.

34. Roberts CJ. Concepts and misconceptions in corneal biomechanics. *J Cataract Refract Surg*. 2014;40(6):862-869. doi:10.1016/j.jcrs.2014.04.019

35. Kobayashi AS, Staberg LG, Schlegel WA. Viscoelastic properties of human cornea. *Exp Mech*. 1973 Dec 1;13(12):497–503.

36. Ahmed HM, Salem NM, Al-Atabany W. Human cornea thermo-viscoelastic behavior modelling using standard linear solid model. *BMC Ophthalmol*. 2023;23(1):250. doi:10.1186/s12886-023-02985-3

37. Phan-Thien N. Understanding Viscoelasticity: An Introduction to Rheology. 2 ed. Berlin Heidelberg: Springer; 2013.

38. Brison HF, Brison LC. Polymer engineering science and viscoelasticity. 2 ed. Berlin Heidelberg: Springer; 2013.

39. Glass DH, Roberts CJ, Litsky AS, Weber PA. A viscoelastic biomechanical model of the cornea describing the effect of viscosity and elasticity on hysteresis. *Invest Ophthalmol Vis Sci*. 2008;49(9):3919-3926. doi:10.1167/iovs.07-1321

40. Galindo Moreno JM. *Análisis numérico experimental del comportamiento de materiales viscoelásticos procedentes de neumáticos fuera de uso*. Trabajo fin de grado. Universidad de Málaga;2020.

41. Kok S, Botha N, Inglis HM. Calibrating corneal material model parameters using only inflation data: an ill-posed problem. *Int J Numer Method Biomed Eng*. 2014;30(12):1460-1475. doi:10.1002/cnm.2667

42. Kling S, Bekesi N, Dorronsoro C, Pascual D, Marcos S. Corneal viscoelastic properties from finite-element analysis of *in vivo* air-puff deformation. *PLoS One*. 2014;9(8):e104904. doi:10.1371/journal.pone.0104904

43. Jannesari M, Mosaddegh P, Kadkhodaei M, Kasprzak H, Jabbarvand Behrouz M. Numerical and clinical investigation on the material model of the cornea in Corvis tonometry tests: differentiation between hyperelasticity and viscoelasticity. *Mech Time-Depend Mater*. 2019;23(3):373–84.

44. Kelly, PA. Mechanics Lecture Notes: An introduction to Solid Mechanics. Accedido el 24 de noviembre de 2024. Disponible en: http://homepages.engineering.auckland.ac.nz/~pkel015/SolidMechanicsBooks/index.html

45. Lombardo G, Serrao S, Rosati M, Lombardo M. Analysis of the viscoelastic properties of the human cornea using Scheimpflug imaging in inflation experiment of eye globes. *PLoS One*. 2014;9(11):e112169. doi:10.1371/journal.pone.0112169

46. Esporcatte LPG, Salomão MQ, Lopes BT, et al. Biomechanical diagnostics of the cornea. *Eye Vis (Lond)*. 2020;7:9. doi:10.1186/s40662-020-0174-x

47. Wilson A, Marshall J. A review of corneal biomechanics: Mechanisms for measurement and the implications for refractive surgery. *Indian J Ophthalmol*. 2020;68(12):2679-2690. doi:10.4103/ijo.IJO_2146_20

48. Peris Martínez C, Ausín González E. Concepto de ectasia corneal. En: Cezón J, ed. *Técnicas de Modelado Corneal. Desde la Ortoqueratología hasta el Cross-Linking*. Sociedad española de cirugia ocular IMPL; 2009:163-178

49. McGhee CN, Kim BZ, Wilson PJ. Contemporary Treatment Paradigms in Keratoconus. *Cornea*. 2015;34(10):16-23. doi:10.1097/ICO.0000000000000504

50. Smadja D, Touboul D, Cohen A, et al. Detection of subclinical keratoconus using an automated decision tree classification. *Am J Ophthalmol*. 2013;156(2):237-246. doi:10.1016/j.ajo.2013.03.034

51. Ambrósio R, Correia FF, Lopes B, et al. Corneal Biomechanics in Ectatic Diseases: Refractive Surgery Implications. *Open Ophthalmol J*. 2017;11:176-193. doi:10.2174/1874364101711010176

52. Ortiz D, Piñero D, Shabayek MH, Arnalich-Montiel F, Alió JL. Corneal biomechanical properties in normal, post-laser in situ keratomileusis, and keratoconic eyes. *J Cataract Refract Surg*. 2007;33(8):1371-1375. doi:10.1016/j.jcrs.2007.04.021

53. Shah S, Laiquzzaman M, Bhojwani R, Mantry S, Cunliffe I. Assessment of the biomechanical properties of the cornea with the ocular response analyzer in normal and keratoconic eyes. *Invest Ophthalmol Vis Sci*. 2007;48(7):3026-3031. doi:10.1167/iovs.04-0694

54. Sedaghat MR, Ostadi-Moghadam H, Jabbarvand M, Askarizadeh F, Momeni-Moghaddam H, Narooie-Noori F. Corneal hysteresis and corneal resistance factor in pellucid marginal degeneration. *J Curr Ophthalmol*. 2017;30(1):42-47. doi:10.1016/j.joco.2017.08.002

55. Bohac M, Koncarevic M, Pasalic A, et al. Incidence and Clinical Characteristics of Post LASIK Ectasia: A Review of over 30,000 LASIK Cases. *Semin Ophthalmol*. 2018;33(7-8):869-877. doi:10.1080/08820538.2018.1539183

56. Moshirfar M, Tukan AN, Bundogji N, et al. Ectasia After Corneal Refractive Surgery: A Systematic Review. *Ophthalmol Ther*. 2021;10(4):753-776. doi:10.1007/s40123-021-00383-w

57. Zhao L, Yin Y, Hu T, et al. Comprehensive management of post-LASIK ectasia: From prevention to treatment. *Acta Ophthalmol*. 2023;101(5):485-503. doi:10.1111/aos.15636

58. Randleman JB, Woodward M, Lynn MJ, Stulting RD. Risk assessment for ectasia after corneal refractive surgery. *Ophthalmoly*. 2008;115(1):37-50. doi:10.1016/j.ophtha.2007.03.073

59. Bella Gala R*. Cambios en la superficie corneal y calidad óptica en pacientes con queratocono pre y post implantación de anillos intraestromales.* Tesis doctoral. Universidad Complutense de Madrid; 2022.

60. Ariza-Gracia MÁ, Flecha-Lescún J, Büchler P, Calvo B. Corneal Biomechanics After Intrastromal Ring Surgery: Optomechanical In Silico Assessment. *Transl Vis Sci Technol*. 2020;9(11):26. doi:10.1167/tvst.9.11.26

61. Nti AN, Berntsen DA. Optical changes and visual performance with orthokeratology. *Clin Exp Optom*. 2020;103(1):44–54.

62. Li Y, Yang Z, Yan Z, Shi H, Liu Z, Wang K. Revealing and predicting the long-term biomechanical response of orthokeratology by developing a patient-specific computational model. *Sci China Phys Mech Astron*. 2024;68(1):214611.

63. Swarbrick HA, Wong G, O'Leary DJ. Corneal response to orthokeratology. *Optom Vis Sci*. 1998;75(11):791-799. doi:10.1097/00006324-199811000-00019

64. Tsukiyama J, Miyamoto Y, Higaki S, Fukuda M, Shimomura Y. Changes in the anterior and posterior radii of the corneal curvature and anterior chamber depth by orthokeratology. *Eye Contact Lens*. 2008;34(1):17-20. doi:10.1097/ICL.0b013e3180515299

65. Yoon JH, Swarbrick HA. Posterior corneal shape changes in myopic overnight orthokeratology. *Optom Vis Sci*. 2013;90(3):196-204. doi:10.1097/OPX.0b013e31828121eb

66. Alharbi A, Swarbrick HA. The effects of overnight orthokeratology lens wear on corneal thickness. *Invest Ophthalmol Vis Sci*. 2003;44(6):2518-2523. doi:10.1167/iovs.02-0680

67. Nieto-Bona A, Porras-Ángel P, Ayllón-Gordillo AE, Carracedo G, Piñero DP. Short and long term corneal biomechanical analysis after overnight orthokeratology. *Int J Ophthalmol*. 2022;15(7):1128-1134. doi:10.18240/ijo.2022.07.13

68. Weinreb RN, Khaw PT. Primary open-angle glaucoma. *Lancet*. 2004;363(9422):1711-1720. doi:10.1016/S0140-6736(04)16257-0

69. Schuster AK, Erb C, Hoffmann EM, Dietlein T, Pfeiffer N. The Diagnosis and Treatment of Glaucoma. *Dtsch Arztebl Int*. 2020;117(13):225-234. doi:10.3238/arztebl.2020.0225

70. Darbà J, Marsà A. Ambulatory and hospital care of glaucoma in Spain and associated medical costs. *J Med Econ*. 2022;25(1):769-773. doi:10.1080/13696998.2022.2083348

71. Burgoyne CF. A biomechanical paradigm for axonal insult within the optic nerve head in aging and glaucoma. *Exp Eye Res*. 2011;93(2):120-132. doi:10.1016/j.exer.2010.09.005

72. Del Buey-Sayas MÁ, Lanchares-Sancho E, Campins-Falcó P, Pinazo-Durán MD, Peris-Martínez C. Corneal Biomechanical Parameters and Central Corneal Thickness in Glaucoma Patients, Glaucoma Suspects, and a Healthy Population. *J Clin Med*. 2021;10(12):2637. doi:10.3390/jcm10122637

73. Susanna CN, Diniz-Filho A, Daga FB, et al. A Prospective Longitudinal Study to Investigate Corneal Hysteresis as a Risk Factor for Predicting Development of Glaucoma. *Am J Ophthalmol*. 2018;187:148-152. doi:10.1016/j.ajo.2017.12.018

74. Mangouritsas G, Morphis G, Mourtzoukos S, Feretis E. Association between corneal hysteresis and central corneal thickness in glaucomatous and non-glaucomatous eyes. *Acta Ophthalmol*. 2009;87(8):901-905. doi:10.1111/j.1755-3768.2008.01370.x

75. Murphy ML, Pokrovskaya O, Galligan M, O'Brien C. Corneal hysteresis in patients with glaucoma-like optic discs, ocular hypertension and glaucoma. *BMC Ophthalmol*. 2017;17(1):1. doi:10.1186/s12886-016-0396-9

76. Zimprich L, Diedrich J, Bleeker A, Schweitzer JA. Corneal Hysteresis as a Biomarker of Glaucoma: Current Insights. *Clin Ophthalmol*. 2020;14:2255-2264. doi:10.2147/OPTH.S236114

77. Koomson NY, Kobia-Acquah E, Abdul-Kabir M, Aderonke UM, Kwaw RJ, Arkhurst EE. Relationship between peripheral refraction, axial lengths and parental myopia of young adult myopes. *J Optom*. 2022;15(2):122-128. doi:10.1016/j.optom.2020.10.007

78. Leske MC, Hyman L, Hussein M, Heijl A, Bengtsson B. Comparison of glaucomatous progression between untreated patients with normal-tension glaucoma and patients with therapeutically reduced intraocular pressures. The effectiveness of intraocular pressure reduction in the treatment of normal-tension glaucoma. *Am J Ophthalmol*. 1999;127(5):625-626.

79. Medeiros FA, Meira-Freitas D, Lisboa R, Kuang TM, Zangwill LM, Weinreb RN. Corneal hysteresis as a risk factor for glaucoma progression: a prospective longitudinal study. *Ophthalmol*. 2013;120(8):1533-1540. doi:10.1016/j.ophtha.2013.01.032

80. Venkataraman P, Madhuri MB, Mohan N. Corneal Biomechanics in Glaucoma – A Review of the Current Concepts and Practice. *TNOA Journal of Ophthalmic Science and Research*. 2020;58(2):94-100. doi: 10.4103/tjosr.tjosr_16_20

81. Deol M, Taylor DA, Radcliffe NM. Corneal hysteresis and its relevance to glaucoma. *Curr Opin Ophthalmol*. 2015;26(2):96-102. doi:10.1097/ICU.0000000000000130

82. Piñero DP, Alcón N. Corneal biomechanics: a review. *Clin Exp Optom*. 2015;98(2):107-116. doi:10.1111/cxo.12230

83. Crespo MA, Jimenez HJ, Deshmukh T, et al. *In Vivo* Determination of the Human Corneal Elastic Modulus Using Vibrational Optical Coherence Tomography. *Transl Vis Sci Technol*. 2022;11(7):11. doi:10.1167/tvst.11.7.11

84. Randall J, Vaughan JM. The measurement and interpretation of Brillouin scattering in the lens of the eye. *Proc R Soc Lond B Biol Sci*. 1982;214(1197):449-470. doi:10.1098/rspb.1982.0021

85. Kaushik S, Pandav SS. Ocular Response Analyzer. *J Curr Glaucoma Pract*. 2012;6(1):17-19. doi:10.5005/jp-journals-10008-1103

86. Terai N, Raiskup F, Haustein M, Pillunat LE, Spoerl E. Identification of biomechanical properties of the cornea: the ocular response analyzer. *Curr Eye Res*. 2012;37(7):553-562. doi:10.3109/02713683.2012.669007

87. Hwang HS, Park SK, Kim MS. The biomechanical properties of the cornea and anterior segment parameters. *BMC Ophthalmol*. 2013;13:49. doi:10.1186/1471-2415-13-49

88. Roberts CJ, Mahmoud AM, Bons JP, et al. Introduction of Two Novel Stiffness Parameters and Interpretation of Air Puff-Induced Biomechanical Deformation Parameters With a Dynamic Scheimpflug Analyzer. *J Refract Surg*. 2017;33(4):266-273. doi:10.3928/1081597X-20161221-03

89. Ambrósio R, Ramos I, Luz A, Faria FC, Steinmueller A, Krug M, et al. Dynamic ultra high speed Scheimpflug imaging for assessing corneal biomechanical properties. *Rev Bras Oftalmol*. 2013;72:99–102.

90. Lan G, Twa MD, Song C, et al. *In vivo* corneal elastography: A topical review of challenges and opportunities. *Comput Struct Biotechnol J*. 2023;21:2664-2687. doi:10.1016/j.csbj.2023.04.009

91. Wang S, Larin KV. Shear wave imaging optical coherence tomography (SWI-OCT) for ocular tissue biomechanics. *Opt Lett*. 2014;39(1):41-44. doi:10.1364/OL.39.000041

92. Lan G, Aglyamov S, Larin KV, Twa MD. *In vivo* human corneal natural frequency quantification using dynamic optical coherence elastography: Repeatability and reproducibility. *J Biomech*. 2021;121:110427. doi:10.1016/j.jbiomech.2021.110427

93. Akca BI, Chang EW, Kling S, et al. Observation of sound-induced corneal vibrational modes by optical coherence tomography. *Biomed Opt Express*. 2015;6(9):3313-3319. doi:10.1364/BOE.6.003313

94. Silver FH, Kelkar N, Deshmukh T, Horvath I, Shah RG. Mechano-Vibrational Spectroscopy of Tissues and Materials Using Vibrational Optical Coherence Tomography: A New Non-Invasive and Non-Destructive Technique. *Prog Mater Sci.* 2020;2(2):1–19.

95. Lan G, Larin KV, Aglyamov S, Twa MD. Characterization of natural frequencies from nanoscale tissue oscillations using dynamic optical coherence elastography. *Biomed Opt Express*. 2020;11(6):3301-3318. doi:10.1364/BOE.391324

96. Komninou MA, Seiler TG, Enzmann V. Corneal biomechanics and diagnostics: a review. *Int Ophthalmol*. 2024;44(1):132. doi:10.1007/s10792-024-03057-1

97. Fahd DC, Cherfan CG, Raad C, Asouad M, Awwad ST. Assessment of anterior and posterior corneal indices using two Scheimpflug analyzers. *Arq Bras Oftalmol*. 2014;77(1):17-20. doi:10.5935/0004-2749.20140006

98. GALILEI G4 ColorZ. www.ziemergroup.com. Accedido el 25 de febrero de 2025. Disponible en: https://www.ziemergroup.com/en/products/diagnostic-devices/galilei-g4/

99. Feizi S. Galilei Dual Scheimpflug Analyzer. En: *Diagnostics in Ocular Imaging*. Berlin Heidelberg: Springer; 2021:163-182

100. Ramón AFS, Castellanos M A, Ruiz Quintero NC, Naranjo T. Reproducibilidad de la medida del ángulo iridocorneal con el uso de Pentacam®, cámara rotatoria tipo Scheimpflug. *Rev Mex Oftalmol*. 2009;83(2)1:106-109

101. Oliveira CM, Ribeiro C, Franco S. Corneal imaging with slit-scanning and Scheimpflug imaging techniques. *Clin Exp Optom*. 2011;94(1):33-42. doi:10.1111/j.1444-0938.2010.00509.x

102. Karmiris E, Soulantzou K, Machairoudia G, Ntravalias T, Tsiogka A, Chalkiadaki E. Corneal Densitometry Assessed With Scheimpflug Camera in Healthy Corneas and Correlation With Specular Microscopy Values and Age. *Cornea*. 2022;41(1):60-68. doi:10.1097/ICO.0000000000002722

103. Consejo A, Trillo-Moreno I, Remon L. Corneal tissue changes following short-term soft contact lens wear of different materials. *Ophthalmic Physiol Opt*. 2023;43(1):35-45. doi:10.1111/opo.13067

104. Wilkinson JM, Cozine EW, Kahn AR. Refractive Eye Surgery: Helping Patients Make Informed Decisions About LASIK. *Am Fam Physician*. 2017;95(10):637-644.

105. Sinha Roy A, Shetty R, Kummelil MK. Keratoconus: a biomechanical perspective on loss of corneal stiffness. *Indian J Ophthalmol*. 2013;61(8):392-393. doi:10.4103/0301-4738.116057

106. Naderan M, Jahanrad A, Farjadnia M. Ocular, corneal, and internal aberrations in eyes with keratoconus, forme fruste keratoconus, and healthy eyes. *Int Ophthalmol*. 2018;38(4):1565-1573. doi:10.1007/s10792-017-0620-5

107. The Advanced Glaucoma Intervention Study (AGIS): 7. The relationship between control of intraocular pressure and visual field deterioration.The AGIS Investigators. *Am J Ophthalmol*. 2000;130(4):429-440. doi:10.1016/s0002-9394(00)00538-9

108. Lichter PR, Musch DC, Gillespie BW, Guire KE, Janz NK, Wren PA, et al. Interim clinical outcomes in the collaborative initial glaucoma treatment study comparing initial treatment randomized to medications or surgery. *Ophthalmoly*. 2001;108(11):1943–53.

109. Leske MC, Heijl A, Hussein M, et al. Factors for glaucoma progression and the effect of treatment: the early manifest glaucoma trial. *Arch Ophthalmol*. 2003;121(1):48-56. doi:10.1001/archopht.121.1.48

110. Lee SY, Bae HW, Kwon HJ, Seong GJ, Kim CY. Correction: Utility of Goldmann applanation tonometry for monitoring intraocular pressure in glaucoma patients with a history of laser refractory surgery. *PLoS One*. 2018;13(10). doi:10.1371/journal.pone.0206564

111. Doughty MJ, Zaman ML. Human corneal thickness and its impact on intraocular pressure measures: a review and meta-analysis approach. *Surv Ophthalmol*. 2000;44(5):367-408. doi:10.1016/s0039-6257(00)00110-7

112. Liu J, Roberts CJ. Influence of corneal biomechanical properties on intraocular pressure measurement: quantitative analysis. *J Cataract Refract Surg*. 2005;31(1):146-155. doi:10.1016/j.jcrs.2004.09.031

113. Doughty MJ, Jonuscheit S. Corneal structure, transparency, thickness and optical density (densitometry), especially as relevant to contact lens wear-a review. *Cont Lens Anterior Eye*. 2019;42(3):238-245. doi:10.1016/j.clae.2018.11.014

114. Seitz ME, Wiseman ME, Hilker I, Loos J, Tian M, Li J, et al. Influence of silicone distribution and mobility on the oxygen permeability of model silicone hydrogels. *Polymer*. 2017;118:150–162.

115. Orssengo GJ, Pye DC. Determination of the true intraocular pressure and modulus of elasticity of the human cornea *in vivo*. *Bull Math Biol*. 1999;61(3):551-572. doi:10.1006/bulm.1999.0102

116. Pérez Marrero MJ, Bastidas Narváez LA, Velázquez Pinillos NM, et al. Presión de perfusión ocular en sujetos sin enfermedad ocular. *Rev. Cub. Oftalmología*. 2022;35(3). Accedido el 18 de marzo de 2025. Disponible en: http://scielo.sld.cu/scielo.php?script=sci_abstract&pid=S0864-21762022000300006&lng=es&nrm=iso&tlng=es

117. Luce DA. Determining *in vivo* biomechanical properties of the cornea with an ocular response analyzer. *J Cataract Refract Surg*. 2005;31(1):156-162. doi:10.1016/j.jcrs.2004.10.044

118. Edmund C. Corneal elasticity and ocular rigidity in normal and keratoconic eyes. *Acta Ophthalmol (Copenh)*. 1988;66(2):134-140. doi:10.1111/j.1755-3768.1988.tb04000.x

119. Daxer A, Misof K, Grabner B, Ettl A, Fratzl P. Collagen fibrils in the human corneal stroma: structure and aging. *Invest Ophthalmol Vis Sci*. 1998;39(3):644-648.

120. Dana D, Mihaela C, Raluca I, et al. Corneal hysteresis and primary open angle glaucoma. *Rom J Ophthalmol*. 2015;59(4):252-254.

121. Nossair AA, Kassem MK, Eltanamly RM, Alahmadawy YA. Corneal Hysteresis, Central Corneal Thickness, and Intraocular Pressure in Rheumatoid Arthritis, and Their Relation to Disease Activity. *Middle East Afr J Ophthalmol*. 2021;28(3):174-179. doi:10.4103/meajo.meajo_434_20

122. Murtagh P, O'Brien C. Corneal Hysteresis, Intraocular Pressure, and Progression of Glaucoma: Time for a "Hyst-Oric" Change in Clinical Practice? *J Clin Med*. 2022;11(10):2895. doi:10.3390/jcm11102895

123. Roberts CJ, Mahmoud AM, Fleming GP. Comparison of elastic and viscoelastic biomechanical metrics in ocular hypertension and normal controls. *Invest Ophthalmol Vis Sci*. 2023;64(8):4720.

124. Bullimore MA, Johnson LA. Overnight orthokeratology. *Cont Lens Anterior Eye*. 2020;43(4):322-332. doi:10.1016/j.clae.2020.03.018

125. Pérez Corral JE. *Caracterización de la regresión diurna en ortoqueratología.* Tesis Doctoral. Universitat Politècnica de Catalunya; 2021.

126. Hocaoğlu M, Kara C, Şen EM, Öztürk F. Relationships between corneal biomechanics and the structural and functional parameters of glaucoma damage. *Arq Bras Oftalmol*. 2020;83(2):132-140. doi:10.5935/0004-2749.20200019

127. Azuara-Blanco A, Harris A, Cantor LB, Abreu MM, Weinland M. Effects of short term increase of intraocular pressure on optic disc cupping. *Br J Ophthalmol*. 1998;82(8):880-883. doi:10.1136/bjo.82.8.880

128. Vinciguerra R, Elsheikh A, Roberts CJ, et al. Influence of Pachymetry and Intraocular Pressure on Dynamic Corneal Response Parameters in Healthy Patients. *J Refract Surg*. 2016;32(8):550-561. doi:10.3928/1081597X-20160524-01

129. Tonnu PA, Ho T, Newson T, et al. The influence of central corneal thickness and age on intraocular pressure measured by pneumotonometry, non-contact tonometry, the Tono-Pen XL, and Goldmann applanation tonometry. *Br J Ophthalmol*. 2005;89(7):851-854. doi:10.1136/bjo.2004.056622

130. Molina N, Milla E, Bitrian E, Larena C, Martínez L. Comparación del tonómetro de Goldmann, neumotonómetro de contacto y el efecto del grosor corneal. *Arch Soc Esp Oftalmol*. 2010;85(10):325-328. doi:10.1016/j.oftal.2010.09.003

131. Toro Utrera PM. *Características morfológicas, biomecánica y tonometría comparada en queratoplastia.* Tesis doctoral. Universidad Complutense de Madrid; 2022.

132. Wu S, Xu J. Incidence and risk factors for post-penetrating keratoplasty glaucoma: A systematic review and meta-analysis. *PLoS One*. 2017;12(4). doi:10.1371/journal.pone.0176261

133. Silver FH, Shah RG, Benedetto D. Non-Invasive and Non-Destructive Determination of Corneal and Scleral Biomechanics Using Vibrational Optical Coherence Tomography: Preliminary Observations. *Mater. Sci. Appl*. 2018;9(7):657–69.

134. Sridhar MS. Anatomy of cornea and ocular surface. *Indian J Ophthalmol*. 2018;66(2):190-194. doi:10.4103/ijo.IJO_646_17

135. Tsubota K, Mashima Y, Murata H, Sato N, Ogata T. Corneal epithelium in keratoconus. *Cornea*. 1995;14(1):77-83.

136. Daher ND, Saad AS, Jimenez HJ, et al. Identification of the Vibrational Optical Coherence Tomography Corneal Cellular Peak. *Transl Vis Sci Technol*. 2023;12(4):11. doi:10.1167/tvst.12.4.11

6. ANEXO

6.1. ANEXO I. Factor de impacto publicaciones y contribución autoría.

En esta sección se detallan los artículos publicados, acompañados del factor de impacto y las áreas temáticas de cada revista en el siguiente orden: JIF/JCI (año)- Factor-Categoría-Rango-Cuartil. De acuerdo con lo estipulado en el Real Decreto 99/2011, se incluye también en este anexo la contribución específica realizada por el doctorando en cada una de las publicaciones.

1. Ávila FJ, Marcellán MC, Remón L. On the Relationship between Corneal Biomechanics, Macrostructure, and Optical Properties. *J Imaging*. 2021;7(12):280. https://doi.org/10.3390/jimaging7120280

   JCI (2021): 0,56-Imaging science & photographic technology-17/31-Q3

   Contribución al artículo:

   - Revisión y edición del artículo.
   - Validación.

2. Marcellán MC, Remón L, Ávila FJ. Corneal hysteresis and intraocular pressure are altered in silicone-hydrogel soft contact lenses wearers. *Int Ophthalmol*. 2022;42(9):2801-2809. https://doi.org/10.1007/s10792-022-02270-0

   JIF (2022): 1,6- Ophthalmology- 50/62-Q4

   JCI (2022): 0,65- Ophthalmology-52/95-Q3

   Contribución al artículo:

   - Investigación.
   - Revisión y edición del artículo.

3. Del Barco Ó, Ávila FJ, Marcellán MC, Remón L. Corneal retardation time as an ocular hypertension disease indicator. *Biomed Phys Eng Express*. 2023;10(1). https://doi.org/10.1088/2057-1976/ad12fa.

   JIF (2023): 1,3-Radiology, nuclear medicine & medical imaging-139/204-Q3

   JCI (2023):0,44-Radiology,nuclear medicine & medical imaging-132/204-Q3

   Contribución al artículo:

   - Investigación.
   - Revisión y edición del artículo.

4. Ávila FJ, Marcellán MC, Remón L. *In Vivo* Biomechanical Response of the Human Cornea to Acoustic Waves. *Optics*. 2023; 4(4):584-594. https://doi.org/10.3390/opt4040043

   JIF (2023):1,1-Optics-94/119-Q4

   JCI (2023): 0,31-Optics-97/120-Q4

   Contribución al artículo:

   - Metodología.
   - Investigación.
   - Revisión y edición del artículo.

5. Ávila FJ, del Barco Ó, Marcellán MC, Remón L. A Comprehensive Study on Elasticity and Viscosity in Biomechanics and Optical Properties of the Living Human Cornea. *Photonics*. 2024; 11(6):524. https://doi.org/10.3390/photonics11060524

   JIF (2023): 2,1-Optics-59/119-Q2

   JCI (2023):0,61-Optics-56/120-Q2

   Contribución al artículo:

   - Investigación
   - Visualización.

6. Ávila FJ, del Barco O, Marcellán MC, Remón L. Aberrometric, Geometrical and Biomechanical Characterization of Sound-Induced Vibrational Modes of the Living Human Cornea. *Optics*. 2025; 6(1):5. https://doi.org/10.3390/opt6010005

   JIF (2023):1,1-Optics-94/119-Q4

   JCI (2023): 0,31-Optics-97/120-Q4

   Contribución al artículo:

   - Metodología
   - Investigación